GEOMAR REPORT

GEOMAR

Helmholtz-Zentrum für Ozeanforschung Kiel

RV SONNE
Fahrtbericht / Cruise Report
SO226 - CHRIMP
CHatham RIse Methane Pockmarks

07.01. - 06.02.2013 / Auckland – Lyttelton
07.02. – 01.03.2013 / Lyttelton - Wellington

Berichte aus dem GEOMAR
Helmholtz-Zentrum für Ozeanforschung Kiel

Nr. 7 (N. Ser.)
Juni 2013

GEOMAR

Helmholtz-Zentrum für Ozeanforschung Kiel

RV SONNE
Fahrtbericht / Cruise Report
SO226 - CHRIMP
CHatham RIse Methane Pockmarks

07.01. - 06.02.2013 / Auckland – Lyttelton
07.02. – 01.03.2013 / Lyttelton - Wellington

Berichte aus dem GEOMAR
Helmholtz-Zentrum für Ozeanforschung Kiel

Nr. 7 (N. Ser.)

Juni 2013

ISSN Nr.: 2193-8113

GEOMAR
Helmholtz-Zentrum für Ozeanforschung Kiel

Das GEOMAR Helmholtz-Zentrum für Ozeanforschung Kiel ist Mitglied der Helmholtz-Gemeinschaft Deutscher Forschungszentren e.V.

The GEOMAR Helmholtz Centre for Ocean Research Kiel is a member of the Helmholtz Association of German Research Centres

Herausgeber / Editor:
Jörg Bialas / Ingo Klaucke / Jasmin Mögeltönder

GEOMAR Report
ISSN Nr.: 2193-8113, DOI 10.3289/GEOMAR_REP_NS_7_2013

Helmholtz-Zentrum für Ozeanforschung Kiel / Helmholtz Centre for Ocean Research Kiel
GEOMAR
Dienstgebäude Westufer / West Shore Building
Düsternbrooker Weg 20
D-24105 Kiel
Germany

Helmholtz-Zentrum für Ozeanforschung Kiel / Helmholtz Centre for Ocean Research Kiel
GEOMAR
Dienstgebäude Ostufer / East Shore Building
Wischhofstr. 1-3
D-24148 Kiel
Germany

Tel.: +49 431 600-0
Fax: +49 431 600-2805
www.geomar.de

Content

1. Summary

[*Davy et al.*, 2010a] reported on pockmark observations along the Chatham Rise, offshore New Zealand's South Island. The observed structures fall into three categories: features of approx. 150 m diameter are found in water depths of 500 m – 700 m, depressions with diameters of up to 5 km and the largest structures with diameters of up to 11 km were observed in water depth of 800 - 1100 m. Seismic sections across the pockmarks were available at only a few locations and mainly consisted of Parasound data. Multiple layers of small pockmarks could be correlated with sediment interfaces of increased amplitudes that correspond to the transitions between glacial maxima and minima. Consequently [*Davy et al.*, 2010a] assumed that sealevel lowstands during glacial maxima caused the dissolution of gas hydrates and hence triggered the formation of pockmarks.

Project SO226 CHRIMP aimed to test this hypothesis with an extended data base. Additional bathymetric coverage revealed multiple occurrences of large and medium size structures. Three working areas were selected along the Chatham Rise each representing one of the three types / sizes of seafloor depression.

Area one was chosen to be centred around 178°40'E with the largest pockmark structure of up to 15 km diameter. From the extended bathymetric coverage a south-west to north-east oriented alignment of three similar structures was observed. Seismic sections show a highly variable sedimentation. Inside the structures all sediments had been fully eroded to a surface that can be mapped throughout the entire region. All observed pockmarks show a radial eroded rim to the South-West with a base that corresponds to the above mentioned erosional surface. Near vertical faults and blanking patterns are found underneath the eroded rim of the structures. Shallow bright spots with negative polarity are interpreted as indicators for free gas. Nevertheless no signs were found for active fluid venting above the structure or in the surrounding.

The second area centred around 177°05'E hosts medium-size pockmarks. Five depressions were mapped, but some of them might be formed by overlapping pockmarks. Partly resedimented the structures show an eroded southern part with a sharp radial rim. Indifferent from area one a roughly 250 m wide blanking zone was found underneath one of the pockmarks. The area is imaged right above a conical shaped upward extension of a deeper sediment interface. From the 3D data the interface shows a rough topography. The conical structure and the blanking area are interpreted as an ancient feeder channel. This chimney terminates at an erosional interface, which forms the base of the seafloor depression. Multiple events of erosion, sedimentation and slumping have been identified above the erosional surface. Again water column imaging and geochemical analyses do not show indications for active methane venting within this area.

The third working area was chosen to be centred 174°35'E where a large zone of small pockmarks was known from earlier mapping. A 2D seismic profile confirms the existence of stacked pockmark layers. The wide funnel shaped opening of the buried pockmarks terminates at distinguished sediment interfaces that show an increased reflection amplitude. This corresponds to the interpretation of [*Davy et al.*, 2010a]. At greater depth the horizontal layering of the sediments is not interrupted. As with the previous two working areas there is no sign of a BSR and active methane venting could not be confirmed by water column imaging or geochemical analyses.

In summary all three areas do show images of gas migration pathways of various sizes within the deeper sediments. Nevertheless active venting of fluids could not be confirmed. Therefore other models need to be developed to explain todays still sharp defined rims of the pockmark-like seafloor depressions.

2. Introduction

2.1. Objectives of the cruise SO226

Methane is one of the most aggressive greenhouse gases driving climate change. Unfortunately the amount and the dynamics of natural methane reservoirs and sources (e.g. as gas hydrate layers along the continental margins) are not completely understood. Improving our understanding and modelling of climate dynamics requires detailed quantitative knowledge of natural reservoirs and sources of methane, such as the widespread gas hydrate deposits of the continental margins. Increasing numbers of active and passive locations of fluid and gas expulsion (cold seeps) are known from these areas. At present only seeps from shallow water contribute methane directly to the atmosphere. [Schmale et al., 2005] showed that gas bubbles rising from greater depth than 100 m will be dissolved in the water column. Bubbles rising to the sea surface have lost almost all their methane due to osmotic processes [McGinnis et al., 2006]. Contrary observations from the Gulf of Mexico show that an oil film can protect the bubbles from osmotic gas exchange and hence result in a methane contribution to the atmosphere [Solomon et al., 2009]. Estimates on the relevance of marine methane release are based on recent measurements, but much higher flow rates have been inferred for the past. Therefore it is still under discussion to which extend todays results are relevant for the geological past [*Gerald R. Dickens et al.*, 1997; *Kennett et al.*, 2000; *Paull et al.*, 1991; *Svensen et al.*, 2004].

In the context of marine Methane release the existence of marine gas hydrates is of certain relevance. Occurrence of marine gas hydrates depends on temperature, pressure, available gas and fresh water. Usually they do not appear at the seafloor but a few tens of meters below. Therefore changes in pressure and bottom water temperature will influence the formation or dissolution of gas hydrates. As such the gas hydrate stability zone (GHSZ) provides a large buffer for Methane [G.R. Dickens, 2001]. Pressure increase due to sea level rise may increase the GHSZ and bound more Methane, while an increase of bottom water temperature will decrease the GHSZ and reduce the uptake of Methane [Kennett et al., 2000]. In general both parameters vary slowly and hence changes do not result in large Methane contribution to the atmosphere. An exception could be a sudden dissolution of larger quantities of gas hydrate with a related expulsion of Methane. Such focused fluid flow appears as funnel-shaped depressions at the seafloor, so called “pockmarks”. Typical dimensions are within a few hundreds of meters. However, five to twelve kilometre wide “giant pockmarks” (GP) are known as well. Although full understanding of the mechanism of formation of these pockmarks is lacking the GPs are thought to be responsible for massive gas release causing the Palaeocene/Eocene Thermal Maximum (PETM) at about 55 million years ago. A current model expects a volume of gas to move pore water through the sediment. Fluidised sediments than allow a sudden gas release into the ocean [Cathles et al., 2010], during which the gas is not completely dissolved in the water column and Methane may reach the atmosphere [Schmale et al., 2005].

Offshore New Zealand a large number of pockmarks has been identified at the southern slope of the Chatham Rise. Among these are a few giant pockmarks ,[*Davy et al.*, 2010a]. The 1000 km long and 100 km wide ridge separates subtropical water masses (East Cape current) in the North from sub-antarctic water currents (Southland current) in the South by the Sub Tropical Front (STF; Fig. 2.1.1.) [Chiswell, 2002; Sutton, 2001]. The STF is bound to the bathymetry of the Chatham Rise and hence stayed stable during glacial cycles [Sikes et al., 2002]. Therefore pockmark systems can be studied in the context of exceptionally stable water temperature during glacial sea level variations.

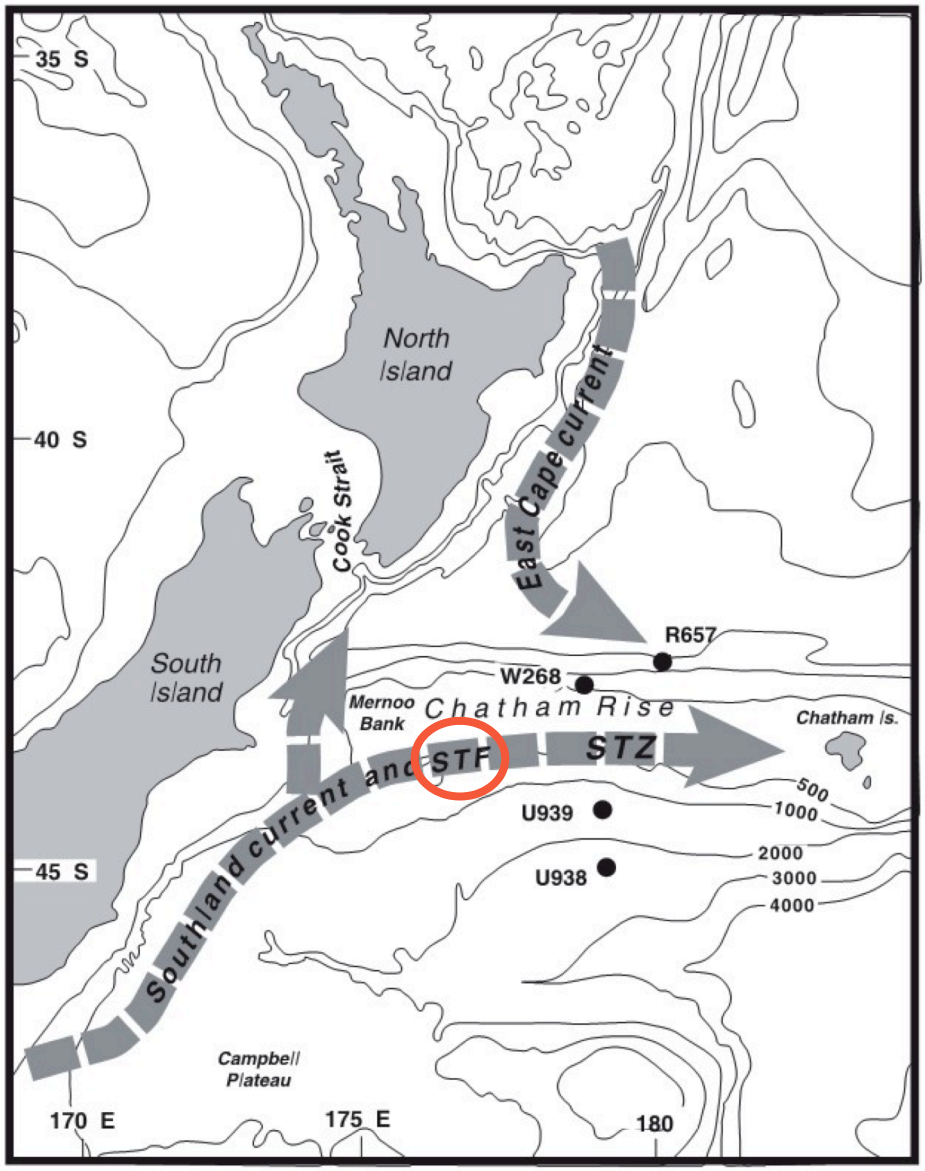

Figure 2.1.1. Water bodies from Sikes et al.

2.2. Regional Geology and Tectonics

The northern side of the Chatham Rise (Fig. 2.2.1.) was a convergent margin of Gondwana from the Permian to the Late Cretaceous. In the Late Cretaceous c. 105 Ma the convergent margin began to jam [Bradshaw 1989] following the entry of the buoyant c. 20 My-old Hikurangi Plateau Large Igneous Province into the margin [Wood and Davy, 1994, Davy and Wood 1994, Davy et al 2008] (Fig. 2.2.2.).

Reyners et al. (2011) identified a base of Hikurangi Plateau (HKP) layer with a Vp > 8.5 km/s. Such a velocity is also observed beneath the Ontong Java Plateau and Reyners et al. (2011) suggested it may be due to an underplated eclogite layer formed during the combined Ontong Java/Manihiki/Hikurangi Plateau formation [Taylor 2006]. Partly based on such high velocity observations Reyners et al. (2011) suggested the Hikurangi Plateau had been subducted as far south as Fiordland in the South Island.

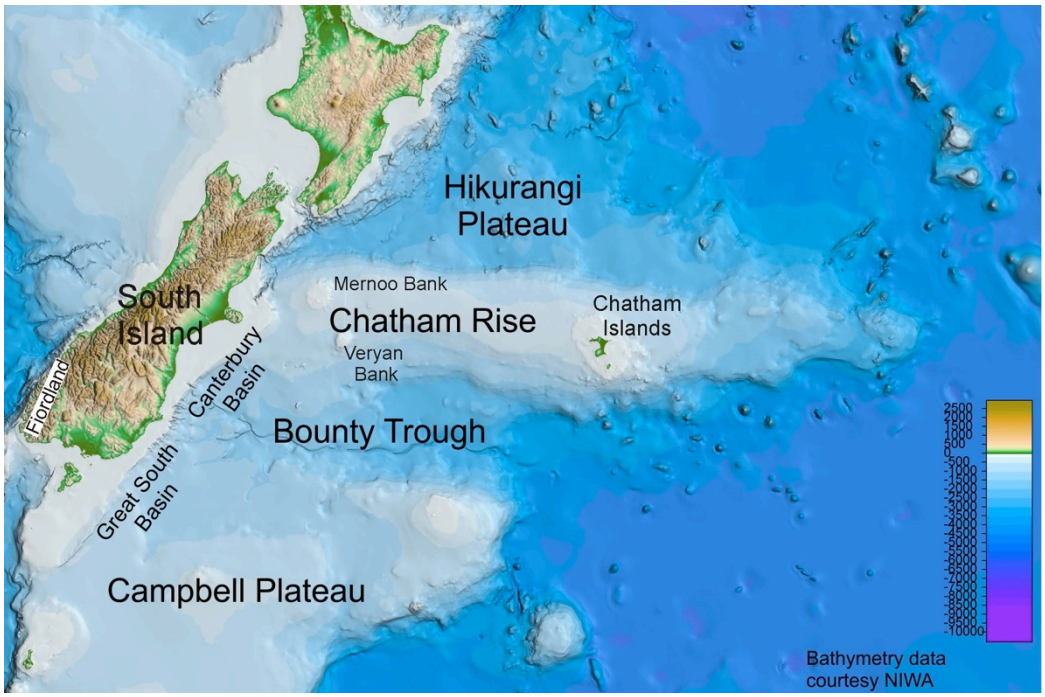

Figure 2.2.1. Regional morphology and features

Although the extent of plateau subduction offshore has yet to be defined subduction of the 20-30 My-old bouyant Hikurangi Plateau beneath the Chatham Rise will have elevated the accretionary prism well above sea-level. A deep crustal seismic reflection line, HKDC1 (Fig. 2.2.3.) collected by Geco Resolution in 2000 as part of the New Zealand UNCLOS extended continental shelf studies shows the paleo-Cretaceous subduction margin, a subducted Hikurangi Plateau and a Cretaceous unit (unit "MES") interpreted to have been eroded from the uplifted Chatham Rise Crest.

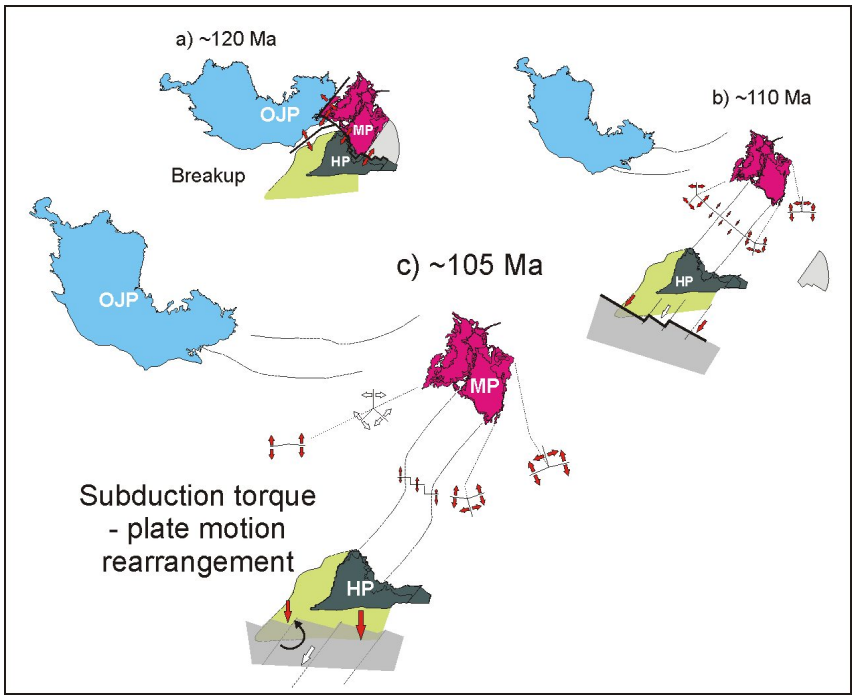

Figure 2.2.2. Cartoon of proposed Hikurangi Plateau breakup and Gondwana subduction (modified from Davy et al. 2008). The cartoon includes an extended Hikurangi Plateau extent (light green area) as proposed by Reyners et al. (2011).

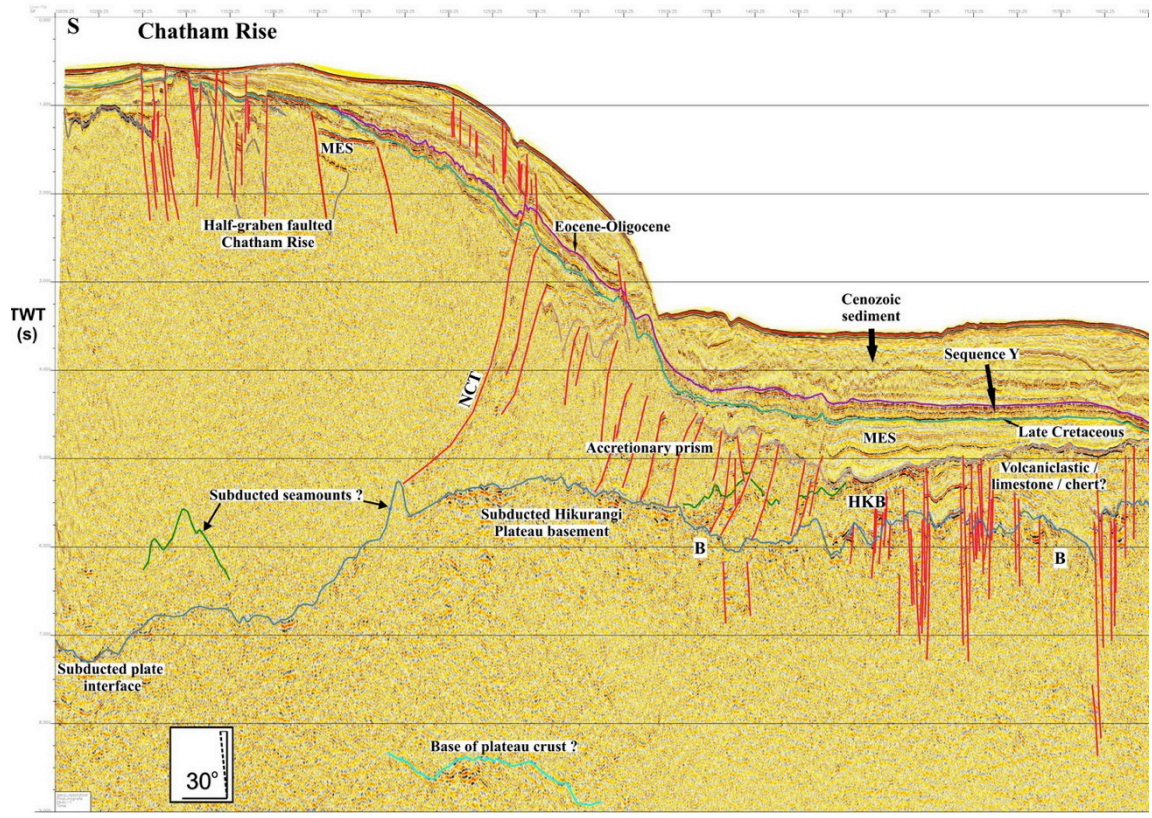

Figure 2.2.3. Southern segment of line HKDC1 (modified from Davy et al. 2008) showing the fossil Gondwana subduction margin (northern Chatham Rise) with the Hikurangi Plateau subducted at least as far south as the Chatham Rise crest. Location is shown in Figure 2.1.4.

Uplift episodes on the Chatham Islands were examined by Adams et al. 2008 using Rb-Sr metamorphic and U-Pb detrital zircon ages. Cover sandstones returned a detrital zircon age of 101-119 Ma and Chatham Schists returned detrital zircon age peaks of 230-250 Ma and other minor peaks in the Late Triassic to Late Permian.The peaks are very similar to age peaks of Torlesse greywacke onshore South Island, New Zealand. Chatham Schist metamorhic ages are 180-198 Ma suggesting earlier periods of margin uplift. Schist only occurs on the eastern half of the Chatham Rise with greywacke exposed on the western half.

Davy ey al. (2008) suggested a northeast offset in the Chatham Rise, between East and West Chatham Rise, running between c. 178.6o and 180o. The satellite free-air gravity anomaly (Fig. 2.2.4.) [Sandwell and Smith 2010] provides support for this segmentation which occurred, most probably, as a consequence of Hikurangi Plateau subduction. Fig. 2.2.4. also highlights how the giant pockmark described in Davy et al. (2010) lies on the southwestern end of this line of the Chatham Rise segmentation. The crest of the Chatham Rise is dominated by linear half-graben basins which are well imaged in the free-air gravity anomaly.

Wood and Herzer (1993) examined seismic reflection lines and outcrop geology of the Chatham Rise, They found greywacke/schist basement, some exposed near the Chatham Rise crest, disrupted everywhere by south-facing half-graben depressions. The half-graben are filled with up to several kilometres of cretaceous sediments. Overlying Cenozoic sediments are principally limestone and greensand. The crest of the Chatham Rise was starved of limestone in the early Neogene with a thin limestone and volcanogenic sediment cover.

Plate convergent motion and the rise of the South Island Southern Alps beginning in mid Neogene provided increased terrigenous input particularly to the western Chatham Rise. The Chatham Rise has been rich in basaltic volcanic activity from the Cretaceous to the Pliocene, with the latter occurring at Veryan Bank (Fig. 2.2.1.) and numerous volcanic knolls within a 100 km radius.

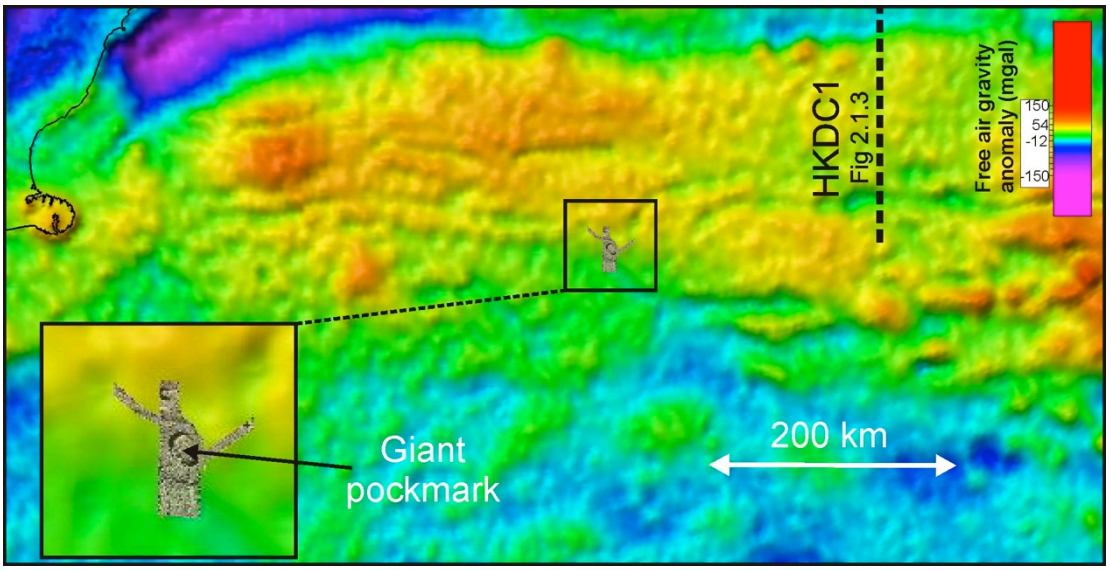

Figure 2.2.4. Free air gravity anomaly map (Sandwell and Smith 1997). The region of the SO226 site 1 including an extract of existing multi-beam data with a giant pockmark evident (Davy et al. 2010). The location of line HKDC1 – Figure 2.2.3. – is also shown.

The Cenozoic sedimentary succession around Chatham Rise has been drilled during several DSDP and ODP campaigns (sites DSDP 594, and ODP 1122-1125; Lewis et al. 1984; Carter et al. 1999). Miocene to Recent deposits largely consist of hemipelagic to pelagic, interbedded nannofossil mudstones and clayey nannofossil chalk [Lewis et al. 1986; Carter et al. 1999]. Cyclic patterns in the lithological records have been interpreted to reflect periodic inflow of cold, corrosive bottom waters from the south [Carter et al. 2004].

An early Oligocene hiatus at ODP site 1124 has been related to the Marshall Paraconformity [Carter et al. 2004], which has been widely encountered in New Zealand. An additional hiatus at this site separates dark Eocene mudstones from Paleocene nannofossil chalk [Carter et al. 1999].

2.3. New Zealand oceanography

2.3.1. Physiography

Relative to its land area New Zealand has a large continental shelf region and the New Zealand Plateau markedly interrupts the generally west to east flow of the two major surface water masses, which surround it.

Extending south down the east coast of the North Island is the extensive, abyssal Hikurangi Plateau. To the south the plateau rises up along the northern flank of the Chatham Rise. The Chatham Rise extends eastwards from the coast of the South Island, and shoals to average depths of ~300 m. Mernoo Saddle separates the Rise from the continental shelf of emergent New Zealand. South of Chatham Rise is the Bounty Trough which extends ~1000 km east of the continental margin of the South Island. The Trough is bounded to the north by the submerged continental mass of the Chatham Rise. The Bounty Trough contains two fan systems, the Otago Fan Complex at its head and the Bounty Fan at its base, which merges with the 4500 m deep abyssal plain of the South-west Pacific. These two fan systems are linked by the Bounty Channel and levee system – a conduit for feeding sediment eroded off the South Island down to the abyssal Bounty Fan.

2.3.2. Sediments

The majority of the region surrounding New Zealand is mantled by a drape of terrigenous mud and sand or biogenic gravel, sand and ooze. Primary sources of terrigenous material are the background supply of sediment from active erosion of uplifting mountain chains and volcanoclastic

contributions from intermittent large eruptions. This material is transferred to the deep sea via seafloor failure, fall of volcanic ash, and dispersion via submarine channels. Biogenic sources are dominated by calcareous nannoplankton and foraminifera, with minor siliceous components. Broad regional differences in biogenic supply are a result of both differing production and dilution by terrigenous sediment.

The crest of the Chatham Rise is predominately composed of Paleogene and Miocene chalk deposits [Wood et al. 1989], exposed in places due to episodic current winnowing, and draped by thin, impersistent deposits of authigenic and biogenic silty sand, localized accumulations of phosphorite nodules [Cullen 1987, McDougall 1982] and localised biogenic gravel and sand deposits with some terrigenous cobbles and pebbles [McDougall 1982]. Pelagic carbonate and hemipelagic sediment mantles both the northern and southern flanks of the Chatham Rise, where sediment cover occurs on steep flanks it is patchy and coarse due to erosion and winnowing by associated deep currents, with mass failure also playing a role.

In contrast Bounty Troughs crossed by submarine canyons, and channels is dominated by hemipelagic and terrigenous sedimentation. The head of the system generally consists of muddy sand with associated calcareous and terrigenous gravel and gravelly sand [e.g., McDougall 1982, Herzer 1981]. Modern turbidity current activity is absent in the bathyal to abyssal reaches of the Bounty Channel and Trough [Carter & Carter 1993], resulting in overlying pelagic and hemipelagic ooze.

2.3.3. Water masses

Within the New Zealand region there are two surface and three subsurface water masses. The surface water masses are separated from each other by oceanic fronts which are characterized by rapid spatial changes in water properties [e.g. Heath 1985, Carter *et al.* 1998].

North of the Subtropical Front (STF) surface waters are highly saline, nutrient-depleted, sourced by warm Subtropical Water (STW) from the north, whereas south of the STF surface waters have lower salinity and comprise nutrient-rich, derived from cool Subantarctic Surface Water (SAW) south of New Zealand. These surface water masses meet across the STF. This occurs along the continental margin off the south-eastern South Island turning east along Chatham Rise at ~43°S, following approximately the 15°C isotherm in summer. The STF is a complex and irregular frontal zone comprising large meanders and eddies, constrained by easterly flows along the flanks of Chatham Rise [Chiswell, 1994].

Antarctic Intermediate Water (AAIW), a major northward-spreading water mass, occurs immediately below surface water masses at depths of ~600–1450 m. AAIW is characterized by salinities of 34.3–34.5‰ and temperatures of 3–7°C. AAIW in this location is strongly influenced by bathymetry with those waters bathing the southern sector of the New Zealand region being sourced from the south and taking the shortest route from the Antarctic Convergence. However AAIW in the north enters the region from the western South Pacific Ocean via the Coral and Tasman Seas before extending around the northern tip of New Zealand [Tomczak and Godfrey, 1994]. This northern-sourced AAIW is distinguished on the basis of a slightly higher salinity minimum [Stanton, 2002]. Subantarctic mode water, often considered to be a component of AAIW, lies north of the Subantarctic Front at depths of ~300–700 m as an isothermal subsurface layer. Circumpolar Deep Water (CPDW) underlies AAIW down to the seafloor in this region.

2.3.4. Currents

Major surface currents off New Zealand (Fig. 2.1.1) originate from two arms of the east-flowing Tasman Inflow. This inflow is sourced from the South Pacific western boundary current, which flows down the coast of Australia, before separating from the Australian landmass at c. 31-32°S. The bulk of the flow crosses the Tasman Sea as the Tasman Inflow [Stanton 1981] bringing in STW down the east side of northern New Zealand. The warm EAUC flows south-east around East Cape

[Heath 1985], where it is called the East Cape Current (ECC), then south down to Cook Strait where it is deflected eastwards along the STF. Associated with this current system is the semi-permanent Wairarapa Eddy.

Warm STW also flows south along the west coast of the southern South Island becoming the Southland Current that flows around southern New Zealand and then swings northwards along the east coast of the South Island mixing with cooler Subantarctic water across the Southland Front [Heath, 1972]. Part of the Southland Current (SC) crosses Chatham Rise over the Mernoo Saddle while a second component turns east along the southern flank of Chatham Rise and STF resulting in cool SAW veering east as it meets Chatham Rise.

The main inflow of deep water into the Pacific Ocean is via the DWBC that extends around the eastern plateau–rise complex of New Zealand. The path of this deep flow is constrained by bathymetry. Hence, the current path passes around the eastern end of Chatham Rise.

2.4 Previous investigations

Pockmarks were first identified on the southern Chatham Rise by the 2006 Oceans 2020 survey TAN0610 9 [Nodder et al. 2009] although it was the compilation of multi-beam bathymetry from the region, described in Davy et al. (2010), that highlighted the wide-ranging extent and nature of pockmarks on the Chatham Rise.

Davy et al (2010) identified gas escape features extending over a region of 20,000 km^2 between 173^o and 180^oE (Fig. 2.4.1) which included:

a) circular, remarkably uniformly distributed, typically 150-200 m in diameter, 2–8 m deep pockmarks which occupy about 1% of the sea floor between 500 and 700 m water (Fig. 2.4.2)
b) irregularly shaped but dominantly ellipsoid features, estimated to occupy about 50% of the sea floor between 800 and 1,100 m. These pockmarks are 1–5 km in diameter, and 50 to 150 m deep (Fig. 2.4.3)
c) Two near circular depressions with diameters of 8–11 km characterized by an annular ring that is 1500 m wide, 80 – 100 m deep and asymmetric in cross section (Fig. 2.4.4). The slope of the outer and inner ring slopes are roughly 15° and 2°, respectively. The two large, near-circular features that have been mapped show an interruption of the annular ring in the Northeast. Up to 10 further examples of this type were anticipated to be discovered as more complete multi-beam coverage was obtained. No pockmarks of this size have been found elsewhere in the world.

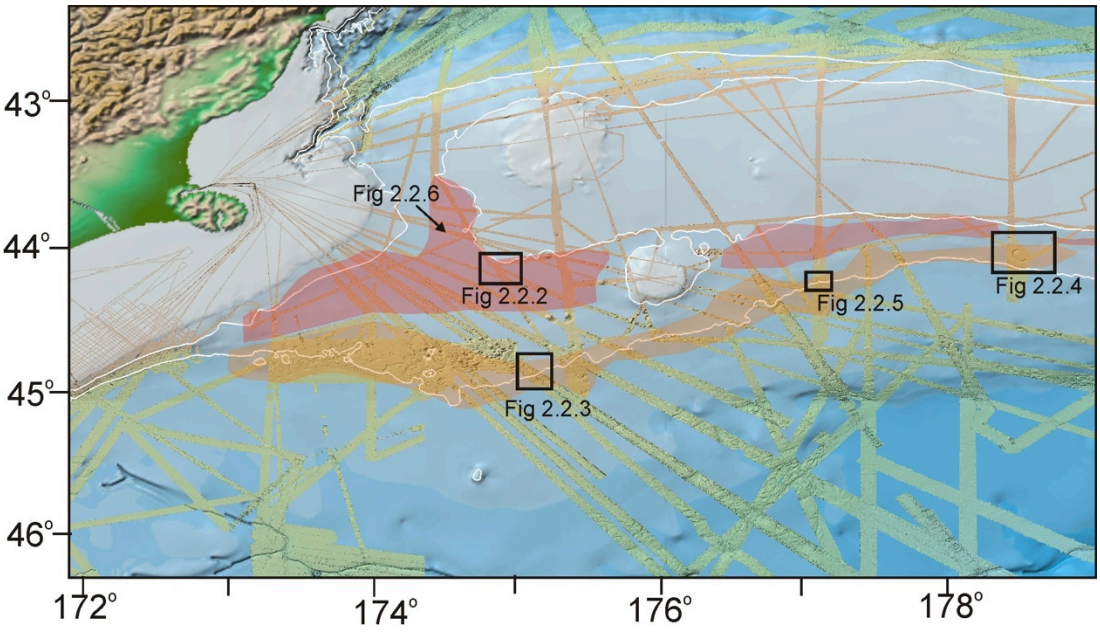

Figure 2.4.1. Swath bathymetry coverage, zones of pockmarks on the Southern Chatham Rise and location boxes for Figures 2.23.2-2.3.6. Red zones contain small pock marks (diameter c. 200 m). Orange zones contain medium (1-5 km diameter) and giant (c. 20 km diameter) pockmarks. The 500 m and 1000 m contours are plotted as white lines.

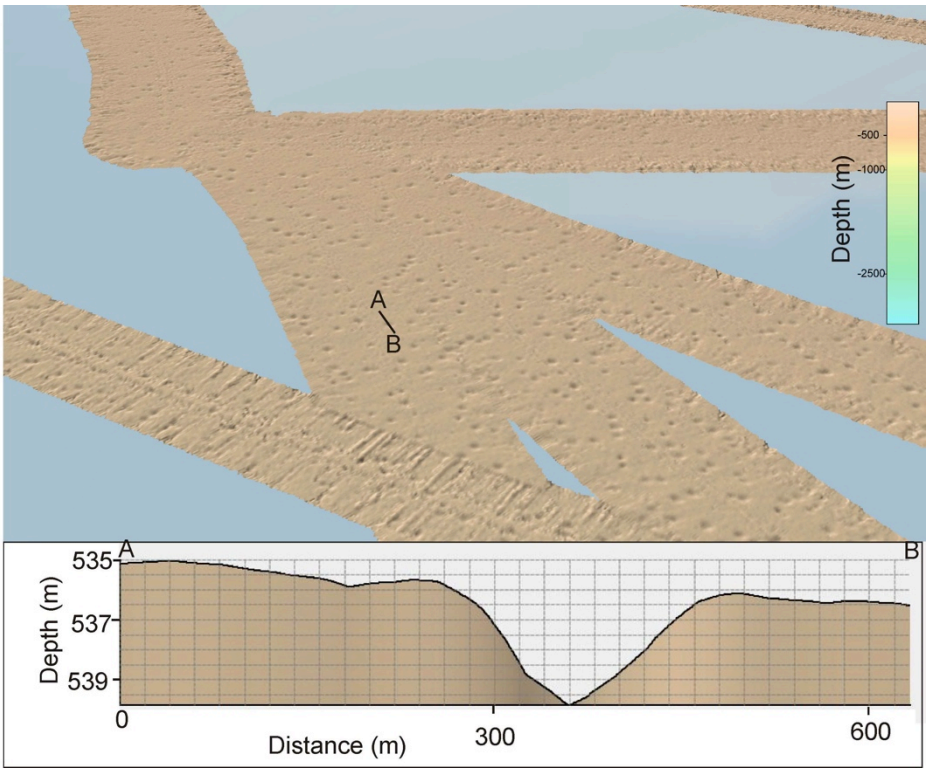

Figure 2.4.2. Small pockmarks plotted in this shade illuminated image of the seafloor. The pockmarks become scarce near 500 m water depth and are absent c. 20 m shallower. Location is shown in Figure 2.4.1.

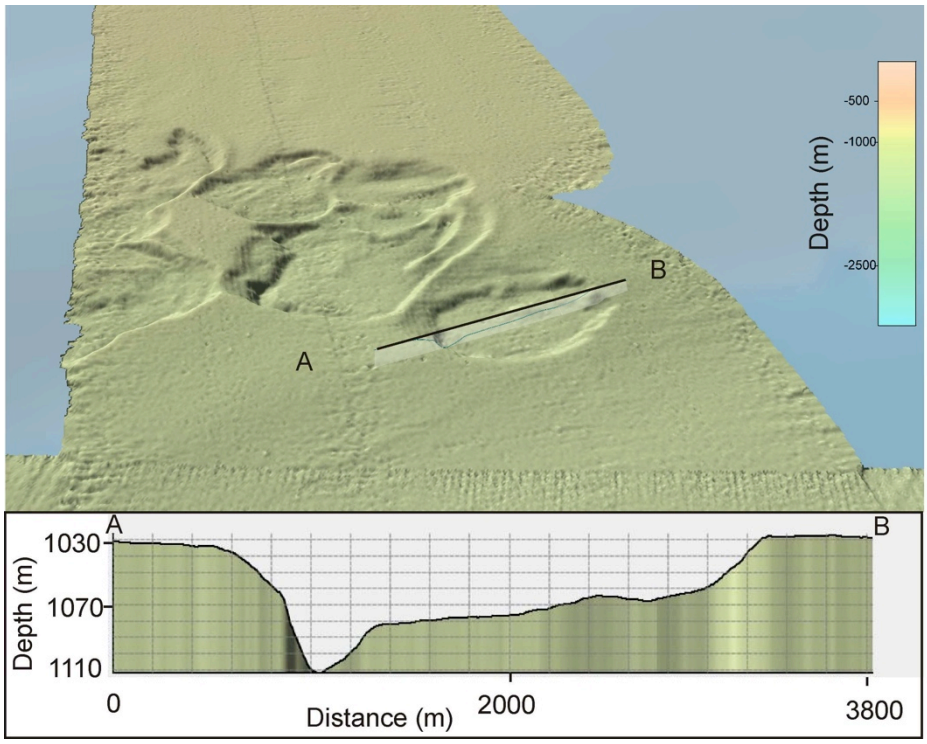

Figure 2.4.3. Medium pockmarks plotted in this shade illuminated image of the seafloor. The pockmarks occur between c. 800-1000 m. Location is shown in Figure 2.4.1.

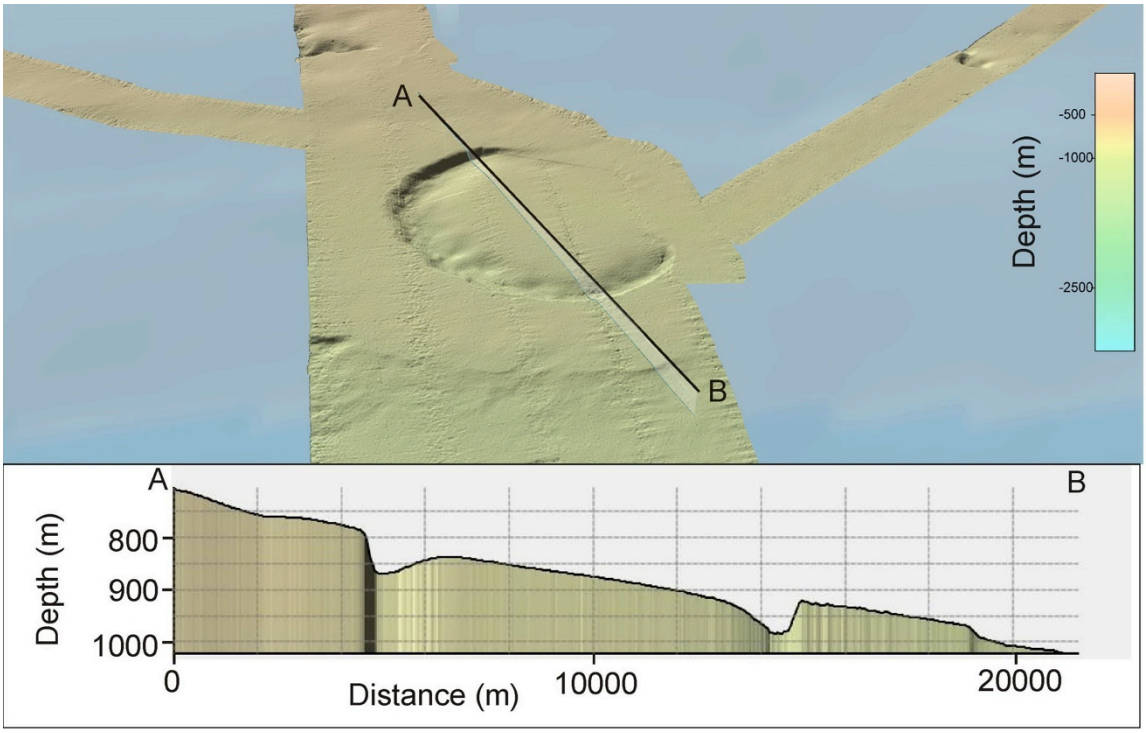

Figure 2.4.4. A giant pockmark plotted in this shade illuminated image of the seafloor. The pockmark occurs between c. 800-900 m. Location is shown in Figure 2.4.1.

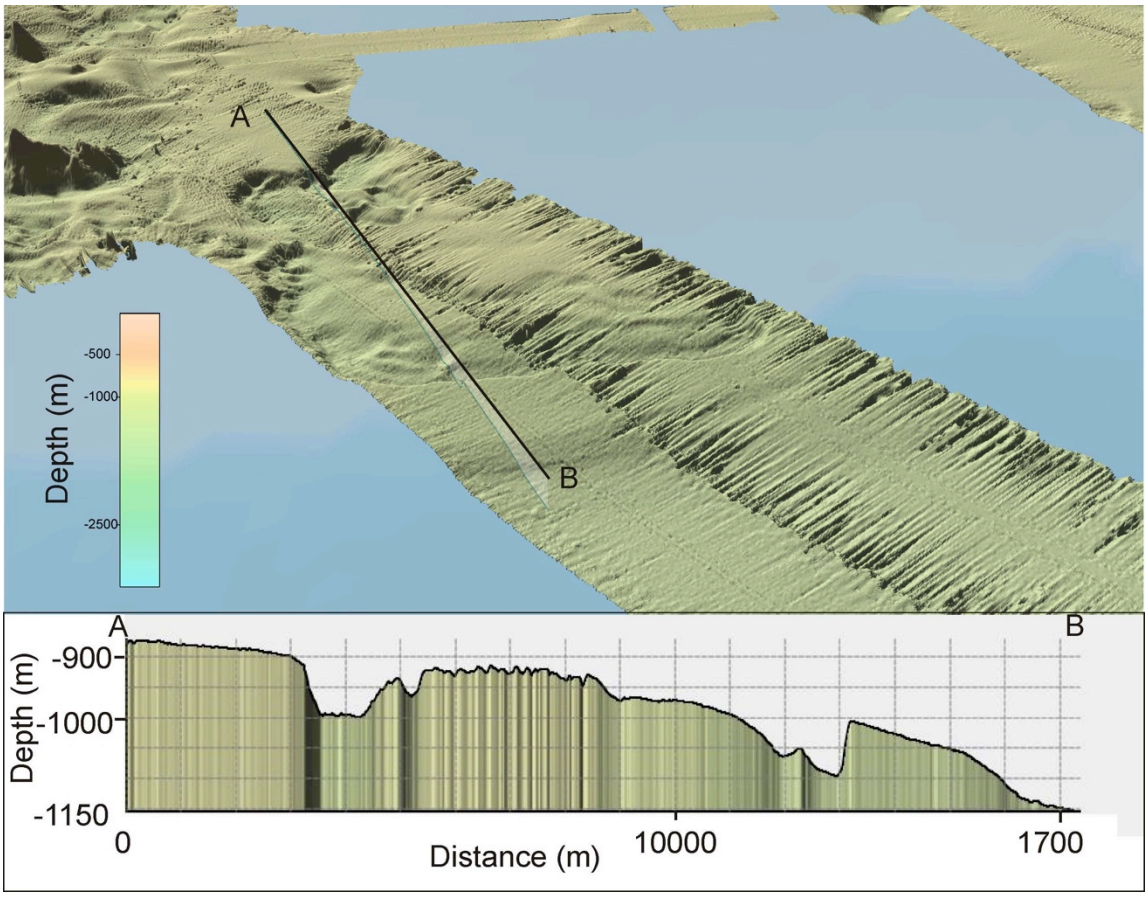

Figure 2.4.5. A giant pockmark plotted in this shade illuminated image of the seafloor. The pockmark occurs between c. 800-900 m. Location is shown in Figure 2.4.1.

PARASOUND sub-bottom profiler data collected by the RV SONNE in 2003 and RV POLARSTERN in 2010 also show buried pockmarks (Fig. 2.4.6). Davy et al. (2010) noted that between 600-700 m water depths these pockmarks were only observed on high amplitude subsurface reflectors, some of which were unconformities. The pockmarks were not observed on the reflection horizons between the high-amplitude reflectors.

Using published sediment accumulation rates from the Bounty Trough region [Carter et al. 2000] and by correlation of PARASOUND seismic horizon patterns with oxygen isotope curves Davy et al. (2010) identified the more reflective horizons as peak glacial stages over the last 0.6 Ma. They further inferred that gas was escaping at the profile location principally during the peak of glaciation or the immediately consequent warming transition. The c, 500 m upper cut-off of small pockmarks matches with the depth of top of gas hydrate stability at this location and was a strong indicator that the shallow pockmarks are derived from melting gas hydrate during interglacial development.

Davy et al. (2010) further postulated that during peak glacial stages lowered pressures at the base of the gas hydrate zone would have led to disassociation of gas hydrate leading to gas accumulations which when released formed the medium to giant sized pockmarks.

Pockmarks have since been mapped along the Canterbury shelf [Davy et al. in prep] as well as the Pegasus basin in the very north-western Chatham Rise.

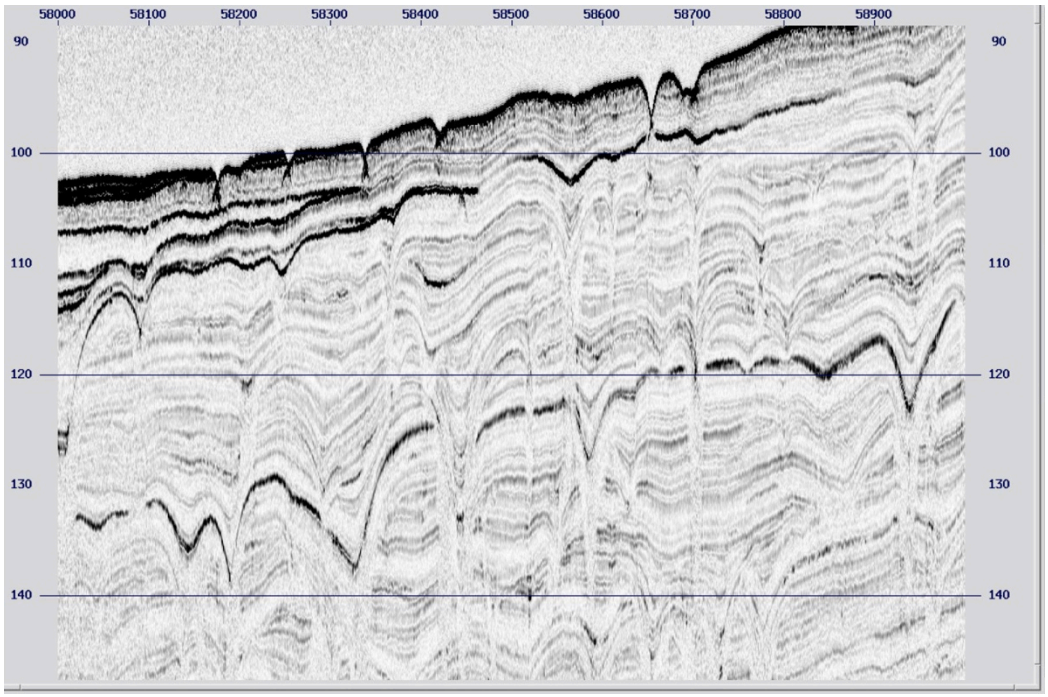

Figure 2.4.6. A PARASOUND image collected in 2010 by the RV POLARSTERN. Paleo-pockmarks dominate the c.50 msec TWT of seismic record shown.

The pockmarks on the Canterbury shelf are elongated by up to 200% parallel to the direction of the Southland Current which is a strong current forming the southern margin of the Sub-Tropical Front (STF) a major ocean boundary between the Sub-Tropical Water and the Sub-Antarctic Water [Chiswell 2002].

Similarly the medium and giant pockmarks on the south-western Chatham Rise are asymmetric and they are clearly influenced in their erosional/depositional pattern by the Southland Current (Fig. 2.1.1).

3 Participants

3.1. Scientists

3.1.1. Scientists of the cruise SO-226/1

#	Name	Aufgabe	Institut
1	Jörg Bialas	Chief scientist / Seismic	GEOMAR
2	Brian Davy	Seismic / Observer	GNS
3	Sudipta Sarkar	Seismic Prozessing	Uni Southampton
4	Cord Papenberg	Navigation / Processing	GEOMAR
5	Stephanie Koch	Seismic Prozessing	GEOMAR
6	Thomas Eckhardt	Seismic	GEOMAR
7	Anke Dannowski	OBS	GEOMAR
8	Henning Schröder	OBS	GEOMAR
9	Felix Gross	Bathymetry & Parasound	GEOMAR
10	Klaus Steffen	Technician	GEOMAR

11	Gero Wetzel	Electronic Engineer	GEOMAR
12	Jasper Hoffmann	Bathymetry & Parasound	GEOMAR
13	Jess Hillmann	Bathymetry & Parasound	Uni OTAGO
14	Christin McLachlen	Bathymetry & Parasound	Uni OTAGO
15	Karsten Kröger	Seismic / Observer	GNS
16	Sean Crossen	Seismic	Uni Auckland
17	Kate Waghorn	Seismic	Uni Auckland

3.1.2. Scientists of the cruise SO-226/2

#	Name	Expertise	Institute
1	Ingo Klaucke	Chief scientist / sidescan	GEOMAR
2	Wilhelm Weinrebe	Sidescan / Bathymetry	GEOMAR
3	Ines Dumke	Sidescan	GEOMAR
4	Jens Schneider v. Deimling	Parasound & WCI	GEOMAR
5	Malte Rolfs	Geology	Windkraft Union & GE-OMAR
6	Martin Wollatz-Vogt	Electronic Engineer	GEOMAR
7	Stefanie Semper	Parasound	GEOMAR
8	Rick Coffin	Organic geochemistry	NRL
9	Paula Rose	Inorganic geochemistry	NRL
10	Santiago Carrizosa	Geochemistry	NRL
11	Curt Millholland	Core processing	NRL
12	Thomas Boyd	Biogeochemistry	NRL
13	Ross Downer	Coring technician	NRL
14	Layton Bryant	Coring technician	NRL
15	Michael Nies	Coring technician	NRL
16	John Woods	Geochemistry	NRL
17	Brandon Yoza	Geochemistry	NRL
18	John Mitchell	OFOS	NIWA
19	Scott Nodder	OFOS	NIWA
20	Jess Hillmann	Bathymetry & Parasound	Uni OTAGO
21	Dimitar Saturov	Methane sensors	CONTROS
22	Kate Waghorn	Bathymetry & Parasound	Uni Auckland

3.2. Crew

3.2.1. Crew of the cruise SO-226/1

#	rank or rating	family name	given name
1	Captain/Master	Mallon	Lutz
2	Ch. Mate	Korte	Detlef
3	Officer Nav. Watch	Buechele	Heinz-Ulrich
4	Officer Nav. Watch	Henning	Tim
5	Surgeon	Dr. Heuser	Sabine
6	Ch. Engineer	Rex	Andreas
7	2. Engineer	Klinder	Klaus Dieter
8	Officer Eng. Watch	Pieper	Carsten
9	Electrician	Rieper	Uwe
10	Ch. Electron	Grossmann	Matthias
11	System Manager	Meinecke	Stefan
12	Fitter	Blohm	Volker
13	Motorman	Krawczak	Ryszard
14	Motorman	Roob	Christian
15	Apprentice MPR	Grawe	Manuel
16	Apprentice MPR	Kallenbach	Christian
17	Ch. Cook	Wieden	Wilhelm
18	2nd Cook	Matter	Sebastian
19	Ch. Steward	Schmandke	Harald
20	2nd Steward	Royo	Luis
21	Boatswain	Schrapel	Andreas
22	Able Bodied Seaman	Staengl	Guenter
23	Able Bodied Seaman	Altendorf	Denis
24	Able Bodied Seaman	Fricke	Ingo
25	Able Bodied Seaman	Kraft	Juergen
26	Able Bodied Seaman	Heibeck	Frank

3.2.2. Crew of the cruise SO-226/2

#	rank or rating	family name	given name
1	Captain/Master	Meyer	Oliver
2	Ch. Mate	Korte	Detlef
3	Officer Nav. Watch	Göbel	Jens-Christian

4	Officer Nav. Watch	Henning	Tim
5	Surgeon	Dr. Bauer	Bodo
6	Ch. Engineer	Guzman-Navarrete	Werner
7	2. Engineer	Klinder	Klaus Dieter
8	Officer Eng. Watch	Genschow	Steffen
9	Electrician	Beyer	Thomas
10	Ch. Elec. Engineer	Grossmann	Matthias
11	Elec. Eng. (addtl)	Leppin	Joerg
12	System Manager	Meinecke	Stefan
13	Fitter	Blohm	Volker
14	Motorman	Krawczak	Ryszard
15	Motorman	Roob	Christian
16	Apprentice MPR	Grawe	Manuel
17	Apprentice MPR	Kallenbach	Christian
18	Ch. Cook	Tiemann	Frank
19	2nd Cook	Matter	Sebastian
20	Ch. Steward	Schmandke	Harald
21	2nd Steward	Steep	Maik
22	Boatswain	Schrapel	Andreas
23	Able Bodied Seaman	Staengl	Guenter
24	Able Bodied Seaman	Altendorf	Denis
25	Able Bodied Seaman	Fricke	Ingo
26	Able Bodied Seaman	Kraft	Juergen
27	Able Bodied Seaman	Ross	Reno
28	Able Bodied Seaman	Barkow	Michael

3.3 Addresses of participating institutions

GEOMAR Helmholtz Centre for Ocean Research Kiel, Marine Geodynamics
Wischhofstr. 1-3, 24148 Kiel, Germany
Ph.: +49-431-600-2271, Fx.: +49 431 600 2922
http://www.geomar.de/forschen/fb4/fb4-gdy/schwerpunkte/

GNS GNS Science
1 Fairway Dr, Avalon, Lower Hutt 5011, New Zealand
Ph.: +64 4-570 1444, Fx.: +64 4 570 4600
http://www.gns.cri.nz/

NIWA National Institute of Water and Atmospheric Research
301 Evans Bay Parade, Wellington 6021, New Zealand
ph: +64 4 386 0300, fax: +64 4 386 0574
http://www.niwa.co.nz/

OTAGO University of Otago, Geology
Clocktower Building, 364 Leith Walk, Dunedin, 9016, New Zealand
Tel ++64 3 479 7519, Fax ++64 3 479 7527
http://www.otago.ac.nz/geology/index.html

SOTON University of Southampton
University Road, Southampton SO17 1BJ, Great Britain
Ph.: +44 (023) 8059 6569, Fx.: +44 (023) 8059 6554
http://www.southampton.ac.uk/soes/

UOA University of Auckland, School of Environment
Private Bag 92019, Auckland, New Zealand
Ph.: +64 9 373 7513 (overseas), Fax: +64 9 373 7431
http://www.env.auckland.ac.nz/uoa/

CONTROS CONTROS Systems & Solutions GmbH
Wischhofstrasse 1-3, Bld. 2, 24148 Kiel, Germany
Ph.: +49 (0) 431-260 95 900, Fax: +49 (0) 431-260 95 90
http://www.contros.eu/index.html

4. Agenda of the cruise

4.1. Agenda oft the cruise SO-226/Leg 1

On Monday 07th January 2013 17 scientists joined RV SONNE in the port of Auckland to prepare cruise SO-226/1 CHRIMP. Two 20" containers were loaded on board while a 40" container was unloaded at the berth. During the following days laboratories were installed with research equipment and computers and on deck the seismic equipment and trawl doors of the 3D P-Cable system were prepared. Dr. Pecher from Auckland University, PI of the co-operating New Zealand Marsden Project Chatham Rise, was invited for a science meeting where the last target selections were discussed. A safety instruction for all scientists was completed. On Wednesday 09th January 2013 RV SONNE left the port of Auckland at 16:00 and set course to the 600 nm distant working area at Chatham Rise.

On Thursday 10th January 2013 a safety exercise for crew and scientists was undertaken.

The voyage was interrupted on Friday 11th January 2013 when RV SONNE reached a water depth of more than 1000 m in order to gain a water sound profile for the multibeam data and to complete a depth test of the acoustic releases used with the Ocean-Bottom Seismometers.

RV SONNE approached to Chatham Rise on 03:00 on Saturday 12th January 2013 and the acquisition of bathymetry and PARASOUND was started. At 06:00 three OBS were deployed for test purposes during the upcoming 2D reconnaissance multichannel seismic profiles. While sailing across the working area the outlook at the bridge did not spot any sights of mammals. A Streamer and a single GI-Airgun were deployed at 07:00.

On Monday 14th January 2013 the streamer and the airgun were recovered at 06:40. All three OBS were back on board at 08:30. Additional courses with bathymetry and PARASOUND recording were sailed while the 2D seismic data were analysed to identify the best location for the 3D seismic volume. The decision was made in favour for a new discovered giant pockmark site, as active flares were observed along the rim of that structure. On 18:00 the deployment of 19 OBS was started and could be completed until 23:00. Further mapping was done during the night as the first deployment of the 3D P-Cable system with the trawl doors should be undertaken during daylight.

On Tuesday 15th January 2013 the 3D system was deployed and the first airgun shot was fired at 13:40.

On Wednesday 16th January 2013 weather conditions became much worse than announced. On 11:45 the airgun was recovered. Wind conditions had raised to force 7 Bft. instead of the announced 5 – 6 Bft. At 14:30 the entire system need to be recovered as weather conditions did not improve. Bathymetric mapping and PARASOUND were used to search for further pockmark structures in the working area.

On Thursday 17th January 2013 a second CTD was deployed at the Southern slope of Chatham Rise (CR) to adopt the sound velocity profile to the different conditions of the currents North and South of the CR. At 12:00 the 3D P-Cable system was deployed again. As another storm with up to7 Bft. wind speed and >5 m wave height was announced seismic profiling was interrupted again on 19:15. RV SONNE headed to the SW where less strong weather conditions were announced.

On Saturday 19th January 2013 weather conditions improved again and the 3D system was deployed at 09:00. During Monday wave swell increased up to 4 m but with long wavelength. The trawl doors sailed well until one of the swivel break. The P-Cable system was recovered for repair at 16:30 and redeployed at 20:20. Later in the evening the signal transmission became instable and the entire system was recovered at 02:00 on Tuesday 22th January 2013. Profiles were laid for multibeam bathymetry mapping and PARASOUND to fill gaps in the existing map and to look for additional depressions in the working area.

As the search for the cable failure continued during the day the seismic system was reset to 2D mode and the streamer was deployed at 13:30. The 2D profiles were completed on 23th January 2013 at 08:15 and the system was again rebuilt to deploy the 3D P-Cable at 10:20. During the day weather conditions got worse. In the evening the port side trawl door flipped around. It could be adjusted again without recovery. The system operated well while weather conditions calm down again. Nevertheless the wave state stayed high with about 3 m swell and the port side trawl door needs to be recovered during the afternoon of Thursday 24th January 2013 after it sailed across the data umbilical. The measurements continued until Friday 25th January 2013 07:20 when the compressor failed.

The repair was completed at 11:20 and the P-Cable acquisition continued until Saturday 26th January 2013. During the night the streamer system generated some internal trigger signals and caused incomplete data acquisition when regularly interrogated. At 05:00 the data connection was interrupted and the P-Cable needs to be recovered. As a major part of the cube has been sailed already and the OBS tend to run out of battery, the morning hours were used to recover the 19 OBS. The operation went smooth and all instruments returned within 7 hrs. Until the afternoon the P-Cable system was tested on deck and could be deployed again. Profiling continued for about 6 hours. when the data connection failed again. The port door was recovered and the first break-out with connecting cables was replaced. At 01:20 on Sunday 27th January 2013 the test of the system was okay and it was deployed again. Unfortunately the P-Cable became instable again after 2 hours. At 05:00 in the morning the data connection to the cross cable failed again and the system was recovered. At 07:20 the 2D streamer configuration was deployed for the attempt of filling gaps in the 3D coverage. Until 16:30 profiles were shot across all major gaps and profiling continued on a set of 2D lines investigating structures that have been imaged on PARASOUND and previous 2D lines in more detail.

On Monday 28th January 2013 we finished our work program at site 1 and recovered the airgun and the streamer. During the 70 nm transit towards working area 2 a test deployment of the life boats was completed. Upon arrival at site 2 10 OBS were deployed at 15:50 and reconnaissance 2D seismic profiling began. Based on the 2D images that were provide for analyses in KingDom software right after completion of each line a new target area for a 3D box was defined. The 10 OBS were recovered during the night of Wednesday 29th January 2013. 18 OBS were deployed again across the 3D area until 08:00. During the time intensive tests of the cables of the P-Cable system were undertaken, with no save result. The P-Cable could be deployed on 08:30. About 2 hrs after the start of profiling data the connection became instable and internal triggers were generated again. The search for a cable failure points towards a possible damage within the data umbilical. Therefore the

port door was recovered and the umbilical was replaced. Profiling could be continued after 20:20 on the 30th January 2013

The P-Cable survey could be continued until Sunday 03th February 2013 at 18:30 without any interruptions. By then a good coverage had been obtained. Due to an unfavourable weather forecast we decided to stop the survey and recover the OBS.

After a 113 nm transit RV SONNE arrived at working area 3. As weather conditions already changed we decided to deploy the 2D seismic streamer only. At 15:30 a streamer and an airgun were deployed for a short survey above an existing PARASOUND line. Weather conditions changed rapidly within 20 min around 20:00 hours and all equipment was recovered. As the weather forecast announced winds of 8 Bft. and wave heights of 5.5 m RV SONNE set course towards the bay of Lyttleton to wait for an improvement. As the weather reports did not change to better conditions for the coming days it was decided to dock in the port of Lyttleton on Wednesday 06th February 2013 already.

4.2. Cruise narrative leg-2

The day of Thursday 7th February 2013 was spent exchanging information with the scientific crew of the previous leg. A wealth of good seismic data had to be talked through and additional New Zealand partners (I. Pecher and A. Gorman) joined in the discussion. Most members of the scientific party had arrived by today, except for two New Zealand scientists expected to arrive one day later. In the afternoon scientific equipment arriving from the United States, New Zealand or by airmail from Germany was delivered to the ship.

Friday 8th February was dedicated to setting up the scientific equipment in the different laboratories on board. A major difficulty was to install the mobile ELAC multibeam transducers under the moon pool. The transducers do not fit through the moon pool and divers had to fix the transducer from underneath the ship. By noon the last members of the scientific party had arrived.

Saturday 9th February started with RV SONNE changing berth at 10:30 for refuelling after having been cleared by Customs. At 17:30 local time the pilot finally came on board and guided us out of the harbour of Lyttelton. We went for one day of transit into the easternmost working area. Once outside the New Zealand 12 miles zone, the multibeam and sediment echosounder have been switched on.

Sunday 10th February saw our arrival in the easternmost working area 1 at 20:00 and we started our work program with a CTD cast in order to get the latest sound velocity profile. Subsequently, we spent the night with bathymetric profiles in order to fill gaps in the existing bathymetric chart that our colleagues of leg one had already started.

On Monday 11th February the Posidonia USBL antenna was calibrated at 08:00 and a first piston core with 5.74 m recovery was taken in order to obtain a background geochemical profile. Subsequently, starting at 14:00 the DTS sidescan sonar was deployed for a detailed survey of the two large depressions in area 1.

The sidescan survey continued without problems until Wednesday, 13th February when the instrument was recovered at 13:00. The remainder of the day was dedicated to piston core sampling across the southwestern large depression. As the first core only recovered less than 3 m of core the corer was modified from 9 m barrel to just 6 m. Despite this short length and only 4.5 m of recovery the maximum pull was on the order of 90 kn. Here, three cores were taken for geochemistry, paleoceanography and geotechnics. The geochemistry core was processed onboard in order to retrieve the pore water and run pore water analyses, the paleoceanography core was split and described while the geotechnics core was cut into sections for further analyses back in the lab. The next station was supposed to recover older strata, but instead of the feared for bent or broken barrels, the piston corer was firmly stuck in the sediments. The maximum pull of the winch of 150 kn was insufficient to recover the piston corer. It took all the seamanship of the crew in order to pull out the corer, but eventually at 23:00 the coring cable broke at the connection to the coring weight.

We lost the weight and the corer, but recovered the trigger outrigger and the Posidonia transponder. During this maximum pull one of the fibres of the cable also snapped at roughly 950 m cable length and 1000 metres of the cable had to be cut off before a new termination could be fixed.

After loosing the piston corer the night and morning hours of Thursday 14th February were spent searching for gas flares in the water column using the ELAC multibeam system. The search was in vain and the potential flares reported by the scientific party of the previous leg are most likely schools of fish. As the broken cable had to be taken off the drum and a new cable termination had to be fixed, work continued with bathymetric mapping under good weather conditions but with steadily increasing swell. By the late afternoon, the cable was again ready for use and a series of nine multi-corer stations were undertaken across the northeastern depression in the working area.

By 02:30 on Friday 15th February the multicorer stations had been completed and the same locations were targeted by piston coring starting at 10:00 with a couple of bathymetric profiles in between for filling some gaps. The first two stations were quite successful with more than 5 metres of muddy sediments recovered. On the third location at the bottom of the depression two attempts resulted in a broken barrel and, unfortunately, also in one lost piston. With no more spare piston, the decision was made to concentrate on sampling the infill sediments of the depression rather than trying to sample the oldest sediments outcropping at the base of the depression.

Starting at 22:00 multicores were taken prior to the piston cores that started Saturday 16th February at 04:30 and recovered up to 7 m of mostly muddy sediments. The coring work continued until 14:30 and was followed by an OFOS transect across the series of multicorer stations taken in the night of Thursday to Friday. The video image clearly showed hard rock outcrops at the base of the depression, thus explaining the failed attempts to core this location. OFOS was back on deck by 22:00 and the night was spent filling gaps in the bathymetry in order to determine the full extent of the depressions mapped so far in area 1.

By 11:00 on Sunday 17th February the first station of a series of four short gravity cores for backscatter characterisation was reached. Three of these stations did not recover a core besides some sandy deposits in the core catcher. At 17:00 a series of six additional multi-core stations on several of the previous coring sites was undertaken and completed by the early morning hours of the next day.

After finishing the multi-core stations at 04:00 on Monday 18th February we started our transit to working area 2 while running the multibeam bathymetry system. At 21:00 a CTD cast was taken together with a methane sensor and at 22:30 the sidescan sonar was deployed for a 48 hours survey of area 2.

The sidescan was recovered on Wednesday 20th February at 18:00 followed by a series of six multicorer stations across one of the depressions in working area 2.

By 02:00 on Thursday 21th February the multicorer stations were completed and the same stations, except one that did not recover any sediment and that was deemed to hard to core, were cored using a 9 m long piston corer for a total of 9 cores. Piston coring finished by 21:30 and was followed by additional multicorer stations.

At 09:00 on Friday 22th February the multicorer stations had been finished and were soon followed by a last set of five piston cores across the structure that had been investigated with 3D-seismics on leg one. Coring was completed by 19:30 and followed by bathymetric mapping of a wide area upslope from the known seafloor depressions.

At 13:00 on Saturday 23th February the bathymetric surveying was interrupted for a short, 3 hours OFOS transect across the coring stations in area 2 and the dedicated bathymetry and Parasound profiles continued during the night and during Sunday, February 24 with increasing swell during the night of Saturday to Sunday and then slowly decreasing again.

By 10:00 Monday 25th February we had reached our third and final working area and deployed the sidescan sonar for a short survey. The sidescan was recovered at 22:00 and was soon followed by a series of multi-cores.

Multicoring went on until 05:00 on Tuesday 26th February when we started a series of 9-m piston cores. Coring went smoothly until the third to last station at 20:00 when a broken barrel was retrieved. This coring site was abandoned. The next site retrieved 1.5 m of sandy deposits with the core liner being shattered further up the core. We suspect that the corer fell over at this site. The final station (attempted at 11:30) also fell over, but this time the core barrel was bent and only 60 cm of mostly fine sand was retrieved. We decided that this location could not be cored with our equipment and thus concluded piston coring for this voyage.

At this time, we also noticed that the coring wire had a kink that needed to be cut off and the wire had to be re-terminated for a final series of four multi-cores starting at 03:00 on Wednesday 27th February and finishing at 08:00. This concluded sediment sampling for this voyage as the number and type of samples to be landed at Wellington port had to be communicated 48 hours in advance to the New Zealand Biosecurity Office. At 09:00 the OFOS was deployed for a final four hour transect across the coring sites at area 3. Finally, starting at 14:30 we expanded on the known bathymetry of area 3 until we had to leave the working area and start our transit to Wellington at 08:00 on Thursday 28th February. At this time northerly winds had increased and slowed down our progress.

We arrived at the pilot station outside Wellington harbour at 08:00 on Friday 1st March and docked at Aotea quay at 09:00 ending our 20 day research cruise to Chatham Rise.

5. Scientific Equipment

5.1. Shipboard Equipment

5.1.1. Navigation

Several Ashtec AC12 and Garmin GPS receivers were set up to provide position information of the various systems. Onboard a GPS antenna was mounted on one of the containers (Fig. 5.1.1.1.). Additional GPS receivers were mounted on the two trawl doors for the 3-D P-Cable system. NMEA strings from the remote GPS were transmitted via radio link onboard R/V SONNE. RS232 links submitted the position information to the OFOP PC (Fig 5.1.1.2.). OFOP was used to display the ships and trawl doors positions on top of a bathymetric map. Track keeping accuracy could be controlled by the display of the waypoints. In addition offsets between trawl doors and trawl door – ship were displayed. A connecting line between the trawl doors is drawn in user-selected intervals. Its width can be adjusted to the expected CDP coverage. Storage of the coverage lines enables to redraw the achieved coverage any time. At the same time the GPS navigation data is processed already for calculation of the real streamer positions. Even in the case one of the trawl door GPS receivers is lost the cross cable position can be estimated and a true CDP coverage map is provided. At a later stage of the survey the coverage map is used to identify remaining gaps. Additional profiles will then be used to fill the gaps (Fig. 5.1.1.3.).

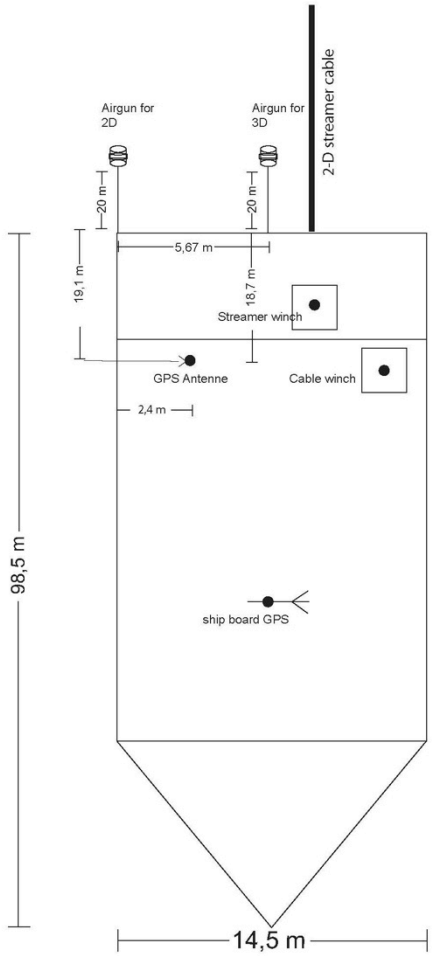

Figure 5.1.1.1. Measures used fort he positioning of gun and streamers during the seismic surveys

With the P-Cable system the streamer sections are not distributed along a straight line. Due to drag forces in the water the cross cable can best be described forming a shape somewhere between a triangular and a half circle. Navigation processing sets out to calculate the exact shape by using the GPS positions of the trawl doors and the first arrival time of the direct wave from the airgun signal. During the course of profiling the trawl doors were effected by water currents and sea state. Therefore offsets between starboard and port side door and the airgun in the centre are varying depending on the heading of the sail line (Fig. 5.1.1.4.). Based on GPS positions of the trawl doors and the first arrival of the airgun shots at the front most streamer hydrophone the position of each streamer segment is calculated. Triangulation is applied and provides coordinates for the streamer groups within a range of less than 5 m. The assumption of a catenary shaped outline for the cross cable provides best results (Fig. 5.1.1.4.). Based on the resulting shot table interpolation, stacking and migration of the entire data cube can be done. For the raw processing onboard RV SONNE a migration grid of 6.25 m * 6.25 m could be achieved.

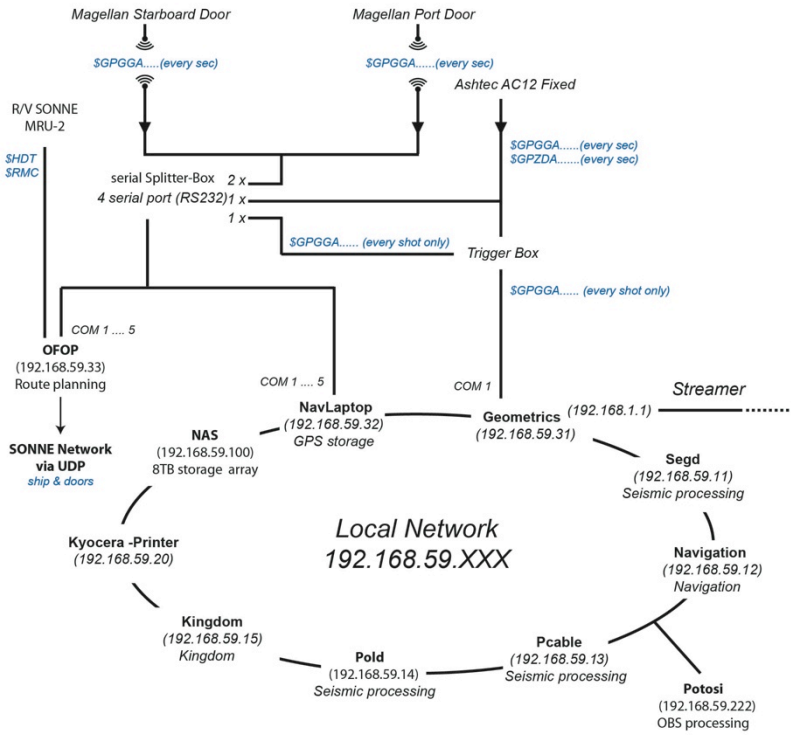

Figure 5.1.1.2. Local Area Network set up for the seismic data handling

For 2-D multichannel acquisition the streamer was deployed through the rear A-frame. The streamer composes of 137.5 m active length and 55 m tow cable. Three birds submersed the streamer. During rough seas streamer depth was chosen at 3 m while during flat seas the scheduled depth was 2 m. The GI-Airgun was deployed and towed from the starboard derrick at the aft (Fig. 5.1.1.1.). Due to the small group offset of 1.52 m within the streamer sections a 2D migration with 0.7 m trace offset could be achieved.

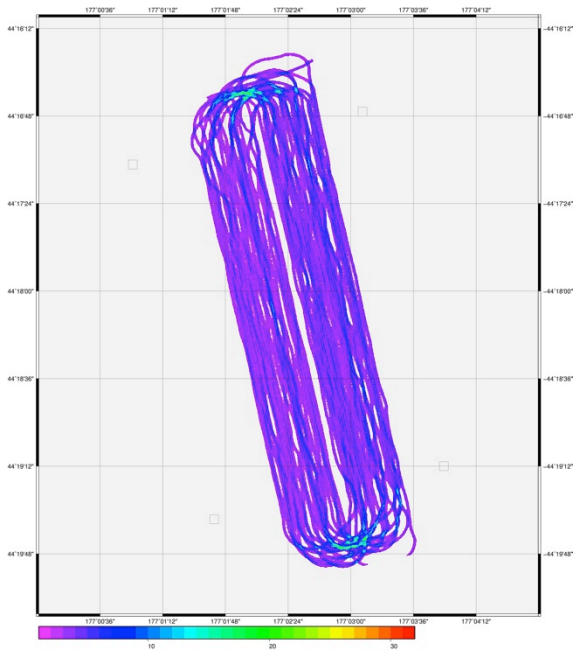

Figure 5.1.1.3. Coverage map from a 3D area. Colours indicate fold on a 3 m by 3 m grid

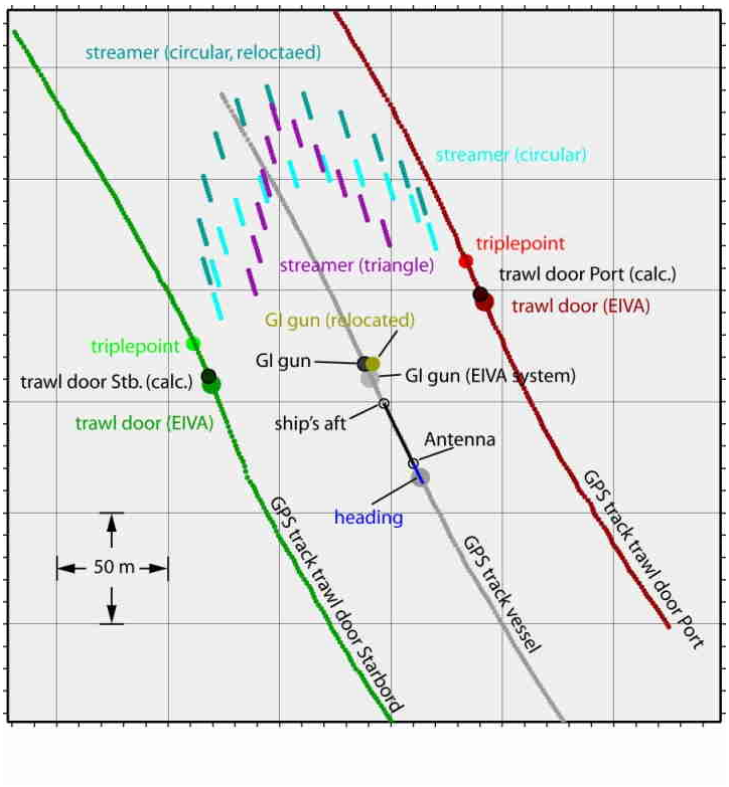

Figure 5.1.1.4. Schematic drawing for the triangulation of the P-Cable streamers and the airgun (EIVA system was notused during SO226)

5.1.2. Simrad EM-120 Multibeam

5.1.2.1. Data Acquisition

The RV SONNE is equipped with the SIMRAD EM 120 multi-beam echo sounder (Kongsberg) for continuous mapping of the seafloor. The SIMRAD EM 120 echo sounder system consists of several units; A transmit (TX) and a receive (RX) transducer array in a fixed mills cross configuration below the keel of the vessel, the deck unit contains the preamplifiers for the received signals, the TX/RX unit contains the transmit and receive electronics and processors for beam-forming and control of all parameters with respect to gain, ping, range and swath angle. There are serial interfaces for motion sensor data such as roll, pitch, yaw, and heave, time synchronization, and GPS (no DGPS available during this cruise). Furthermore the system contains a SIS (Seafloor Information System) workstation as an operator station. The operator station processes the collected data, applies all corrections, displays the results and logs the data to internal disks.

The acoustic signal generated by the hull mounted transducer has a main operational frequency around 12 kHz (frequencies in the range of 11.25 to 12.60 kHz are employed to code the different transmit sectors) with a total angular coverage sector of up to 150° (75° per port/starboard side). A single swath is received as 191 beams by the transducer unit through the hydrophones in the receiver unit. The beam spacing can be defined as either equidistant, equiangular, or a combination both. The variation of angular coverage sector and beam pointing angles was set between 50 and 70 degrees, depending on water depth, data quality and coverage requirements to fill survey gaps. During the survey the transmit fan is split into individual sectors with independent active steering according to the current vessels pitch and yaw values. Pitch and roll movements within $^{+}$/- 10 degrees are automatically compensated by the system. Overall, the SIMRAD EM 120 system can map the seafloor with a swath width of up to approximately six times the water depth.

The EM120 data quality is highly dependent upon the signal to noise ratio being influenced by weather conditions, type of the seafloor, interference with other sounders, ship movement, and speed. Combined seismo-acoustic studies were conducted at ship speeds between 3 kn and 4 kn,

dedicated multibeam surveys were run at 6-8 knots, and during transit the survey speed was 10-12 kn.

5.1.2.2. Data Processing

Multibeam data were processed on- and off-board using the MBSystem Software©, Sonar Scope©, Fledermaus© and Hypack/Hysweep©. The raw data were converted to a format compatible with the MBSystem Software for initial editing and processing. This made it possible to edit the data in 2D and 3D using Mbedit and Mbeditviz, respectively. The data were edited to remove spikes and other anomalous soundings. A filter was applied using Mbclean to remove the outermost ten beams from each side of the swath as these were found to be consistently erroneous. Mbgrid was used to create GMT grids of the edited data for export to Fledermaus and creation of GeoTIFF files for use in ArcGIS and seismic analysis in Kingdom Suite. The grids were created using a Gaussian weighted mean algorithm at a grid size according to the local water depth (e.g. 25 x 25 m). A minimum ship speed filter of 3.0 km/h was applied to eliminate any soundings collected at low speed.

Unfortunately, a significant roll offset was identified towards the end of the cruise and some roll calibration lines were run in the fairly flat and shallow working area 3. A first analysis in Mbsystem gives a roll bias of -0.2° (Fig. 5.1.2.1.). Thus, part of the data need to be re-processed in the future because substantial amounts of uncorrected roll-biased data have probably been flagged bad during 3D editing.

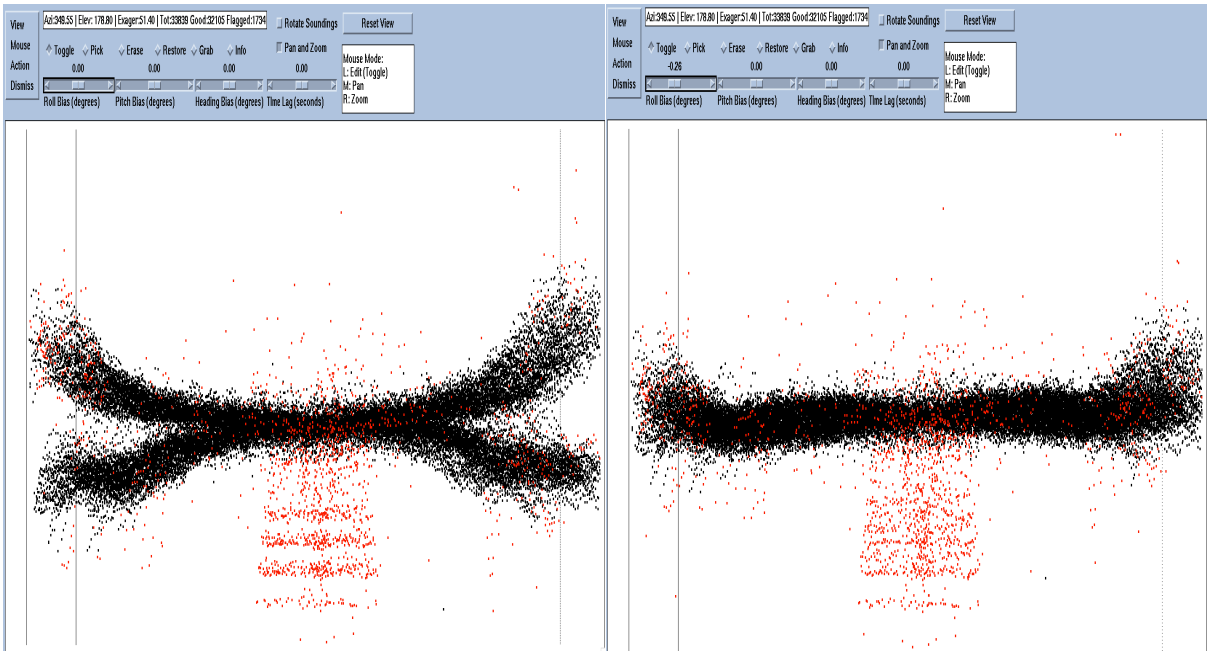

Figure 5.1.2.1. Cross sectional view of two lines run in opposite direction to investigate roll-bias values. Black dots represent accepted soundings, red ones rejected ones. The left picture shows uncorrected data, the right corrected values (-0.2° roll offset)

Another source of significant errors may appear from changes in the sound velocity profiles in the working areas. Fig. 5.1.2.2. represents a residual plot from raw data records at an a priori flat seafloor.

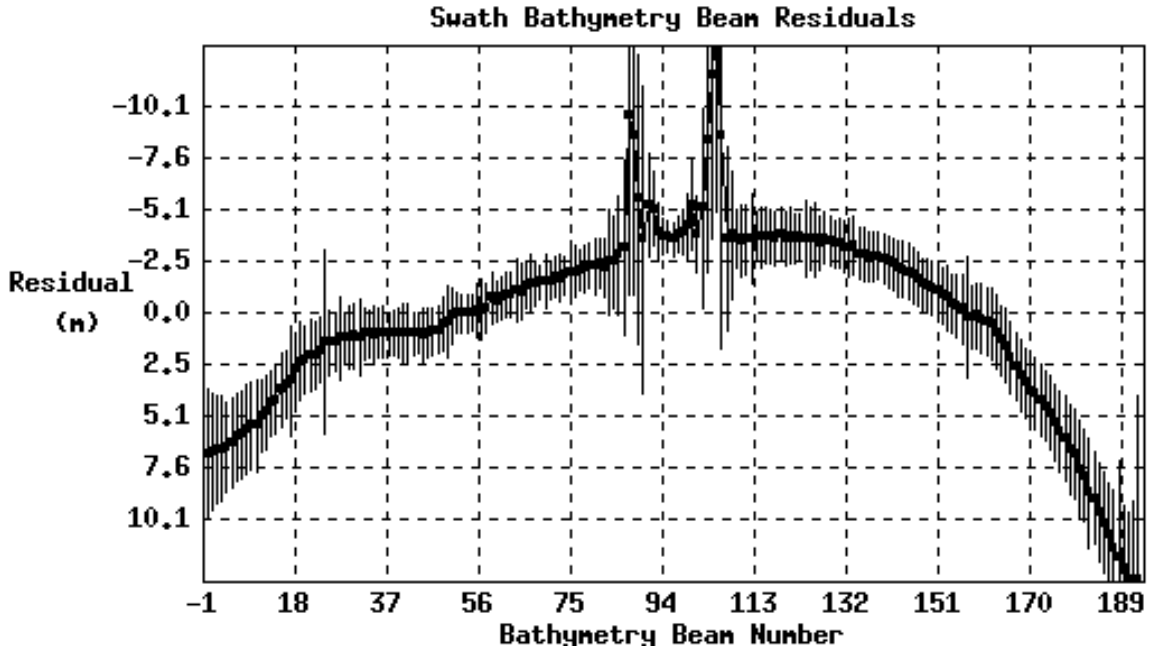

Fig. 5.1.2.2. Residual plot generated with mbvelocitytool demonstrating strong sidelobe artefacts in the centre beams, and odd sound velocity correction offset towards the outer beams, even though the respective CTD profile was gathered just 4 hours before.

In the case of a flat seafloor the residuals will accurately reflect any problems with the water velocity profile. If the water velocity profile was correct, then the residual plot will be roughly flat. In our case quick changes in water velocity profiles seem to have caused a significant depth offset on the outer beam data. A careful review of these data is suggested to figure out which sound velocity profiles have to be used for the bathymetric calculations, because the profiles show a strong tempo-spatial variation in the working areas.

Backscatter data were processed using Sonar Scope and Fledermaus for seafloor classification [Lamarche and Lucieer, 2011] and/or to locate shallow gas deposits [Schneider von Deimling et al. 2013]. The raw data were first pre-processed and the lines were edited to remove any data collected whilst the ship was turning. Only the north-south parallel lines were used in backscatter processing as overlapping lines are problematic in creating mosaics of backscatter data. The selected lines were then cleaned to remove anomalous bathymetry values; cleaning was done with reference to range, depth and across distance histograms. Compensation curves were plotted for each sounding mode to enable correction of the nadir effect. Statistically compensated backscatter mosaics were then created using the compensation curves. Segmentation of the seafloor based on the backscatter mosaics was carried out using the segmentation algorithms developed by Karoui et al. (2009).

For hitherto unknown reasons, the snippet/sidescan datagram shows a lot a gaps in the data gathered during leg-2 (KONGSBERG Sonar Record Viewer). At the same time the bathymetric and beam amplitude values appear correct.

5.1.3. Multibeam (SB3050, 50 kHz) Acoustic water column investigations

5.1.3.1. Acoustic water column imaging

The novel 50 kHz multibeam SB3050 manufactured by L-3 ELAC Nautik GmbH was installed on RV SONNE in the Littleton harbor near Christchurch on February 8th due to its water column imaging (WCI) and recording functionality.

The SB3050 uses a Mills-Cross setup with 50 kHz transmit- and receive-transducers (2°x3°) and was mounted by one diver underneath the moonpool of RV SONNE (Fig. 5.1.3.1.).

Figure 5.1.3.1. Pictures of the SB3050 mounting (left) for later underwater attachment to a pole underneath the forward moonpool of RV SONNE (right) via divers.

In single ping mode one transmission cycle is characterized by the formation of three simultaneously yaw and pitch stabilized transmit-sub fans with subsequent roll-stabilization during receive. The center transmit-sub fan has the frequency F1 slightly different from the respective outer sub fans with frequency F2 to foster reception signal separation. The system covers a maximum of 140° swath width.

In multi ping mode, a second swath is formed also having three transmit sub-fans with frequencies F3 and F4, respectively. 64 reception staves record the incoming echo signals. The transceiver electronic (SEE37) of the SB3050 then performs A/D conversion of the voltage and reception signal processing of the echo time series for further multibeam processing. 4 PCs (one for each frequency F1-F4) perform real-time hybrid time-delay beam forming to generate up to 191 equi-angle beams (or up to 386 equi-distant beams). The beam formed data were processed in the bottom detection algorithm (BDA) and streamed to the "Operator PC" to display and store bathymetric data in the XSE file format and HYPACK/HYSWEEP.

For this new installation on SONNE the reference point was set to the position of the ships MRU projected on to the water line (Fig. 5.1.3.2.)

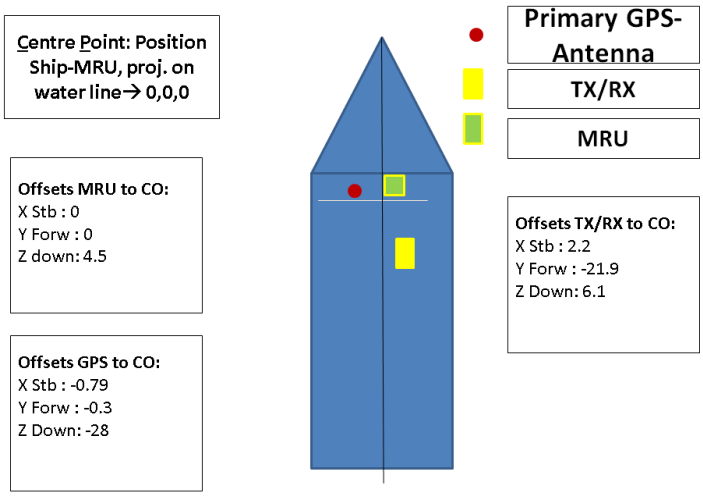

Figure 5.1.3.2. Offsets between MRU, the transducers (TX/RX) and the primary (stbd) GPS-Antenna according to the "left-hand" rule. All offsets relate to the local origin co-ordinate set to the MRU's position projected onto the static water level (Centre Point Position). TX/RX denotes transducer installed underneath the moonpool.

Limited transducer cable length required the systems deck unit to be placed in the "Gesteinssägeraum" on RV SONNE next to the Geolab. From here data was streamed via Gigabit Ethernet to the recording computers in the Geolab.

Besides bathymetric and sidescan data, uncompressed beam formed time series data of each beam were streamed to the "WCI PC" with a maximum sample rate of one half of the pulse length to visualize the water column backscattering data over travel time in each direction. Alternatively, raw stave data (not beam formed) can be recorded by the "WCI PC".

Water column imaging and logging was performed during most surveys with reduced ship speed (2-5 kn) to (1) lower pole-vibration and propeller noise (2) reduce surficial bubble entrainment, and (3) not to lose the spatial coherence of potential rising and current-deflected gas bubbles streams [Schneider von Deimling and Papenberg, 2012]. Multiping mode was chosen for enhanced coverage and the pulse length was preferentially set between 1-10 ms. Depending on the water depth, the transmission source level was either reduced to a power of -20dB or 0dB and the reception gain and TVG were correspondingly adapted to visualize features in the water column. The water column data were streamed over a gigabit-ethernet controller to the WCI computer and stored on a raid 0 system connected via E-SATA for enhanced performance. Even though fast gigabit-ethernet was used for data streaming, the high data rate of ~20MB/s caused significant time latency between echo reception and WCI echogram visualization of approximately 10 seconds. However, this delay had no implication on the total data storage and investigations during postprocessing.

5.1.3.2. Positioning, motion data

For accurate positioning and ship movement corrections the ships DGPS system and motion data (TSS1) from the shipborn MRU5 were connected to the multibeam electronic and the sonar control PC via Hypack/Hysweep (Fig. 5.1.3.2.). Good satellite coverage was given during any course and time. To correct the refraction of the sonar signal on its way through the water column sound velocity profiles were gathered with profiling CTD measurements. To assign the depth measurement to a geographic position, the GPS navigation of the Ashtech MD-XII GPS system was used. The water resistant IXSEA Octans 3000 was permanently installed in the moonpool as a MRU backup system (data logged for later postprocessing) as well as for accurate heading information, because a data string problem between the ship's gyro and the SB3050 (NMEA HEHDT) required the heading to be used from the Octans. Because the Octans currently provides only one digital output the TTS motion data were taken from the MRU5. The GPS reference ellipsoid was set to WGS84.

5.1.3.3. Postprocessing

Water column imaging (WCI) data were streamed via Gigabit Ethernet to a raid system in order to cope with the high data rates of ~1GB per Minute. Besides online inspection with the WCIViewer developed by our SUGAR partner L-3 ELAC Nautik System, the data were converted via the GEOMAR in house conversion tool "wci2gwc" run on LINUX 64bit to generate QPS-IVS GWC file format with a downsampling factor of 16. This allowed echogram visualization of the data in the latest FMMidwater 7.3.3 version several hours after recording. The full water column traces (not downsampled) were converted on batch for data evaluation after the cruise.

5.1.4 PARASOUND

RV SONNE embraces a hull-mounted parametric sub-bottom profiler Atlas Hydrographic PARASOUND P70 that was operated to provide high-resolution data with up to 150m penetration. In addition it was used for flare imaging. The system was operated in a 24-hour schedule. PARASOUND P70 works as a parametric sounder providing narrow beam sediment echo sounder, providing primary frequencies of 18 (PHF) and adjustable 18.5 – 28 kHz, thus generating parametric secondary frequencies in the range of 0.5 – 10 kHz (SLF) and 36.5 – 48 kHz (SHF) respectively. The secondary frequencies develop through nonlinear acoustic interaction of the primary waves at high signal amplitudes. This interaction occurs in the emission cone of the high-frequency primary signals which is limited to an aperture angle of 4° for the PARASOUND P70. This narrow aperture angles

is achieved by using an array of 128 transducers on a rectangular plate of approximately 1 m² surface area. Therefore the footprint size is 7% of the water depth and vertical and lateral resolution is significantly improved compared to conventional 3.5 kHz echo sounder systems. The system provides features like recording of the 18 kHz primary signal and both secondary frequencies, continuous recording of the whole water column, beam steering, different types of source signals (continuous wave, chirp, barker coded) and signal shaping. Digitization takes place at 96 kHz to provide sufficient sampling rates for the high secondary frequency. A down-mixing algorithm in the frequency domain is used to reduce the amount of data and allow data distribution over Ethernet.

For the standard operation a parametric frequency of 4 kHz and a sinusoidal source wavelet of 2 periods was chosen to provide a good balance between signal penetration and vertical resolution. The 18 kHz signal was also recorded permanently. As recent problems with the single pulse mode were known by the vessel's staff, the system was used in the quasi-equidistant mode during the cruise. Therefore all flare imaging tasks were realized in the quasi-equidistant mode, too.

Unfortunately, technical problems occurred especially during the first days of the cruise. The system was crashing at least 5 times a day, which lead to a loss of data.

Nevertheless the data gaps rarely exceeded some minutes and the overall data quality and penetration were very good. After consulting Atlas Hydrographic, some of the system's hardware were replaced. Once this malfunction was solved, the system worked reliable throughout SO226-1 and no complications occurred during the SO226-2.

All recorded raw data were stored in the ASD data format (Atlas Hydrographic), which contains the data of the full water column of each ping as well as the full set of system parameters and signal amplitude and phase. In addition, a 400 m-long reception window centred on the seafloor was recorded in the compressed PS3 data format after mixing the signal back to a final sampling rate of 24 bit. This format is in wide usage in the PARASOUND user community and the limited reception window provides a detailed view on the sub-bottom structures.

All data of the first leg were converted to SEG-Y format during the cruise using the software package ps32sgy (Hanno Keil, University Bremen). The software allows generation of one SEG-Y file for longer time periods, by converting and compiling ps3 data. If seismic data were collected simultaneously, one SEG-Y file was created for the length of each seismic profile. Especially during the 3d seismic acquisition using the P-Cable system, PHF and SLF profiles were stored according to seismic profiles. In all other cases ca. 2h-long profile slices were generated (e.g. during transit, bathymetry surveys). The PARASOUND data were loaded into the seismic interpretation software HIS Kingdom. This approach allowed us to obtain a first impression of sea floor morphology variations, sediment coverage and sedimentation patterns along the ship's track.

5.1.5 CTD

Conductivity, temperature and depth (CTD) data were gathered using the SBE 99plus CTD system. The true speed of sound in the water column was derived from the CTD cast after Delgrosso. As for Multibeam calibration only the sound velocity file was needed, no further work was carried out with the collected data.

Sound velocity profiles were gathered by CTD downcasts carried by a rosette water sampler unit and/or attached to the OFOS. The respective sound velocity profiles were derived from the CTD measurements (DelGrosso) and loaded into SIS to automatically correct for attenuation and sound refractions effects in the water column.

5.1.6. OFOS/OFOP

The Ocean Floor Observing System (OFOS) imaging system was used to characterize the faunal communities living on the surface of the seafloor across each of the three main survey areas. Unfortunately, due to technical difficulties, only high resolution video data were acquired (i.e., no still

photographs). A CTD and Contros methane sensors were also interfaced with the OFOS during these deployments. The Ocean Floor Observation Protocol (OFOP), developed by Dr. Jens Greinert (GEOMAR, Germany), was used for logging observed features on the seafloor (biological and geological).

Figure 5.1.6.1. The Ocean Floor Observing System (OFOS) imaging system onboard RV Sonne (Image from the worldwide web – Google Image search).

A total of three transects were run: a 6.5 hour continuous transect across one of the large "pockmark" features in the northeast of Area 1 (Station 55), a 4 hour transect across Area 2 and a 5 hour deployment over the small "pockmarks" in Area 3.

5.2. Geophysical Instrumentation

5.2.1. GI-gun

For the high-resolution seismic acquisition a GI-gun manufactured by Sercel Marine Sources Division was used. The compressed air was supplied by the super charger of R/V SONNE with a pressure of 210 bar. The GI-gun was attached with chains to a steel frame and towed either from the centre or at the starboard side at 20 m behind the stern in a depth of 2 m (Fig. 5.1.1.1.). The setup with the floatation is shown in Fig. 5.2.1.

Along the first profiles the gun was operated with a volume of 3.8 l (105 cinch generator chamber, 105 cinch injector chamber) as it was known for a well balanced ratio of depth penetration and frequency content of the source signal. The profiles were acquired with a shot interval of 5s during 3D or 7s during 2D survey. The injector was fired at a delay of 63 ms. Additional profiles were used to test a smaller volume of 1.6 l (45 / 45 cinch; injector 40 ms). It turned out that sediment conditions were favourable enough to allow a depth penetration of the gun equivalent to the larger volume. A minor loss in energy appeared with late time arrivals. It could easily be compensated by the increased fold, resulting from the shorter shot interval of 3 s. Further for the 2D seismic profiles and the second 3D cube similar conditions could be confirmed and the gun was used to the benefit of higher resolution at shallow sediment layers.

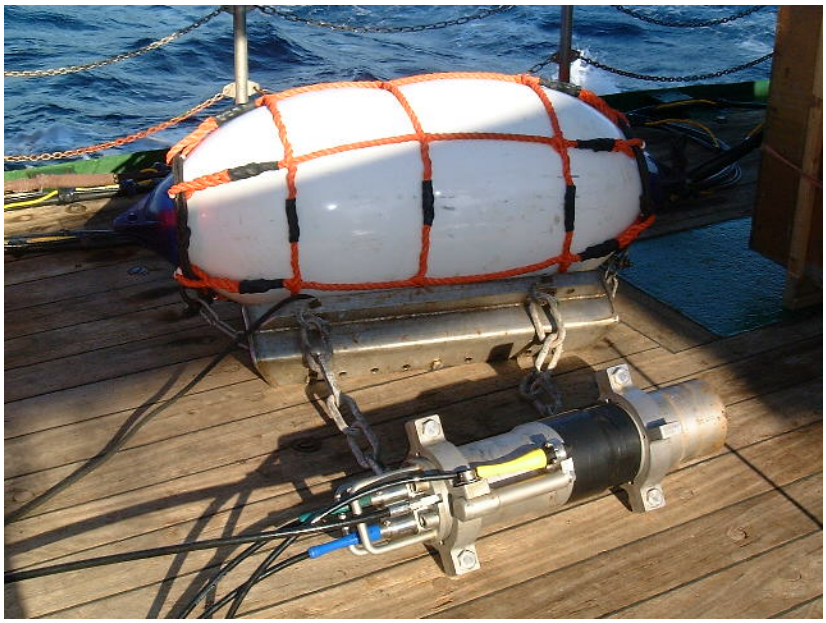

Figure 5.2.1. GI-gun mounted below the carrier to which a Polyform floatation is attached.

5.2.2. External trigger during SO226-1

With the development of the 3-D P-Cable system GEOMAR has build its own GPS based trigger system. The shipboard GPS receiver delivers ZDA and PPS to a timing box. The timing box allows selecting the shot interval by a wheel switch in full second intervals. The TTL trigger pulse is delivered to a distribution box, from which the LongShot gun controller and the Geometrics streamer system receive the signal. Together with the trigger generation a time stamp is written to an internal SD memory card with shot coordinates.

To ensure all systems trigger with the same reference all trigger circuits were adjusted to work on the uprising flank (TTL+). The LongShot gun controller was set to a 40 ms aim point and adjusted later to 50 ms aim point. The automatic adjustment based on the received shot signal from the gun hydrophone usually was within +/- 1 ms.

5.2.3. P-Cable

The P-Cable (VBPR patent of 2003) system design is designed to high resolution imaging of shallow horizons. GEOMAR is holding an academic license of the P-Cable system covering development and application of such a system.

Compared to standard reflection seismic applications in 2-D and 3-D the basic difference is that the P-Cable is build by a cross cable towed perpendicular to the ships heading (Fig. 5.2.3.1.). Instead of a few single streamers the P-Cable uses a large number of short streamer sections towed parallel from the cross cable. Drawback is the limited depth penetration due to the short receiver offsets, which are not favourable for the removal of the multiple energy. This is well compensated by the reduced costs of the system and the ability to operate it even from small multi purpose vessels, the usual academic platform for marine research.

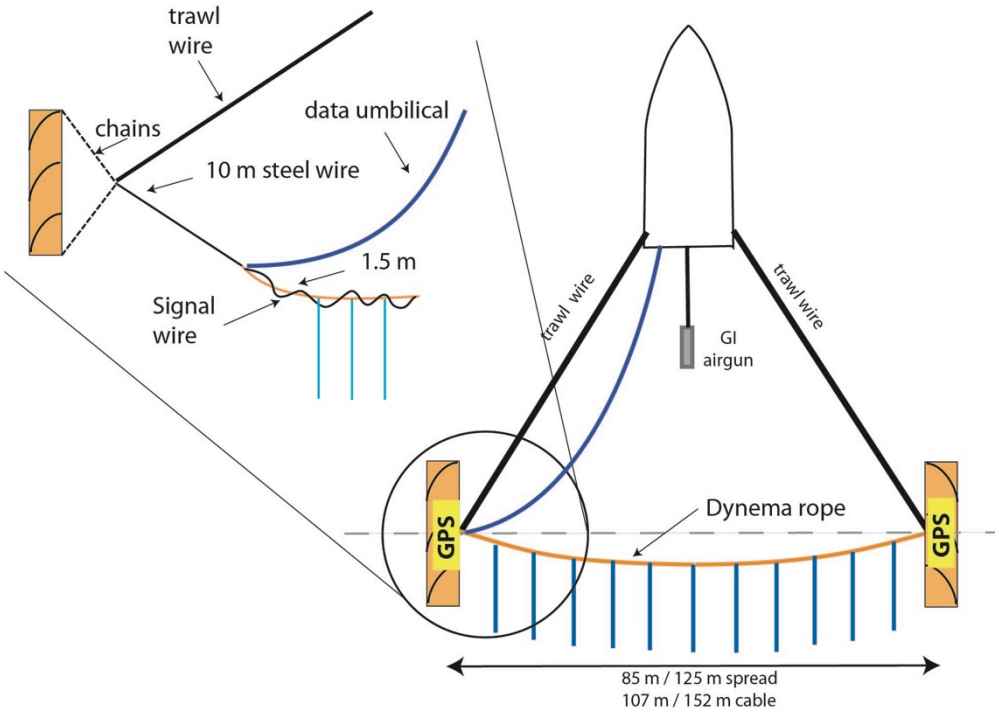

Figure 5.2.3.1. Drawing of the P-Cable design applied during the SO-226 cruise

Fig. 5.2.3.1. shows the basic principle of the P-Cable design. The advantages of the GEOMAR development are two fold. The cross cable is based on a strength member, a Dynema rope, which takes the stretch forces of the trawl doors (Fig. 5.2.3.2.). Attached to this rope is the data cable with the streamer connections (Fig. 5.2.3.3.). The cross cable is stretched by two trawl doors, floating at the sea surface. GEOMAR developed a modular cross cable, which allows exchange of each single streamer connector (node) in case of a malfunction. This allows easy service and reduced service costs. As well the modular design allows to insert connecting cables of different length between the nodes. Floats attached to each break out help to keep the streamers at 2 m depth (Fig. 5.2.3.4.). The current grade of the system provides 10 active nodes connected either by 14 m or 9 m long data cables. On both sides the first node is located 11.5 m off the triple point, the connection of trawl wire, cross cable and trawl door. Each one of the trawl doors provides a lifting force of 2 tons. In order to ensure a continuous inline coverage the maximum shot rate of the gun (5 s / 3 s) requires a maximum speed of 3 kn or 3.5 kn.

Upon deployment the door next to the umbilical is released from its rest position (Fig. 5.2.3.5.) while the ship sails at 1.5 kn through water against wind and waves. The door is lowered into the water while a 10 m long lead cable between door and connection point of cross cable is kept on board. Next the data cable from the recording device to the door is hooked to the connection between lead wire and cross cable. Now trawl wire, data cable and cross cable are paid out simultaneously (Fig. 5.2.3.5.). At the same time streamer sections are connected to the nodes of the cross cable. Floats are fixed to each node in order to keep the cross cable at even depth (Fig. 5.2.3.4.). When the entire cross cable is payed out a support rope on the support winch is used for secure transmit of the cross cable from the support winch to the lead wire of the second trawl door (Fig. 5.2.3.5.). Now both trawl wires are given out until the final length with sufficient stretch of the trawl doors is reached (Fig. 5.2.3.5.).

Figure 5.2.3.2. Photographs of the trawl doors. Left: trawl door preparation on board. Top right: trawl doors in rest position at the aft of RV SONNE. Bottom right: trawl door in operation (photos courtesy F. Gross)

Figure 5.2.3.4. Floats are fixed on the cross cable in order to keep it at about 2 m depth during profiling. Top left: cross cable on winch with break out in front. Top right: droplead and streamer connected to break out. Bottom left: floats compensate weight of the break out. Bottom right: cross cable deployment

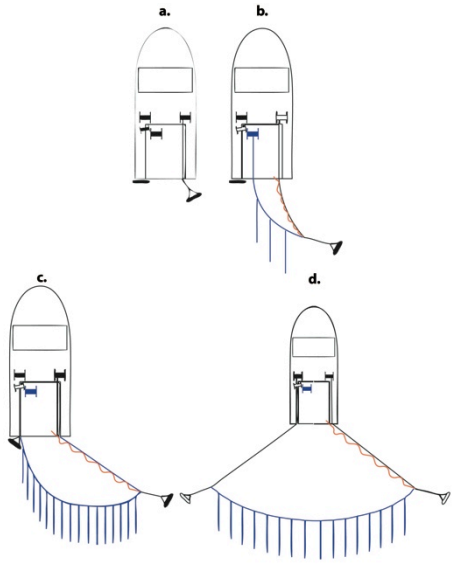

Figure 5.2.3.5. Drawing illustrating the steps during deployment

5.2.4 OBS-Instrumentation

A total of 19 ocean bottom seismometers (OBS) were available for the SO226 CHRIMP cruise. Altogether 50 sites were deployed to complement the seismic 2D and 3D streamer and P-cable measurement. The principle design of the GEOMAR-OBS is described in detail by Flueh and Bialas (1996). Two types of OBS were used:

5.2.4.1. The GEOMAR three-leg Ocean Bottom Seismometers:

The system components are mounted on a steel tube, which holds the buoyancy body on its top. The buoyancy body is made of syntactic foam and is rated, as are all other components of the system, for a water depth of 6000 m. Attached to the buoyant body are a radio beacon, a flash light, a flag and a swimming line for retrieving from aboard the vessel. The release transponder for the acoustic release is also mounted here. The sensors are an E-2PD hydrophone from OAS Inc., or a HTI-01-PCA hydrophone from HIGH TECH, and a three-component seismometer (KUM). The seismometer is only connected via a cable to the OBS and stands free on the seafloor after it was released from the OBS frame. As recording devices broadband seismocorders (MBS) of SEND GmbH were used, which are contained in their own pressure tubes. The recording sampling rate was chosen with 1000 Hz.

5.2.4.2. The GEOMAR Ocean Bottom Seismometer 2002 (OBS-2002):

This is a newer design based on experiences gained with three-leg GEOMAR Ocean Bottom Seismometer [OBS, Bialas and Flueh, 1999]. Fig. 5.2.4.1. shows the basic system. It is constructed to carry a hydrophone and a small seismometer for higher frequency active seismic profiling. However, due to the modular design of the front end it can be adapted to different seismometers and hydrophones or pressure sensors.

The sensitive seismometer is deployed between the anchor and the OBS frame, which allows good coupling with the sea floor. The three component seismometer (KUM), usually used for active seismic profiling, is housed in a titanium tube, modified from a package built by Tim Owen (Cam-

bridge) earlier. Geophones of 4.5 Hz natural frequency were used during SO-226. While deployed to the sea floor the entire system rests horizontally on the anchor frame. After releasing its anchor weight the instrument turns 90° into the vertical and ascends to the surface with the floatation on top. This ensures a maximally reduced system height and water current sensibility at the ground (during measurement). On the other hand the sensors are well protected against damage during recovery and the transponder is kept under water, allowing permanent ranging, while the instrument floats at the surface.

During cruise SO226 on RV SONNE tests on the position of the geophone were performed. One instrument was deployed for several times with two geophones and one hydrophone. One geophone was attached as described and seen on the picture. The second geophone was attached to an arm, thus, the geophone can stand free on the seafloor when released (Fig. 5.2.4.2.).

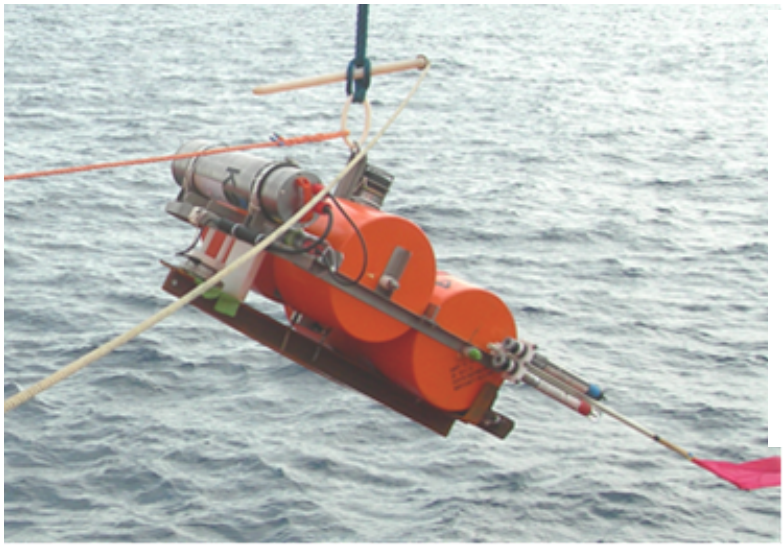

Figure 5.2.4.1. GEOMAR Ocean Bottom Seismometer (OBS-2002) before deployment.

Figure 5.2.4.2. Modified OBS-2002 with an extra geophone.

5.2.4.3. Recording and processing of OBS-Data

Figure 5.2.4.3. Three-leg GEOMAR Ocean Bottom Seismometer. Geophone will be release from the arm when standing on the seafloor.

The so-called Marine Broadband Seismic recorder [MBS; Bialas and Flueh, 1999], manufactured by SEND GmbH, was developed based upon experience with the DAT-based recording unit Methusalem [Flueh and Bialas, 1996] over previous years. This recorder involves no mechanically driven recording media, and the PCMCIA technology enables static flash memory cards to be used as non-powered storage media. Read/write errors due to failure in tape handling operations should not occur with this system. In addition, a data compression algorithm is implemented to increase data capacity. Redesign of the electronic layout enables decreased power consumption (1.5 W) of about 25% compared to the Methusalem system. Depending on the sampling rate, data output could be in 16 to 18 bit signed data. Based on digital decimation filtering, the system was developed to serve a variety of seismic recording requirements. Therefore, the bandwidth reaches from 0.1 Hz for seismological observations to the 50 Hz range for refraction seismic experiments and up to 10 kHz for high resolution seismic surveys. The basic system is adapted to the required frequency range by setting up the appropriate analogue front module. Alternatively, 1, 2, 3 or 4 analogue input channels may be processed.

The instrument can be parameterised and programmed via a RS232 interface. The time base is based on a DTCXO with a 0.05 ppm accuracy over temperature. Setting and synchronising the time as well as monitoring the drift is carried out automatically by synchronisation signals (DCF77 format) from a GPS-based coded time signal generator. Clock synchronisation and drift are checked after recovery and compared with the original GPS units. After software pre-amplification the signals are low-pass filtered using a 5-pole Bessel filter with a -3 dB corner frequency of 10 kHz. Then each channel is digitised using a sigma-delta A/D converter at a resolution of 22 bits producing 32-bit signed digital data. After delta modulation and Huffman coding the samples are saved on PCMCIA storage cards together with timing information. Up to 4 storage cards may be used. Data compression allows increase of this capacity. Recently, technical specifications of microdrives (disk drives of PCMCIA type II technology) have been modified to operate below 10° C, therefore 2 GB drives are now available for data storage. After recording, playback of the data is done by copying the flashcards to a PC workstation. During this transcription the data are decompressed and formatted according to the PASSCAL data scheme. This enables full compatibility with the established processing system and it can be easily transformed into standard seismological data formats.

A standard pre-processing of the active source seismic data was done following GEOMAR standard procedures. Raw data were first processed with software from the manufacturer of the seismic recorders (SEND GmbH) and internal time slips, etc. were corrected. Data were than stored in PASSCAL format. Later, dat2segy program was used to cut out shots by cutting the single SEG-Y trace (the ref2segy output) into traces with a defined time length based on the geometry and shooting time information in the ukooa file. In addition, a time offset of the trace and a reduction velocity was set (to determine the time of the first sample within a record). Also the clock drift of the recorder (skew) is taken into account and corrected for. The final SEG-Y format consists of the file

header followed by the traces. Each trace is built up by a trace header followed by the data samples. The output of the dat2segy program can be used as input for further processing for example using Seismic Unix (SU).

5.3. Sidescan sonar

High-resolution backscatter information of pockmark structures offshore New Zealand was to be obtained using the DTS-1 sidescan sonar system (Fig. 5.3.1.) operated by GEOMAR. The DTS-1 sidescan sonar is a dual-frequency, chirp sidescan sonar (EdgeTech Full-Spectrum) working with 75 and 410 kHz centre frequencies. The 410 kHz sidescan sonar emits a pulse of 40 kHz bandwidth and 2.4 ms duration (giving a range resolution of 1.8 cm), and the 75 kHz sidescan sonar provides a choice between two pulses of 7.5 and 2 kHz bandwidth and 14 and 50 ms pulse length, respectively. They provide a maximum across-track resolution of 10 cm. With typical towing speeds of 2.5 to 3.0 kn and a range of 750 m for the 75 kHz sidescan sonar, maximum along-track resolution is on the order of 1.3 metres. In addition to the sidescan sonar sensors, the DTS-1 contains a 2-16 kHz chirp subbottom profiler providing a choice of three different pulses of 20 ms pulse length each. The 2-10 kHz, 2-12 kHz or 2-15 kHz pulse gives a nominal vertical resolution between 6 and 10 cm. The sidescan sonar and the subbottom profiler can be run with different trigger modes, internal, external, coupled and gated triggers. Coupled and gated trigger modes also allow specifying trigger delays. The sonar electronics provide four serial ports (RS232) to attach up to four additional sensors. One of these ports is used for a Honeywell attitude sensor providing information on heading, roll and pitch and a second port is used for a Sea&Sun pressure sensor. Finally, there is the possibility of recording data directly in the underwater unit through a mass-storage option with a total storage capacity of 30 GByte (plus 30 Gbyte emergency backup).

The sonar electronic is housed in a titanium pressure vessel mounted on a towfish of 2.8 m x 0.8 m x 0.9 m in dimension (Fig. 5.3.1.). The towfish houses a second titanium pressure vessel containing the underwater part of the telemetry system (SEND DSC-Link). In addition, a releaser capable to work with the USBL positioning system POSIDONIA (IXSEA-OCEANO) with separate receiver head, and an emergency flash and radio beacon (NOVATECH) are included in the towfish. The towfish is also equipped with a deflector at the rear in order to reduce negative pitch of the towfish due to the weight of the depressor and buoyancy of the towfish.

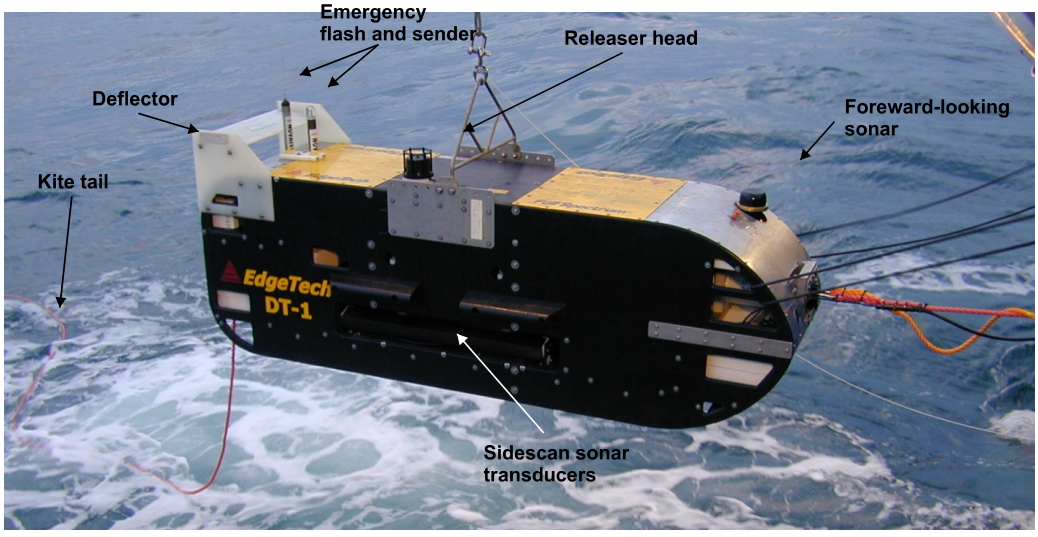

Figure 5.3.1. A picture of the DTS-1 sidescan sonar towfish. The forward-looking sonar is no longer mounted.

The towfish is connected to the sea cable via the depressor through a 45-m long umbilical cable (Fig. 5.3.2.). The umbilical cable is tied to a buoyant rope that takes up the actual towing forces. An

additional rope has been taped to the buoyant rope and serves to pull in the instrument during recovery.

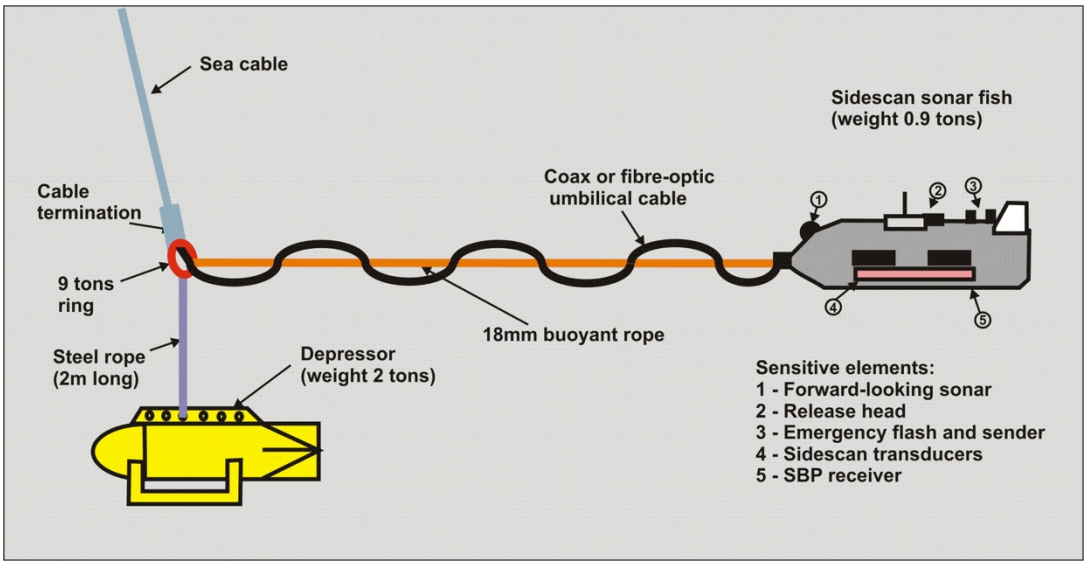

Figure 5.3.2. The DTS-1 towing configuration.

The main operations of the DTS-1 sidescan sonar are run using HydroStar Online, the multibeam bathymetry software developed by ELAC Nautik GmbH and adapted to the acquisition of EdgeTech sidescan sonar data. This software package allows onscreen presentation of the data, of the tow fish's attitude, and the tow fish's navigation when connected to the POSIDONIA USBL positioning system. It also allows setting the main parameters of the sonar electronics, such as selected pulse, range, power output, gain, ping rate, and range of registered data. HydroStar Online also allows activating data storage either in XSE-format on the HydroStar Online PC or in JSF-format underwater on the full-spectrum deep-water unit FS-DW. Simultaneous storage in both XSE and JSF-formats is also possible. Accessing the underwater electronics directly via the surface full-spectrum interface-unit FS-IU and modifying the sonar.ini file of the FS-DW allows changing additional settings such as trigger mode. The FS-IU also runs JStar, a diagnostic software tool that also allows running some basic data acquisition and data display functions. HydroStar Online creates a new XSE-file when a file size of 25 MB is reached, while a new JSF-file is created every 40 MB. How fast this file size is reached depends on the amount of data generated, which depends on the use or not use of the high-frequency (410 kHz) sidescan sonar. The amount of data generated is also a function of the sidescan sonar and subbottom pulses and of the data window that is specified in the initialisation file (sonar.ini) on the FS-DW. The data window specifies the range over which data are sampled.

The subbottom profiler data have to be corrected for varying water depths in which the towfish is flying. These corrections are based on depth information provided by the pressure sensor mounted on the towfish and have been carried out with in-house processing scripts based on GMT and Seismic Unix software packages.

5.4. Geologic Instrumentation

5.4.1. Piston Corer

The following description provides an overview of piston coring installation and operations. Piston coring required cable termination. An Electroline ME200 termination was used and tested on deck for a 10,000 pound pull. Re-termination was conducted twice while at sea, after losing a piston corer and after kinking the cable during retrieval operation

Figure 5.4.1.1. Cable termination on the ship coaxial cable for piston coring lead by Ross Downer (Milbar-Hydrotest Inc.)

Piston Coring was conducted using a 3100 head weight with a changeable pipe assembly for 6 and 9 meters cores. Barrel used were N90 high strength alloy to prevented bending barrels on deployment. This material allows a 45° bend before breaking. Core sleeves were 2- 7/8 inches wide and 9 ft long. Trigger arm was equipped with a 150 lb weight and set for a 12 ft drop. The 9 m barrels were used for the majority of the deployments. Where sediment composition was found to be hard with multi-coring 6 m barrels were deployed.

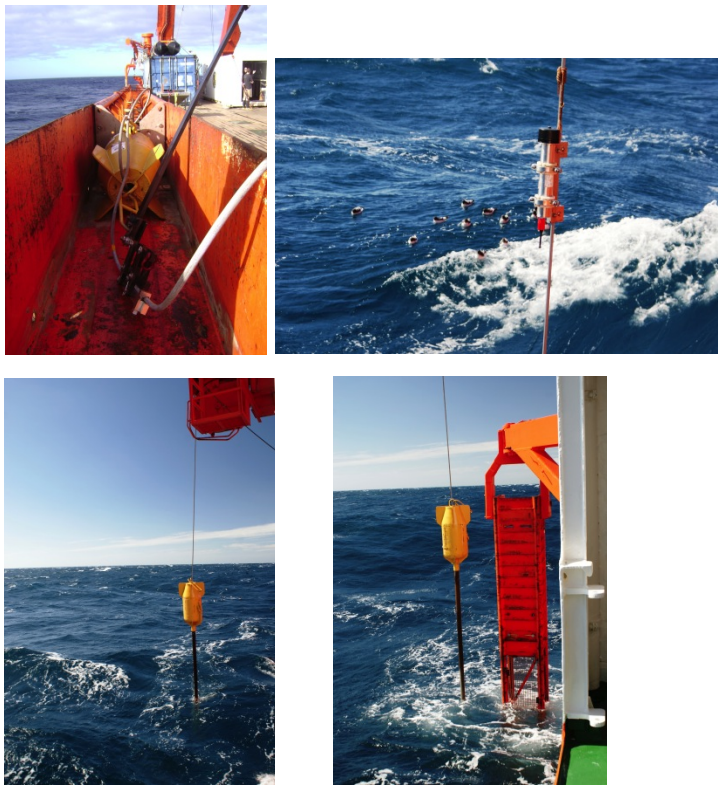

Figure 5.4.1.2. Piston coring conducted of the starboard delivery platform. Core location was determined with a wire mounted transponder

5.4.2. Multi Corer

A 4 or 8 Ocean Instruments deep-ocean multi-corer (MC-800), with 10 cm diameter core tubes, was provide by NIWA (Fig. 5.4.1.3). It was used to sample near and at surface sediments and infaunal communities. The samples will be used for measurement of radiocarbon in organic and inorganic sediment for paleogeochemical flux relative to thorium and lead for current day sedimentation.Multi-corer samples were taken at representative sites within and around the targeted "pock-mark" sea-floor features. Sampling locations were guided by the 2-D and PARASOUND seismic reflection data collected on Leg 1, and side-scan sonar and sea-floor video data collected on Leg 2. Most of the multi-corer sample sites were co-located with the piston corer deployment sites.

Figure 5.4.1.3. Multi-coring deployment was provided by NIWA. Cores obtained were used to assess shallow sediment radiocarbon and thorium and lead samples for assessment of the paleo-geochemical record of vertical CH_4 fluxes relative to modern day sedimentation.

5.4.3. On board Laboratory

An on board laboratory was used to assess porewater geochemical profiles in shallow sediment cores to locate areas with methane vertical diffusion or advection. Analyses focus on porewater concentration of sulfate, chloride, dissolved inorganic carbon (DIC) and sediment methane (CH_4).

5.4.3.1. Gas-Chromatograph

Figure 5.4.3.1. Methane concentrations were determined from 3-ml sediment plugs using headspace techniques and were quantified against certified gas standards (Scott Gas, Plumbsteadville PA). Headspace analysis was performed on board using a GC-FID Shimadzu GC-14A gas chromatograph equipped with a Hayesep 0.80/100 column. Methane concentrations are presented in millimolar units (mM).

5.4.3.2. Ion-Chromatograph

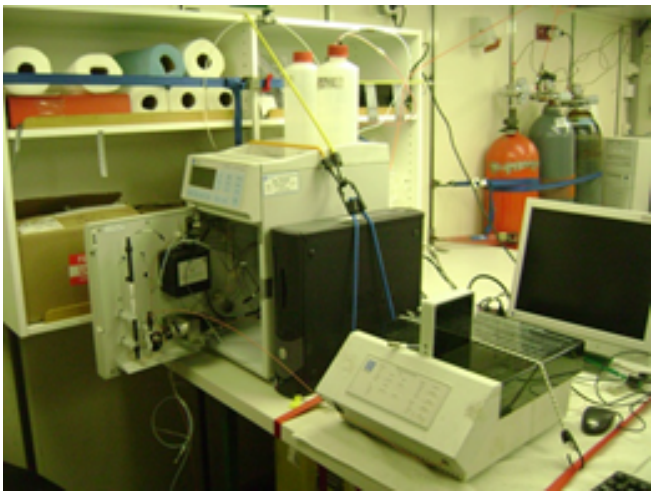

Figure 5.4.3.2. Porewater sulfate and chloride concentrations were measured with a Dionex DX-120 ion chromatograph equipped with an AS-9HC column. Samples were diluted 1:50 (vol/vol) prior to analysis and measured against a 1:50 diluted IAPSO standard seawater (28.9 mM SO_4^{-2}, 559 mM Cl^-). Sulfate and chloride are presented in millimolar units (mM). Limits of detection are <0.1 mM

5.4.3.3.Coulometer

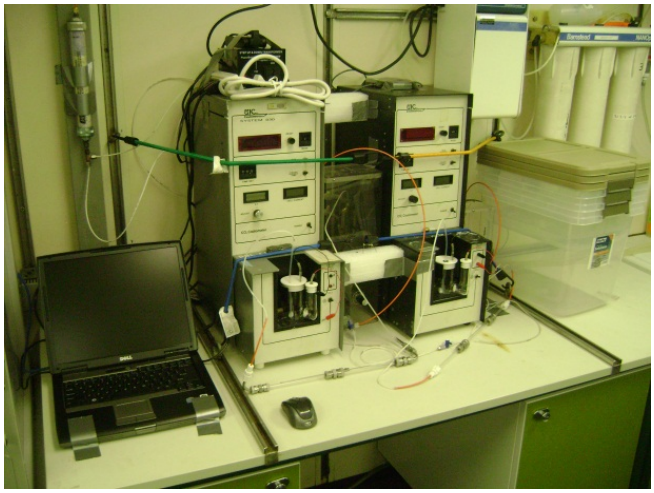

Figure 5.4.3.3. Pore water dissolved inorganic carbon (DIC) concentrations were measured using a UIC coulometer and standardized against a certified reference material (CRM, Batch 58). DIC concentrations are presented in millimolar units (mM)

5.4.3.4. Radiocarbon Natural Abundance Analysis

To conduct analyses of sediment samples for radiocarbon natural abundance is was necessary to determine levels of radiocarbon background present in the work areas. This survey was conducted in different shipboard laboratories and the NRL portable lab van. Ashed Whatmann GF-F filters were soaked in propanol and areas around a meter square were swiped at different well traveled/active locations. At the GNS radioisotope laboratory filters were folded up and placed in combustion tube with carrier after drying in vacuum oven. CO_2 was generated by sealed tube combustion tube. Sample processing and data presentation was conducted according to Stuiver and Polach (1977). The blank corrected fraction modern was normalized to $\delta^{13}C$ of -25‰ defined by Donahue et al. (1990).

5.4.3.5. Geochemical investigations in sediments

Parameters for the porewater data include methane, sulfate, chloride, sulfide, and dissolved inorganic carbon concentration and stable carbon isotope ratio. Porewater geochemical data are plotted for comparison of methane and sulfate concentrations to assess the varying degrees of vertical methane fluxes and resulting methane oxidation [Borowski et al., 1999]. Anaerobic oxidation of methane occurs as:

$$CH_4 + SO_4^{2-} \rightarrow HCO_3^- + HS^- + H_2O$$

in sediment depths where vertical flow of deep sediment methane and sediment surface sulfate converge. This analysis is used to estimate the presence of methane deep in the sediments that could be concentrated in hydrate beds. DIC is added in these plots to support the interpretation of methane oxidation and sulfide is incorporated for comparison with sulfate reduction. Stable carbon isotope analysis of the DIC provides additional interpretation of methane oxidation and contribution to the DIC. In addition radiocarbon isotope analysis and uranium series nuclides will be used to characterize the sedimentary environment age on the Chatham Rise. More specifically, 230Th (t½ = 75,380 y), 210Pb (t½ = 22.3 y) and 231Pa (t½ = 32,760 y) will be used to calculate sediment accumulation rates, determine age of sediment and distinguish changes in sediment chemistry related to glacial-interglacial cycles. These data will be coupled with other geochemical parameters and seismic profiles to determine the timing of pockmark formation and present-day fluxes of sediment CH4.

5.5. CONTROS CH_4 Sensors

A methane concentration and a methane sniffing device have been used in the water column to detect elevated dissolved methane concentration as potential indications for active methane seepage. Two types of CONTROS sensors were used. The one operates optically by a non-dispersive spectrometric infrared method (HISEM) and the other with resistant changes caused by a reactive semiconductor gas sensor (Sniffer). Methane gas molecules diffuse into the sensors through a patented thin-film composite silicone membrane. A pump is connected to the sensor in order to assure a constant flow regime. For measuring the partial pressure of methane infrared absorption in a 100mm cuvette is determined. Electrical resistivity changes of the metal oxide is measured within the Sniffer. Temperature, pressure and humidity were measured for later correction calculations and all data were transferred to an autonomous data logger. The sensors are "plug and play" capable units and are controlled from software designed by CONTROS Systems & Solutions Ltd.

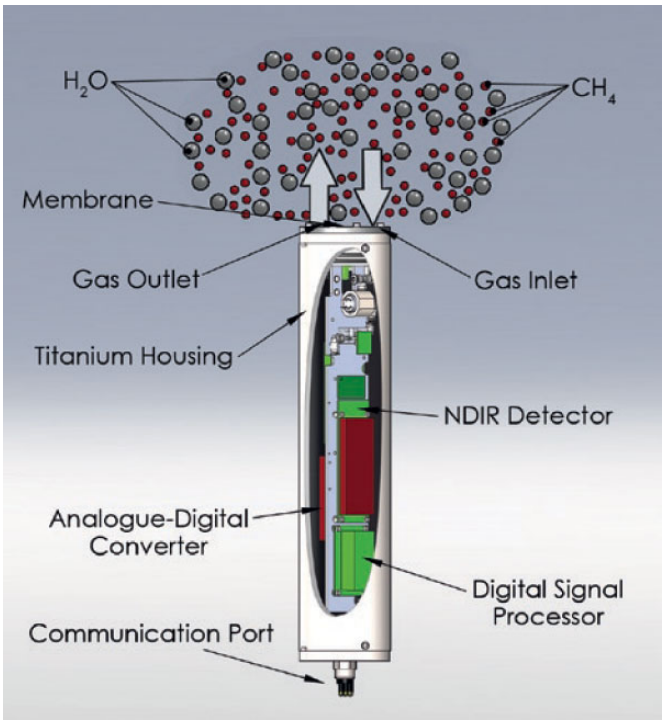

Figure 5.5.1. Principle HISEM CH4

5.6 The Maritime Aerosol Network

The Maritime Aerosol Network (MAN) component of AERONET provides ship-borne aerosol optical depth measurements from the Microtops II sun photometers. These data provide an alternative to observations from islands as well as establish validation points for satellite and aerosol transport models. Since 2004, these instruments have been deployed periodically on ships of opportunity and research vessels to monitor aerosol properties over the world oceans using Solar Light Microtops Sun Photometers and Garmin GPSs.

The Microtops instruments currently in the network have five channels but they may have one of two configurations: 340, 440, 675, 870, 936nm or 440, 500, 675, 870, and 936nm. In addition, the instrument has built-in temperature and pressure sensors as well as the ability to log accurate time and geographical position using a GPS. The Microtops instruments are calibrated at the NASA Goddard Space Flight Center (GSFC) calibration facility via a transfer calibration procedure between the Microtops and the master Cimel sun photometer at GSFC, which has a calibration traceable to a Langley calibration of a Cimel sun photometer on Mauna Loa, Hawaii. In general, the estimated uncertainty of the aerosol optical depth in each channel does not exceed plus or minus 0.02, which is slightly higher than the uncertainty of AERONET field (not master) instruments.

Microtops sampling during cruise SO226B were undertaken on clear days with no upper cloud deck. Sampling days were 9, 12, 15, 15, 16, 17, 18, 20, 23, 25, 26, 27 and 28 February (local). All spectra were copied on the same day as taken and emailed to Dr. Alexander Smirnov at NASA Goddard. The data will be screened for quality at NASA and posted on the AERONET website.

6. Work completed and first results

6.1. Parasound, Bathymetry & Backscatter

6.1.1. CTD casts

In total 7 CTD casts were run during SO226 by the ship's crew. All cast reveal a warm surface layer gradually decreasing from 15°C at the sea surface to 10° around 100 m water depth. Towards deeper water the temperature gradually decreases until ~5° at 1000 m water depth. Significant tempospatial variations occurred in the measured parameters especially in temperature strongly affecting the sound velocity profile. The CTD measurements were either performed by attachment of the sen-

sors to a rosette water sampler or to the OFOS system. Substantial drag of water might have affected the OFOS CTD measurements visible by the large up- and downcast offsets (Fig. 6.1.1.1b).

Another explanation for these offsets may be caused by the tides. It could be observed that the sound velocity not only changed regionally between different working areas, but also locally on a short tidal time scale with strong changes between 80 m and 300m water depth. Such shallow sound velocity inhomogeneity also strongly affect the outer beam data. Therefore, the multibeam data need thorough review in terms of applicability of the respective sound velocity profiles being currently embedded into the raw files.

Table of CTD casts:

Date	Location	Graph No.
10.01.2013	41°39.33 / 178°55.04	CTD-001
16.01.2013	44°14.91 / 178°39.95	CTD-002
28.01.2013	44°20.72 / 177°03.94	CTD-003
16.02.2013		CTD-004
18.02.2013	44°14.02 / 177°15.29	CTD-005
22.02.2013		CTD-006

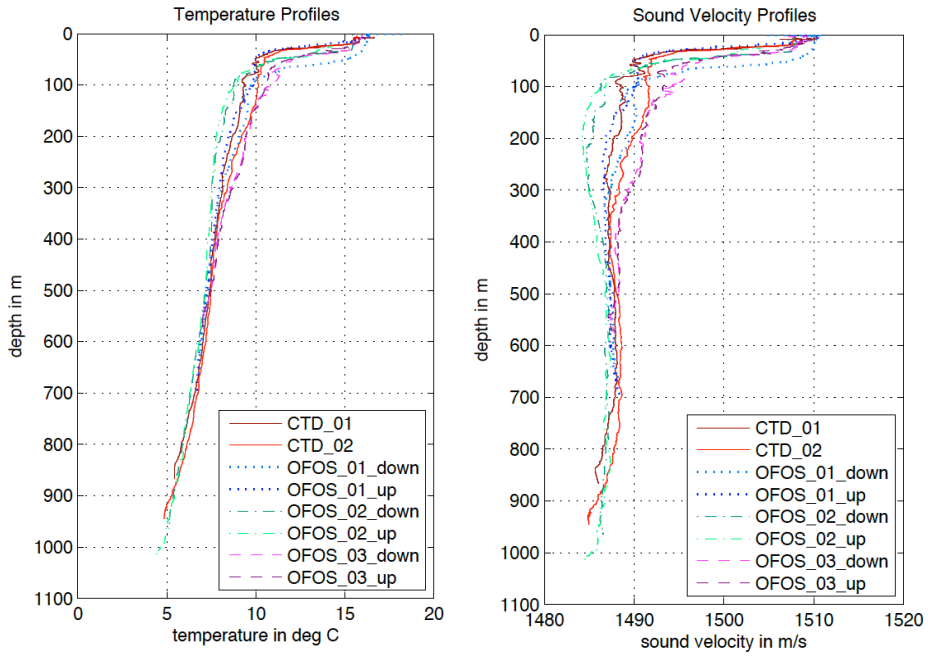

Fig. 6.1.1.1: (a) Temperature and (b) Sound velocity (after DelGrosso) profiles gathered during SO226-2 gathered by CTD/Rosette and OFOS casts.

6.1.2. Area 1 bathymetry

The bathymetry was recorded with the EM120 and in parallel with the SB3050 50 kHz system. No severe interference between both systems has been observed. It remains to be investigated which system performed better at respective water depths. Multibeam bathymetry collected at Area 1 shows two 'giant' pockmark structures, each roughly 10 x 6 km large, at water depths of 600 – 1000 m (Fig. 6.1.2.1, Fig. 6.1.5.1). In addition to these two pockmark structures, four smaller pockmark structures were also discovered in the surrounding area. These range in diameter from 2 – 5 km, placing them in the category of medium-sized pockmarks on the Chatham Rise, as discussed by Davy et al. (2010). The two giant pockmark structures have a similar geometry with a deeper channel incised along the south-west side of the structure.

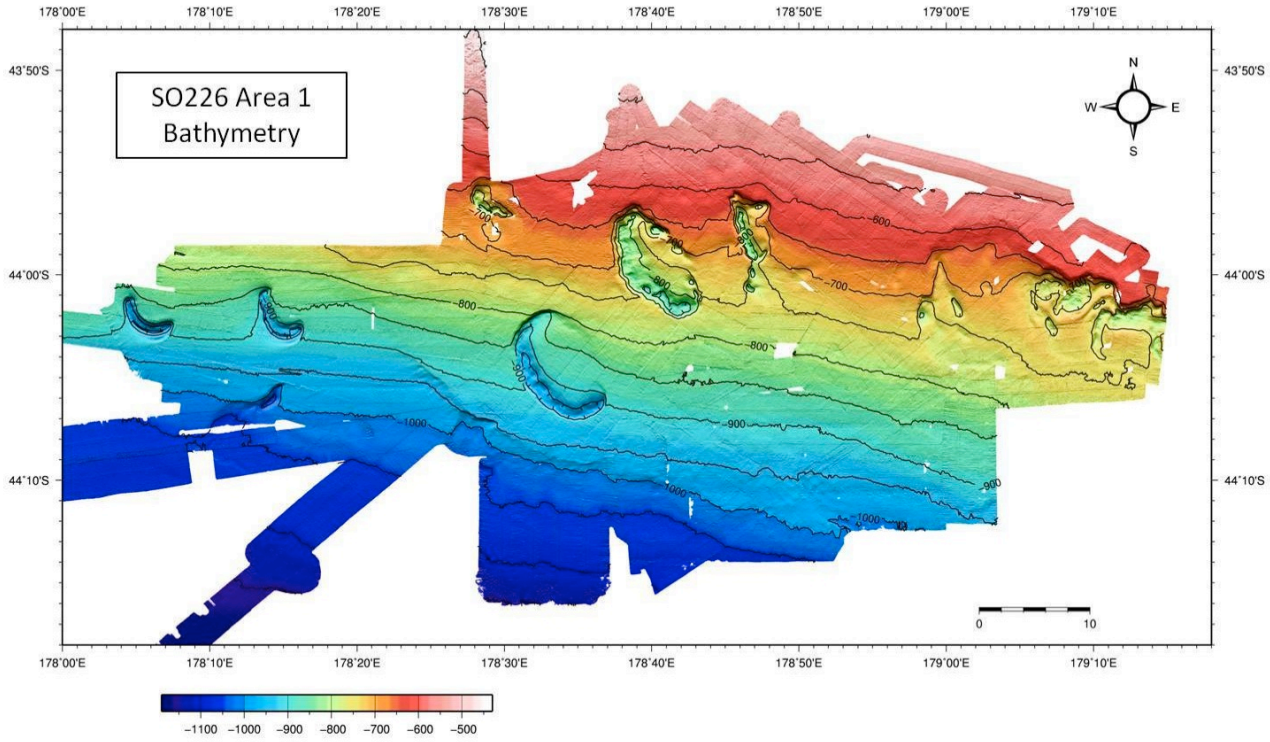

Figure 6.1.2.1. Bathymetric map of Area 1.

These channels are both 100 – 150 m deep relative to the surrounding seafloor. The southern pockmark structure is reasonably circular in shape in comparison to the northern structure which is far more irregular. Gradient presentations (Fig. 6.1.2.3) calculated on the giant depressions' bathymetric grid reveal extraordinary steep wall slope angle up to 28°. The slope angles tend to be higher in the northerly/upslope rim than in the southerly/downslope rim of the depressions walls.

The backscatter mosaic from Area 1 shows significant variation in the vicinity of the pockmark structures (Fig.6.1.2.2.). Alternating bands of high and low backscatter levels around the edge of the southern structure indicate variation in lithology and texture of the seafloor [Goff et al. 2004]. This is supported by evidence from the OFOS transit carried out across one of the depressions which showed large carbonate outcrops along the edge of the structure. Backscatter of the SB3050 has not been evaluated yet due to the missing import functionality into SONARSCOPE and FMGEOCODER.

The primary high and secondary low frequencies of PARASOUND were evaluated online in regard to finding free rising gas in the form of so called "gas flares". According to the results from the SB3050 WCI system (s. section 6.1.5) neither gas flares nor clear indications of shallow gas (no distinct blanking) were observed. Instead, the features found in the water column resemble the ones identified with the SB3050 WCI, i.e. abundant findings of solitary fish and fish shoals, diurnal migration layers (zooplankton), and several scattering layers in the twilight zone (Fig. 6.1.2.3).

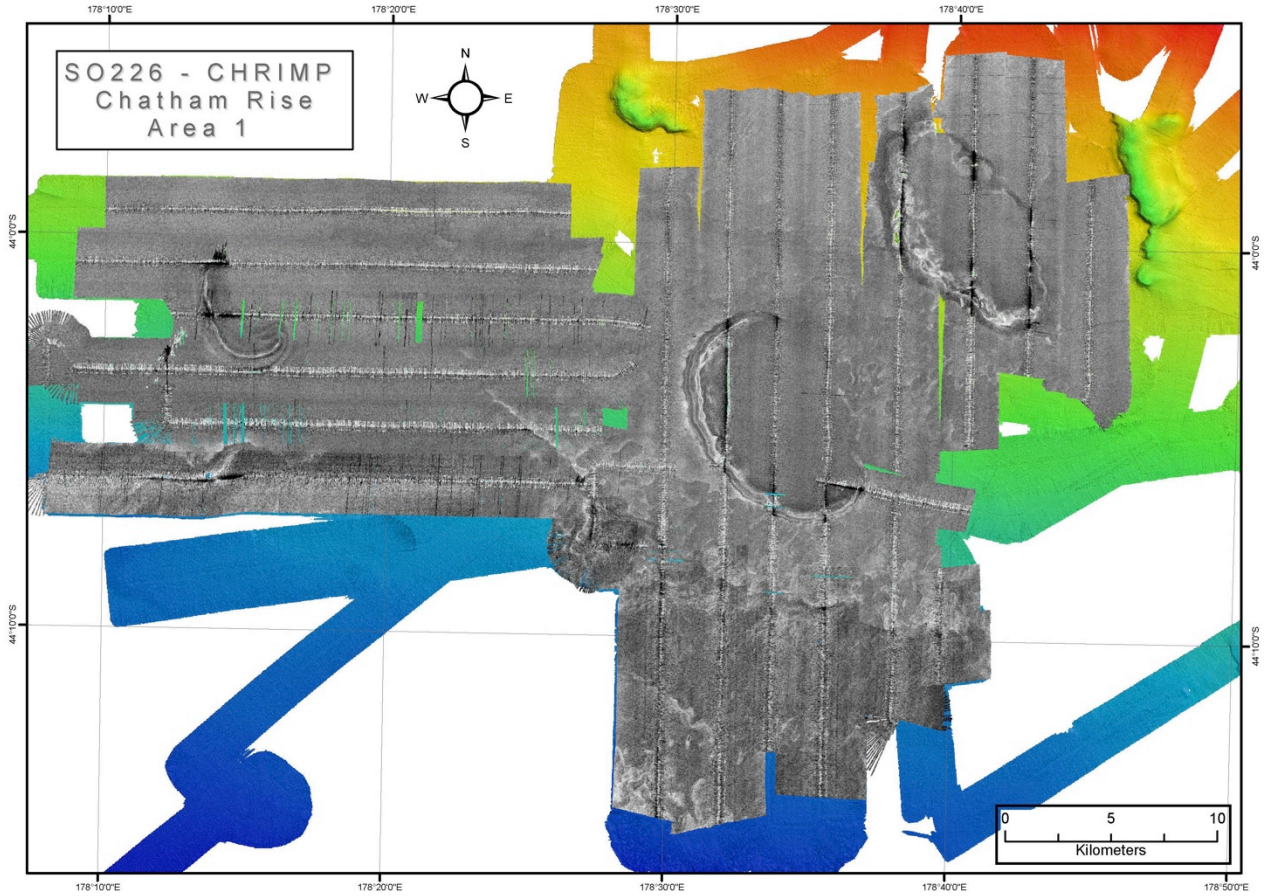

Figure 6.1.2.2. Backscatter mosaic of Area 1.

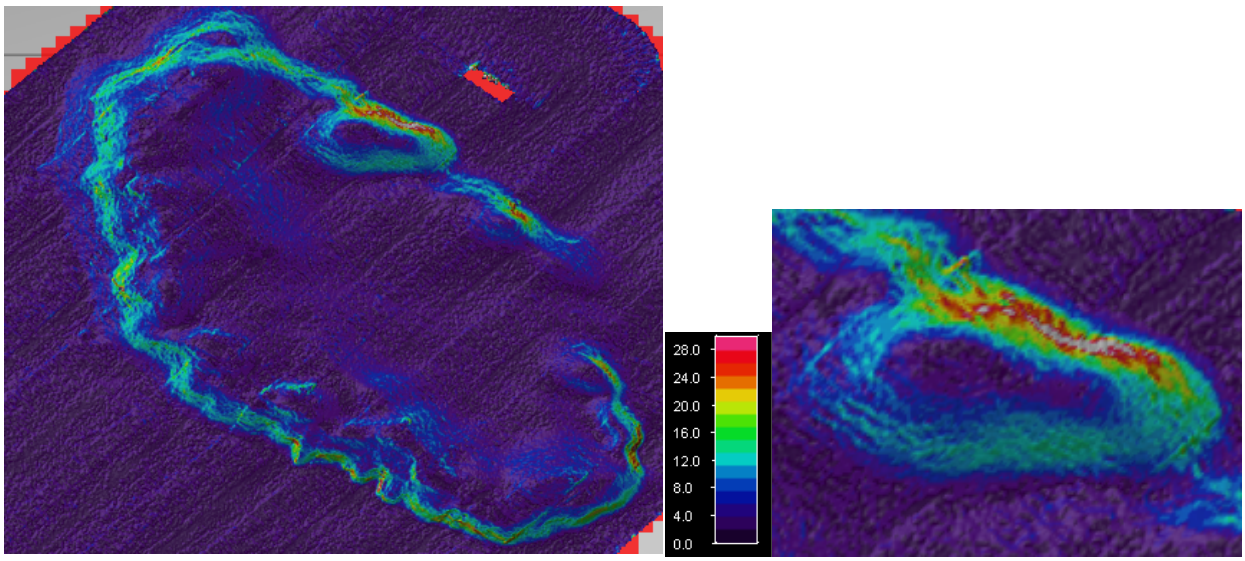

Fig.: 6.1.2.3: Gradient map generated in Fledermaus on the SB3050 data

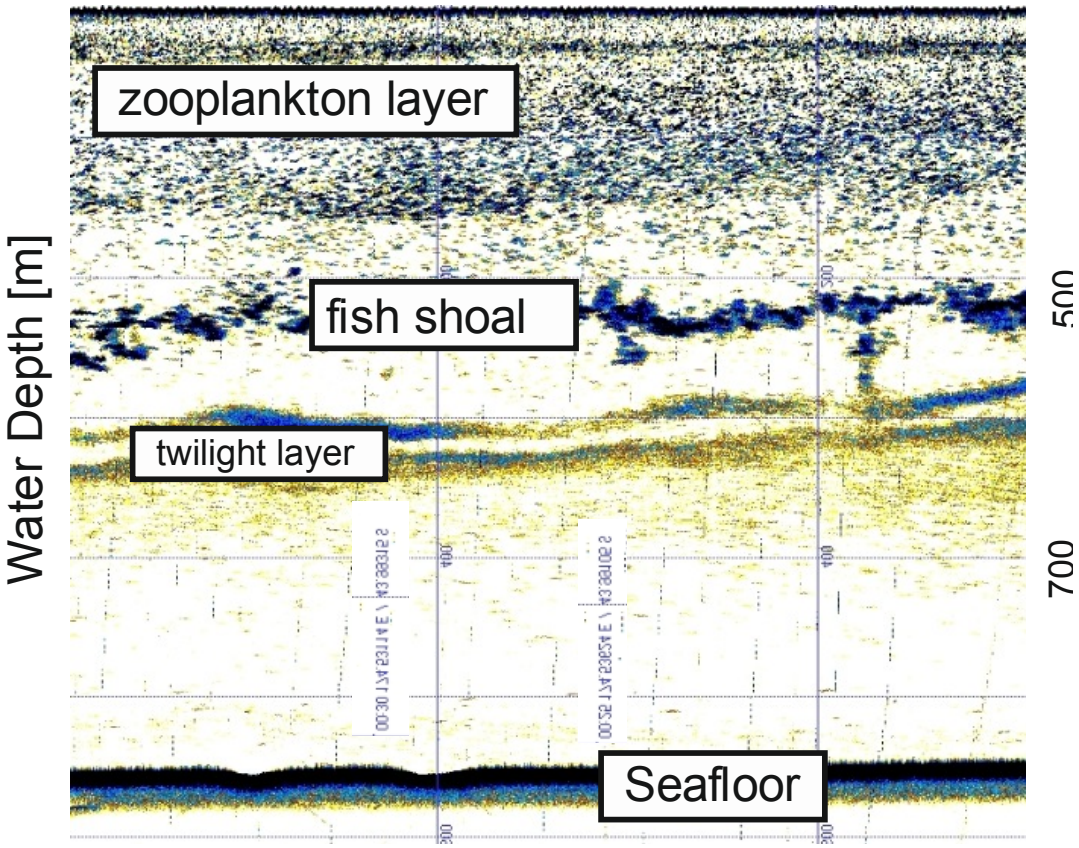

Fig. : 6.1.2.3: Water column backscatter image recorded with the PHF frequency of Parasound .

6.1.3. Area 2 bathymetry

In transit from Area 1 to Area 2 several pockmark structures were crossed at depths of 980 – 1200 m. These structures are relatively circular in shape and significantly smaller than those seen at Area 1, with diameters of 1200 – 3600 m. Multibeam bathymetry data from Area 2 shows numerous structures of a similar size, according to Davy et al. (2010) these are categorised as medium-sized pockmarks (Fig. 6.1.3.1.). The majority of the pockmark structures at Area 2 are irregular in shape and are predominantly elongate along an east-west orientation. They range in size from 2600 – 5500 m in diameter, and are located in water depths of 840 – 1200 m. The pockmark structures are 40 – 60 m deep relative to the surrounding seafloor and have uneven floors. The topography suggests that some of the larger structures may in fact be amalgamations of several smaller structures, which formed over a period of time. Additional data collected during SO226/2 revealed more seafloor depressions to the north-east of Area 2. Subbottom transects were run in parallels with a very good penetration over 100 m into the seabed. Very distinct active and submerged paleo-channels (Fig. 6.1.3.2) were identified in the vicinity of seafloor depression. Those structures continue upslope to depths of 550 m, as at Area 2 some of the depressions appear to be connected. Data collected in transit between the survey areas indicates that these depressions continue to the east and west of Area 2. South to the channel area the data also indicate some local slumping events, which need further review of the bathymetry together with the subbottom records.

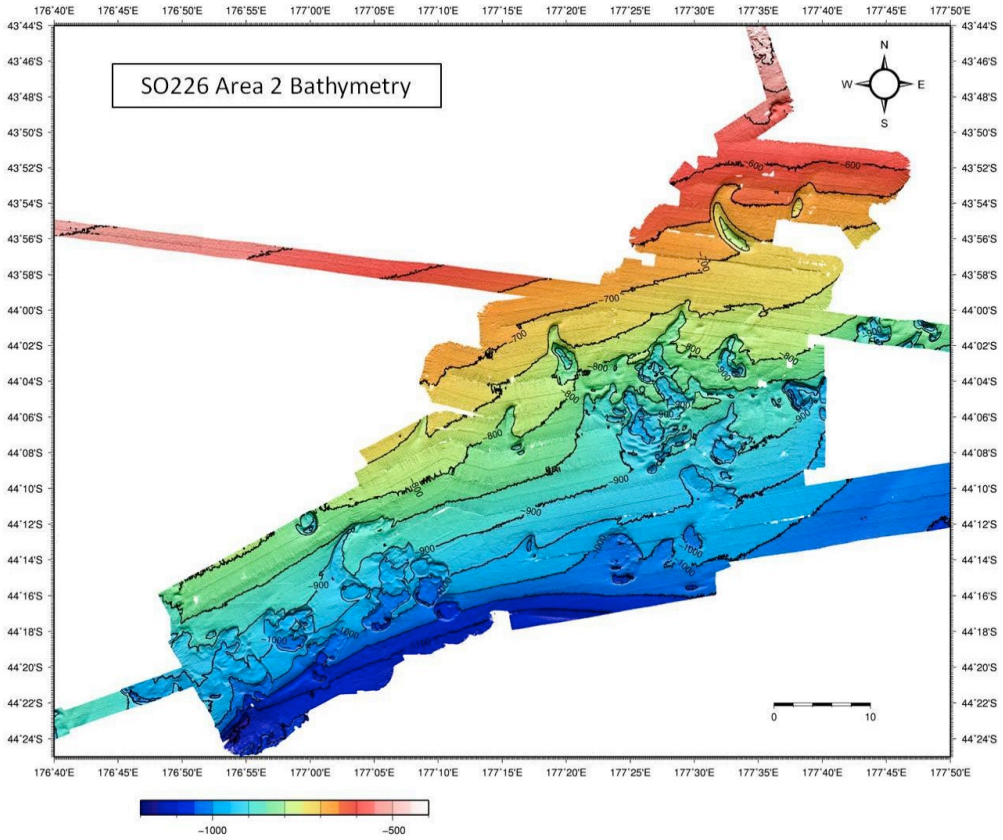

Figure 6.1.3.1. Bathymetric map of Area 2.

The backscatter data collected at Area 2 shows no significant variation in backscatter levels in the vicinity of the seafloor depressions. There is a slight increase in backscatter levels around the perimeter of the most easterly depression; however this may be a function of variation in topography. The northernmost structures show a slight decrease in backscatter level within the depressions, indicating that they are filled with sediment that varies relative to the surrounding substrate. The contrast between the backscatter data collected at the two areas indicates that the variability in backscatter levels at Area 1 is not purely a function of topography. If this were the case then we would expect there to be similar patterns around the structures at Area 2. Therefore, it is probable that the variation in backscatter levels around the giant seafloor depressions at Area 1 indicates a change in seafloor lithology (s. chapter 6.6.1).

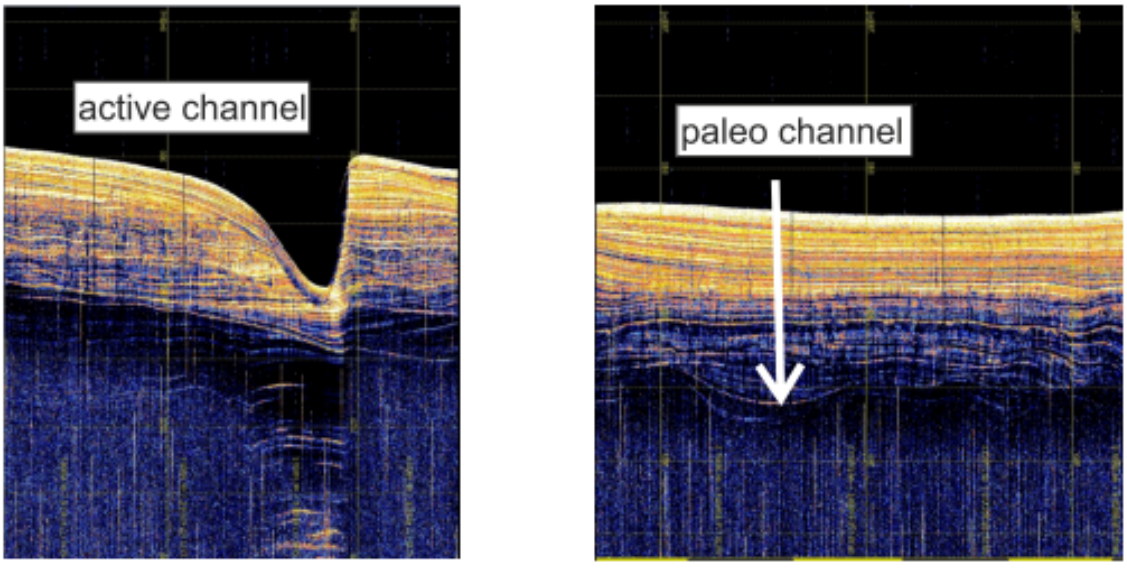

Figure 6.1.3.2: Sub-bottom profiler images of active and paleo channels in the uppermost sediment columns.

6.1.4. Area 3 bathymetry

Multibeam data collected at Area 3 shows numerous small pockmark structures of 100 – 220 m in diameter, located in water depths of 520 – 580 m. Similar structures were observed on the transit from Area 2 to Area 3 at water depths of 520 – 650 m to the north of Veryan Bank. These structures are classified as small pockmarks in accordance with Davy et al. (2010). The seafloor depressions are relatively circular in shape, range in depth from 4 – 10 m and are slightly asymmetric in cross section.

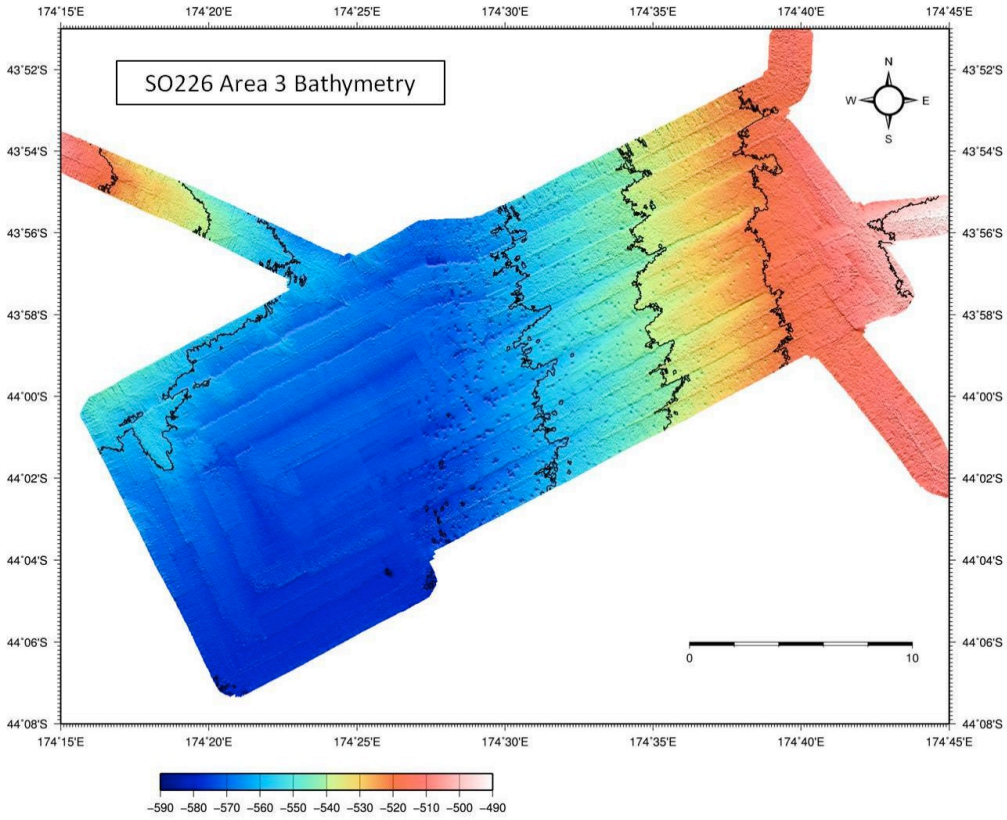

Fig. 6.1.4.1. Bathymetric Map of Area 3.

Backscatter data from Area 3 (Fig. 6.1.4.2) shows some variation across the survey area. To the south-west there is a region where no depressions are observed. This region correlates with a lower backscatter level, indicating a variation in seafloor substrate relative to the rest of the survey area. Some of the depressions are also filled with sediment, which has a lower backscatter signal.

6.1.5. ELAC Multibeam and WCI

The main goal of the SB3050 multibeam studies during this cruise was to identify gas bubble seepage potentially related to the large depressions formerly interpreted as pockmarks [Davy et al., 2010]. Thus we concentrated on the detection of both, gas bubble-mediated echoes from the water column and seep related seabed features [Judd and Hovland, 2007] such as shallow gas blanking, pockmarks and high backscattering patches. The latter may appear with low frequency multibeam systems mediated by methane derived authigenic carbonates or very shallow gas [Schneider von Deimling et al. 2013].

Prior to the surveying a CTD was run to generate an up to date sound velocity profile for the subsequent calibration patch test. Calibration lines for roll were run in a flat area at 700m and at deeper water for pitch, latency and yaw. The calibration was successfully performed in Hysweep and Fig. 6.1.5.1. shows that the calibration worked reasonably well. Calibration values are provided in table 6.1.5.2.

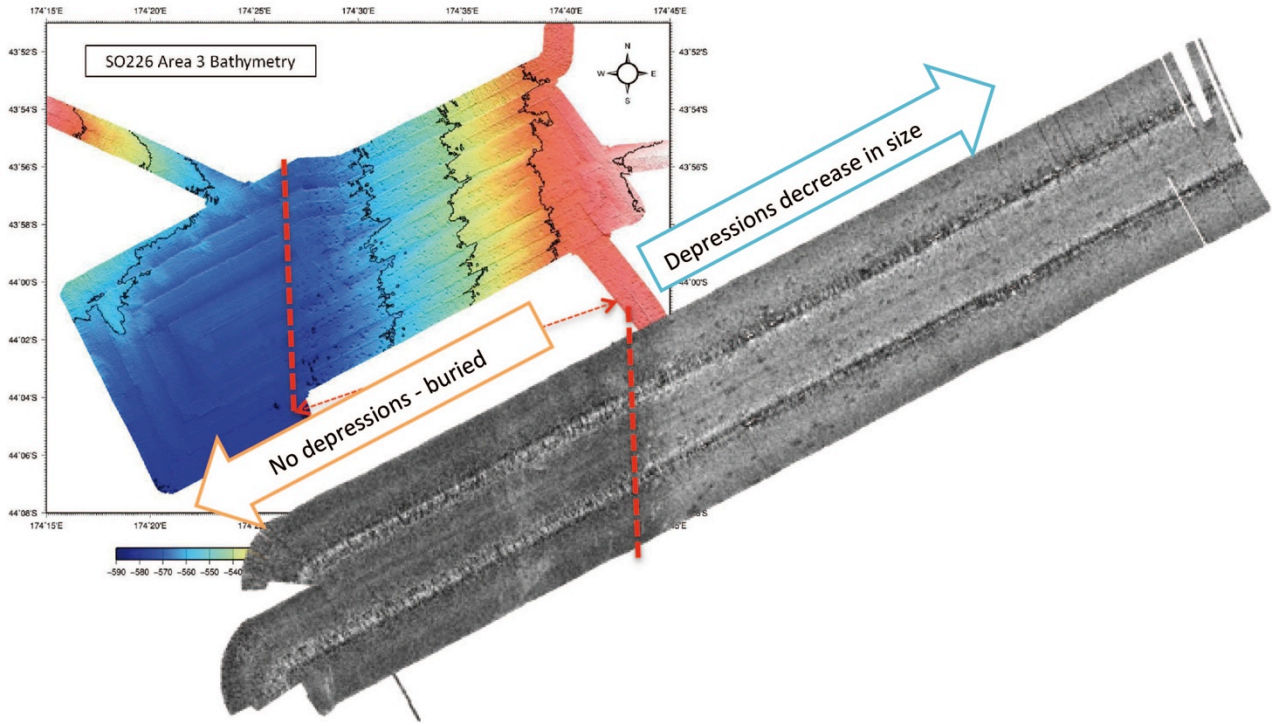

Fig. 6.1.4.2 Variation in backscatter levels at Area 3.

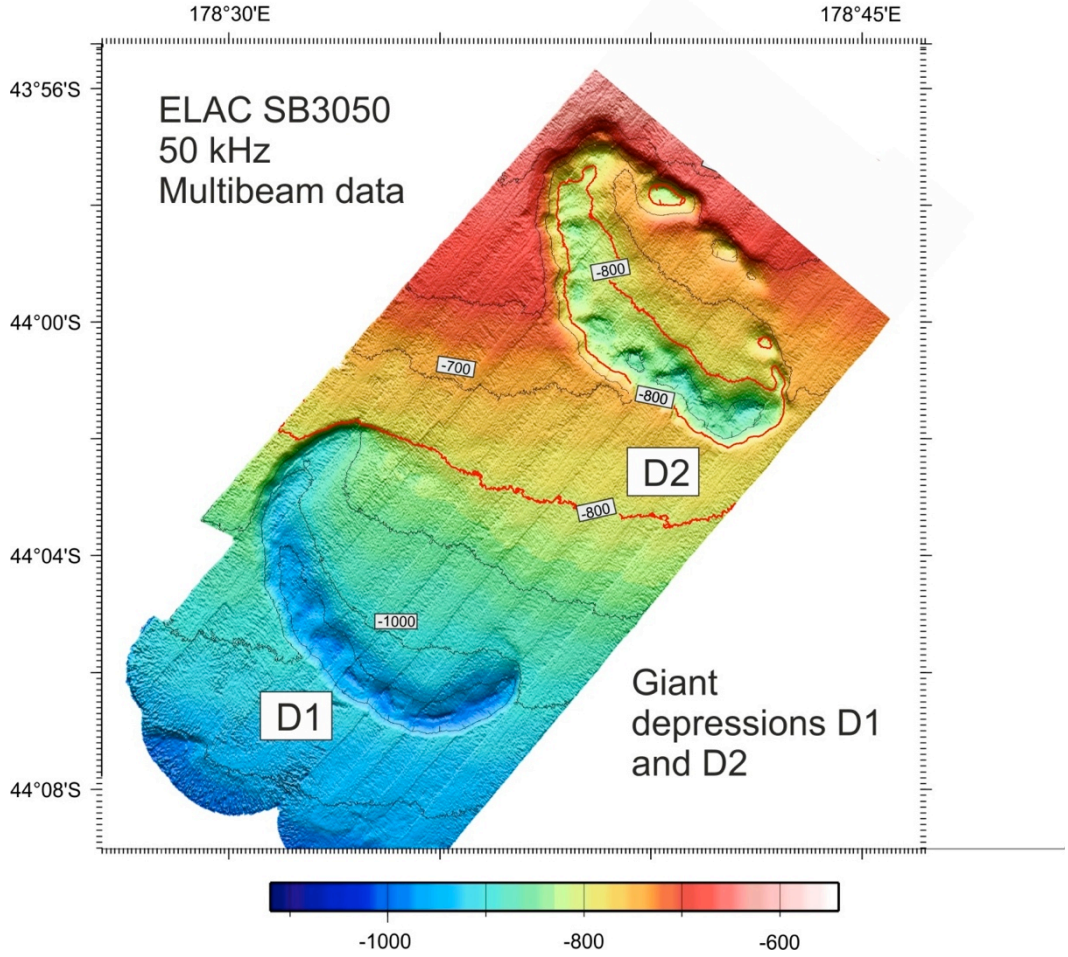

Figure 6.1.5.1. Bathymetric chart of the two giant depressions measured with the SB3050.

Table 6.1.5.2. Calibration offsets between MRU 5, Octans Heading, and SB3050 array

Latency	Roll	Pitch	Yaw
0	1.4°	0.5°	-1.0°

The SB3050 system performed well and worked reliably throughout the cruise. Fig. 6.1.5.3. a and b represent the general WCI data pattern. Very close to the transducer reverberation of the transmit signal gives rise to elevated echo signal strength. Strong ship turning operations and/or significant pitching produced some bubble wash down under the transducer and influenced the first 20 m of signal reception. The damping effect of this bubble wash appeared considerably small. Therefore flare imaging was feasible even at rough weather conditions.

A scattering layer was observed in most of the data characterized by a diurnal up- and downward migration pattern. The migration of this layer took place upwards after sunset and is interpreted as a day and night zooplankton migration layer. The second most prominent scatterer where fish appearing either in the form of singular elevated echoes or as dispersed clouds. Those scatterers concentrated around the migration layers indicating feeding activity of fish on the zooplankton (Fig. 6.1.5.3. c). Further down in the water column a temporal more stationary scattering layer appeared throughout the place. Close to the seabed and especially along morphological features like slopes bottom feeder fish were abundantly present (Fig. 6.1.5.3. b, lower right corner, Fig. 6.1.5.3. e).

Acoustic water column investigations during the first leg of this cruise were realized with PARASOUND. With such a narrow beam (4°) system it is difficult to unambiguously detect gas seepage, because of a lack of spatial coherence. Bubbles rise paths are controlled by ocean currents and as a result the bubbles move out of the acoustic cone. Then it becomes very difficult to discriminate bottom loving fish against gas seepages [Schneider von Deimling et al., 2011]. In contrast swath mapping allows for imaging of the entire water column and for determining the true spatial extend of a gas flare. E.g. Fig. 6.1.5.3. b displays elevated backscatter that could be misinterpreted as a flare. However if this figure is spatial extended (Fig. 6.1.5.3. e) then it becomes obvious that the backscatter represents a 300m broad fish shoal rather than a flare.

The water column imaging appeared to be sensitive for target detection even at larger water depths beyond 1000 m. This becomes obvious by the successful device tracking of a piston core down to the seabed by elevated signals at larger depths (Fig.6.1.5.3 d). Not a single flare has been detected throughout the entire cruise (Leg 2). Given the very broad swath and high sensitivity of the 50 kHz System in terms of gas seepage detection, we exclude active gas seepage in the respective working areas.

Aforementioned depressions used to be associated with gas hydrate dissociation and interpreted as heavy gas release features [Davy et al. 2010]. During our cruise a broad swath of at least 140° allowed for a very wide coverage and unambigious gas flare detection. Most of the data has been reviewed onboard and no gas flares were found neither in the SB3050 nor in the PARASOUND water column data. This corresponds to the geochemical readings from core analysis and water column sensor measurements not indicating any enhancement of methane at all. Overall we conclude that gas escape in the surveyed areas does not occur at the moment.

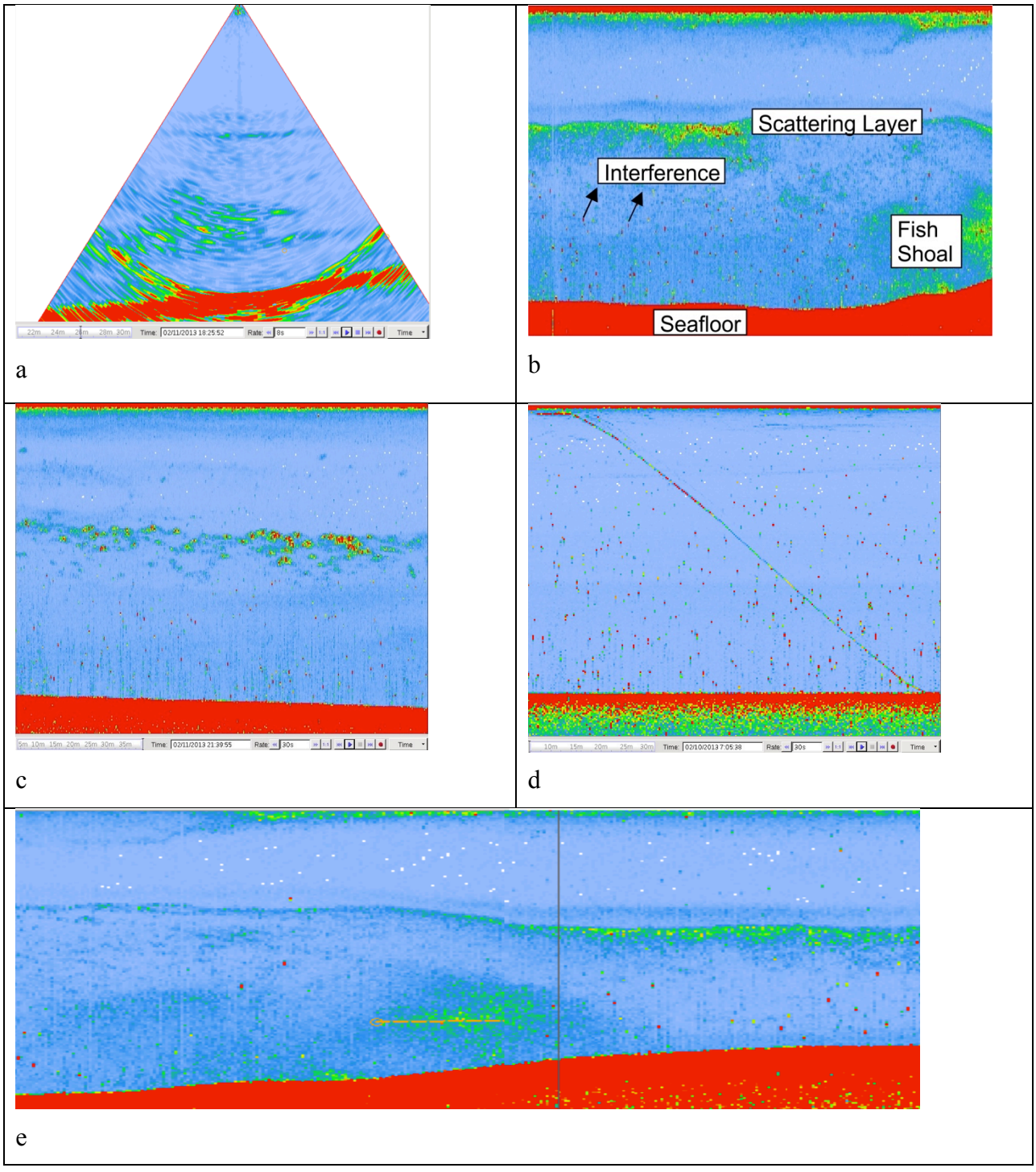

Figure 6.1.5.3. (a) raw swath showing a scattering layer and a large fish shoal at midwater (670 m). High backscattering values are coded in red, and background values in blue. Echogram time series presentation of the WCI data, where all beams have been stacked together in (b) represents a downward migrating biological scattering layer around 250 m water depth and a fish shoal close to the bottom at 740 m water depth. (c) shows some fish shoals around 300 m water depth and (d) the 876 m downcast of the CTD at station 028-1 (e) an example of the swath WCI mapping approach showing the same fish shoal as (b) with spatial extension, horizontal bar (orange) is 260m

6.2. Seismic

6.2.1. Area 1

6.2.1.1. 2D Seismic

The 2D-seismic survey area covers an area of 60 km (E-W) x 35 km (N-S) on the southern Chatham Rise. Eighteen E-W and N-S oriented reflection seismic lines were acquired over two large elliptical depressions (major axis ~ 10 km, oriented NNW-SSE) on the seafloor (Fig. 6.2.1.1.). Six additional seismic lines extended the survey area further to the east (~ 30 km east of the easternmost elliptical depression).

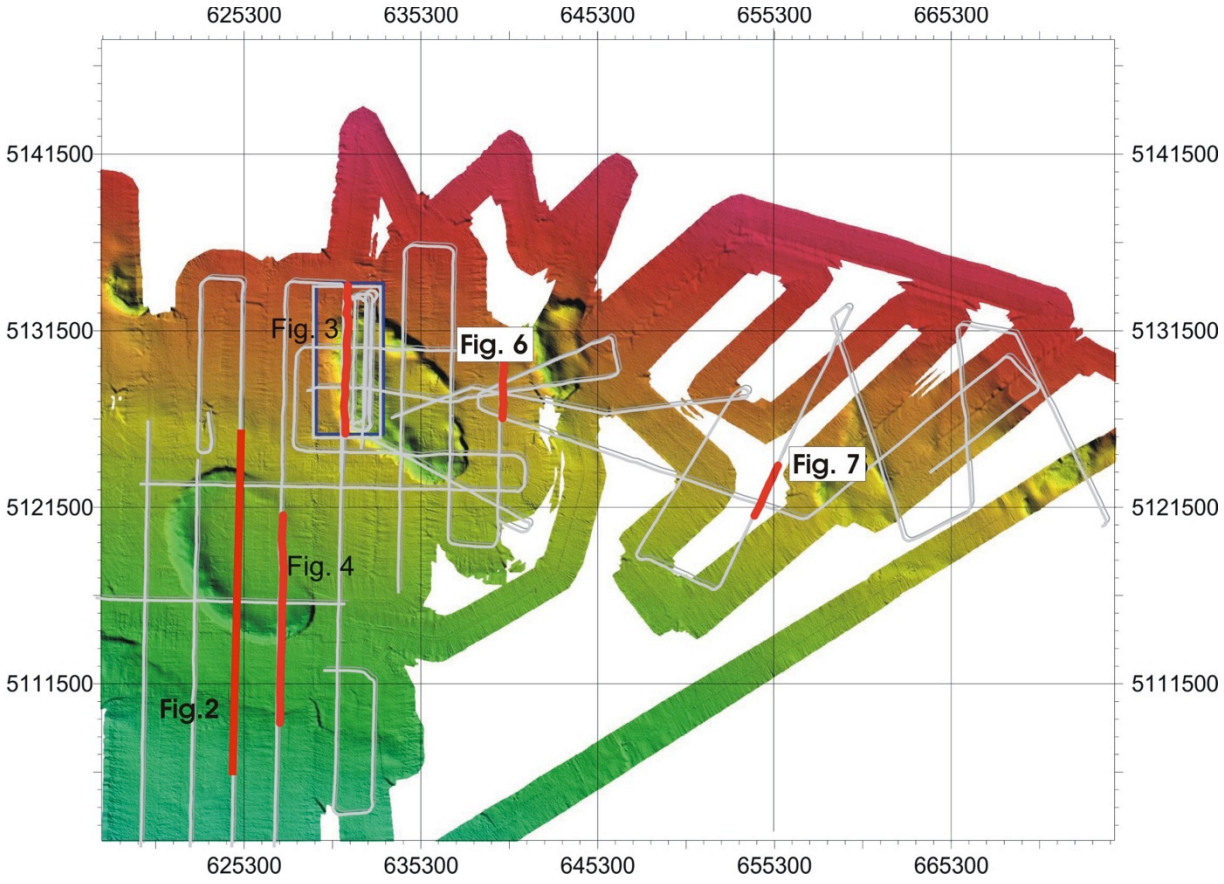

Figure 6.2.1.1. Map of survey area showing two large elliptical depressions previously interpreted as giant pockmarks, and location of 2D seismic survey lines. Illustrated seismic profile locations are indicated on the map.

The seismic reflection survey resolves sedimentary strata down to 1.5 - 2 s TWT. Four reflectors (R1-R4) were used to broadly divide the stratigraphy of the region into five units (Units I-V). Unit I is the bottommost unit with reflector R1 at its top but its base could not be imaged in our data (Figure 6.2.1.2., 6.2.1.3.).

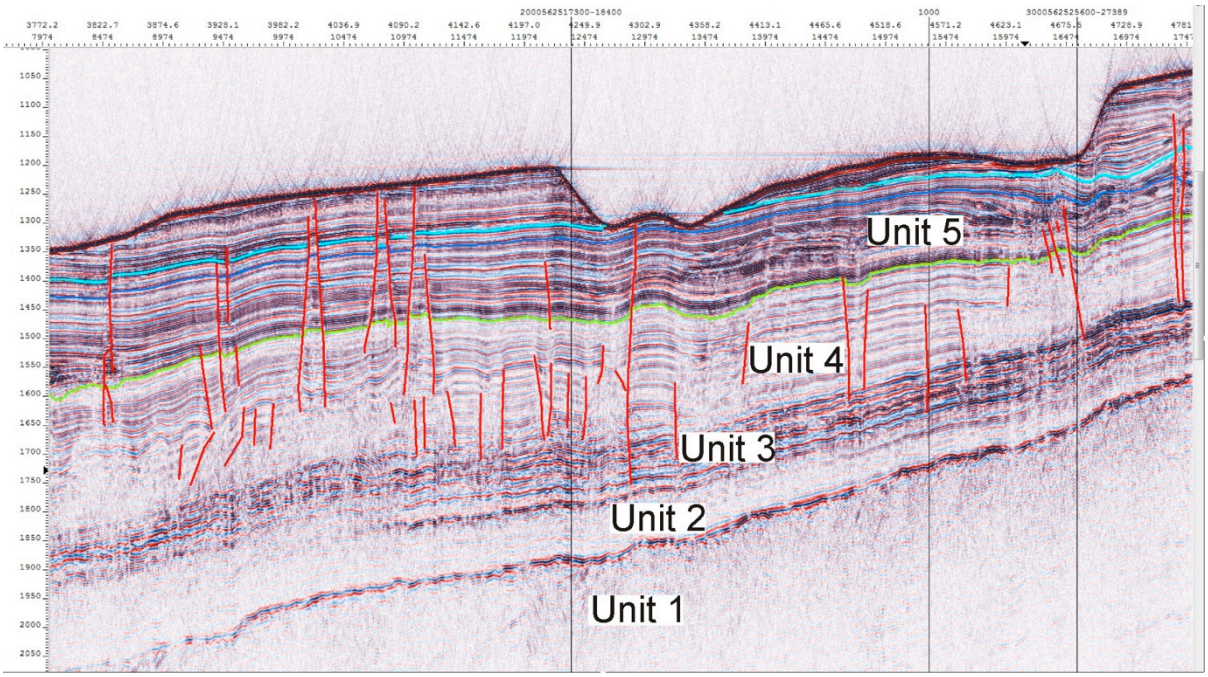

Figure 6.2.1.2. South (left) – North (right) transect across the centre of the south-western pockmark structure showing northward thinning strata. Small-scale faulting and folding occurs predominantly within Unit IV. Some faults extend to the seafloor and associated blanking indicates that they act as gas or fluid conduits

Although Unit I is poorly imaged, reflectors onlapping southward onto seismic basement can be identified. The top of Unit I is defined by a strong normal polarity reflection (R1) and is laterally traceable throughout the survey area. Over most of the area surveyed, this horizon represents an erosional unconformity or peneplanation surface that forms the base of the overlying north eastward thinning sedimentary sequence comprising Units II-V (Fig. 6.2.1.2., 6.2.1.3.).

Unit II is weakly reflective but stratification can still be observed. Unit III is represented by relatively high amplitude, parallel and well-stratified reflectors. However, lens-shaped regions, often showing internal incoherent reflections are observed, especially in the eastern part of the survey area. Unit IV is moderate to weakly reflective showing largely parallel, well-stratified layers and also has lenticular bodies with partially incoherent reflections (see below). The base of units III and IV appear to form relatively sharp contacts that are traceable through most of the area (Fig. 6.2.1.2.-6.2.1.4.).

The base of Unit V has so far not been well-defined, due to lateral pinch out and truncation of reflectors. Unit V generally shows a well-stratified reflection pattern. However, internal erosional surfaces and areas of vertical disruption and up-doming are common (Fig. 6.2.1.4.). Older strata of this unit intersect the seafloor in the southwest of the 2D seismic coverage. These strata thin and are partially eroded and overlain by younger strata thickening towards the north and east (Fig. 6.2.1.2.). Older strata of unit V also occur in the east, where deep erosion has occurred associated with “mega-pockmark” formation

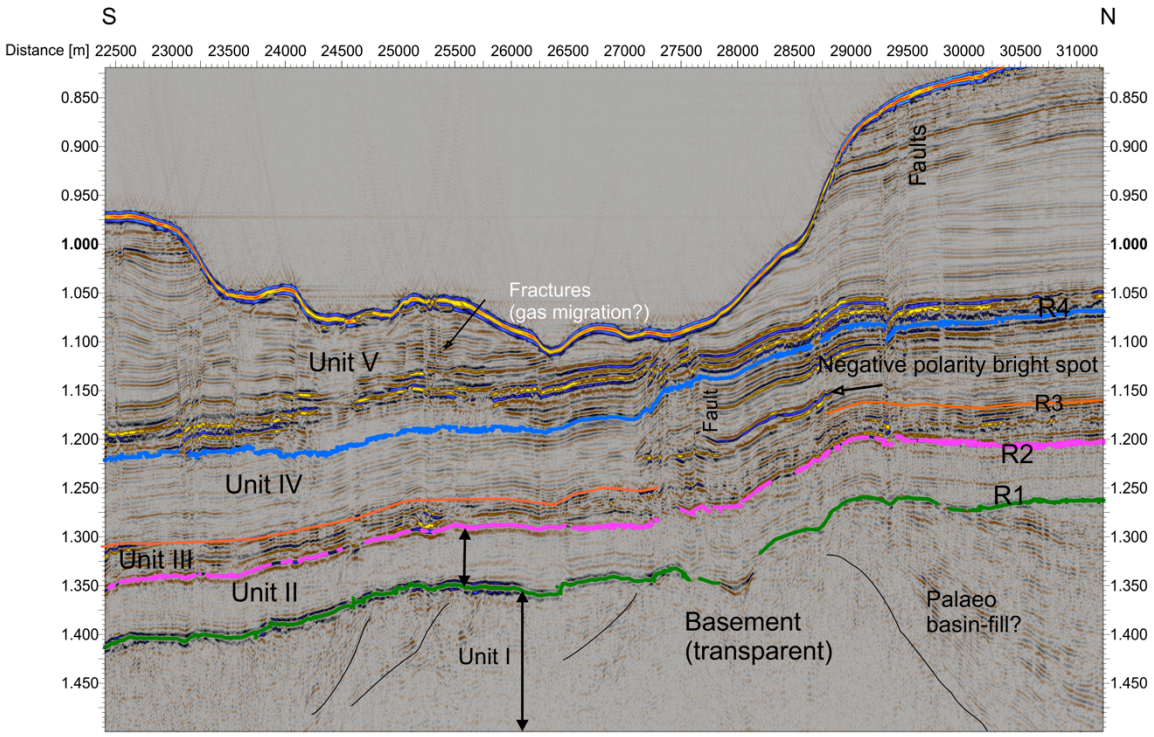

Figure 6.2.1.3. The five mapped stratigraphic units as seen along a N-S seismic profile across the large easternmost depression. Unit I is the basal unit. Parts of Unit I are acoustically transparent and are referred to as seismic basement. R1 is an erosional unconformity. Unit II is weakly reflective. Unit III is moderately to strongly reflective. Unit IV is stratified and moderately reflective. A negative polarity bright area is observed along with a predominance of low frequency reflecting horizons underneath the pockmark structure. Unit V is well-stratified in parts with variable amplitude. Stronger reflections are seen near the base and weaker reflections are mostly in the shallower regions. Faults are common and some extend to the seafloor. Narrow columns of amplitude fading often terminate close to the seafloor. Faults and zones of fine scale fracturing are likely gas conducts to the seafloor. Potential gas chimneys are observed close to the centre of the depression.

Numerous faults are identified in the seismic profiles (Fig. 6.2.1.2.). Many faults are small-scale and terminate near the base of Unit IV although some extend to the seafloor. Small scale folding, local up-doming and fracturing is also common in Unit IV and V. Faulting with an offset of 50 ms or more is largely restricted to Unit I, although some of these faults appear to relate to smaller scale faulting in the overlying units. The largest normal fault was encountered in the far east of the surveyed area at the eastern rim of the easternmost large sea-floor depression.

Structure in unit I is not well imaged but the orientation of onlap of northward dipping strata on acoustic basement appears to follow a WSW-ENE orientation, indicating graben structures oriented in this direction. The northern rim of the northeastern pockmark structure overlies this underlying graben-structure (Fig. 6.2.1.3.). Faults appear to delimit areas of higher reflectivity further south but are not well imaged.

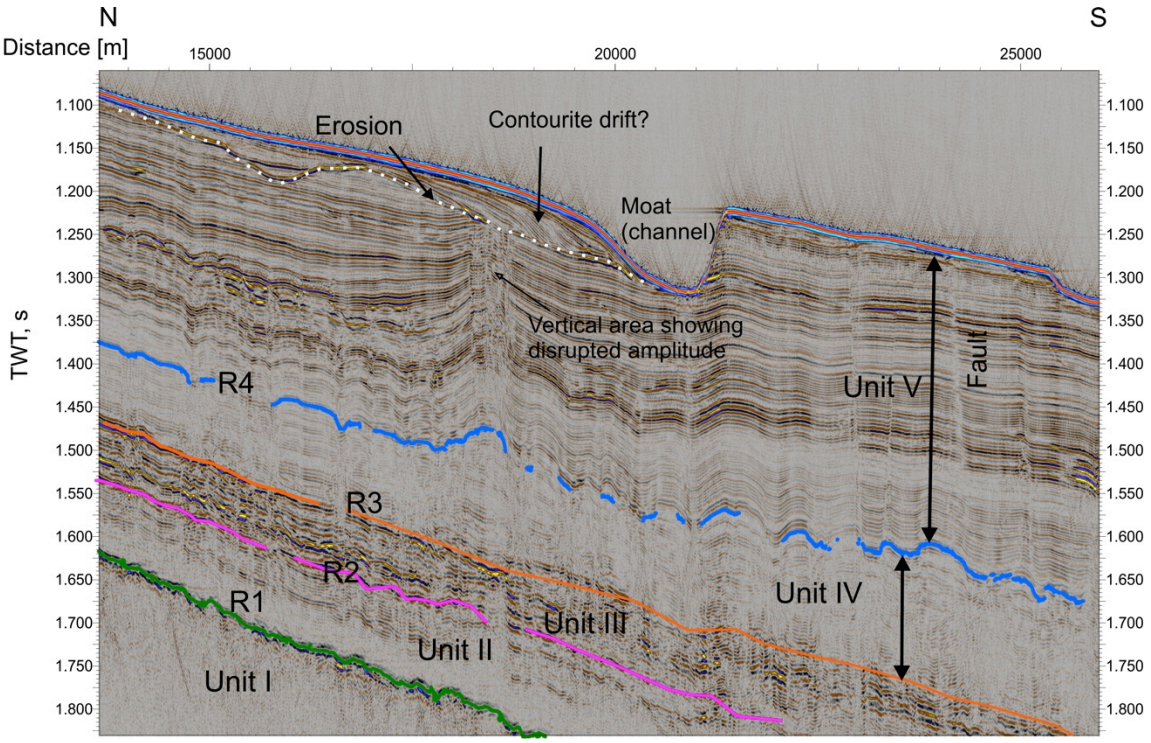

Figure 6.2.1.4. N-S line across the westernmost elliptical "giant pockmark" depression. Small scale faulting is common. The original floor of the pockmark structure (dotted white line) is partially filled by sediments that in profile show typical crossbedding and levee and moat channel geometry observed in contourite drift deposits. A vertical zone showing internally disrupted reflections is probably a chimney or gas migration pathway.

Giant pockmarks as proposed by Davy et al. (2010) were the primary target of the Site 1 survey. The two largest structures are elliptical and 11 km in diameter at their long axis (Fig. 6.2.1.5.). A series of additional more irregular structures of various sizes were intersected ion the eastern part of the survey. Most structures are underlain by largely continuous strata. A later stage infill of the originally up to 180 m deep structures exhibits geometries typical for contourite drift deposits. All structures are also underlain by areas of disturbed bedding and both blanking and brightening of reflectors indicates the presence and escape of gas.

The more irregular seafloor depression in the far east of the survey area is underlain by extensive gas escape structures and buried geometries similar to those seen in the west of the survey area.

A series of seismic anomalies that may be indicative of or related to the presence and migration of gas were encountered in the 2D seismic data:

- Pronounced lateral variation in amplitude and intervals of brightened or reversed polarity reflectors and bright spots occur throughout Units IV and V, particularly underneath seafloor pockmark structures and below gas flares (Fig. 6.2.1.3.).
- Areas of blanking are widespread, often with disruption of stratification. They are commonly rooted in faults and often extend down as far as Unit II
- Lens-shaped low velocity bodies characterized by inverse polarity at the top and normal polarity at the base and chaotic or poorly stratified internal structure are widespread in Units III and IV (Fig. 6.2.1.6.). Overlying strata do not onlap on the lenticular structures, which therefore appear to have formed at a later stage by injection.
- In the eastern half of the site1 survey area, an interval of chaotic reflections (Fig. 6.2.1.7.), up to 200 ms (TWT), was encountered in the upper part of unit V. This interval also contains tilted and up-thrown blocks of undeformed strata. At the top of this interval, brightened inverse polarity reflectors indicate gas-rich sediments. Processes leading to the formation of this interval could be lateral gas injection, mobilization of unconsolidated sediments and

slumping. The latter interpretation is supported by overlying strata apparently infilling a pre-existing topography.

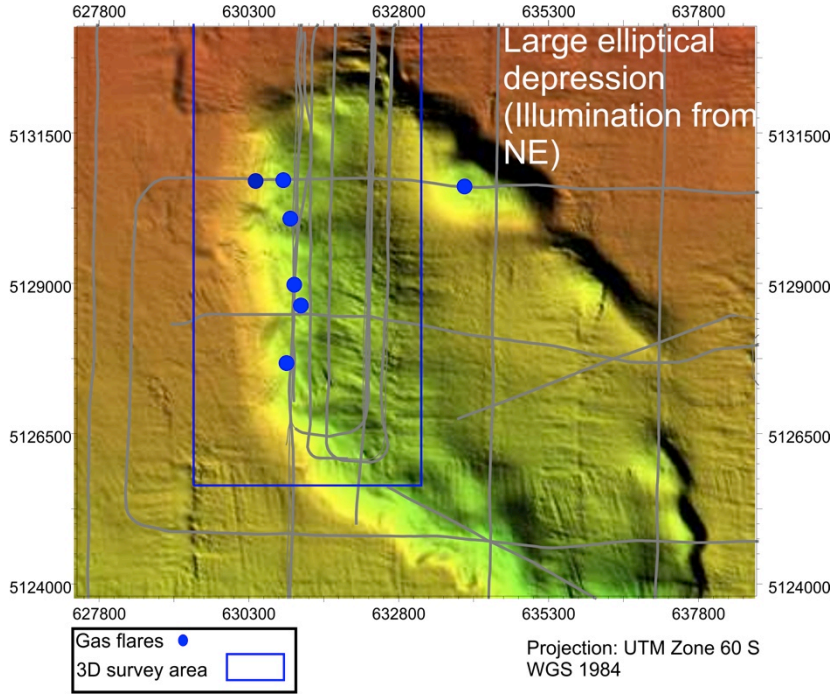

Figure 6.2.1.5. Location of gas flares in the central depression (giant pockmark) and 2D seismic lines crossing the region. The flare positions are based on the observations made on parasound data.

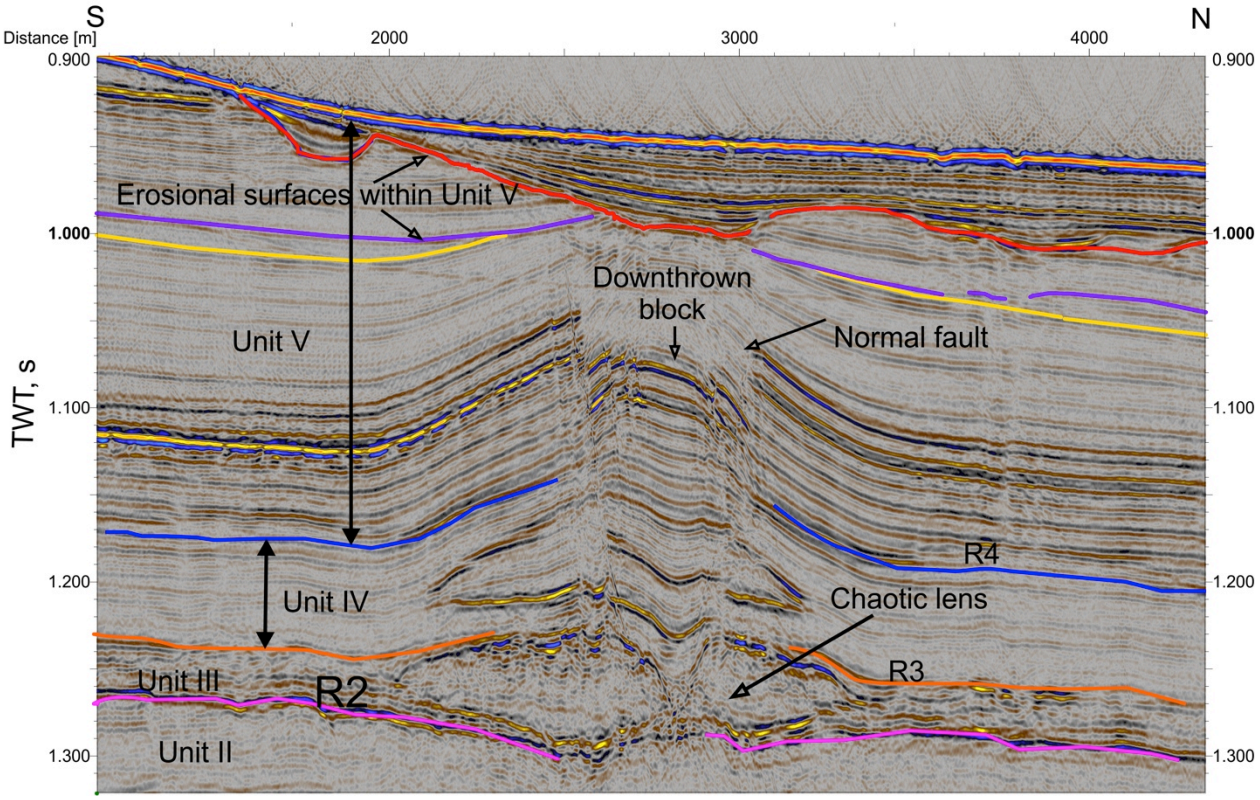

Figure 6.2.1.6. A N-S seismic profile shows two lens-shaped features in Units III and IV. The lens in Unit III shows weak stratification near the base and moderately chaotic reflection near the top. The lenses lie beneath an apparently E-W oriented downthrown block with fractured margins.

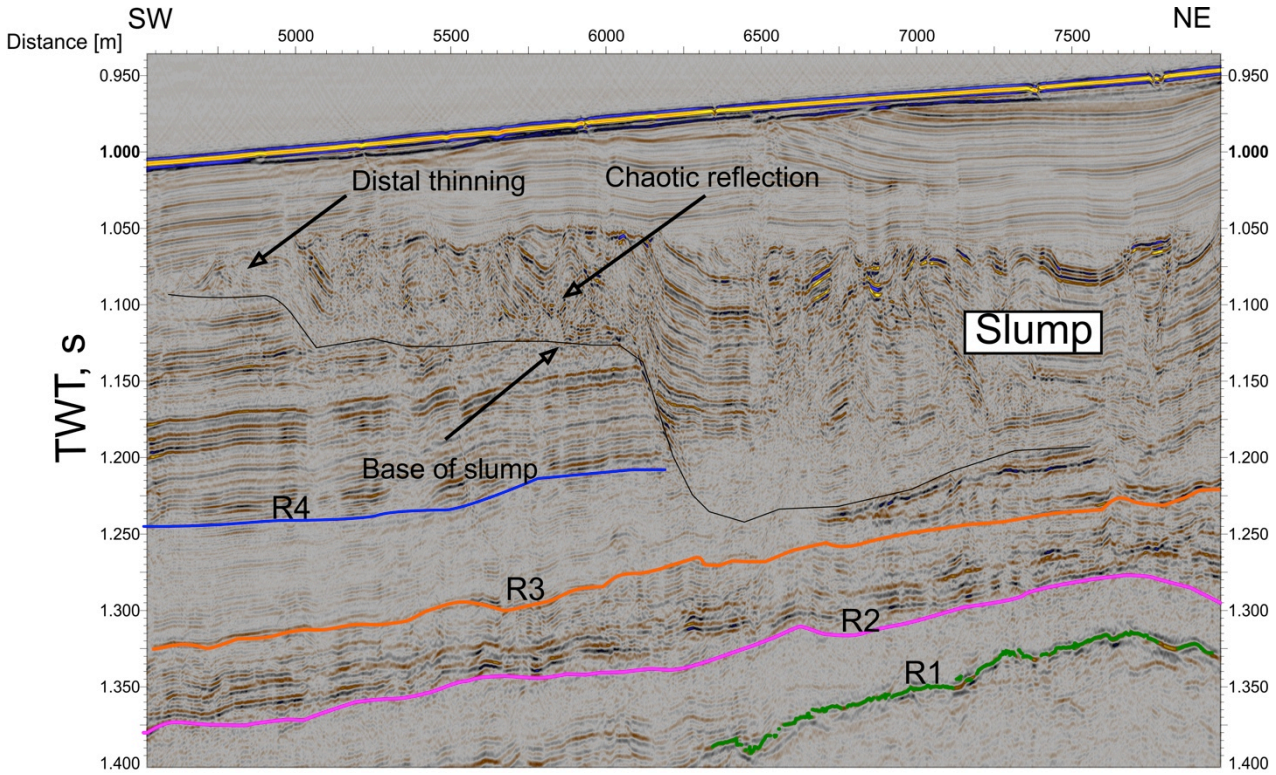

Figure 6.2.1.7. A deformed and chaotic interval within Unit V is shown. Its base truncates underlying strata. The top shows negative polarity reflections. Note the underlying SW limits of a lense in Unit IV.

We find it hard to establish a stratigraphic model for this study area. By inference from regional data, the lowermost horizon (R1) could represent an erosion and peneplanation surface that was formed following Late Cetaceous uplift. The wide-spread early Oligocene Marshall paraconformity [e.g. Carter et al. 2004] could be represented by one of the sharp boundaries observed in the seismic data (e.g. R2 or R3). The sedimentary succession at site 1 is also similar to seismic data shown in Lewis et al. (1986), where a sharp reflection interpreted to be of Oligocene age was identified below the extend of drilled Mid-Miocene to Recent strata. Mid/Late Oligocene to Recent strata around the Chatham Rise typically consist of chalks and nannofossil [Carter et al. 1999; 2004], and are likely to be encountered in the upper part of the sedimentary succession (Unit IV - V). Strong seafloor erosion and pockmark formation prevented us from tying reflectors across the area within Unit V. However, eroded rims of the giant pockmark structures could provide sites to sample sediments of different ages within Unit V.

Many of the giant pockmark structures have common characteristics. These are

- An elliptical to irregular outline
- A typical profile with a sometimes steep incision on the up-dip side and a second often more gentle incision on the down-dip side and a later state sedimentary infill of cross-bedded strata typical of contourite drifts along the center (Fig. 6.2.1.2.-6.2.1.4.)
- Evidence for gas chimneys and gas venting and the rim and towards the centre of giant pockmark structures (Fig. 6.2.1.2.-6.2.1.4.)

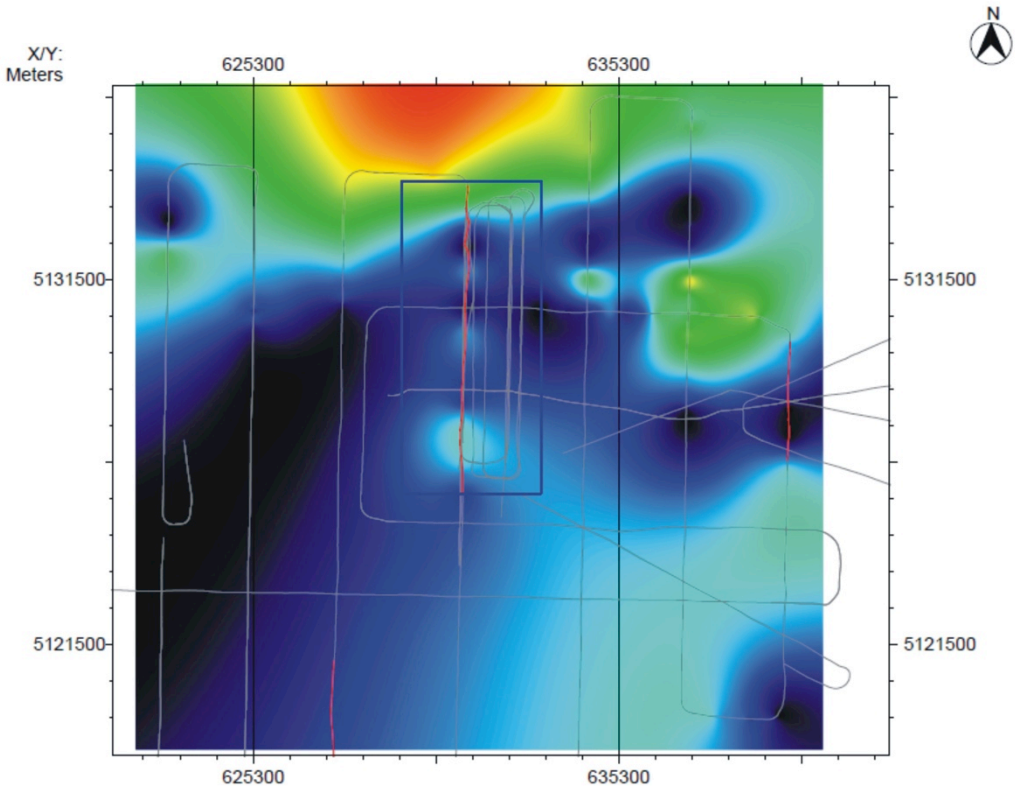

Figure 6.2.1.8. Isochron map of reflective intervals beneath R1, indicating a WSW-ENE structure

The latter suggests that gas venting was the driving factor in the formation of the giant pockmark structures, although large central vents have not been encountered. Various stages of contouritic infilling indicate that currents along the southern Chatham rise have played a role in the shaping of the elliptical to irregular structures. Mapping of northward dipping strata within Unit I showed a WSW – ENE orientation of older strata onlapping basement (Fig. 6.2.1.8.). The coincidence of some of the gas escape structures with the trend of onlap of strata within Unit I indicates a deeper origin of some of the migrating gas.

It is not clear whether gas migration to the seafloor in the past created pockmarks or accumulations at the base of the depressions led to their sudden development as outlined by Davy et al. 2010. Either formation mode structure was likely eroded by currents at a later stage. A detailed analysis of the 3D P-cable seismic survey may help to understand gas migration and its release at the seafloor through time and the role of faults in gas migration.

Bottom simulating reflectors indicating the presence of gas hydrate were not identified anywhere at site I. Integration of OBS data with the 2D and 3D seismic surveys may help to resolve a potential role of gas hydrate in the formation of the observed structures.

6.2.1.2. 3D P-Cable

The region for the 3D cube of working area 1 (Fig. 6.2.1.2.1.) was chosen based on the 2D multichannel seismic reconnaissance lines and findings in the PARASOUND data. The bathymetric mapping revealed a set of three circular to oval shaped pockmark depressions in working area 1. During the 2D seismic survey and the bathymetry mapping with PARASOUND recordings gas flares were observed in the water column. They line up along the western rim of the pockmark mapped in the centre of the working area.

In order to achieve a reasonable coverage with the P-Cable the line spacing for the profiles was set to 40 m. A GI airgun of 105 cinch / 105 cinch was fired every 5 sec. at 210 bar as seismic source.

During 7 days of active profiling a cube with 3.5 km * 6 km could be covered. Without further trace interpolation the cube could be migrated with an inline spacing of 3.125 m and a crossline spacing of 6.5 m.

Due to the short length of the streamer sections and the strumming of the cross cable the signal to noise ratio is not as good as with the much higher fold of the 2D streamer data. Nevertheless all major structural elements that are of importance for the region are well imaged in the cube. A wide spread feature found on the 2D seismic lines are lens shape bodies that are limited to the top with an inverted reflection event. Internal transparency further supports the interpretation of a sediment body with gas content. In the 2D seismic images several of the top layers of the lens shaped bodies show interrupted short length reflection events. These events continue vertically along faults.

Such a lens shaped body is well covered within the 3D data cube. Fig. 6.2.1.2.2. images the lateral extend of the top interface of such a lens shape body. Close to the western termination of the body a fault could be observed, which may serve as gas migration pathway. Images of three prominent reflection events from within the fault area are shown in Fig. 6.2.1.2.2. The outline of the reflection events reflects the circular shape of the fault. Beside these example of a degassing feature above a lens shaped body several other gas migration pathways are visible in the 3D cube. The data quality will be sufficient to fully map and interpret the different fluid flow path that can be observed underneath the active seeps at depth.

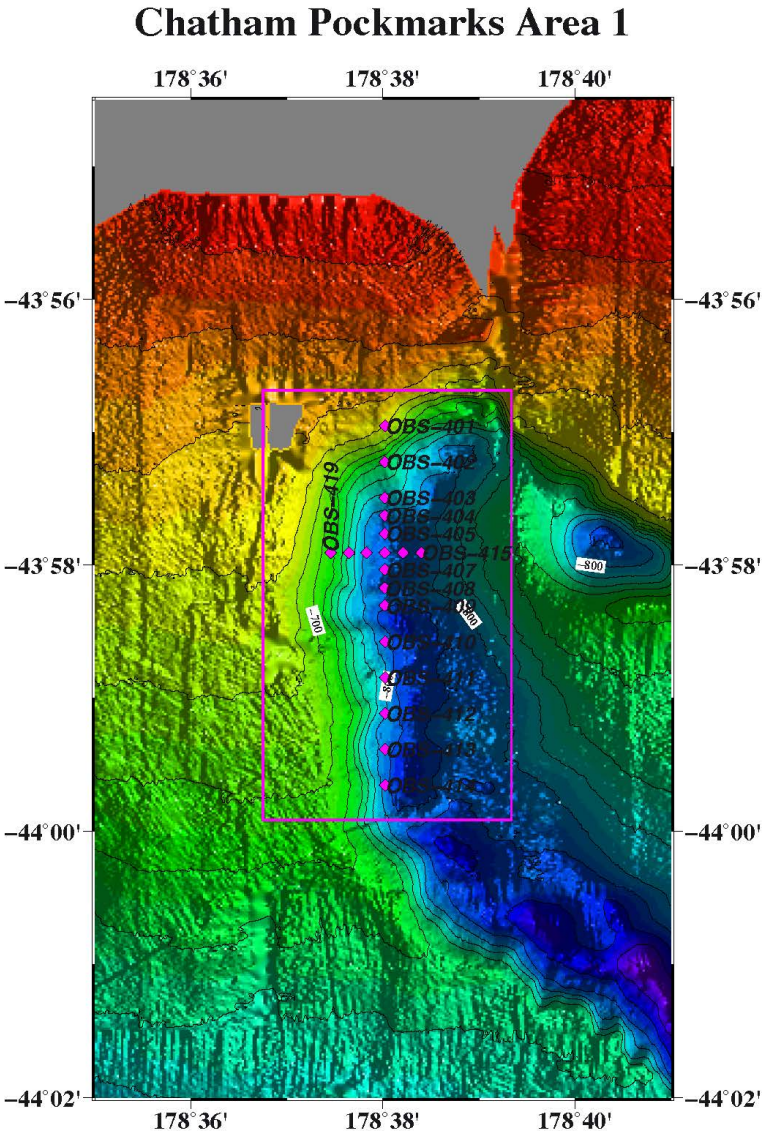

Figure 6.2.1.2.1. Map of the pockmark area 1

purple box indicate the 3D seismic volume area

purple diamonds indicate OBS positions

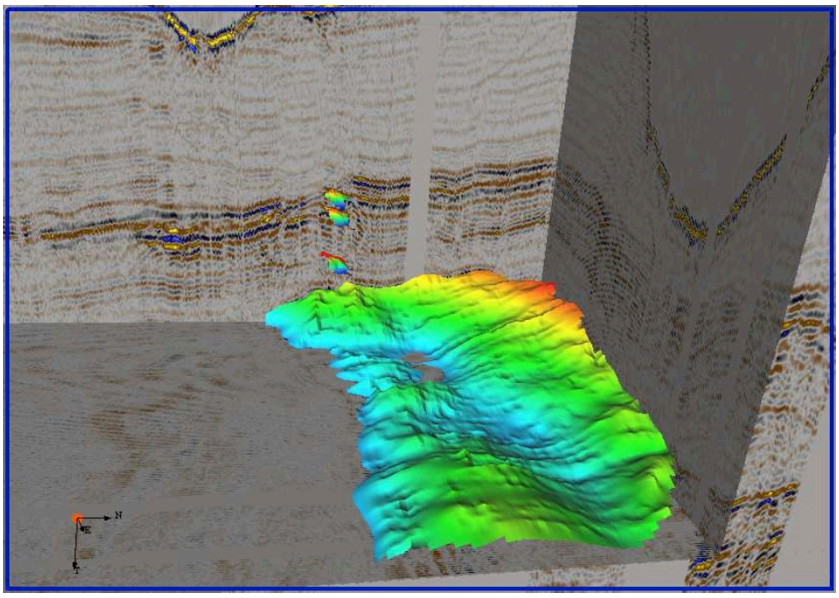

Figure 6.2.1.2.2. 3D chair cut image of working area-1. The top of the gas containing lens shaped body is marked as coloured plane. At the western end of the chair cut the seismic image shows a fault with bright reflections and a thin vertical transparent zone which is interpreted as fluid migration pathway. The bright spots in the fault are mapped in colour.

6.2.1.3. OBS data in area 1

In the first, most eastern area, three OBS equipped with different recorder types (MBS, MES from Send GmbH and Sercel) were deployed. At OBS 101 and OBS 103 two seismometers were attached. The geophones were either directly tightened to the anchor or attached to an arm, lying freely on the ocean bottom after deployment (Fig. 5.2.3.2.). The third instrument OBS 102 contained the Sercel recorder and a standard geophone and hydrophone. The instruments were deployed on the 12th of January. This deployment was meant as a test of different ways to attach the geophones to the OBS and to test the different recorder types, which all can run with high sampling rates of up to 1000 Hz.

After shooting the 2D profiles P1000 to P3000 with the 200 m long streamer, all three instruments were recovered successfully on January 13th. OBS 102 did not record properly and it was decided not to use the Sercel recorders during cruise SO226. OBS 101 (MBS) and 103 (MES) recorded well during the whole deployment. The signal shape and the signal-to-noise ratio of the two recorders were different; thus, it was decided to use MBS recorders for all coming deployments on SO226. The gain was adjusted to prevent the data being clipped. As it turned out, a first comparison of the two geophone attachments resulted in a slight better signal from the free standing seismometer isolated from the possible swinging OBS frame (Fig. 6.2.1.3.1.). Afterwards, it was decided to deploy as many OBS as possible with a free standing geophone. One OBS in every deployment was equipped with two geophones throughout the whole survey to have the possibility of cross-checking the signal quality independent of the deployment site.

On the 14th of January, a total of 19 OBS were deployed along 2 lines in Area 1 (Profile P4000, see Fig. 6.2.1.3.2.). The instrument positions were chosen based on the collected 2D streamer data, PARASOUND data and the observed bathymetry. The two lines are situated in the centre of the 3D-seismic cube. The East-West profile P4001 crosses the North-South trending profile P4002 above OBS 406 and contains 6 OBS. At line P4002 14 instruments were installed. The trigger signal was recorded separately from the P-cable streamer system on one additional MBS recorder in the laboratory. After finishing the 3D shooting, all OBS were successfully recovered during the day of the 26th of January (local time). Except OBS 412 which had corrupted data on the hydrophone channel, all OBS held usable data of high quality. The geophone test showed similar results compare to the first deployment favouring the free standing geophone.

Fig. 6.2.1.3.3. to 6.2.1.3.5. show data examples of the collected profiles. All instruments have a similar high data quality. The sampling rate of the OBS is 1000 Hz; thus a high resolution of the shallow subsurface is obtained. OBS 403 was compared to the P-Cable data of line P5102 (Fig. 6.2.1.3.6.). It shows a good correlation of the seismic phases. This comparison can help to define the reflection phases on all the deployed ocean bottom seismometers on that line. With this data set it will be possible to obtain a velocity field which can be used for the migration of 2D and 3D seismic data.

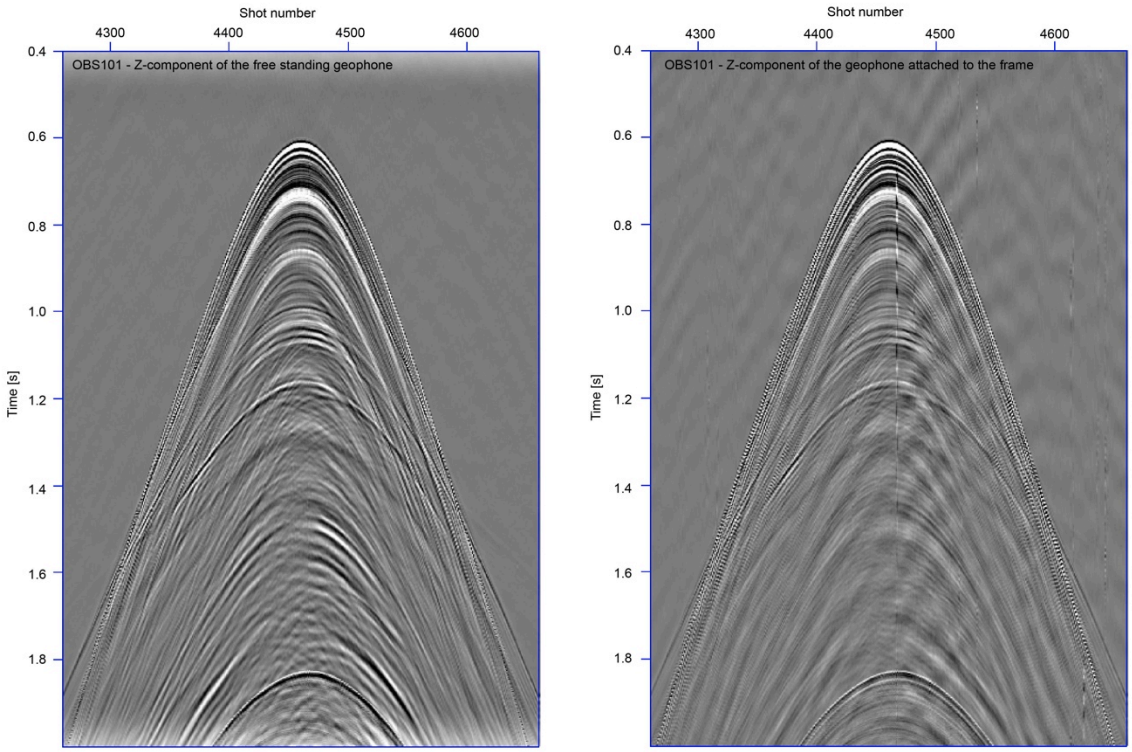

Figure 6.2.1.3.1. First results of a geophone test. Two geophones were deployed at one recording unit. The left the geophone was attached on an arm for the deployment that will be release after the instrument reached the seafloor. Thus, it is free standing on the seafloor, only connected via a data cable to the OBS frame. The right the geophone was attached to the frame standing on the anchor (compare to Fig. 5.2.3.2).

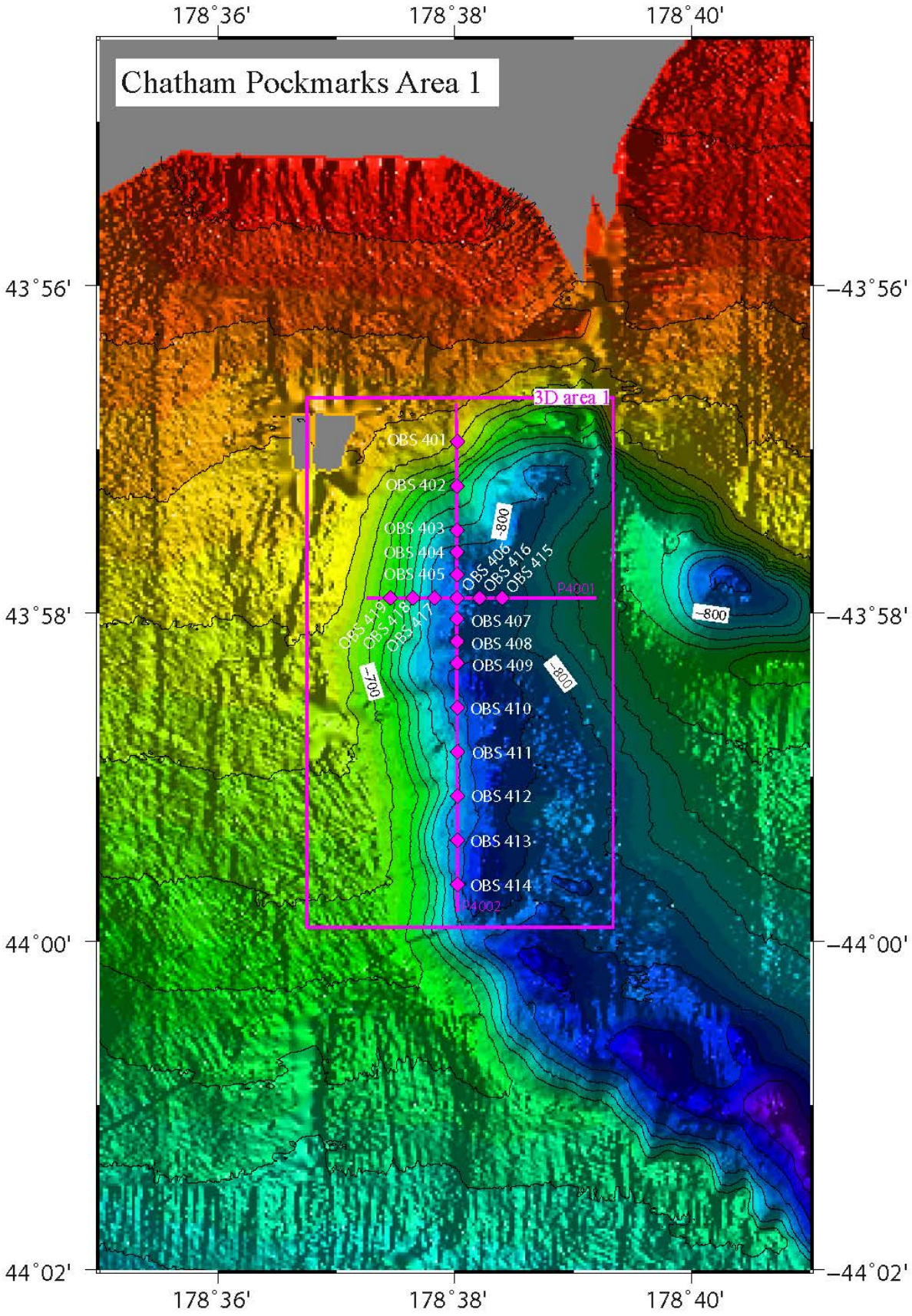

Figure 6.2.1.3.2. Map overview of the deployed ocean bottom seismometers and the profiles.

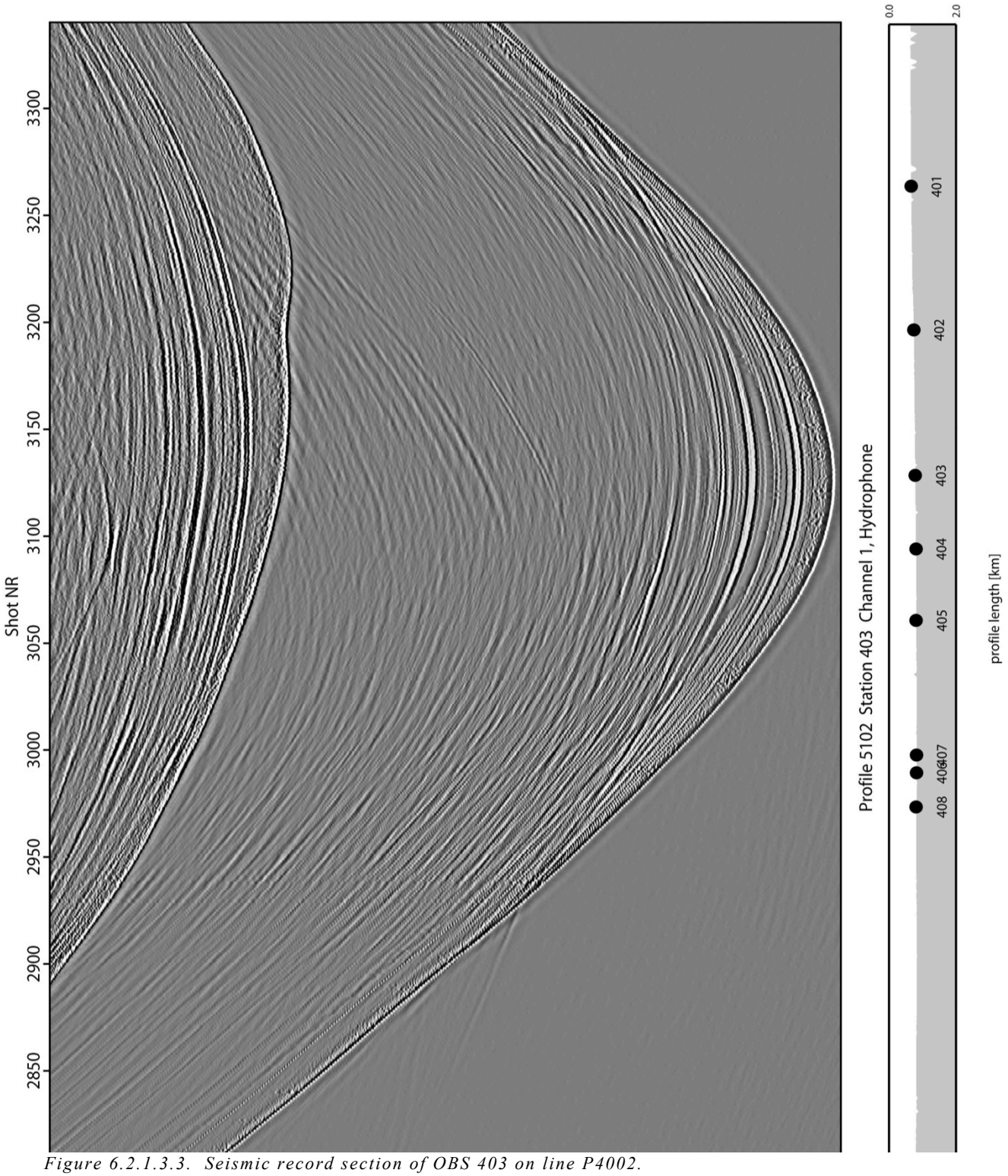

Figure 6.2.1.3.3. Seismic record section of OBS 403 on line P4002.

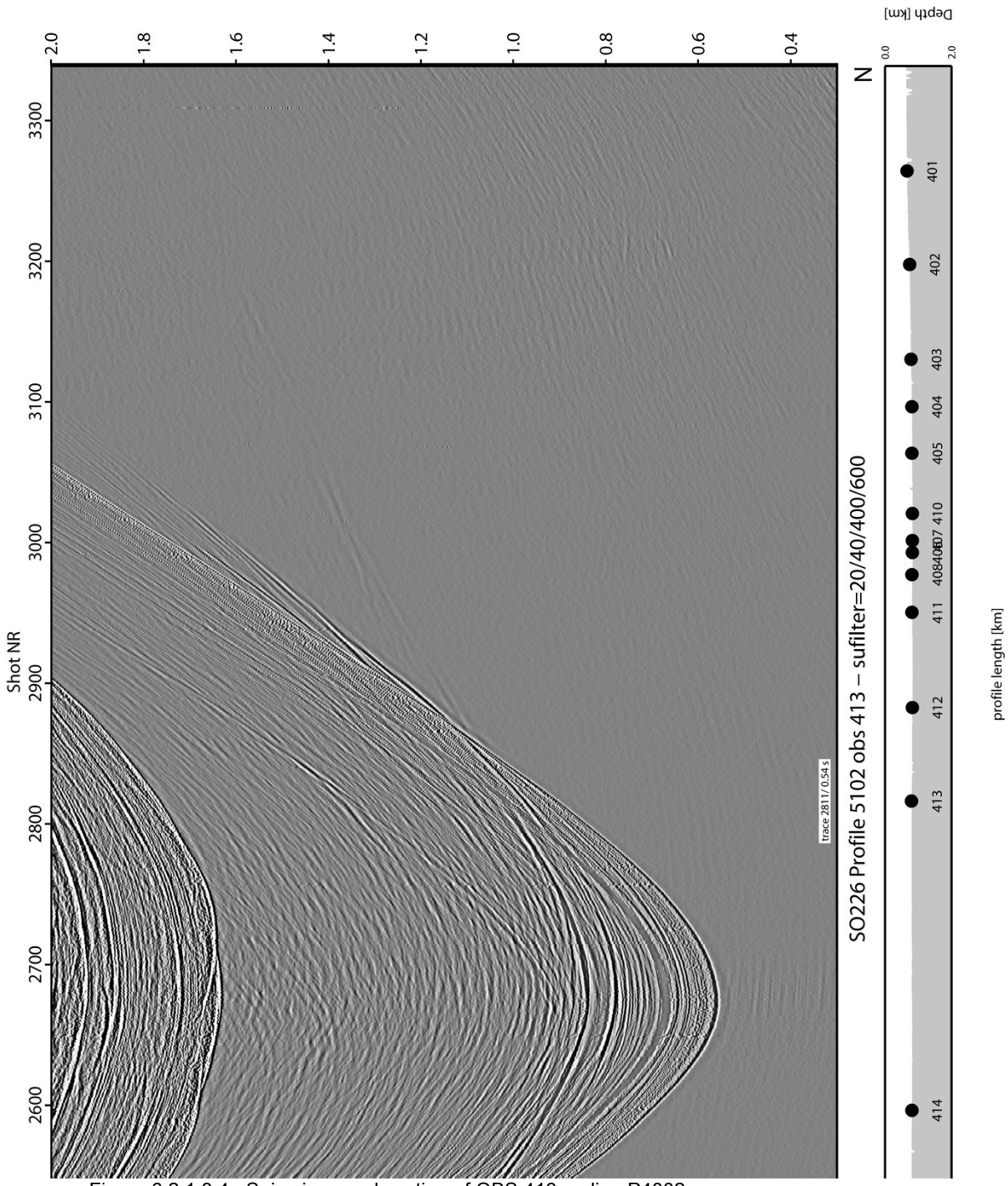

Figure 6.2.1.3.4. Seismic record section of OBS 413 on line P4002.

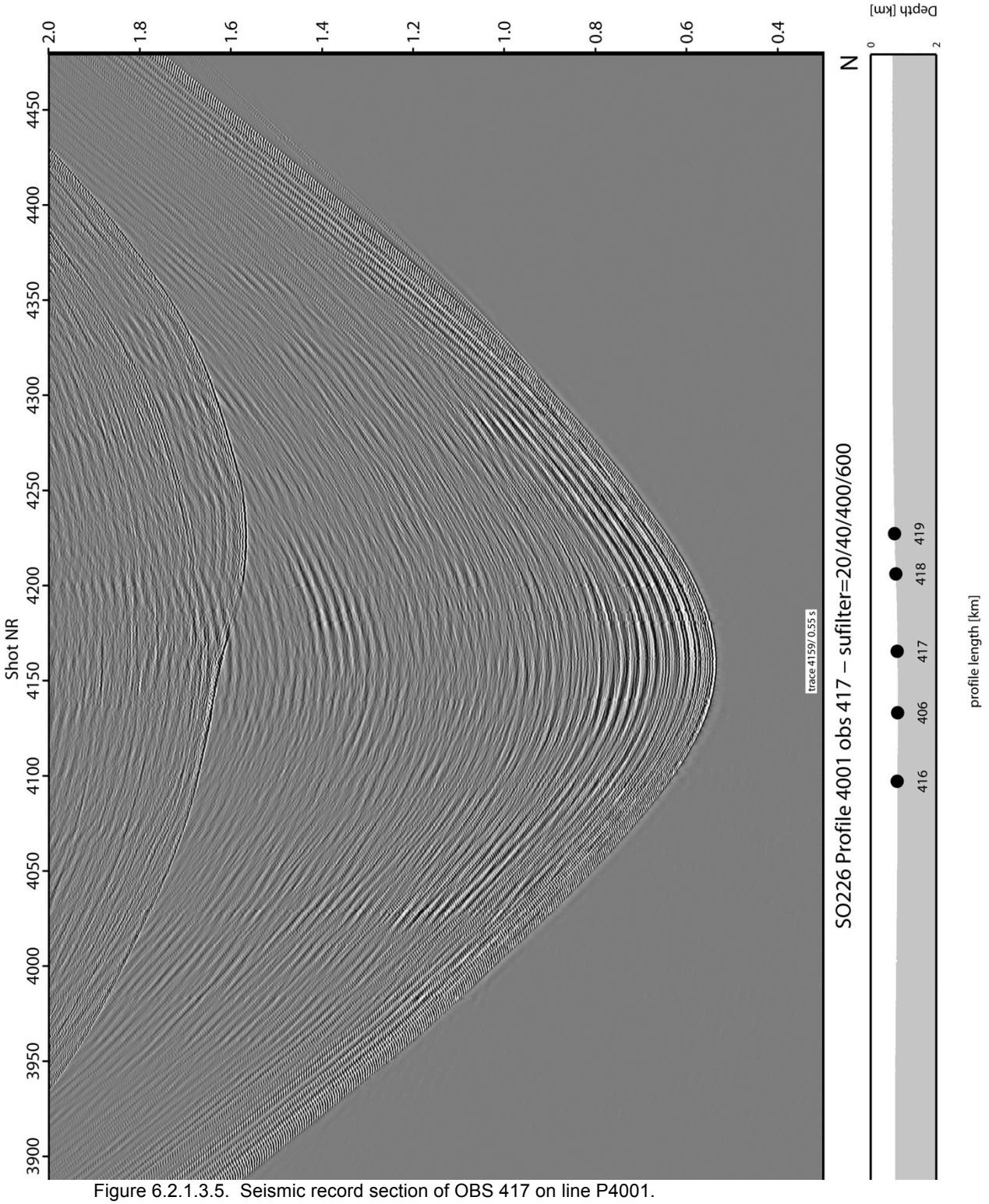

Figure 6.2.1.3.5. Seismic record section of OBS 417 on line P4001.

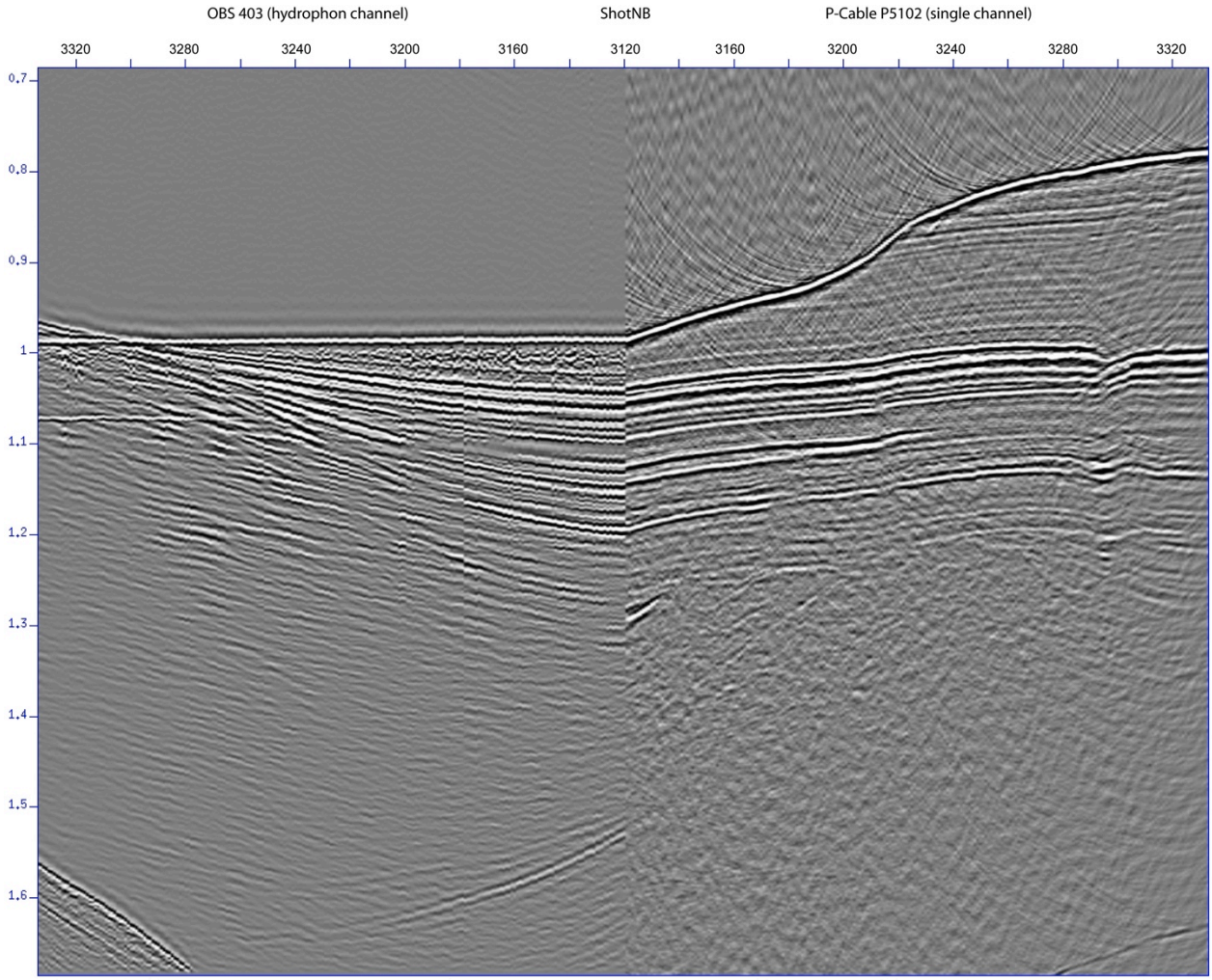

Figure 6.2.1.3.6. Comparison of OBS403 on line P5102 (left part of the figure) and a short streamer section of the P-cable (right part of the figure). A good correlation of the reflected phases is observed.

6.2.2. Area 2

6.2.2.1. 2D Seismic

The 2D survey of site 2 covers a 20 x 25 km wide area on the southern Chatham Rise (Fig. 6.2.2.1.). It shows a stratigraphic succession similar to site 1 (Fig. 6.2.2.2.). Two higher amplitude intervals (Unit III and V) each overlie a less reflective unit (II and IV). Horizon R1 is less well defined in this area but inclined strata can be identified underneath down to 2700 ms. Unit II is thicker whereas Unit III is thinner in site 2 than in site 1 and reflectors are less continuous in Unit II. In the lower part of which is tentatively marked as Unit IV, an undulating and in part poorly stratified unit occurs. It appears to be in unconformable contact with the upper part of Unit IV.

Small scale faulting and folding is typical in units IV and V. Blanking around faults, disruption of sediment layers and updoming is common. Brightening of reflectors along faults also occurs and suggests that faults are gas conduits (Fig. 6.2.2.3.). Multiple erosional stacking of cross-bedded sedimentary bodies indicates widespread channel incision and migration in the upper 200ms (Fig. 6.2.2.3.).

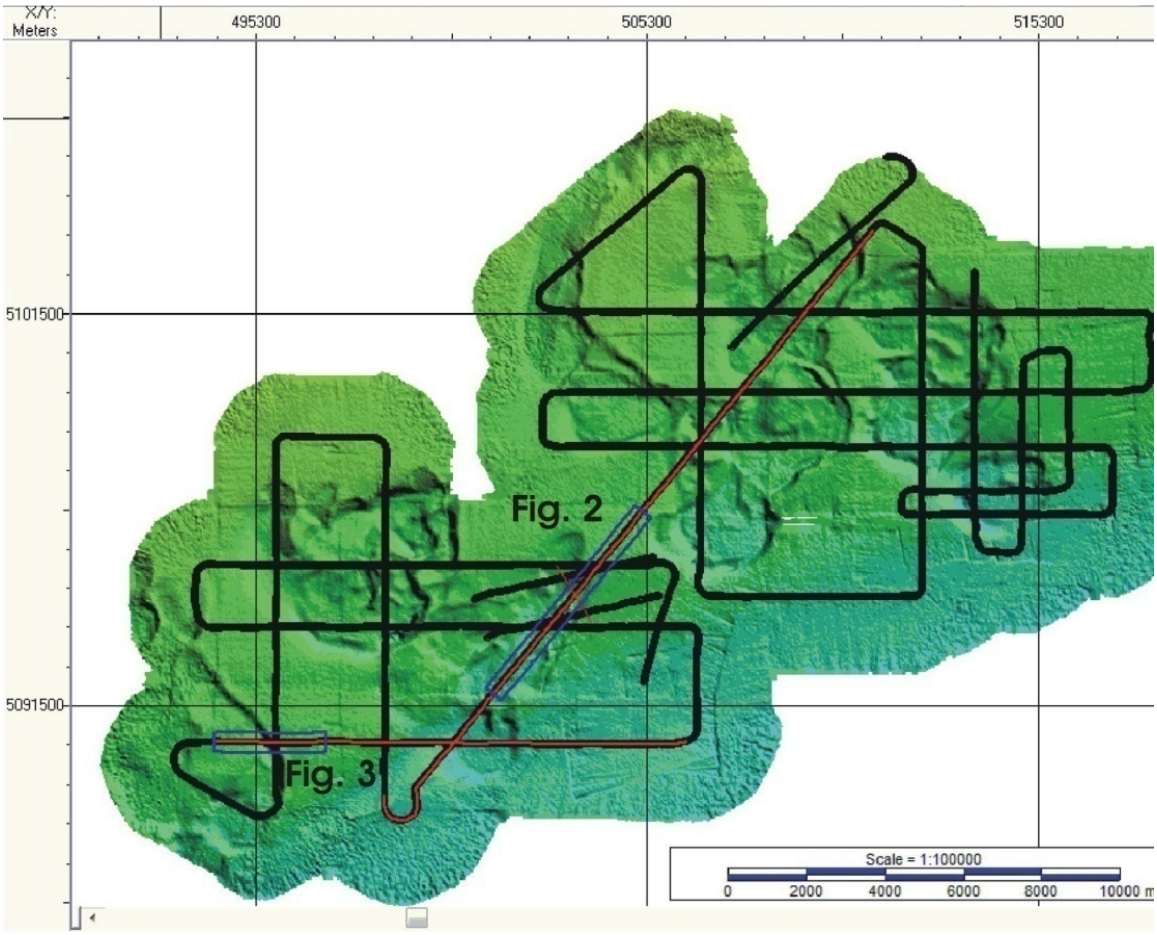

Figure 6.2.2.1. Map showing multi-beam sea floor topography and extend of 2D seismic lines

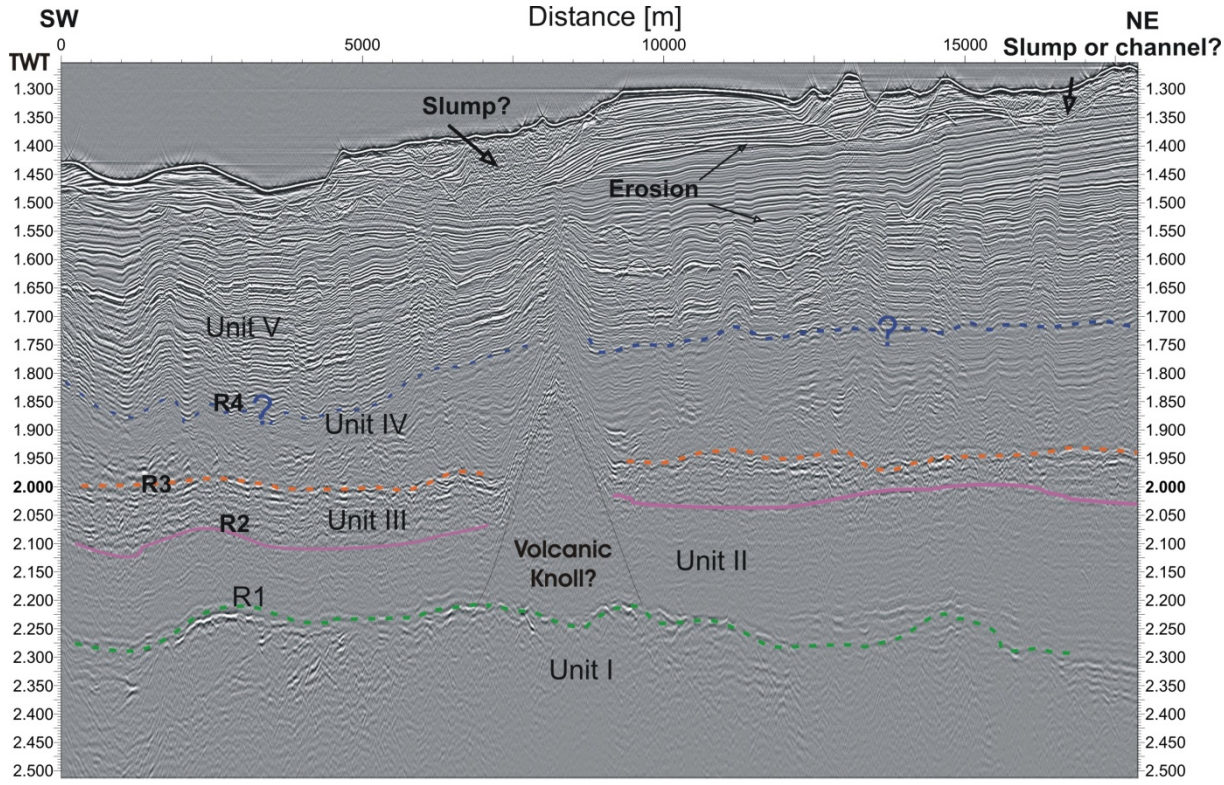

Figure 6.2.2.2. Line through the central part of site 2 and tentative interpretation of seismic stratigraphic units

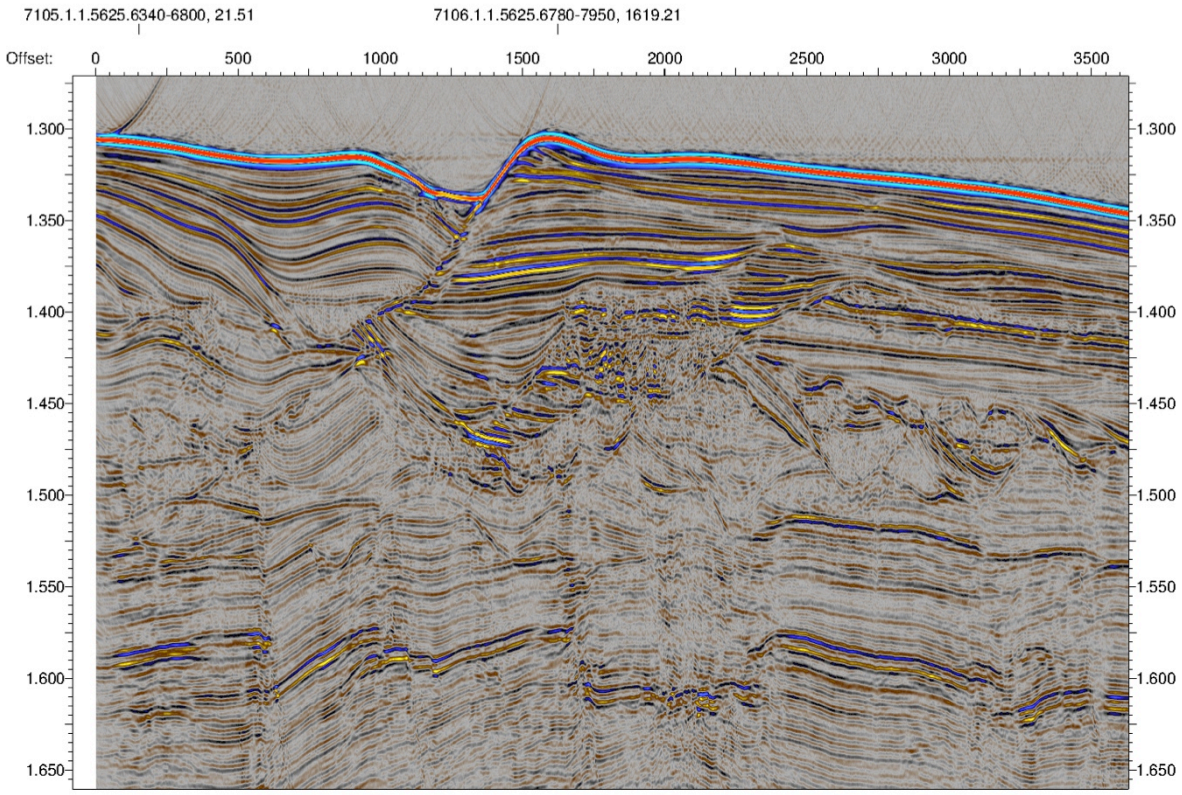

Figure 6.2.2.3. Detail of Unit V, showing stacked incised channels. Note bright reflectors in the lower part that are widely traceable, fracturing and brightening along faults

Differential erosion and channel migration may explain the more complex seafloor topography at site 2. Fractured areas and faults that may be gas conduits rarely reach the surface but are common beneath the stacked channel interval.

At two sites buried mounds that may be Late Cretaceous or younger volcanic knolls were encountered. One of the knolls is located in the northeast of the survey area and the other in the center, at the site of the 3D survey. A similar feature was described in Lewis (1986).

6.2.2.2. 3D P-Cable

As there was no information on the subsurface structure of area 2 available a set of 2D multichannel seismic lines was acquired prior to the final decision on the location of the 3D cube. Test shots undertaken with a small volume GI airgun (45 cinch / 45 cinch) proved that the same depth penetration could be achieved as with the larger (105 cinch / 105 cinch) GI airgun. At the same time the frequency content of the seismic source signal could be expanded to about 350 Hz (250 Hz with 105/105 cinch). Consequently the resolution of the sedimentary layers could be significantly improved.

The location of the 3D cube and the deployment positions of the 18 OBS are shown in Fig. 6.2.2.2.1. Bathymetry mapping revealed a set of seafloor depressions interpreted as pockmark structures. Other than in the first working area the pockmarks are not separated from each other and intersect across their circular structure or seem to be washed out by currents. The 2D survey revealed two different systems of upward migration pathways for fluids. The majority of the pockmarks do show a continuous base horizon (Fig. 6.2.2.2.2.). As with the pockmarks of the previous region it seems that their inner part must have been eroded entirely. The sedimentation has been strongly influenced by contourites. Below the circular and eroded rim of the pockmarks there are several faults were observed that are coinciding with transparent parts in the seismic sections. This type one

structure is similar to the features observed with the pockmarks in the first working area. Two of the investigated pockmarks do show a different structure of a gas chimney at depth (Fig. 6.2.2.2.3.). The second system (type two) is characterised by a 250 m wide transparent zone underneath the pockmark. This is interpreted as an ancient feeder channel and can be traced vertically for about 2 km. Reflection events from an interface imaged beneath this vertical channel bend upwards in conical shape at this location. This feature may be completely covered and imaged by the 3-D seismic volume subsequently acquired (Fig. 6.2.2.2.4.). The horizon below this interface shows a rough topography but no signs for fluid migration pathways. The top of the feeder channel can be imaged until it intersects with the erosional horizon forming the original base of the pockmark. Infilling sediments involving multiple periods of infill are seen above this erosion surface and are extensively imaged elsewhere in Area 2.

An area of 2.8 km * 5 km above a type two feeder channel system was chosen for the 3D survey area. Due to technical problems the offsets of the streamer sections were reduced to 9 m and hence the line spacing of the 3D profiles need to be reduced to about 35 m only. Within five days of continuous profiling the data cube could be well covered. The 45 cinch / 45 cinch GI airgun had been tested for signal quality prior to the start of the cube acquisition. Hence the lines could be recorded with an increased shot rate of 4 sec. The coverage of the cube was successful enough to migrate the data on 3.125 m * 3.125 m grid. Fig. 6.2.2.2.4. shows a chair cut image from the 3D cube volume. The time slice on top highlights the outline of the top end conical shaped reflection interfaces raising from a sediment boundary at 1.95 s TWT. The sidewalls of the chair cut confirm the conical continuity of the structure. Velocity information from the OBS observations is required to further judge on the nature of the conical body.

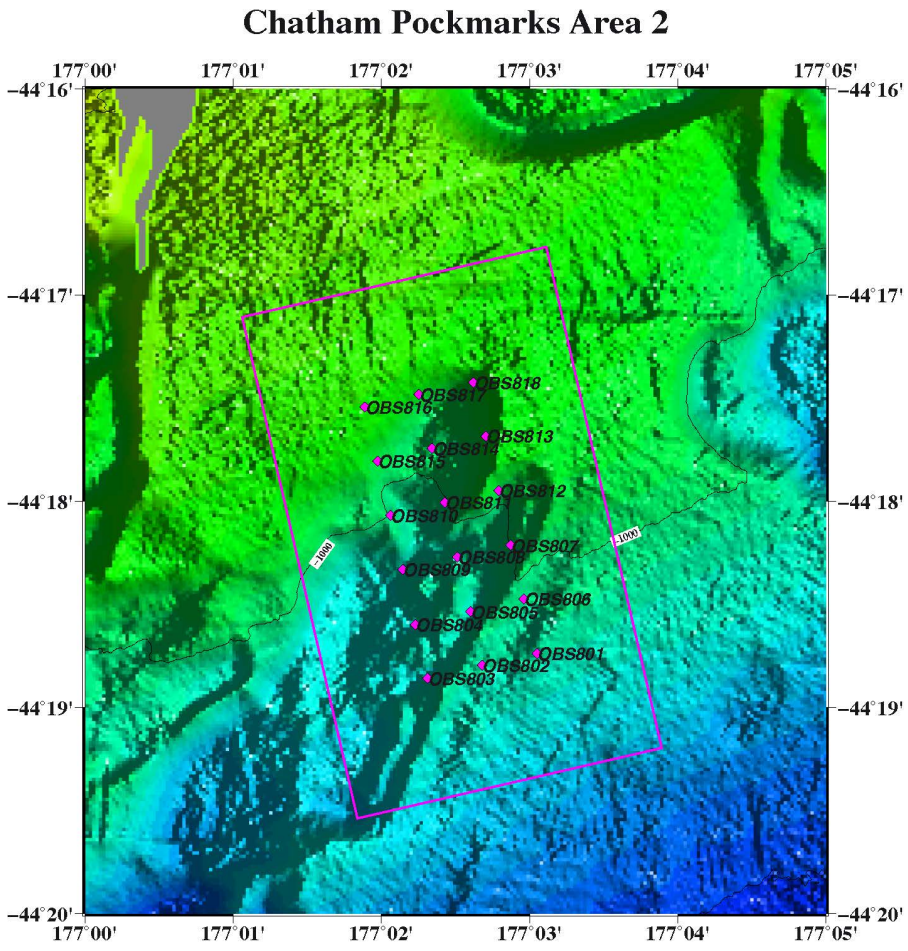

Figure 6.2.2.2.1. Map of the pockmark area 2

purple box indicate the 3D seismic volume area

purple diamonds indicate OBS positions

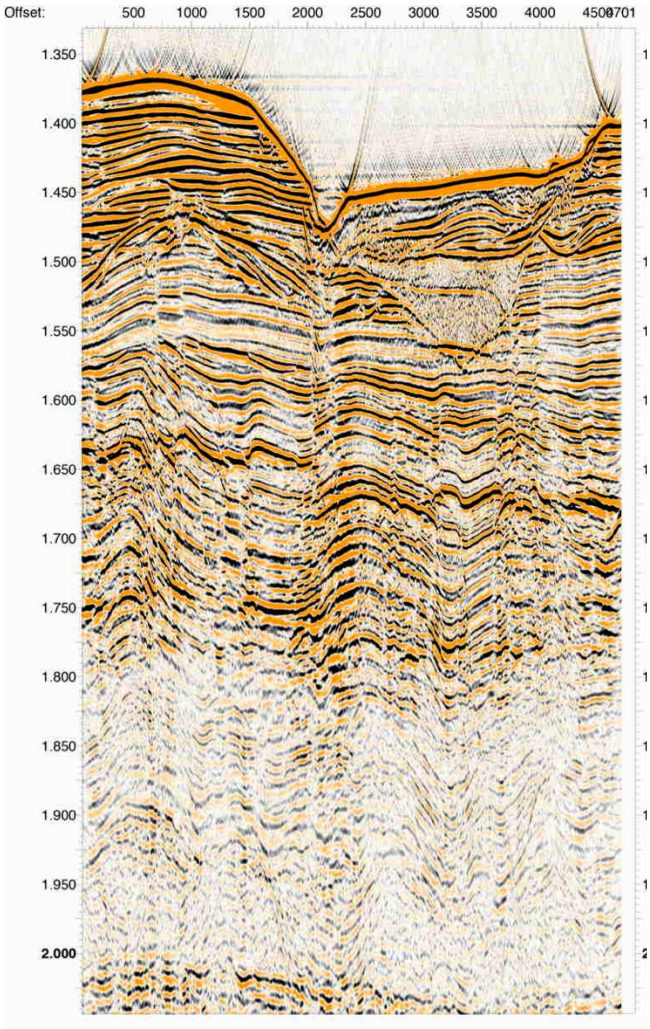

Figure 6.2.2.2.2. 2D seismic image of a pockmark with type one feeder system. Near vertical faults can be traced beyond the rim of the structure all the way to the seafloor. The former eroded base of the pockmark has been covered with sediment refill.

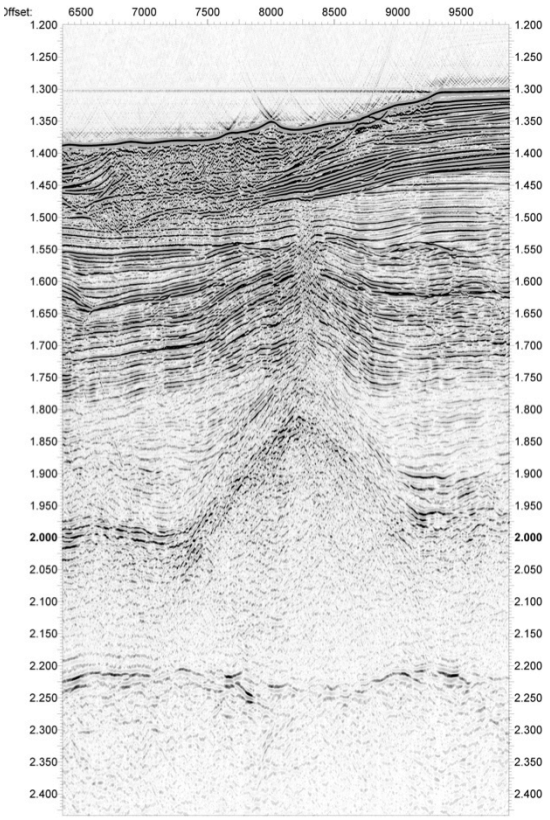

Figure 6.2.2.2.3. 2D seismic image of a pockmark with type two feeder system. A conical shaped uplift of deeper sediment interfaces opens into a broad transparent zone, interpreted as ancient feeder channel.

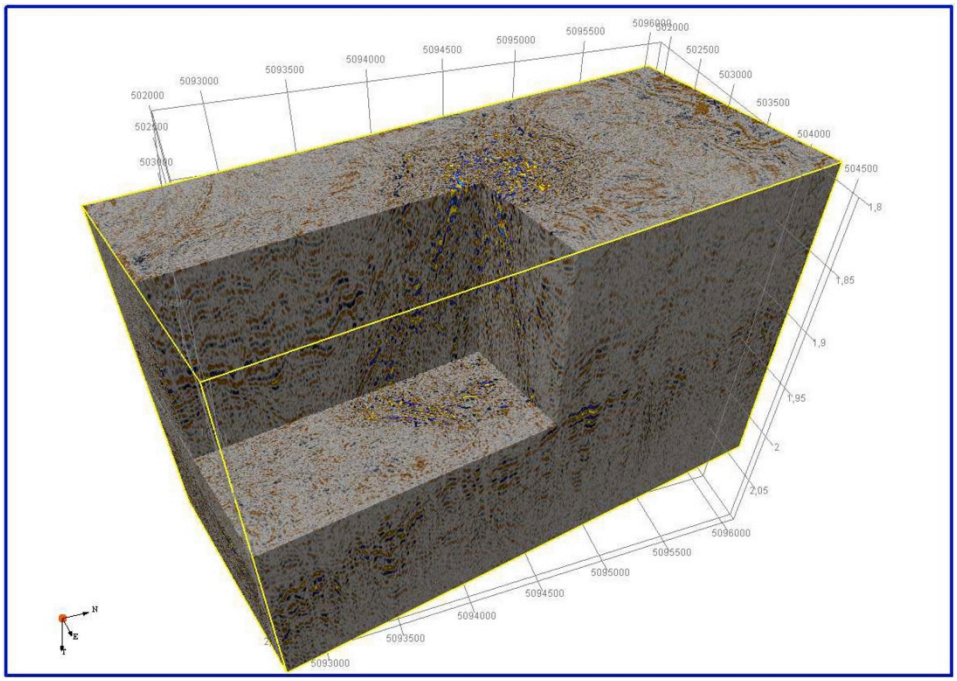

Figure 6.2.2.2.4. 3D chair cut image of working area-2. Blue and yellow amplitudes outline the limits of the conical shaped body leading upwards into a transparent zone.

6.2.3. Area 3

6.2.3.1. 2D Seismic

Working area 3 (Fig. 6.2.3.1.1.) has been chosen according to a PARASOUND profile (Fig. 6.2.3.1.2.) recorded during cruise SO169 in 2003. The bathymetry does show small scale pockmarks, which are limited to water depth shallower than 700 m. The PARASOUND profile shows a succession of 5 sediment packages, which are well separated by strong reflection amplitudes. Pockmark features are visible in the upper most 4 sediment horizons. Pockmarks, which open to the seafloor terminate at the depth of the next prominent reflection interface at about 19 m depth below the seafloor. The same pattern is observed for the deeper packages. Outline of the Pockmark features shows an opening at the depth of the prominent reflectors while the feeder channel terminates downwards at the next interface. The penetration of the PARASOUND signal fades out at about 65 msec below the seafloor (bsf). The prominent reflection horizons are interpreted as ancient seafloor images [*Davy et al.*, 2010b]. [*Davy et al.*, 2010b] correlated the prominent strong reflection interfaces with sea-level low stands during glacial / interglacial changes. Sea-level low stand causes dissociation of the uppermost gas hydrates and may cause the formation of small scale pockmarks, limited to a depth of 700 m where the gas hydrate is stable again.

The 2D seismic profile (GI airgun 45/45 cinch) shows a similar image of the sediment layers (Fig. 6.2.3.1.3.). Due to the deeper penetration of the source signal a further layer of buried pockmarks could be identified below the 65 msec of penetration achieved with the PARASOUND signal. A sediment layer with less strong internal reflection interfaces is found between 75 msec bsf and 115 msec bsf. Buried pockmark features are observed less often. Their depth continuation does not cross the full section of this sediment package but covers about 1/3 of the package thickness. Pockmark features cluster over a limited lateral extend distributed over the package thickness.

Between 115 msec and 150 msec the deepest sediment layer with buried pockmarks is observed. At later arrival times sediments are deposited along horizontal layers. No pockmark features are imaged within these horizons. Two graben like faults are observed in line 9103 (Fig. 6.2.3.1.4.). They are well imaged down to the multiple at 1.5 s TWT. Signs of gas content along these faults are not visible in the seismic image. A BSR, a first order identification of gas hydrates has not been observed in the sections.

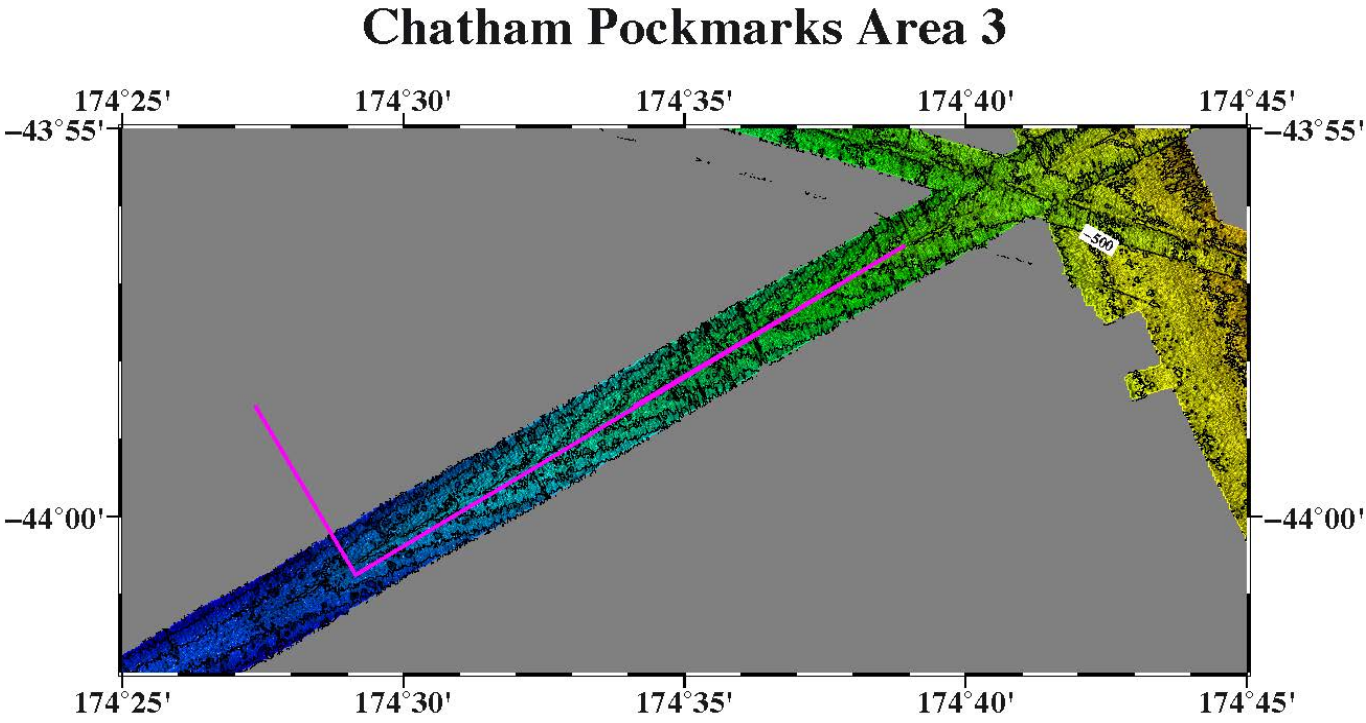

Figure 6.2.3.1.1. Map of the pockmark area 3. Purple line indicates the track of the 2D seismic profile

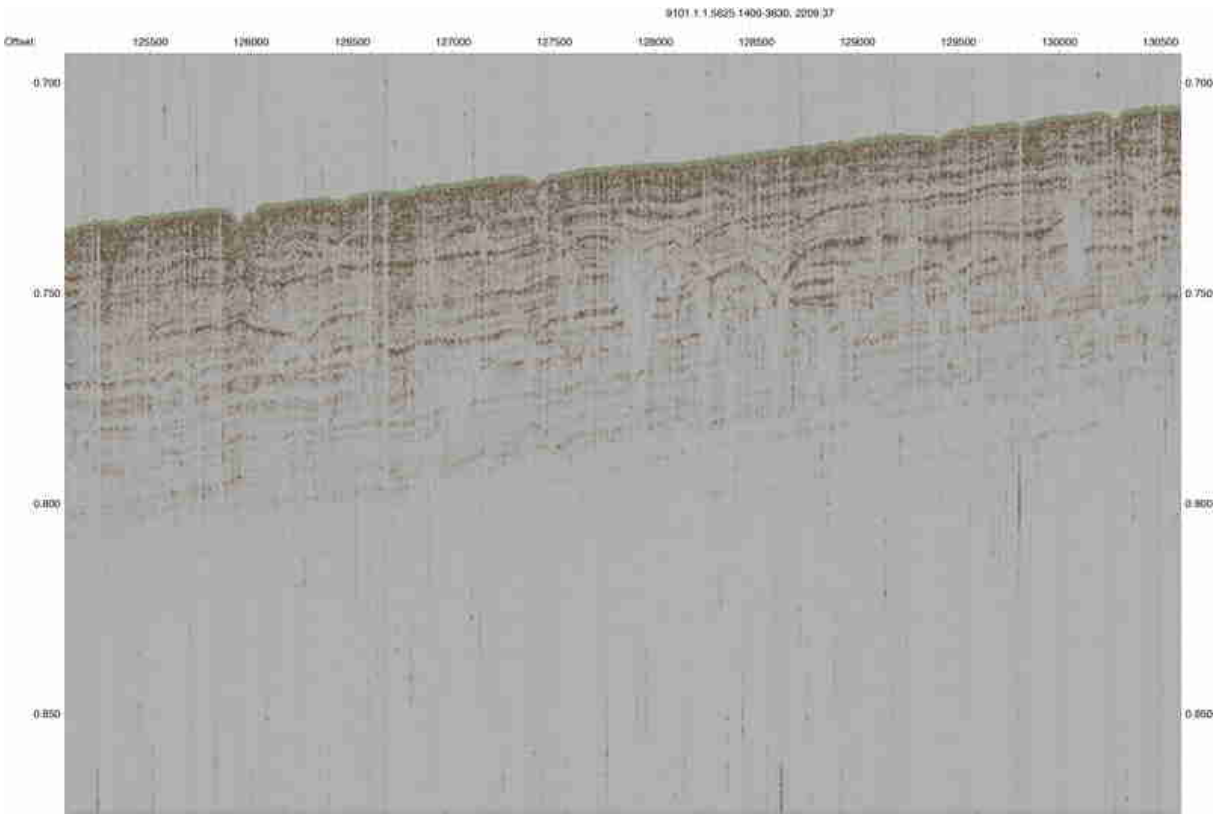

Figure 6.2.3.1.2. Parasound image of the pockmark area 3 recorded during SO169. Muliple sediment layers including recent and buried pockmarks are imaged down to about 65 msec traveltime (TWT)

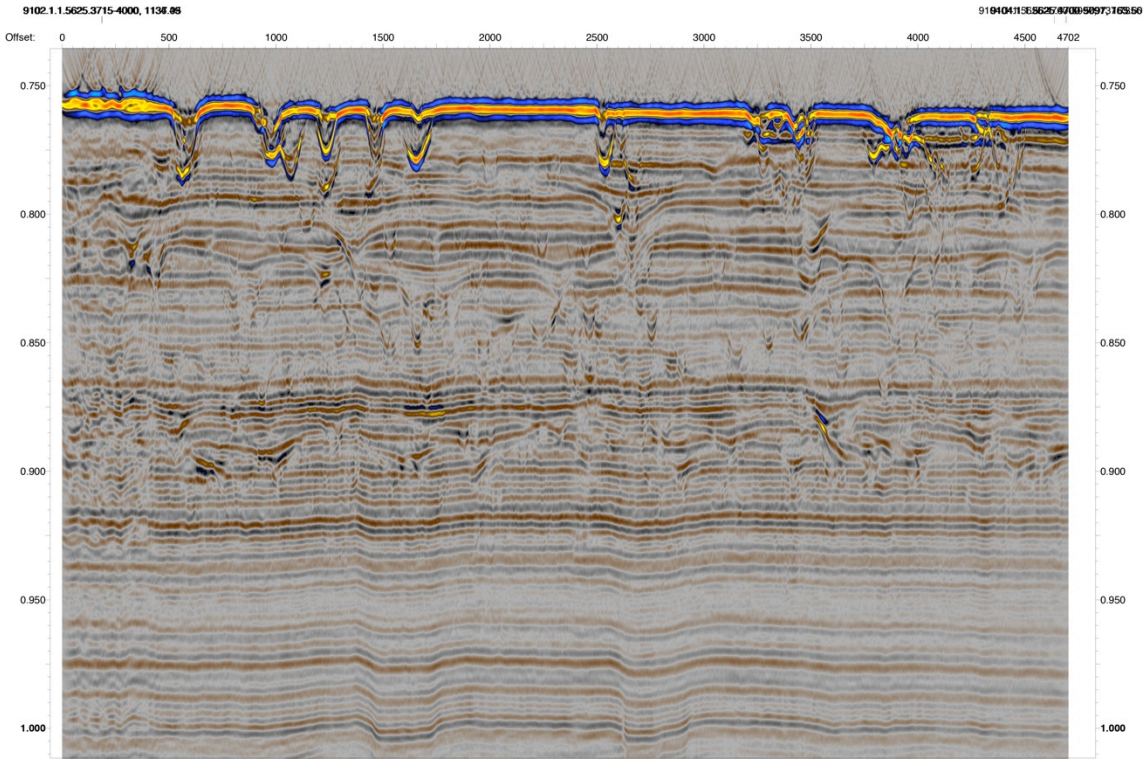

Figure 6.2.3.1.3. 2D seismic image of the pockmark area 3. The profile is coincident with the Parasound line of SO169. Burried pockmarks are imaged down to traveltimes of 150 msec below seafloor.

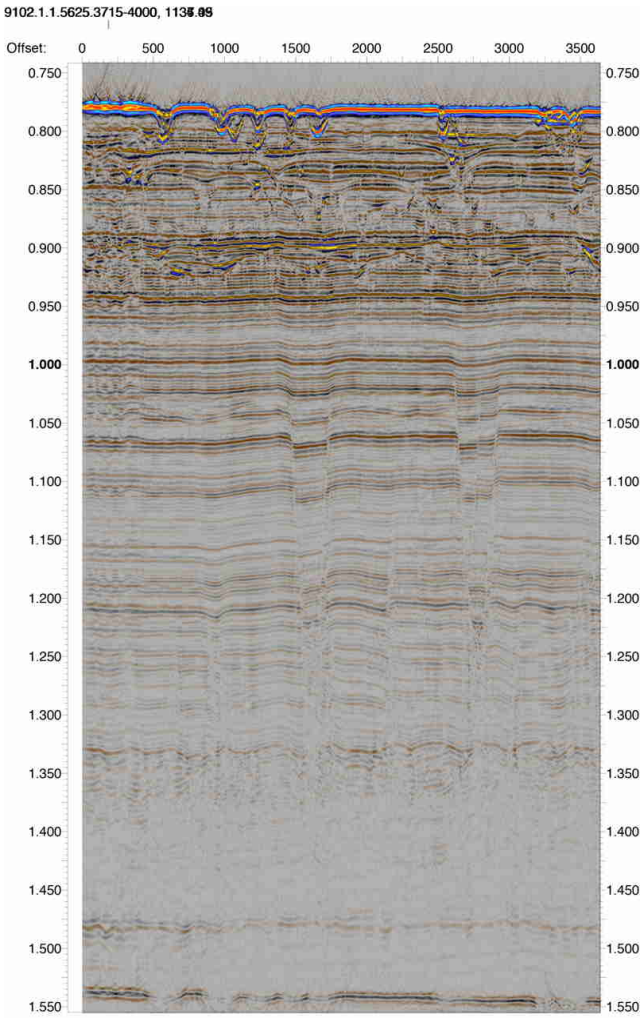

Figure 6.2.3.1.4. 2D seismic image of the pockmark area-3. Buried pockmarks do not appear within sediment reflections deeper than 150 msec traveltime (TWT) below the seafloor. Two graben like faults cut through the strata at least as deep as the multiple event at 15. s (TWT).

6.2.2.3 OBS data and results from Area 2

After reaching the second research area, 10 OBS were deployed in two separated W-E lines on January the 28th. Afterwards the streamer was deployed and several lines of 2D seismics, crossing the OBS were shot during 27 hrs. The shot interval was 3 s with a smaller airgun volume of two times 45 l, than used in the first research area.

The north-eastern line P7115 contains OBS 701 – OBS 705 (Fig. 6.2.2.3.1.) and on the southeastern line P7102 five instruments were deployed (OBS 706 – OBS 710). All instruments were successfully recovered during 5 hours on 29th of January. OBS 701 had a battery problem and though did not record any data; the others did record properly, while on the second line OBS 707 had the same issue.

The main target of the deployment was to provide velocity information for 2D seismic processing and to get a second imaging possibility apart from the streamer seismics.

Shot gather examples from line P7102, OBS 703, and line P7115, OBS 708, are shown in Fig. 6.2.2.3.2. and 6.2.2.3.3., respectively.

After the recovery of the 10 OBS of profiles P07, at February 29th, 18 OBS were directly redeployed in the area of the 3D cube (Profile P08) in lines of three OBS (each line in W-E direction) to cover nearly the whole 3D-cube as seen in map 6.2.2.3.4. The location of the instruments was chosen after analyzing the seismic sections from the 2D shooting. They were centered in the planned 3D cube.

After the 3D shooting, the OBS were recovered during daytime of February the 3rd. Except for one hydrophone channel, all channels recorded and all OBS held data of high quality. Their analysis will provide useful velocity information for the future 3D processing.

Fig. 6.2.2.3.5. shows data from line P8158 (OBS 802), while figure 6.2.2.3.6. shows OBS 809 (line P8131).

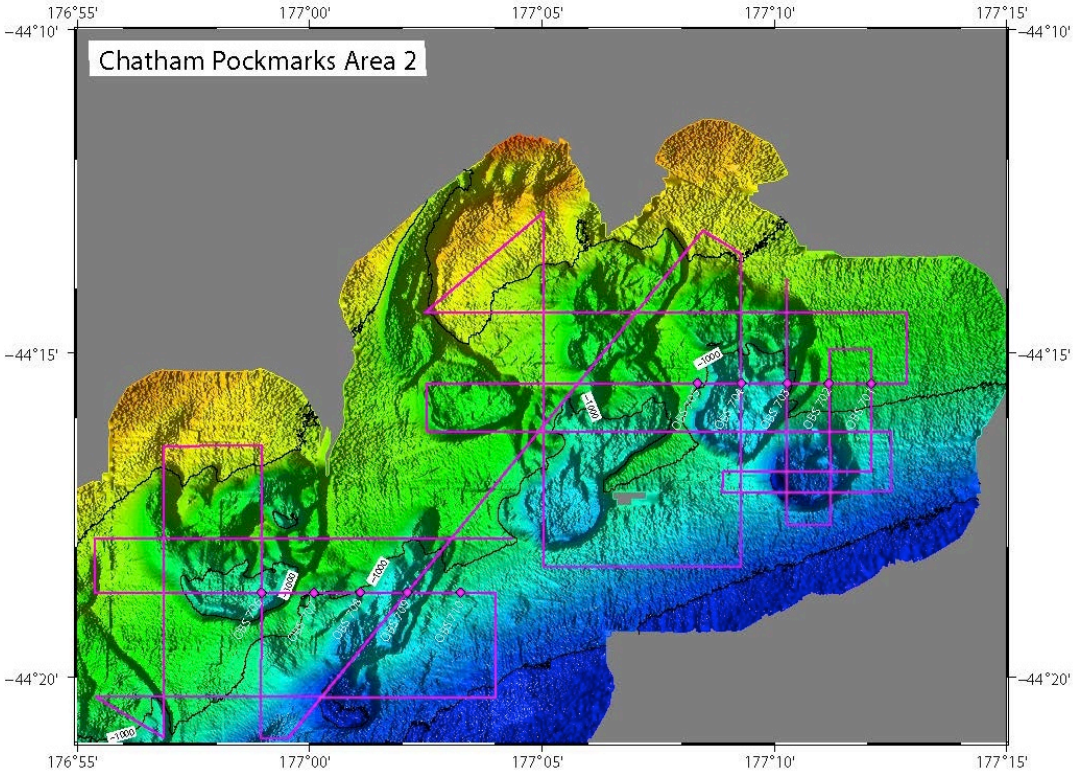

Figure 6.2.2.3.1. Overview map on the deployment of 10 OBS for 2-D shooting along profiles P7000.

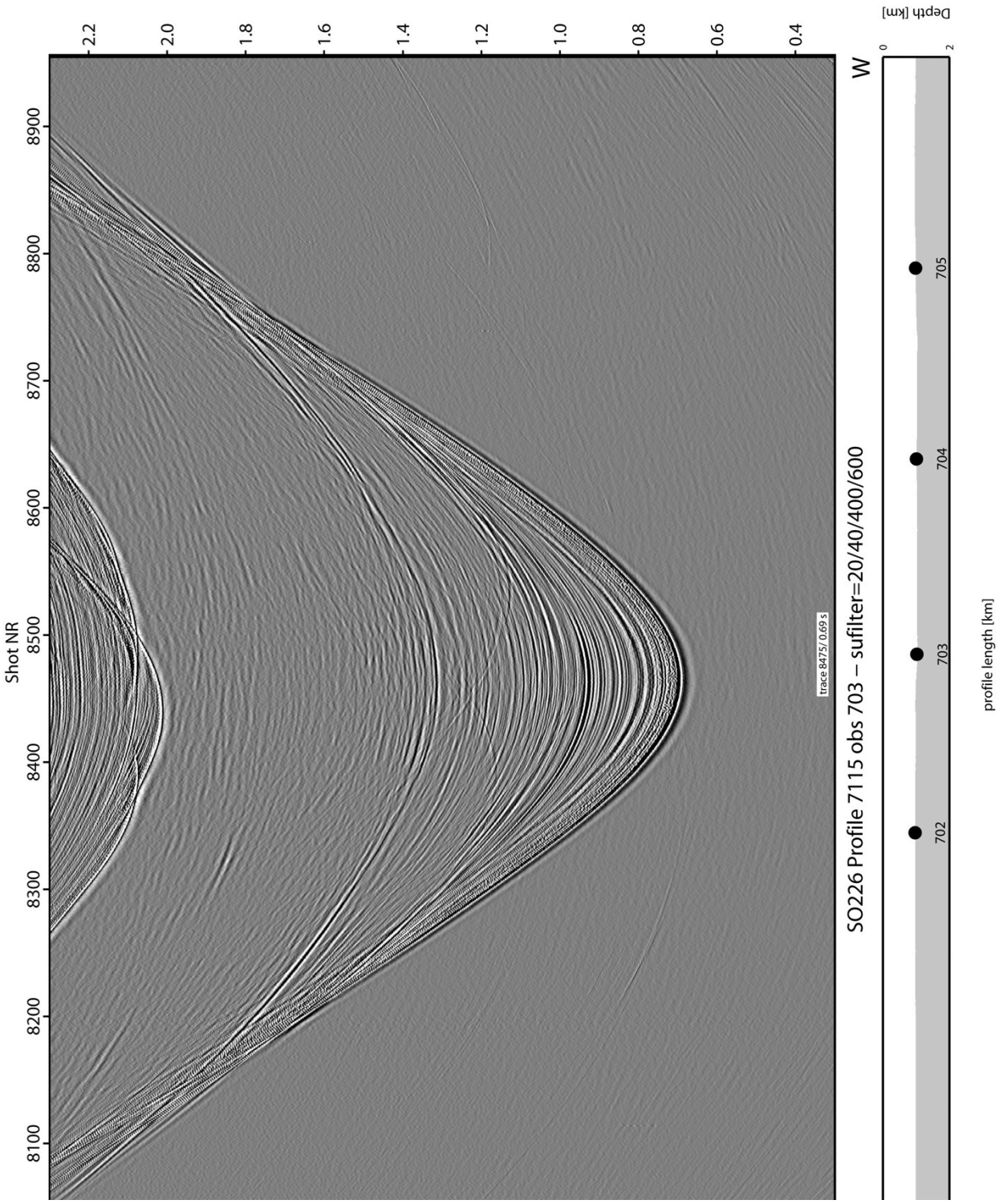

Figure 6.2.2.3.2. Seismic record from OBS 703 on Profile P7102.

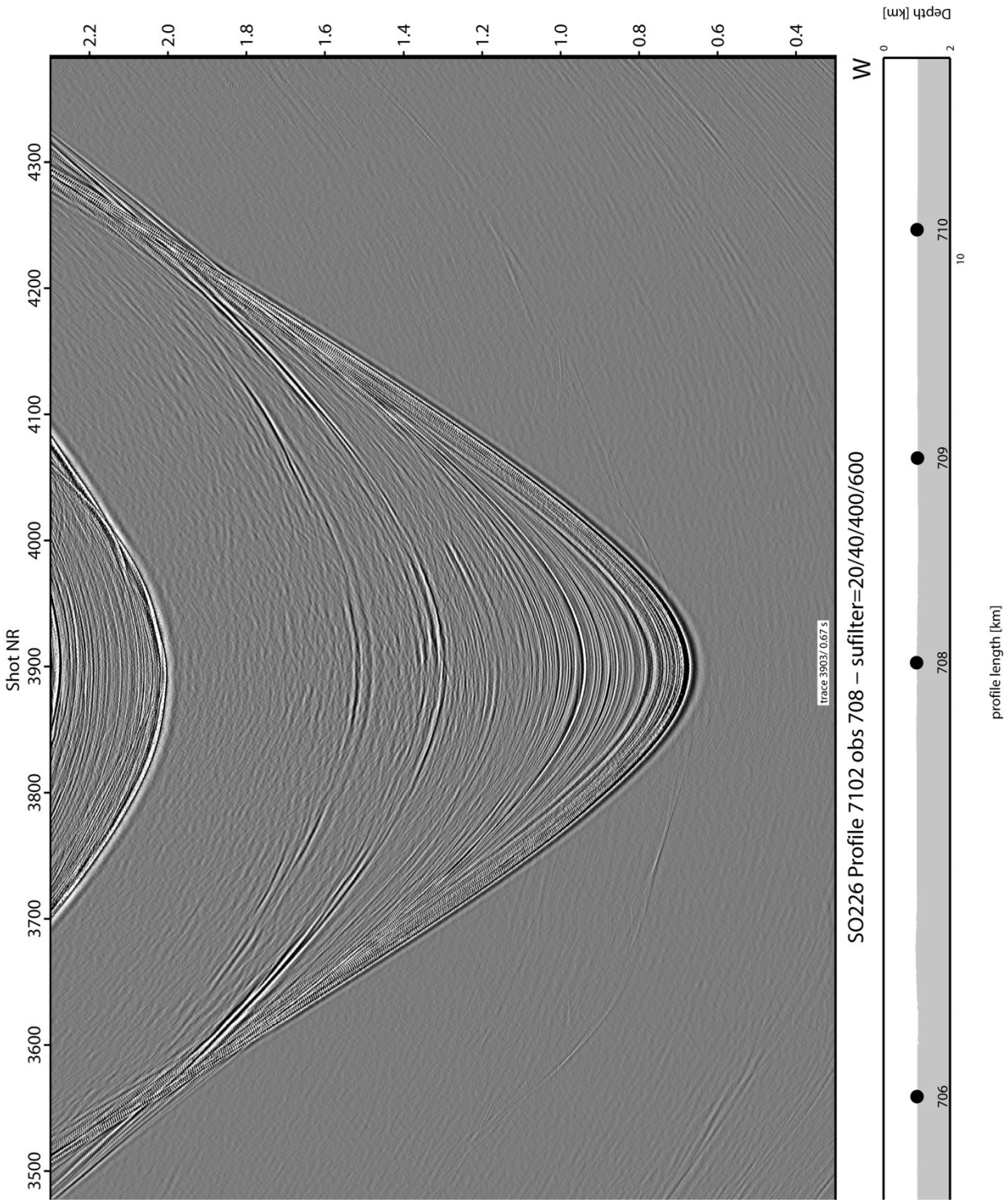

Figure 6.2.2.3.3. Seismic record from OBS 708 on Profile P7115.

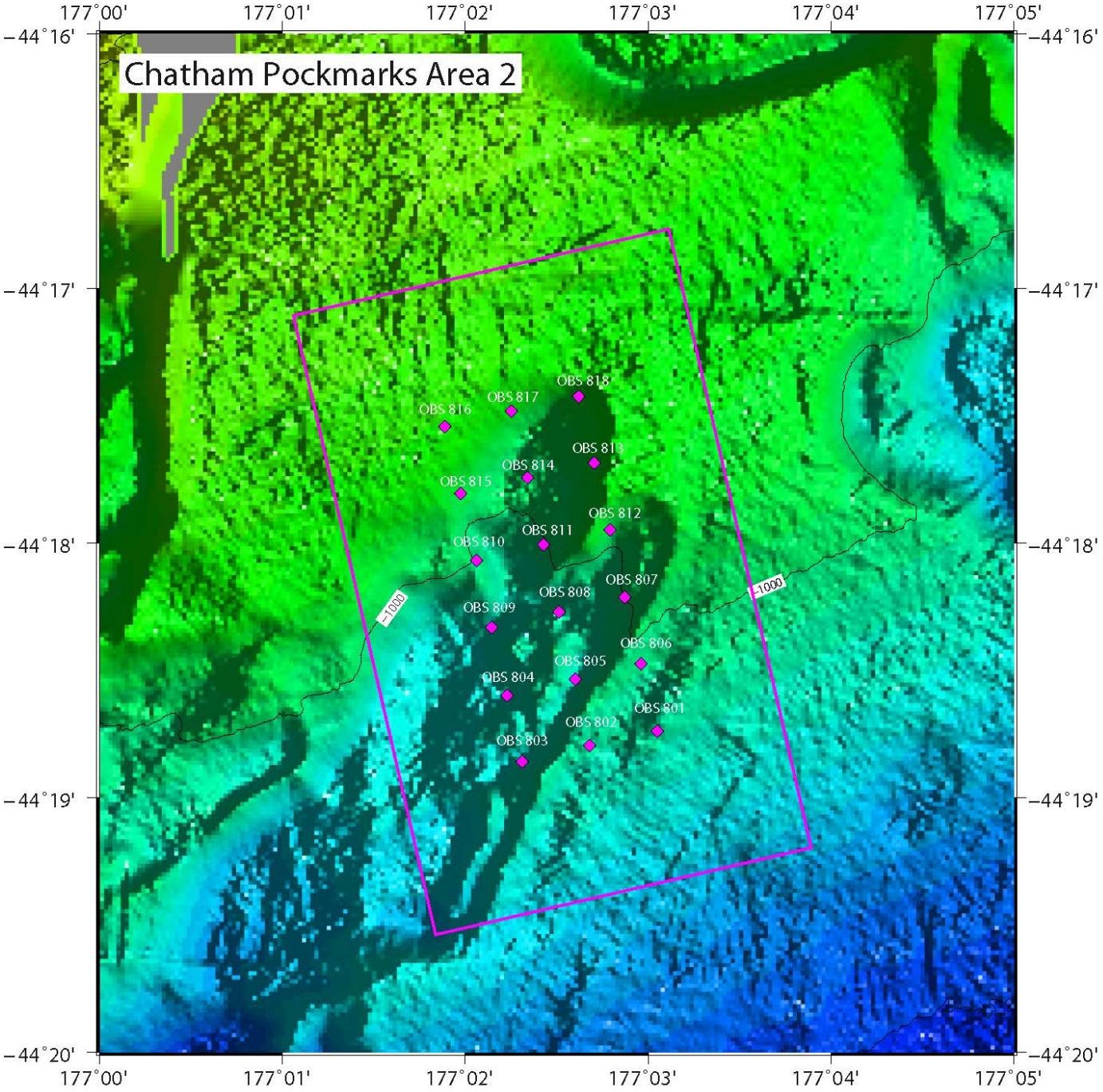

Figure 6.2.2.3.4. Overview map on the deployment of 18 OBS within the area for the 3-D cube (purple rectangular).

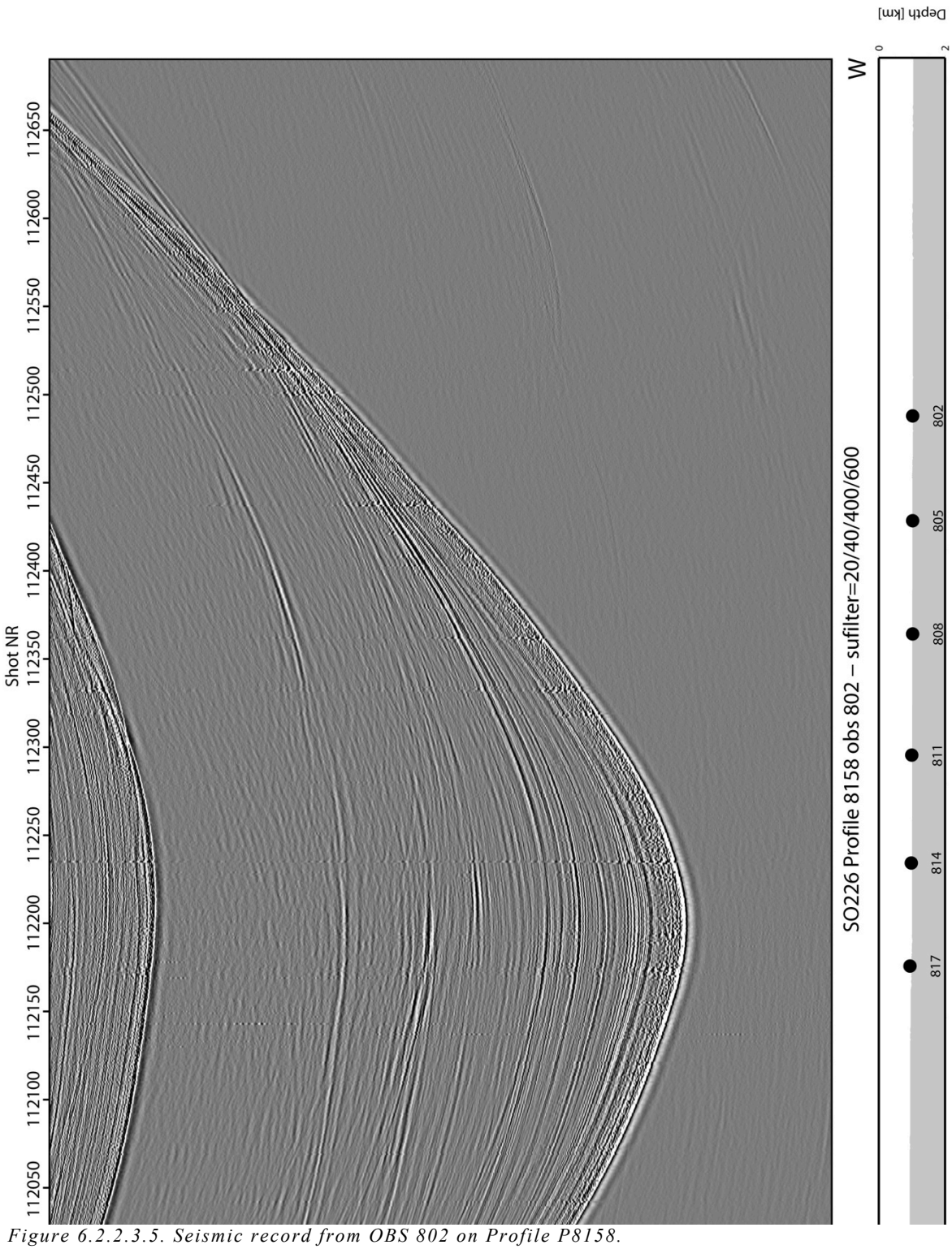

Figure 6.2.2.3.5. Seismic record from OBS 802 on Profile P8158.

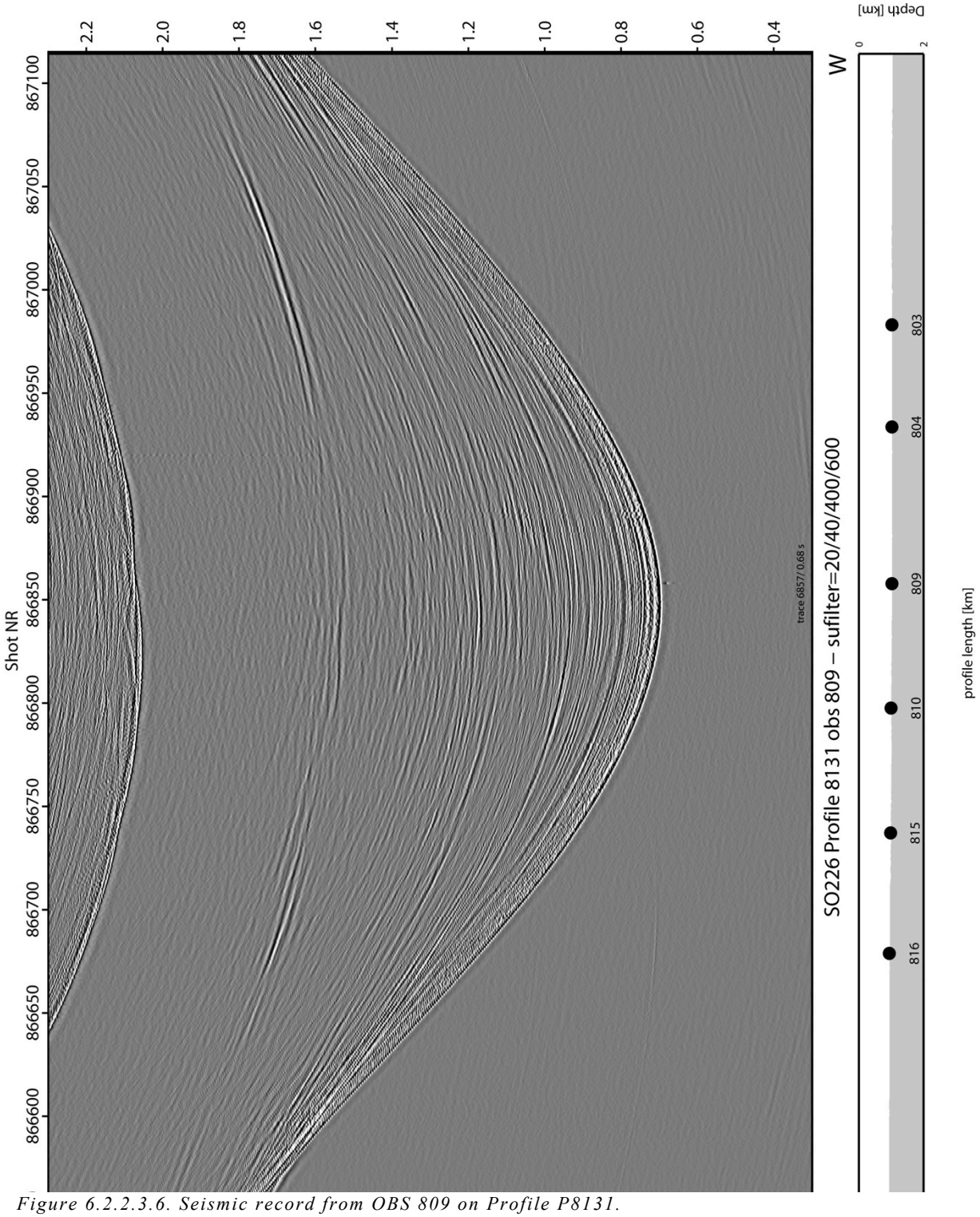

Figure 6.2.2.3.6. Seismic record from OBS 809 on Profile P8131.

6.3. Sidescan Sonar preliminary results

Three sidescan sonar surveys were conducted during the second leg of SO226. Their objectives were the detection of changes in seafloor sediment properties and seafloor morphology, as well as the investigation for patches of authigenic carbonates and gas bubbles which indicate long-lasting and ongoing fluid seepage, respectively.

6.3.1. Area 1

The first sidescan survey (Chrimp1DT) was conducted from 11th February 2:50 to 12th February 23:10 across the two largest seafloor depressions in Area 1. The survey consisted of nine parallel, NE-SW trending profiles of 11 nm length (Fig. 6.3.1.1.). Profiles were spaced 1.3 km apart to ensure some overlap of the outer beams. The DTS1 was towed approximately 100 m above the seafloor at a speed of 3 kn. During acquisition the 75 kHz mode was used with a ping rate of 1 Hz, resulting in a constant range of 750 m. The 2-10 kHz subbottom profiler was also used with a ping rate of 1 Hz and normally pings simultaneously with the sidescan sonar to prevent interference of the two systems. However, during this survey ping times were slightly offset and could not be adapted while the DTS was towed.

The Posidonia USBL system used to determine the towfish position only worked intermittently during the survey. Consequently, the navigation contained gaps and was insufficient for data processing. Towfish navigation was instead calculated via a layback method based on the ship's navigation and the cable length. This method provides a good approximation for the distance behind the ship but does not take into account lateral drift e.g. due to currents.

A first processing attempt revealed that ping times of sidescan sonar and subbottom profiler did not correspond to UTC times but that a 53 minute time shift existed between the bottom PC and the navigation. As it was not possible to modify the data files, these 53 minutes had to be added to the correct navigation so that it matched the times of the data.

Processing of the sidescan data was done using the Caraibes v3.8 software package by IFREMER. Processing steps included manual altitude picking, slant range correction, georeferencing, and mosaicking, resulting in final images with a pixel size of 1 m. Unfortunately, the data showed a consistent increase in amplitude towards the outer beams as the result of an automatic gain correction applied to the raw data. As it was not possible to reverse this correction onboard, this will have to be done during post-processing after the cruise.

The subbottom profiler data were processed using shell scripts based on Seismic Unix and GMT. Processing steps included data conversions, altitude picking, static corrections, and calculating the true water depth from the pressure sensor data. The data showed a high level of coherent noise due to sidescan and subbottom profiler not pinging exactly simultaneously. Because of the noise the data have a relatively low amplitude and penetration, often imaging only the seafloor.

The sidescan data show a smooth and featureless seafloor of low backscatter over most of the survey area. Higher backscatter occurs at the steep southwestern flanks of the two depressions, indicating rougher topography and a very thin or absent cover of soft sediments (Fig. 6.3.1.2. and 6.3.1.3.). Alternating bands of higher and lower backscatter are interpreted as outcropping subsurface strata. Outcropping reflections at steep flanks are also observed in the subbottom profiler data (Fig. 6.3.1.4.). Inside the northern depression, a cluster of small features of low backscatter followed by higher backscatter (as seen from the sonar track) are observed (Fig. 6.3.1.5.). They represent small depressions with lengths of a few tens of meters.

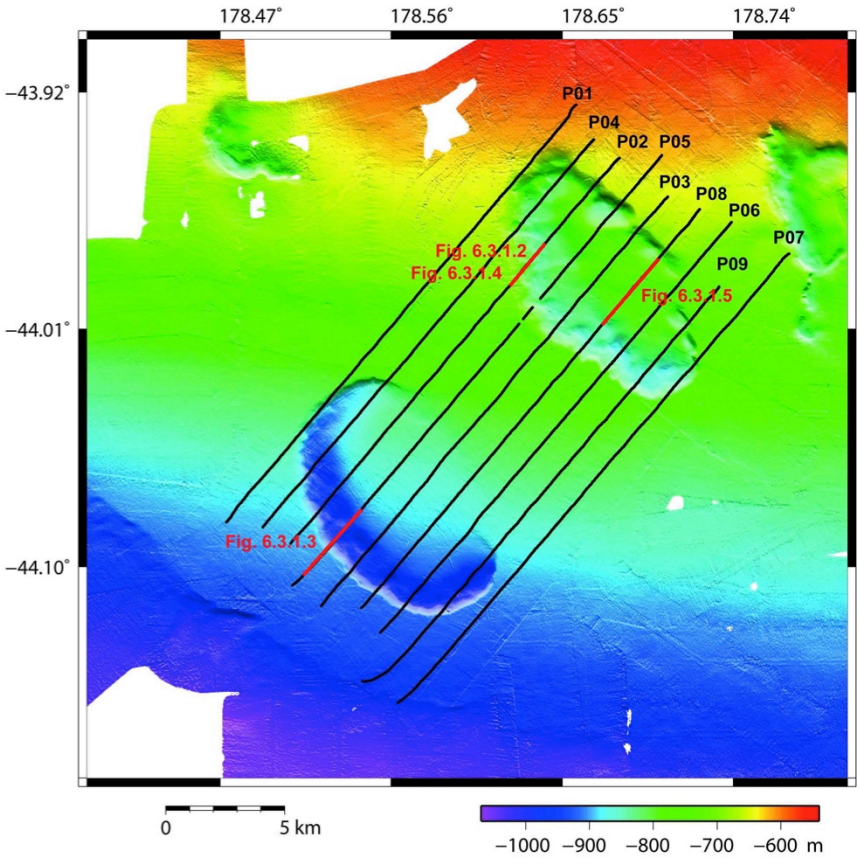

Fig. 6.3.1.1. Bathymetry map of Area 1, showing the sidescan profiles (black lines) and locations of data examples (red sections).

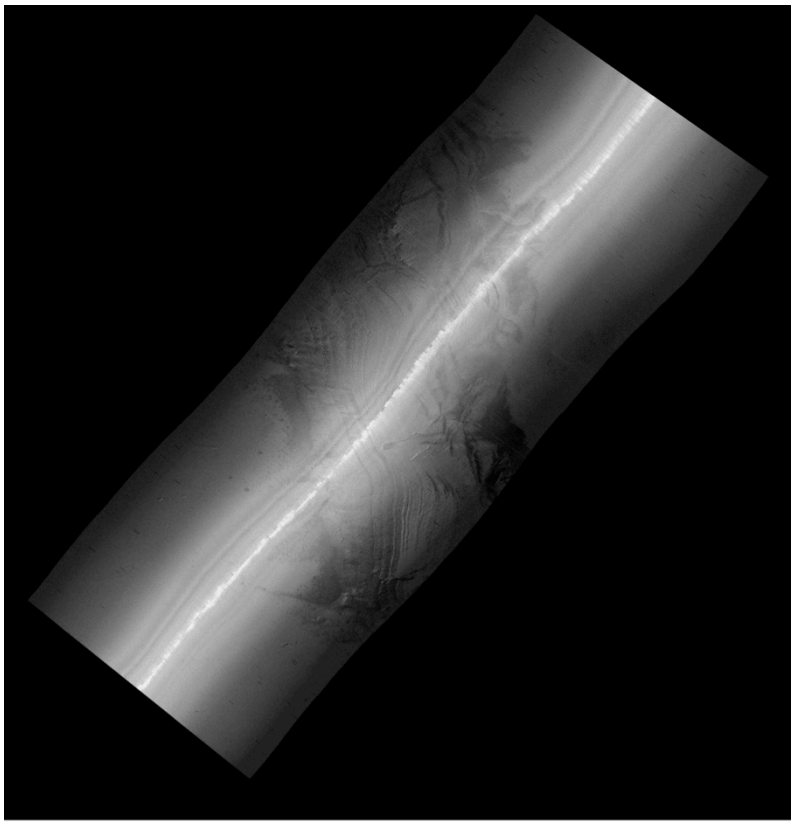

Fig. 6.3.1.2. Sidescan sonar image of the southwestern flank of the northern depression on P02. Structural features and outcropping sediment layers are marked by higher backscatter (dark). See Fig. 6.3.1.1. for location.

Fig. 6.3.1.3. Sidescan sonar image of the southwestern flank of the southern depression on P05. Alternating bands of high and low backscatter indicate outcropping sediment layers. High backscatter is dark. See Fig. 6.3.1.1. for location.

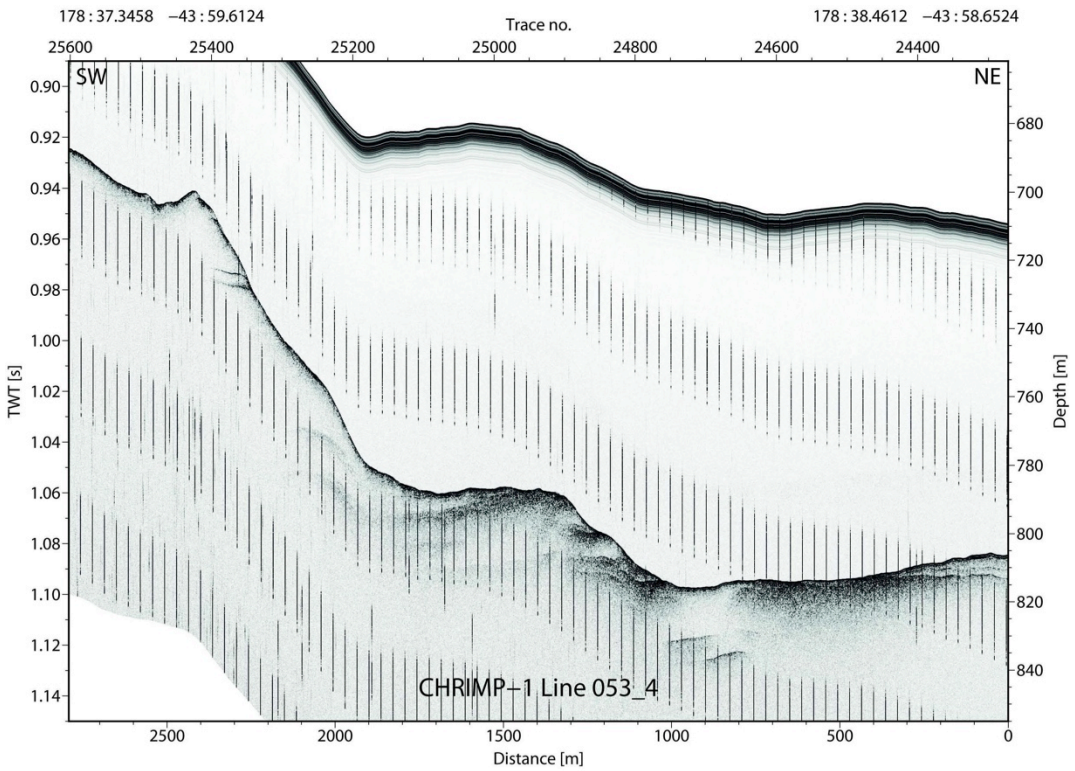

Fig. 6.3.1.4. Subbottom profiler image of the southwestern flank of the northern depression on P02, showing outcropping sediment layers. Note the high noise level due to interference from the sidescan sonar. See Fig. 6.3.1.1. for location.

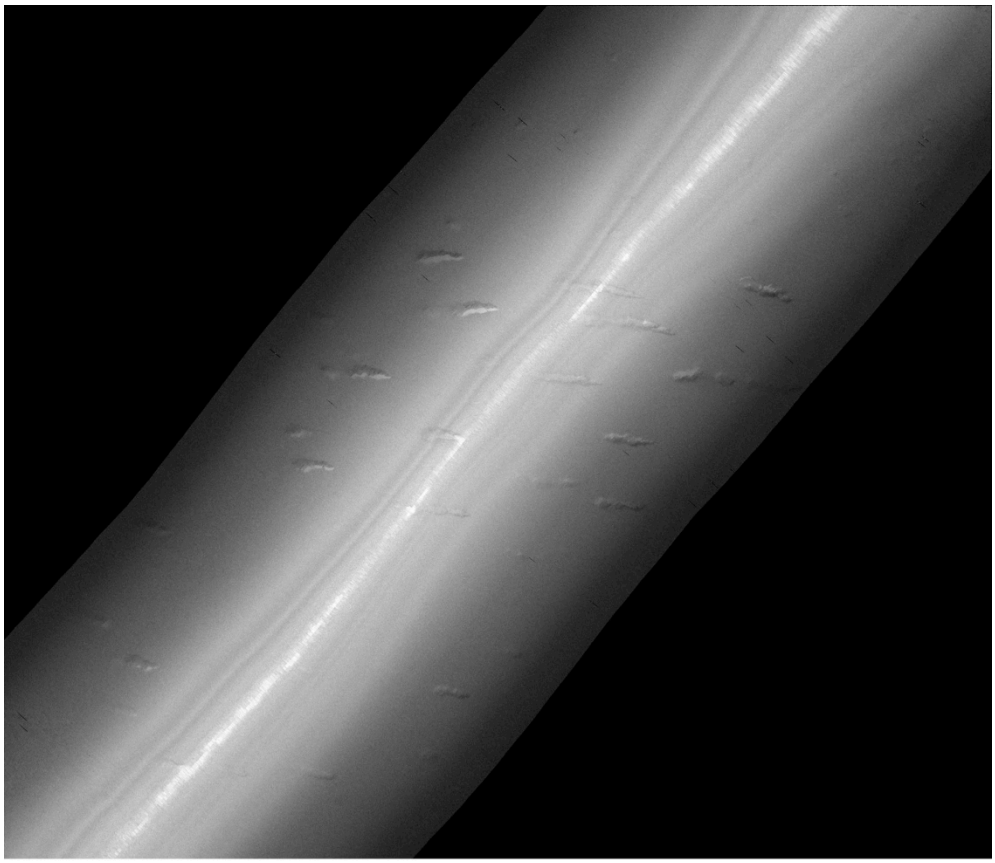

Fig. 6.3.1.5. Small elongate, E-W-oriented depressions inside the northern depression on P08. High backscatter is dark. See Fig. 6.3.1.1. for location.

6.3.2. Area 2

The survey in Area 2 (Chrimp2DT) lasted from 18th February 10:20 until 20th February 04:30 and consisted of eight parallel, NE-SW trending profiles of 12.4 nm length (Fig. 6.3.2.1.). Survey settings were the same as in Area 1, except that sidescan and subbottom profiler now pinged simultaneously and the data were recorded with correct UTC times. Again, the USBL system did not work reliably during most of the survey, requiring navigation to be obtained from the layback method. Sidescan and subbottom profiler data were processed as described above. Simultaneous pinging of the two systems resulted in a much more reduced noise level in the subbottom data.

Like in Area 1, the seafloor in Area 2 is characterized mostly by low backscatter, indicating a smooth and featureless substrate. Elevated backscatter marks the rims of depressions (Fig. 6.3.2.2.), but compared to Area 1 the backscatter is generally more moderate. This is thought to indicate a thicker sediment cover than in the first area, which is in agreement with seismic data. The subbottom profiler has a penetration in the order of 10 m in most of the area. At steeper flanks of depressions, outcropping reflectors are observed (Fig. 6.3.2.3.).

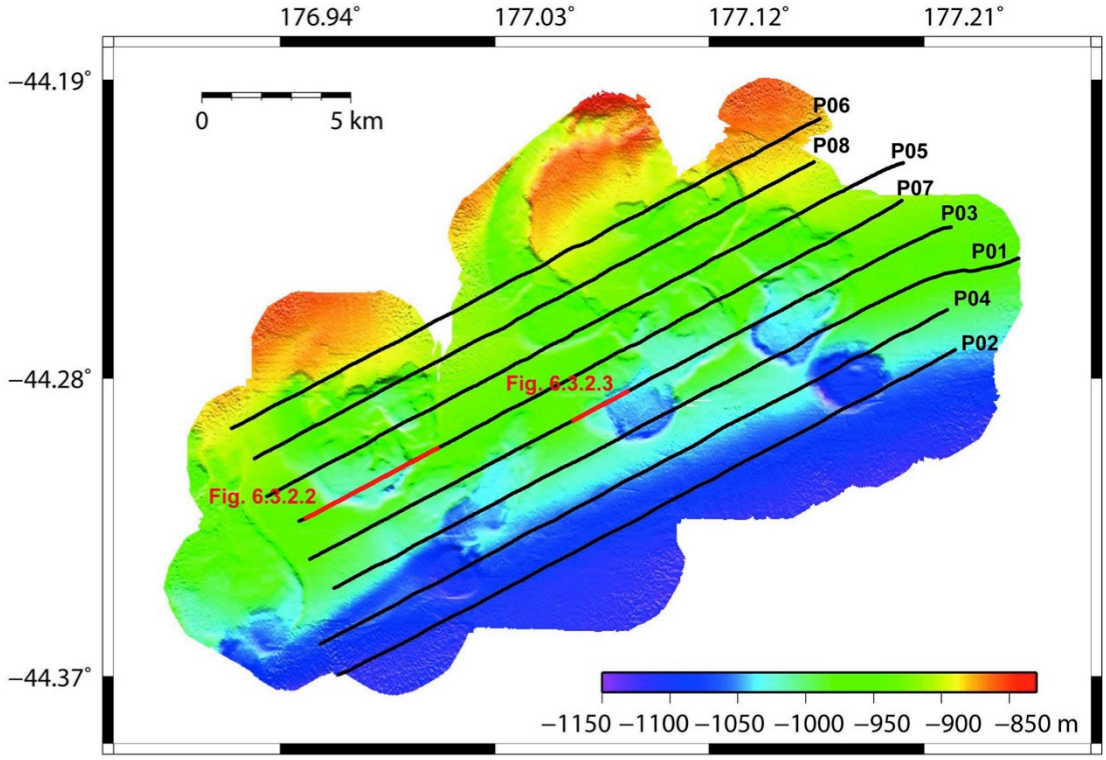

Fig. 6.3.2.1. Bathymetry map of Area 2, showing the sidescan profiles (black lines) and locations of data examples (red sections).

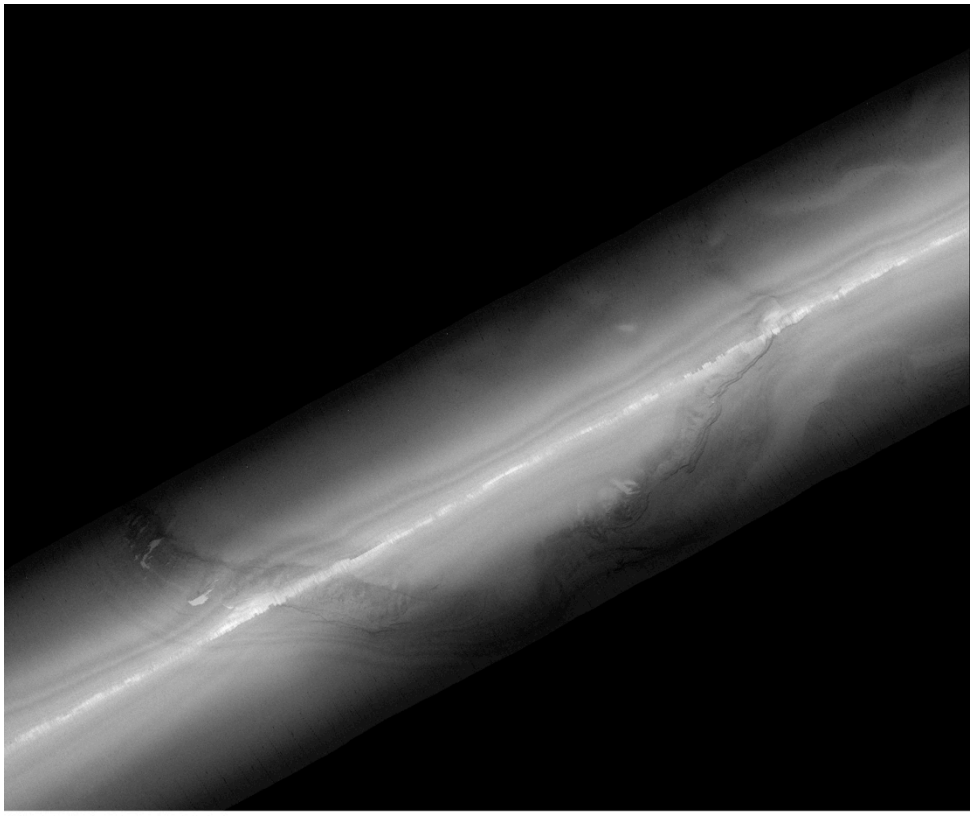

Fig. 6.3.2.2. Sidescan sonar image of the southern flank of the westernmost depression on P07. Alternating bands of higher and lower backscatter indicate outcropping sediment layers. High backscatter is dark. See Fig. 6.3.2.1. for location.

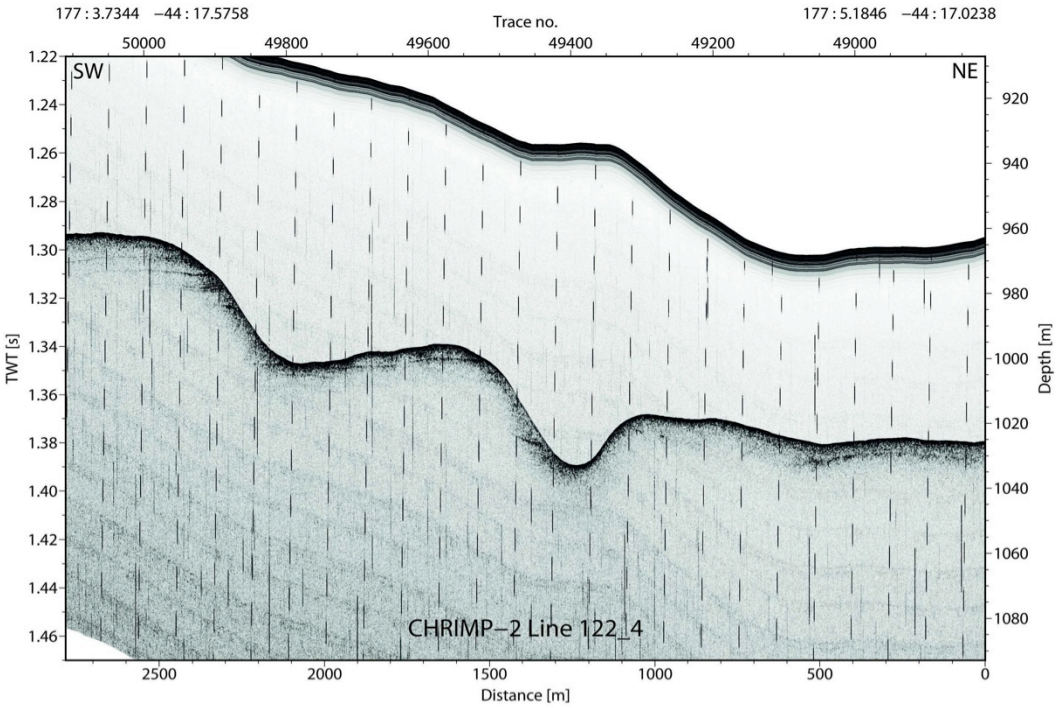

Fig. 6.3.2.3. Subbottom profiler image of the western flank of the central depression on P03, showing a stepwise relief and outcropping reflectors. See Fig. 6.3.2.1. for location.

6.3.3. Area 3

A third sidescan survey was conducted in Area 3 from 24th February 22:00 to 25th February 08:00. This survey consisted of two 11 nm long, NE-SW trending profiles across a field of small depressions apparent in the bathymetry data (Fig. 6.3.3.1.). Survey settings were as described above; towfish navigation was obtained via the layback method. Most of the area features depressions of up to 100 m across that are inferred from patches of low backscatter followed by higher backscatter (Fig. 6.3.3.2.). Depths of the depressions are up to 10 m (Fig. 6.3.3.3.). Towards the southwest, the depressions eventually become smaller in size, measuring only about a few tens of meters across, until they disappear and the seafloor becomes smooth and featureless (Fig. 6.3.3.2.). In the transition zone from large to no depressions penetration of the subbottom profiler data show two subsurface reflectors that are not mapped further north, indicating a change in sediment pattern (Fig. 6.3.3.4.).

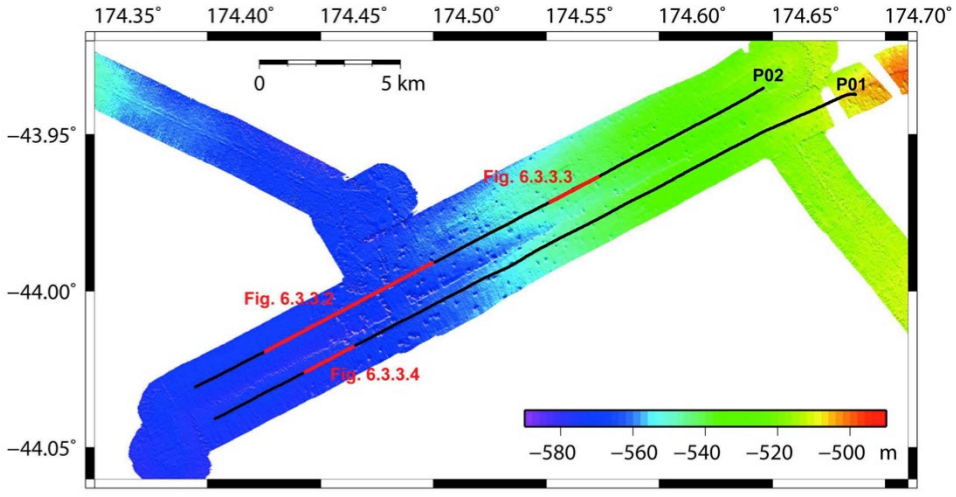

Fig. 6.3.3.1. Bathymetry map of Area 3, showing the sidescan profiles (black lines) and locations of data examples (red sections).

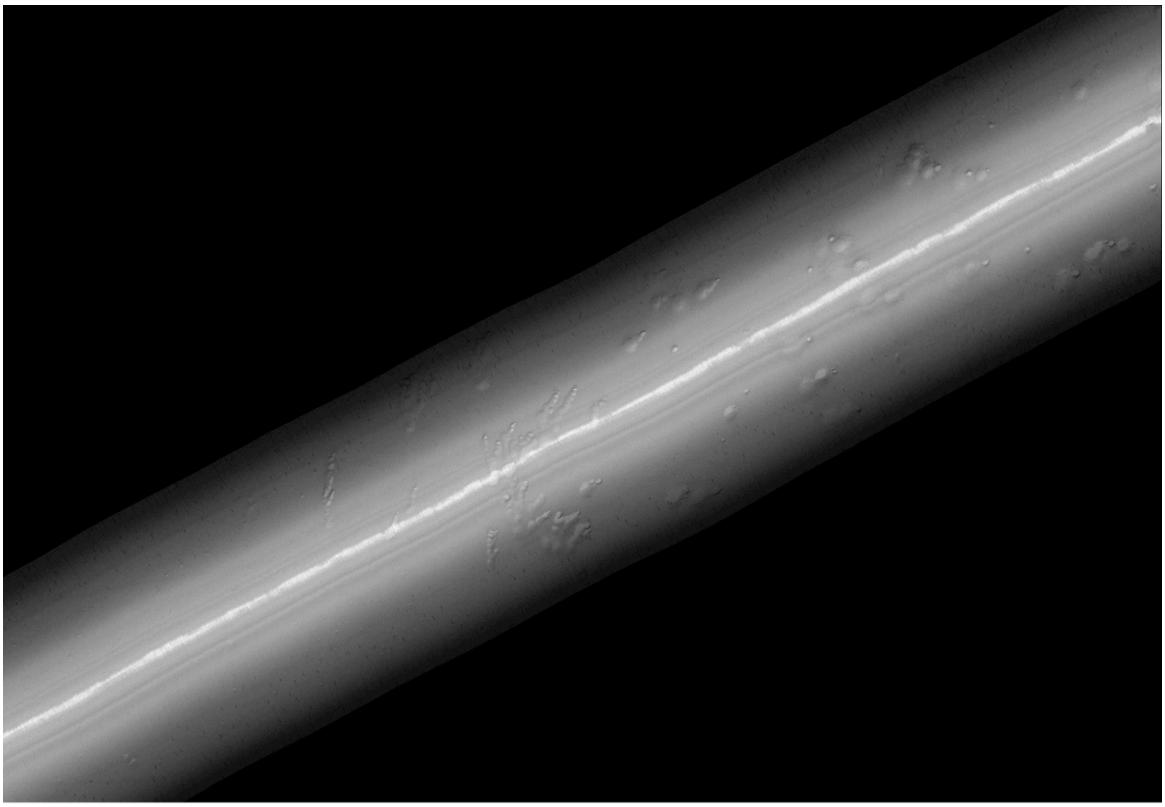

Fig. 6.3.3.2. Sidescan sonar image of the western end of P02, showing an E-W transition from up to 100 m large depressions to smaller, more elongate depressions and a smooth, featureless seafloor. High backscatter is dark. See Fig. 6.3.3.1. for location.

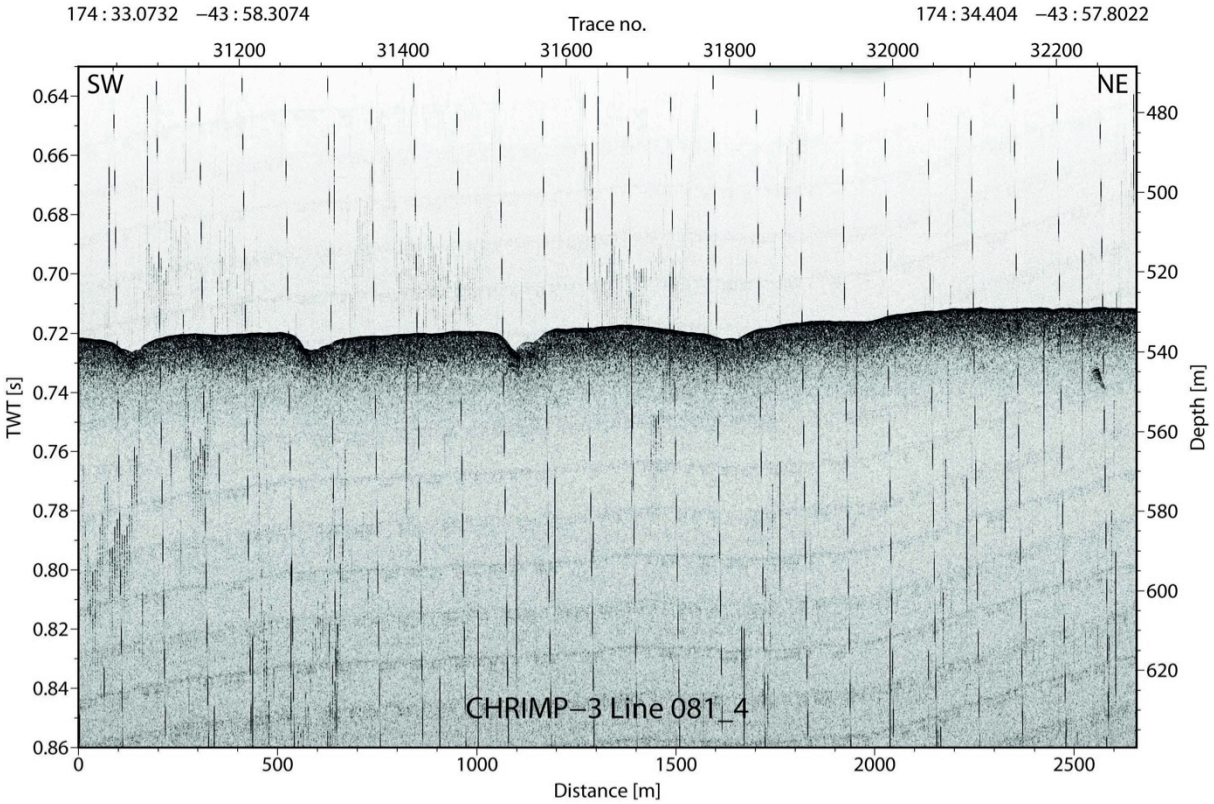

Fig. 6.3.3.3. Subbottom profiler image of seafloor depressions on P02. See Fig. 6.3.3.1. for location.

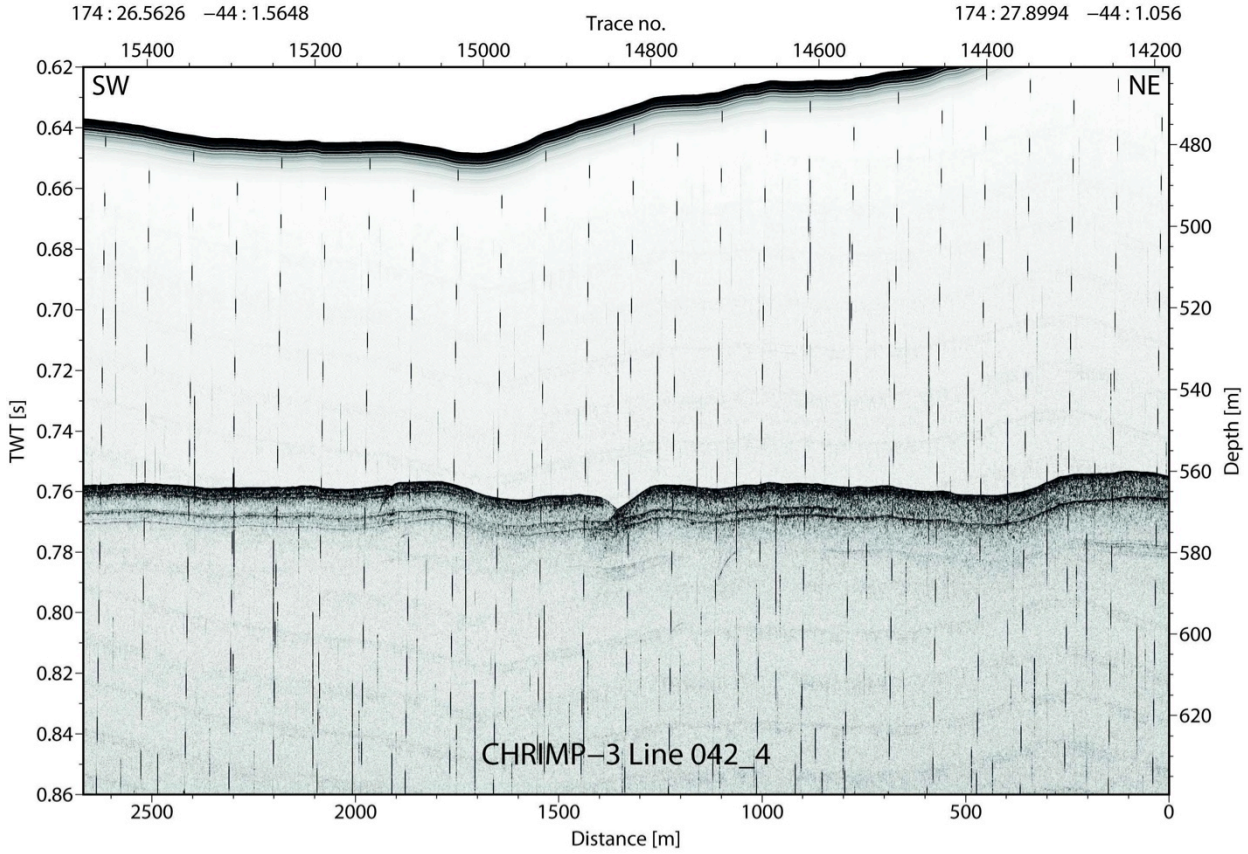

Fig 6.3.3.4. Subbottom profiler image of the transition zone on P01, showing two distinct subsurface reflectors. See Fig. 6.3.3.1. for location.

6.4 OFOS/OFOP General observations

In Area 1, there was a depth-transition from communities dominated by white urchins, anenomes and gastropods to holothurians on soft muddy sediments above the main depression and on its floor. On the steep western flank of the depression, there were numerous low-lying encrusting organisms (sponges, corals) with holothurians also active on outcropping carbonate rocks. Rat-tails dominated the observed fish fauna, although oreos, chimeras and possible bluenose were also observed.

In Area 2, the epifauna were dominated by echinoids (many large black urchins) and holothurians, with a characteristic component of numerous small, round colonial animals. In the OFOP protocols, these were designated as “zooanthids”, but require closer scrutiny by more experienced biological practitioners, as they might be glass-ball sponges or small coral communities (as sampled by one of the multi-corer deployments in this area, Station 81-1).

In Area 3, there were a lot more burrows and mounds than at the other two sites where tracks were the dominant *lebensspuren*. The fauna were characterised by numerous flabellum corals, anenomes, gastropods and occasional sponges.

In a general sense, as mentioned above under the discussion about Area 2, all of the video data needs to be reviewed and the logging re-done by more experienced practitioners than was available during the voyage.

Over the course of each deployment, the OFOP protocols stopped logging periodically. At each drop-out, the existing protocol had to be stopped running and a new protocol instituted, as labelled sequentially in each file. Upon checking the .prot and .observ files after the deployments, it seems that the protocol shut-down occurred when ~490 observations/lines had been compiled in each of these files. Email discussions with Jens Greinert suggest that OFOP should not have any maximum buffer, so the issue has not been able to be rectified at this stage.

6.5. Sediment Geochemistry

This research expedition focuses on three different regions with pockmarks with the intention of studying past and currently active vertical methane migration sites (Table 6.5.1.). Data presented in this report is a summary of the onboard activity. Results organize the selection of samples for radiocarbon, stable carbon and current day radioisotope (thorium and lead) to assess current day and past (~20,000 years back) vertical methane fluxes and subsequent shallow sediment carbon cycling. This study is intended to expand the current understanding of climate change with assessment of past changes. Data presented includes chloride to assess methane hydrate dissociation in cores, or vertical and horizontal transport of porewater. Sulfate, CH_4 and DIC are reviewed to provide estimate of current day vertical gas fluxes.

6.5.1. Area 1

Core site 1 is located northeast of a series of pockmarks on the Chatham Rise at a water column depth that ranges from 686 to 807 meters (Fig. 6.5.1.1.). Sediment characteristics and the need to obtain cores at least 4 meters deep for age dating resulted in the selection of coring sites to the east of the pockmarks. Sand to gravel and chalk sediment to the west resulted in losing one piston corer and breaking two core barrels. After difficulties with piston coring, multi-coring was used to assess the potential to retrieve deep piston cores. Multi-core samples are also used to obtain modern data sediment to assess the current sedimentation rate relative to the vertical methane flux.

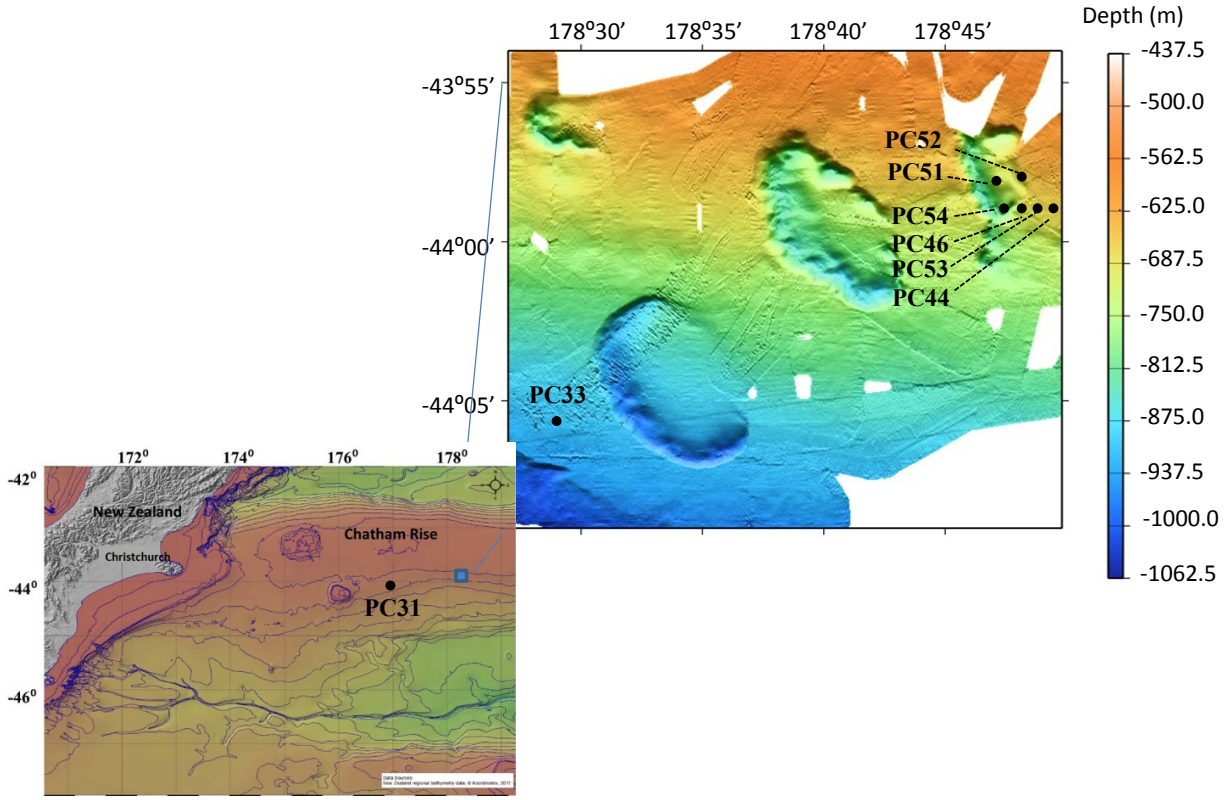

Figure 6.5.1.1. Site 1 coring located on the eastern side of the pockmark. Control cores (PC31 and PC33, not presented in this report) are also shown away from the pockmark.

Core Log

Total # of Cores:	*37*	*Total Length of Core Retrieved (meters):*	*154.95*

Core Number	Date *UTC*	Time at Trigger *UTC*	Transponder Latitude	Transponder Longitude	Water Depth *Meters*	Cable Out at Time of Trigger *Meters*	Est. Max Tension on Pullout *kiloNewtons*	Core Length *Meters*	Notes	Water Depth - Cable Out at Trigger	Percent Recovery	Estimated Core Length	Est. Max Tension on Pullout *Pounds*
30-2-PC9	10-Feb-13	22:45	44° 6.03 S	178° 39.99 E	873	854	56.6	5.74		19	63.78%	5.21	12,724
33-1-PC9	13-Feb-13	2:30	44° 5.72' S	178° 31.25 E	899	884	63.1	3.05		15	33.89%	5.01	14,186
33-2-PC9	13-Feb-13	4:30	44° 5.72' S	178° 31.26 E	900		87	4.2			46.67%	4.25	19,558
33-3-PC6	13-Feb-13	6:30	44° 5.73 S	178° 31.2 E	900		75.7	4.07			67.83%	4.61	17,018
34-1-PC6	13-Feb-13	8:38	44° 5.69 S	178° 32.30 E	976	963	152	0	Whole assembly stuck, snapped cable. Lost bomb, 3 stands of pipe, tip, and piston	13	0.00%	2.20	34,171
44-1-PC9	14-Feb-13	21:38	43° 58.85 S	178° 48.88 E	680	661	41.1	6.04		19	67.11%	5.70	9,240
45-1-PC9	15-Feb-13	0:06	43° 58.86 S	178° 47.57 E	749	732	35.9	6.71		17	74.56%	5.86	8,071
45-2-PC9	15-Feb-13	2:40	43° 58.81 S	178° 47.63 E	743	729	38.7	6.86		14	76.22%	5.78	8,700
46-1-PC9	15-Feb-13	4:29	43° 58.90 S	178° 46.95 E	810	798	26.2	0	Broke off 3rd barrel, No recovery	12	0.00%	6.17	5,890
47-1-PC9	15-Feb-13	6:50	43° 58.91 S	178° 46.74 E	825	807	28	0	Broke off 3rd barrel, No recovery	18	0.00%	6.11	6,295
51-2-PC9	15-Feb-13	16:46	43° 58.20 S	178° 46.82 E	770	750	47.6	6.48		20	72.00%	5.50	10,701
52-1-PC9	15-Feb-13	19:49	43° 57.94 S	178° 47.61 E	702	686	41.7	6.42		16	71.33%	5.68	9,375
53-1-PC9	15-Feb-13	22:09	43° 58.70 S	178° 47.89 E	736	713	32.1	6.15	Top section of core liner stuck in barrel	23	68.33%	5.99	7,216
54-1-PC9	16-Feb-13	0:29	43° 58.89 S	178° 47.22 E	785	766	49.4	6.6		19	73.33%	5.44	11,106
57-1-GC3	16-Feb-13	22:30	43° 56.915 S	178° 35.122 E	631	628	41.7	1.87		3	62.33%	5.68	9,375
58-1-GC3	17-Feb-13	0:50	43° 5.997 S	178° 31.52 E	906	906	32.1	0	No recovery, very sandy	0	0.00%	5.99	7,216
59-1-GC3	17-Feb-13	2:42	44° 7.603 S	178° 36.224 E	928	921	35.7	0	No recovery, very sandy	7	0.00%	5.87	8,026
60-1-GC3	17-Feb-13	4:33	44° 11.239 S	178° 36.338 E	1035	1030	26.2	0	No recovery, very sandy	5	0.00%	6.17	5,890
73-2-PC9	20-Feb-13	15:03	44° 14.37 S	177° 8.47 E	964	944	49.4	6.41		20	71.22%	5.44	11,106
74-1-PC9	20-Feb-13	17:02	44° 14.37 S	177° 8.55 E	960	943	46.4	6.07		17	67.44%	5.53	10,431
75-1-PC9	20-Feb-13	19:38	44° 14.37 S	177° 9.07 E	968	94	31.5			874		6.00	7,082
75-2-PC9	20-Feb-13	21:33	44° 14.39 S	177° 8.97 E	968	949	38.1	6.65		19	73.89%	5.80	8,565
76-1-PC9	21-Feb-13	0:04	44° 14.37 S	177° 10.41 E	970	948	44.7	5.89		22	65.44%	5.59	10,049
76-2-PC9	21-Feb-13	2:03	44° 14.36 S	177° 10.41 E	970	947	39.9	6.48		23	72.00%	5.74	8,970
77-1-PC9	21-Feb-13	4:05	44° 14.36 S	177° 11.16 E	940	919	39.3	6.53		21	72.56%	5.76	8,835
77-2-PC9	21-Feb-13	6:14	44° 14.37 S	177° 11.17 E	936	919	46.6	6.28		17	69.78%	5.53	10,476
77-3-PC9	21-Feb-13	7:56	44° 14.37 S	177° 11.17 E	936	918	38.1			18		5.80	8,565
82-3-PC9	21-Feb-13	21:05	44° 18.49 S	177° 2.37 E	1023	1002	33.9	6.25		21	69.44%	5.93	7,621
83-1-PC9	21-Feb-13	22:51	44° 18.35 S	177° 2.50 E	1013	999	46.4	6.38		14	70.89%	5.53	10,431
84-1-PC9	22-Feb-13	0:52	44° 18.26 S	177° 2.59 E	1019	999	48.2	6.64		20	73.78%	5.48	10,836
85-1-PC9	22-Feb-13	3:01	44° 17.48 S	177° 3.42 E	975	955	34.5			20		5.91	7,756
85-2-PC9	22-Feb-13	5:42	44° 17.54 S	177° 3.43 E	975	954	40.5			21		5.72	9,105
94-3-PC9	25-Feb-13	16:55	43° 59.43 S	174° 28.05 E	569	554	35.7	4.4	Shot 1916 - Paleo core	15	48.89%	5.87	8,026
94-4-PC9	25-Feb-13	19:16	43° 59.44 S	174° 28.04 E	569	554	32.7	6.15	Shot 1916 Geotech core	15	68.33%	5.97	7,351
94-5-PC9	25-Feb-13	20:39	43° 59.43 S	174° 28.09 E	569	553	35.7	6.57	Shot 1916 - Geochem core	16	73.00%	5.87	8,026
95-1-PC9	25-Feb-13	22:05	43° 59.26 S	174° 27.93 E	568	553	31.5	4.27	Shot 2155	15	47.44%	6.00	7,082
96-1-PC9	26-Feb-13	0:05	43° 59.24 S	174° 27.92 E	569	557	35.7	5.79		12	64.33%	5.87	8,026
97-1-PC9	26-Feb-13	1:25	43° 59.17 S	174° 27.86 E	569	554	30.4	4.28		15	47.56%	6.04	6,834
98-1-PC9	26-Feb-13	3:08	44° 0.13 S	174° 28.63 E	571	568	46.4	2.41	Shot 964 - Geotech core	3	26.78%	5.53	10,431
98-2-PC9	26-Feb-13	4:32	44° 0.12 S	174° 28.64 E	571	561	53	5.85	Station Name on Display showed 98, not 98/2	10	65.00%	5.32	11,915
99-1-PC9	26-Feb-13	6:30	43° 58.95 S	174° 27.68 E	575	560	28	0	Broke off 3rd barrel, No recovery	15	0.00%	6.11	6,295
100-1-PC9	26-Feb-13	8:12	43° 58.85 S	174° 27.59 E	568	554	30.4		Imploded middle core liner	14		6.04	6,834
101-1-PC9	26-Feb-13	10:05	44° 1.17 S	174° 27.06 E	572	557	23.8		Bent third barrel	15		6.25	5,350

Table 6.5.1. Sediment piston core locations for SO226/2.

Seismic data from Site 1 was reviewed for strong surface sediment reflections suggesting deep modern sediment and vertical gas migration (Fig. 6.5.1.3.). PC54, PC45, PC53 and PC44 were taken on the south eastern side of Site 1. Line P6110 was selected with observation of strong shallow

seismic reflections suggesting soft sediment and deep reflection patterns indicative of gas (Fig. 6.5.1.2) This feature was also observed in a northern seismic line (P6112), where two core locations were selected to assess the extent of this feature (Fig. 6.5.1.3..).

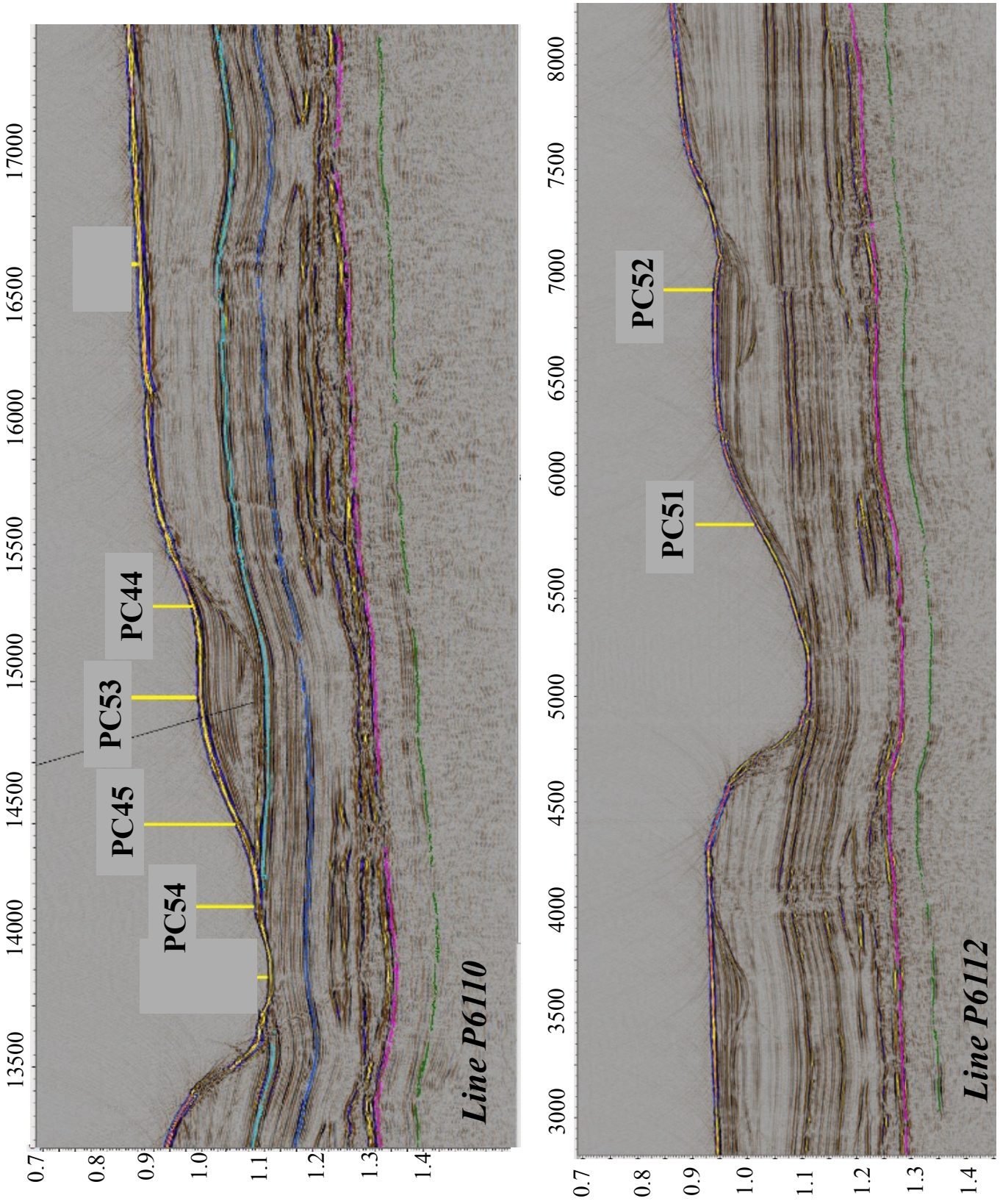

Figure 6.5.1.2. Seismic lines for the Site 1 pockmark research focus. Core sites were located on the eastern side of the pockmark because cores could not be retrieved at western locations.

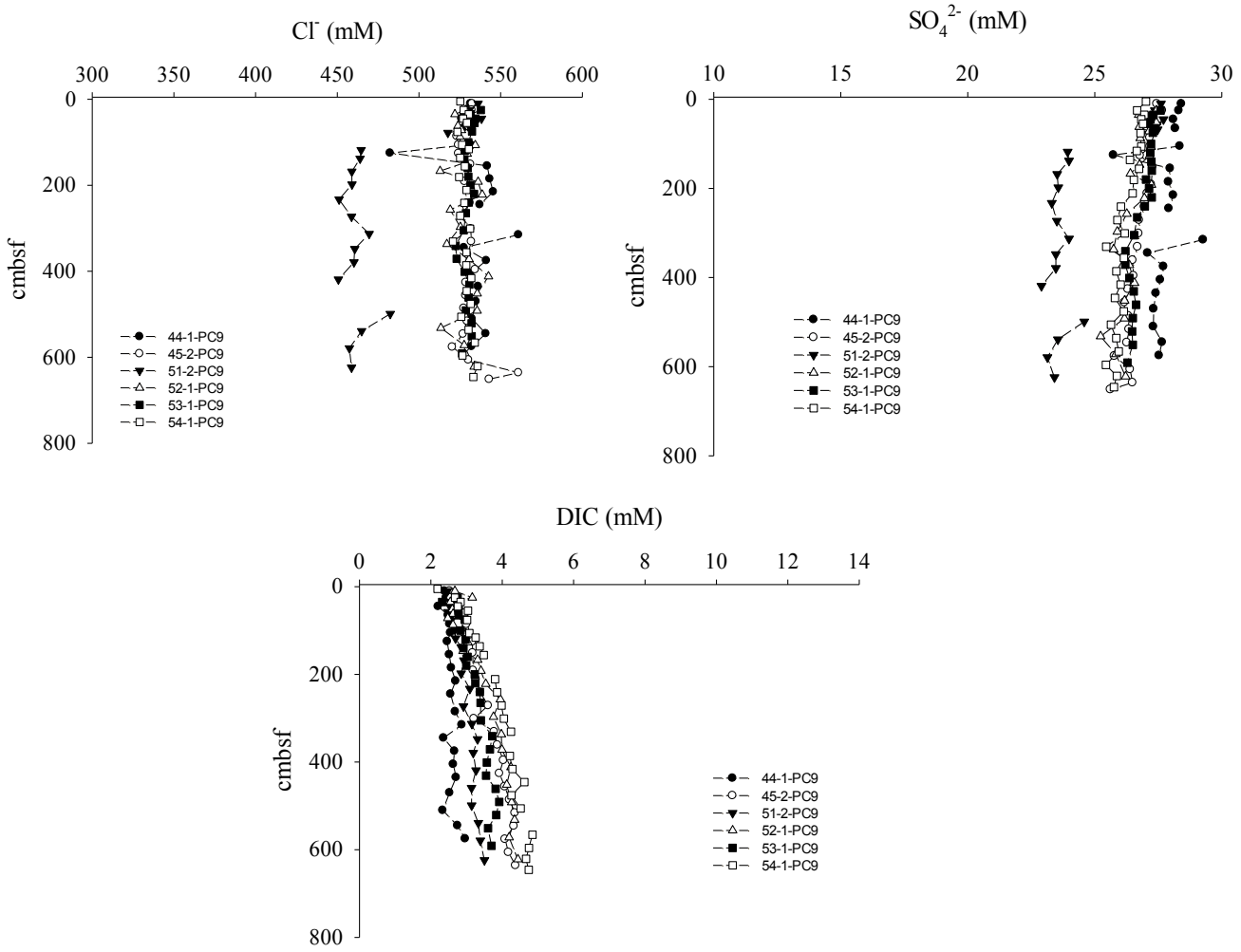

Figure 6.5.1.3. Sulfate, chloride and DIC profiles taken on the eastern side of the pockmark in Site 1.

Geochemical evaluation of the eastern lines across the site 1 pockmark found low background sediment methane and no higher molecular weight gases (Appendix 3). Data presented for the field assessment of the core porewater includes SO_4^{2-}, Cl^-, and DIC (Fig. 6.5.1.3.). The range in SO_4^{2-} concentrations for this location was 22.9 to 29.2 mM. The general trend for SO_4^{2-} profiles at all locations through this region is moderate to no decrease in concentration. The linear trend in the $S0_4^{2-}$ profiles, with no rapid depletion in the shallow sediment characteristic of labile organoclastic cycling, could suggest AOM is responsible for the decline in concentration. However, sediment CH_4 concentrations through the cores were slightly above the limits of detection and indicate that AOM was beyond the core penetration depth. Laboratory stable carbon isotope analyses of DIC and sulfide concentrations will be measured to assess AOM. Chloride concentrations for cores near the Site 1 pockmark ranged from 451 to 543 mM (Fig. 6.5.2.1.). There was a general trend for straight linear cores in the typical range of seawater. However, Cl^- in PC51-1 was observed to be lower through the entire core and decline to the minimum observed value at depth. Another general observation in Cl^- profiles was a replicate image with SO_4^{2-} suggesting low SO_4^{2-} cycling; assuming Cl^- is an independent conservative tracer (Fig. 6.5.1.2.) Porewater DIC concentrations ranged from 2.1 to 5.2 mM with shallow sediment concentrations consistently near the seawater concentration and a gradual increase observed down core. PC54-1 was observed to have the highest DIC concentration toward the bottom of the core. This inverse relationship could indicate low AOM or organoclastic sulfate reduction through the core.

6.5.2. Area 2

Site 2 was located south of Site 1 with water column depths ranging from approximately 1000 to 1100 mbsf (Fig. 6.5.2.1.). In this study area, two regions were focused on after seismic review; Site 2-A (Seismic Line 7114, Fig. 6.5.2.2.) and Site 2-B (Seismic Line 7109, Fig. 6.5.2.2.). Selections of core these sites were based on the interpretation of shallow sediment accumulation and vertical fluxes observed in these seismic profiles. Porewater SO_4^{2-} and DIC concentrations in the cores ranged from 17.1 to 27.6 mM and 1.3 to 12.1 mM, respectively. PC75-2 was observed to have the greatest reduction of SO_4^{2-} and increase of DIC concentrations through a linear pattern suggesting AOM or organoclastic sulfate reduction (Fig. 6.5.2.3.). Through Site 2-A cores porewater chloride concentrations ranged from 489.7 to 540.1 mM. In general profiles were conservative with no vertical patterns, however there were a couple of points observed with lower concentrations (Fig. 6.5.2.3.).

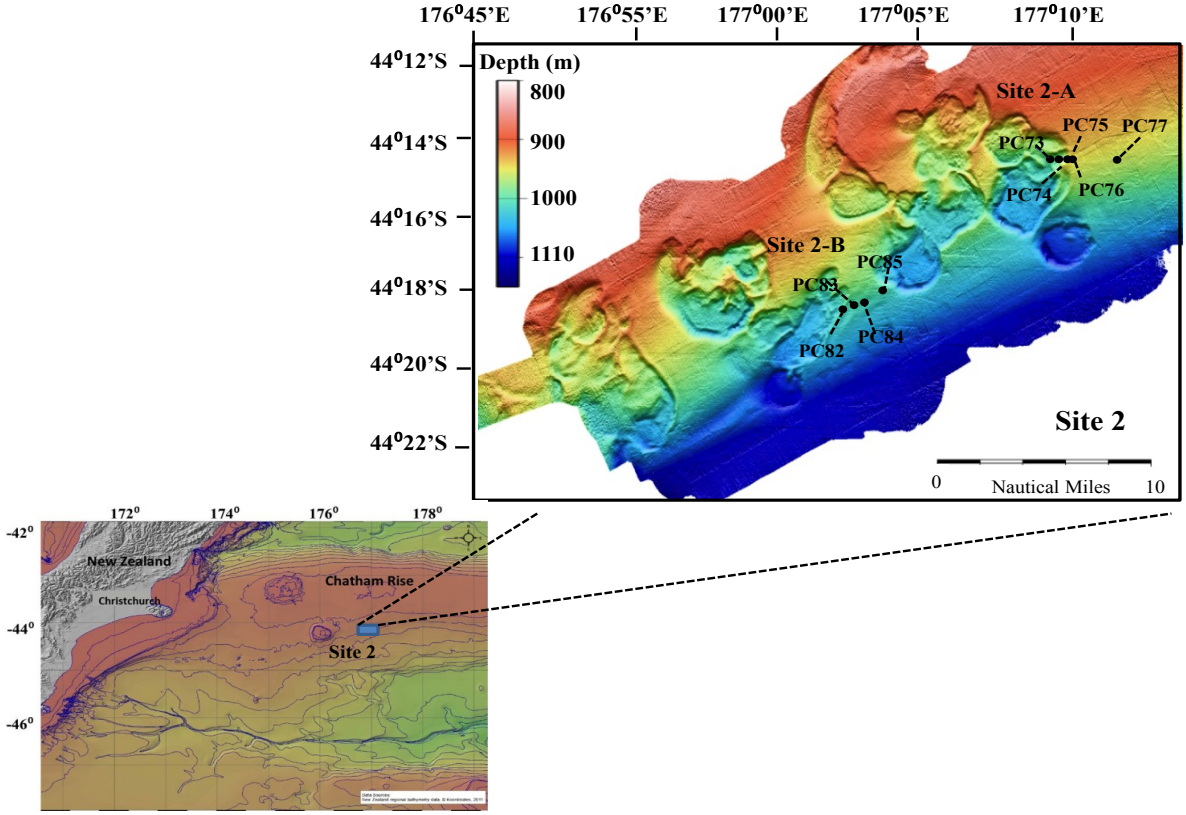

Figure 6.5.2.1. Location of coring Site 2-A and 2-B on the Chatham Rise.

Two regions were focused on after seismic review; Site 2a (Seismic Line 7114, Fig. 6.5.2.4.) and Site 2b (Seismic Line 7109, Fig. 6.5.2.4.). Through Site 2a chloride concentrations in all of the cores ranged from 489.7 to 540.1 mM. In general profiles were conservative with no vertical pattern, however there were a couple of points observed with lower concentrations (Fig. 6.5.3.1.). Porewater SO_4^{2-} and DIC concentrations in the cores ranged from 17.1 to 27.6 mM and 1.3 to 12.1 mM, respectively. PC75-2 was observed to have the greatest reduction of sulfate and increased of DIC through a linear pattern suggesting AOM (Fig. 6.5.3.1.). SO_4^{2-} profile observed in comparison to Site 2A. Where the SO_4^{2-} concentrations at the core sites were linear at Site 2A there was a trend for a consistent concentration from the surface down to approximately 200 cmbsf, with a subsequent shift in the concentration slope below 200 cmbsf. At this site the deeper linear slope is used for estimation of a minimum SO_4^{2-} depth representing AOM and organoclastic sulfate reduction.

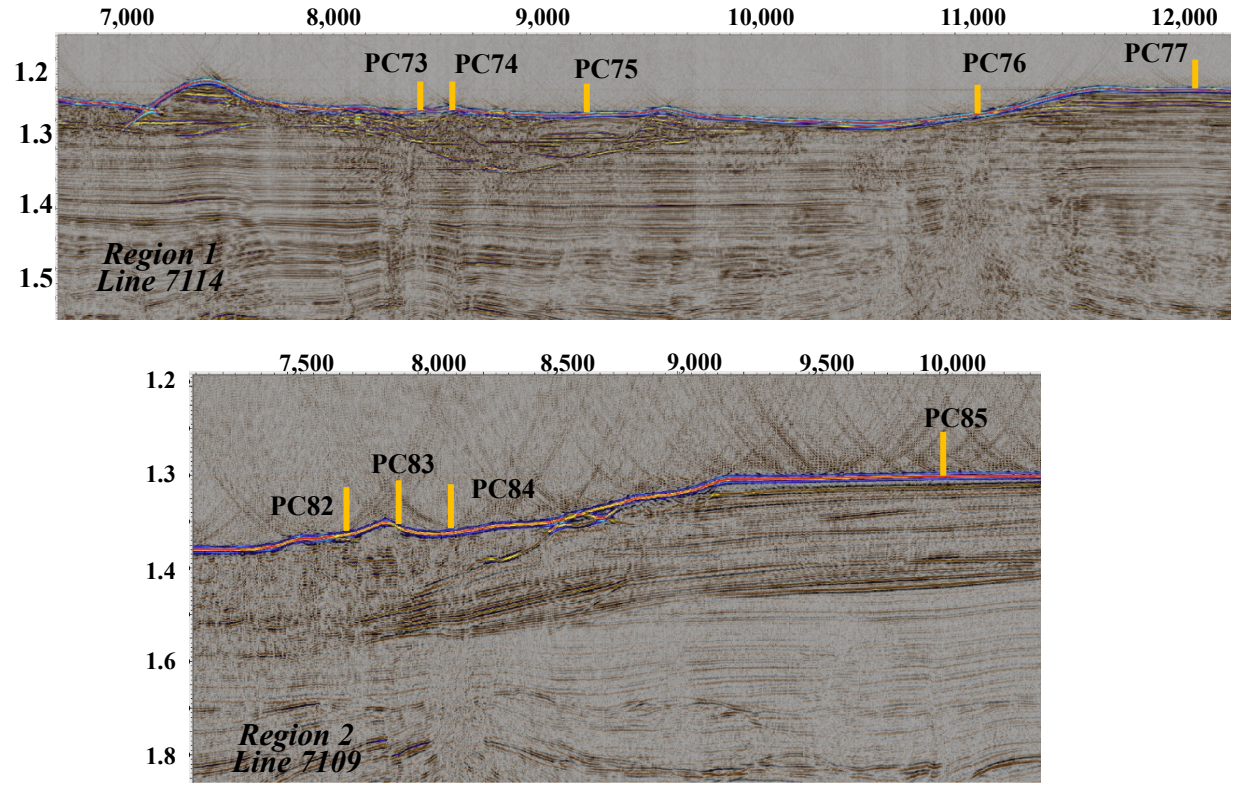

Figure 6.5.2.2. Seismic profiles and core locations for Site 2.

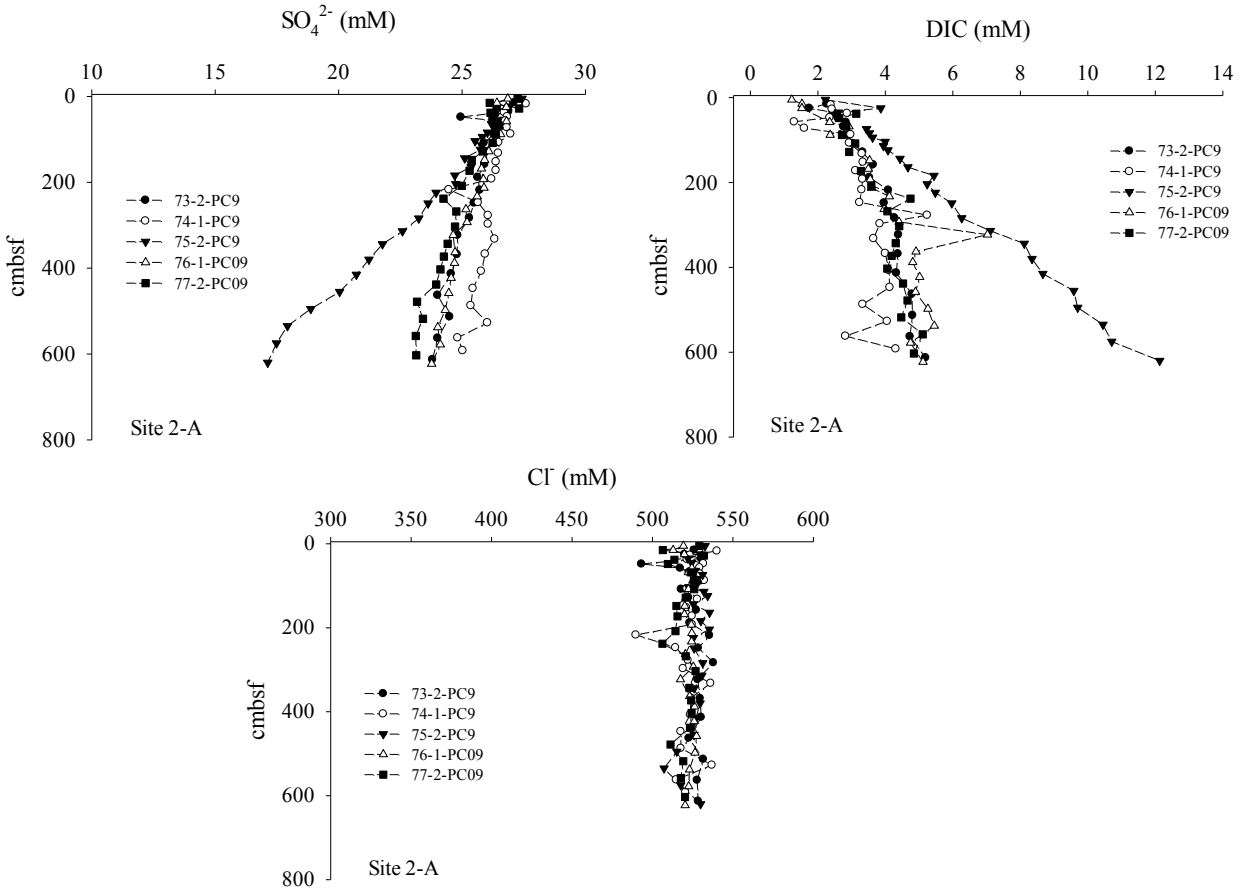

Figure 6.5.2.3. Porewater SO_4^{2-}, DIC and Cl^- profiles from cores taken at Site 2, location A.

At Site 2-B SO_4^{2-} concentrations in porewaters ranged from 27.4 to 22.9 mM (Fig. 6.5.2.4.). Porewater DIC concentrations ranged from 1.9 to 6.1 mM (Fig. 6.5.2.4.). Higher DIC concentrations in pore waters do appear to conicide with lower SO_4^{2-}, suggesting some low rate of biogeochemical sulfate reduction and methane or organic carbon oxidation. Cl^- concentrations ranged from 484.8 to 536.2 mM and did not show strong variations between different core sites or through the vertical profiles (Fig. 6.5.2.4.).

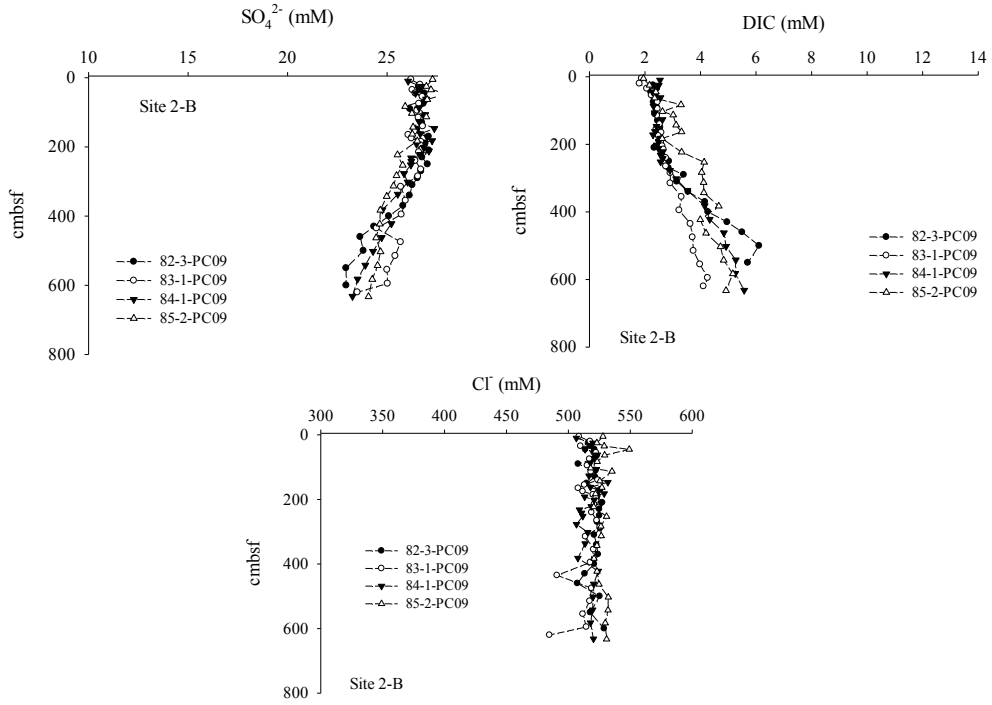

Figure 6.5.2.4. Porewater SO_4^{2-}, DIC and Cl^- profiles from cores taken at Site 2, location B.

6.5.3. Area 3

Site 3 was located at a more shallow region of Chatham Rise with a water column depth of approximately 570 m (Fig. 6.5.3.1.). Multibeam patterns and seismic profiles showed a slight pockmark formation with a split pattern below with disturbance in the bands that indicated vertical migration of fluids and/or gas to the surface (Fig. 6.5.3.1., 6.5.3.2). Three cores were selected in this location, one in center of the flow pattern and the other two on the sides of the center point (Fig. 6.5.3.2., PC95, PC96, PC97). PC94 was selected as a control core in a region with a strong stratification in the seismic pattern. PC98 was located in the center of a small pockmark with a disruption in the seismic pattern immediately below and follow a deep pathway into the sediment (Fig. 6.5.3.2.). Attempts to core at other locations in this region resulted in breaking core barrels, separating the winch cable wires, and minimal sediment samples.

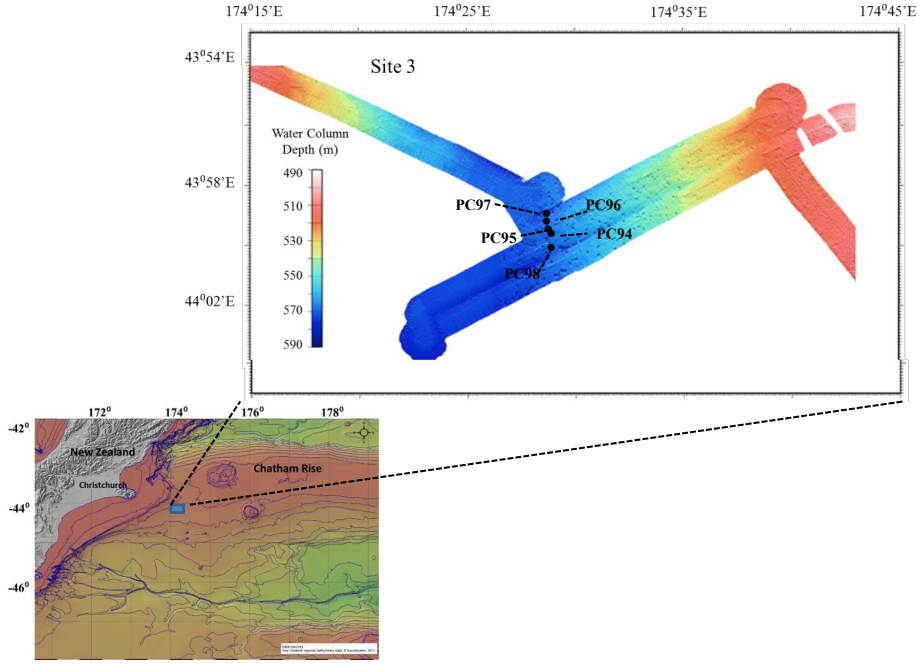

Figure 6.5.3.1. Location of coring Site 3 on the Chatham Rise.

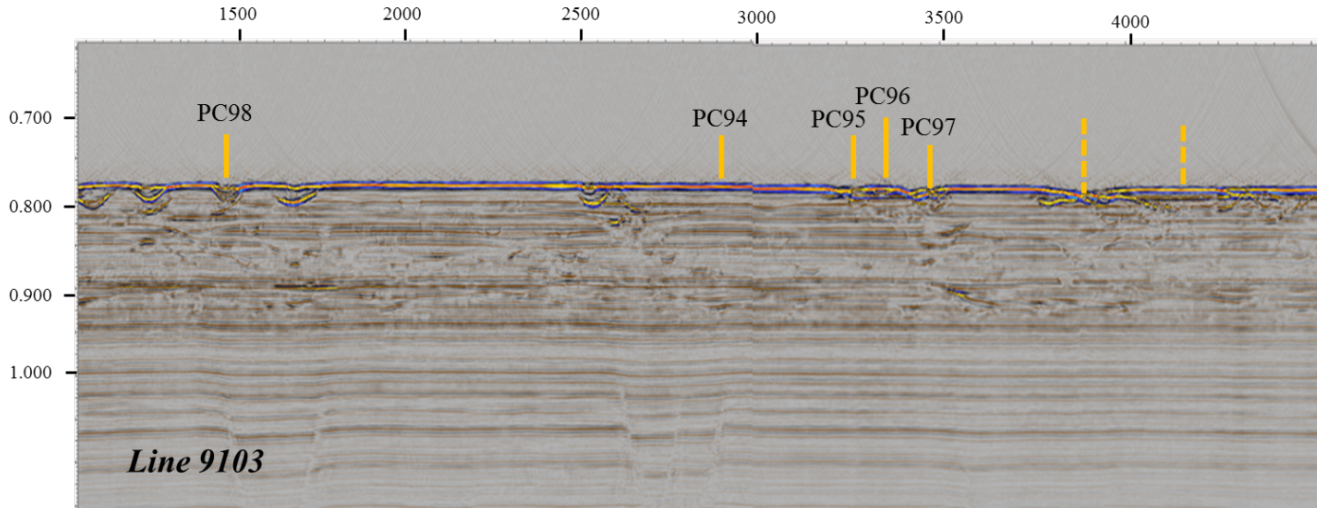

Figure 6.5.3.2. Seismic profiles and core locations for Site 3. Dashed lines represent failed coring sites.

Porewater SO_4^{2-} profiles through the sediment showed small to no changes in concentrations through a depth range of 408 to 633 cmbsf (Appendix 3, Fig. 6.5.3.3.). Dissolved inorganic carbon ranged from form 1.3 to 4.6 mM, generally lower than the other core regions. Some increase in DIC concentration was observed to correspond to the decreases in SO_4^{2-}. Porewater Cl^- concentration ranged 507 to 546 mM and did not show spatial or vertical variations (Fig. 6.5.3.3.).

6.5.4. Porewater Geochemistry Summary

Shallow sediment geochemical cycles that control porewater SO_4^{2-} and DIC are assumed to be AOM or organoclastic sulfate reduction. To evaluate the paleogeochemical CH_4 availability and cycling in the shallow sediment there is a need for thorough assessment of the current day shallow sediment flux and cycling. Studies show that vertical CH_4 fluxes can contribute up to 90% of the

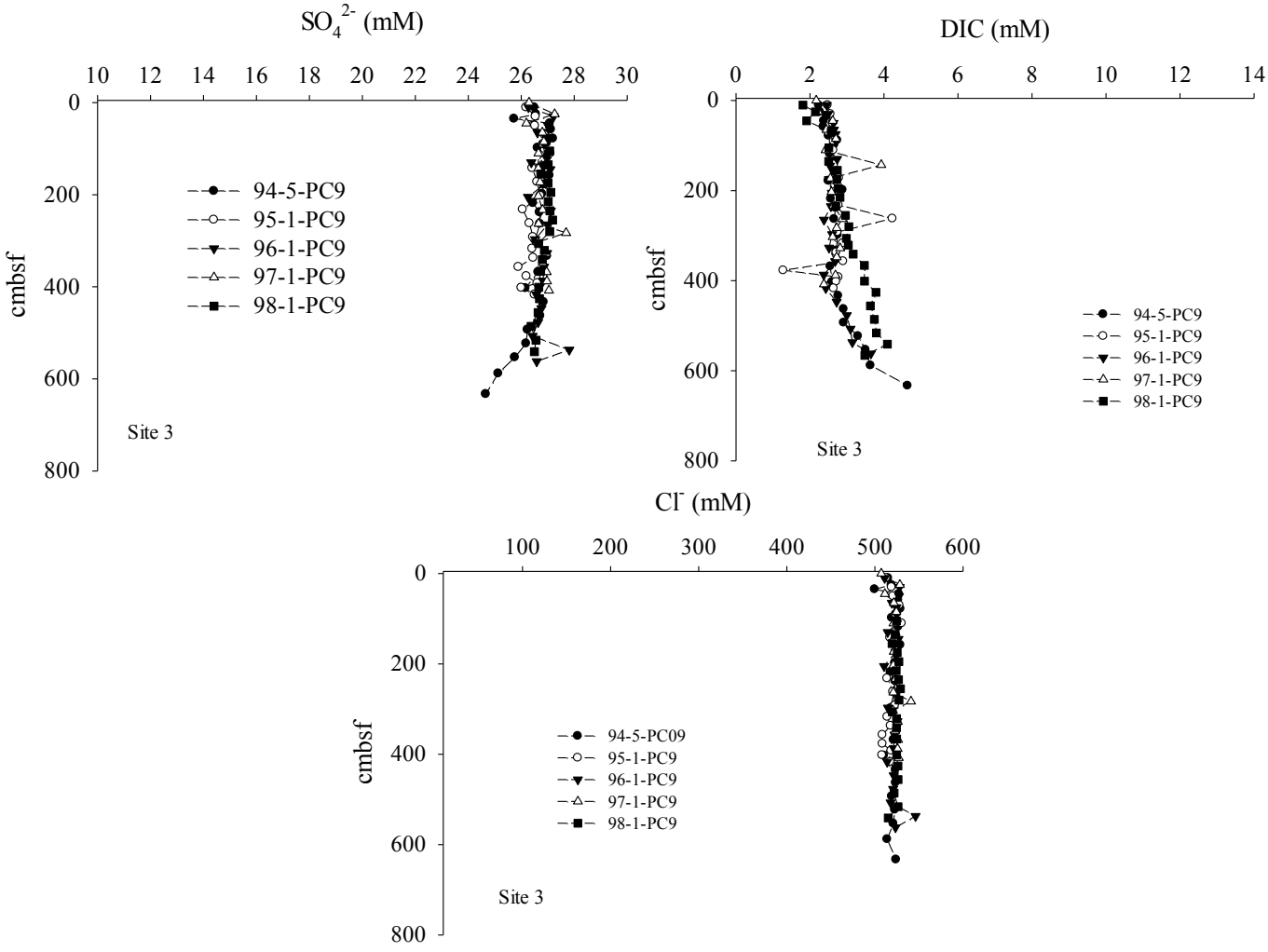

Figure 6.5.3.3. Porewater SO42-, DIC and Cl- profiles from cores taken at Site 3.

shallow sediment organic and inorganic carbon (Coffin et al. submitted-A, submitted-B). We summarize the potential modern day CH_4 input to the study regions with a comparison of sediment porewater Cl^- vs. SO_4^{2-} (Fig. 6.5.3.4.) and SO_4^{2-} vs. DIC (Fig. 6.5.3.5.) data for all of the cores in each region. This summary assumes that Cl^- is a conservative tracer for SO_4^{2-} reduction during AOM and/or organoclastic sulfate reduction (Fig. 6.5.3.4.).

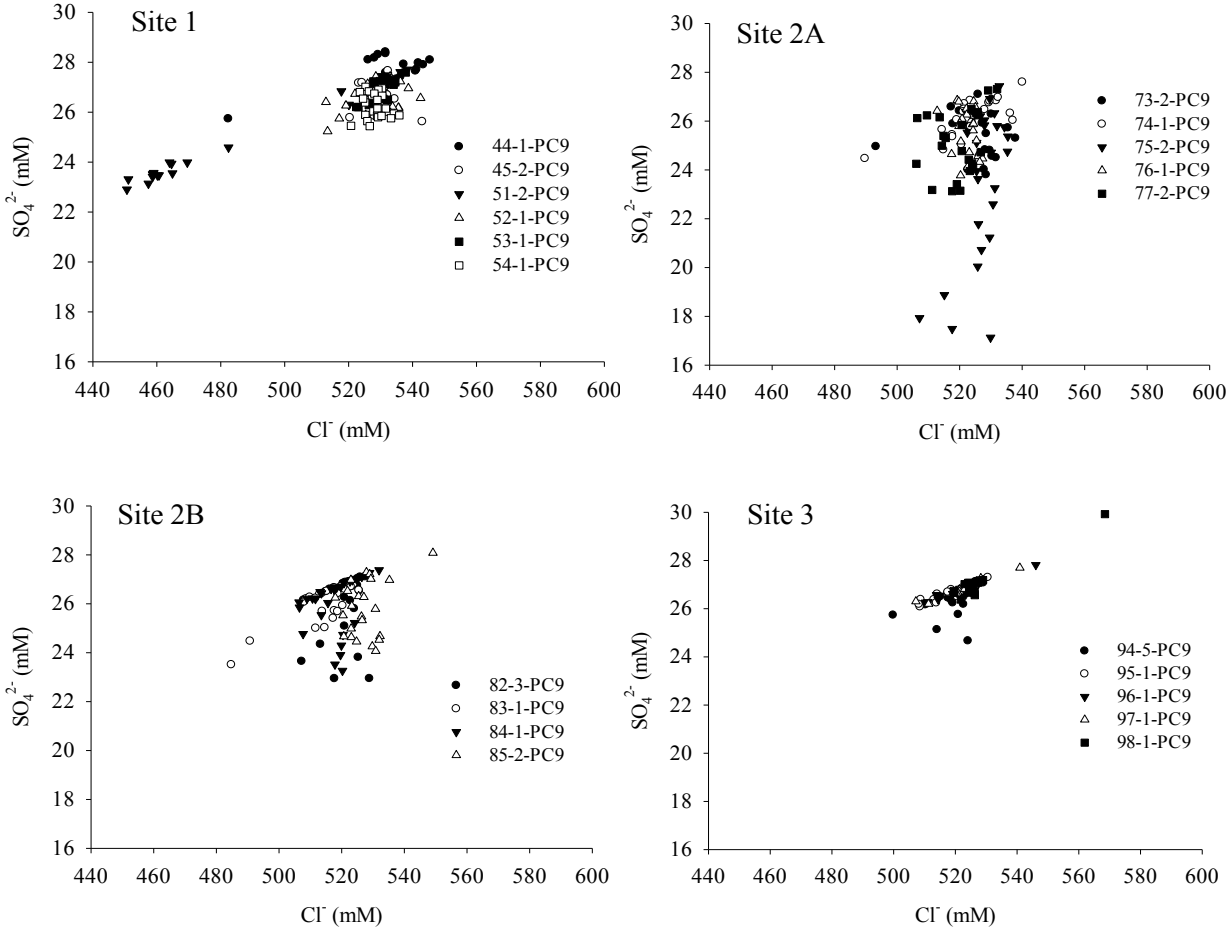

Figure 6.5.3.4. Comparison of the variation in porewater sulfate (SO_4^{2-}) concentrations relative to chloride (Cl^-) in cores from each region.

For this summary porewater SO_4^{2-} falls away from the linear Cl- profile at Sites 2A and 2B relative to Sites 1 and 3, suggesting more active SO_4^{2-} cycling. We also assume that DIC concentrations in the porewaters will increase through oxidation of CH_4 or organic matter during the SO_4^{2-} reduction to sulfide (Fig. 6.5.3.5.; Berner, 1964; Borowski et al., 1996; 1999). Cores taken at Sites 2A and 2B also show a higher porewater DIC concentration relative to a decline in SO_4^{2-} concentration.

The SO_4^{2-} and matching DIC gradients through cores provide the ability to estimate oxidation vertical methane migration and autochthonous organic matter. For this evaluation we predict sediment depth for depletion of SO_4^{2-} concentration to 0 mM using slope of the linear SO_4^{2-} profile (Table 6.5.3.6.). Porewater SO_4^{2-} pattern are less active than other regions where strong AOM and SMT's are estimated to be in the range of 0.1 to 12 mbsf [Coffin et al. 2006; 2008; submitted-A; submitted-B]. Here, the vertical $S0_4^{2-}$ profiles are reviewed for a preliminary estimate of the depth for a depleted, minimum concentration assuming sediment porosity, AOM and organoclastic sulfate reduction control the result. For Site 1 cores were predicted in a range of 22 to 103 meters below the sea floor (mbsf) (Table 6.5.3.6.) with more shallow values showing more variation through the profile (lower R^2). Site 2-A, while still moderate to low in the SO_4^{2-} reduction was the most active in this study with a SO_4^{2-} minimum estimated to range from 16.2 to 77.2 mbsf (Table 6.5.3.6). 75-2-PC9, with the greatest estimate for vertical methane migration was located above an apparent vertical gas flux site observed in the seismic pattern (Fig. 6.5.2.2.). Cores at Site 2-B showed a deeper SO_4^{2-} depletion depth, ranging from 23 to 56 mbsf and Site 3 was even less active in the biogeochemical cycling of SO_4^{2-} with a depleted concentration depth range of 55.4 to 117.3 mbsf. Note through these profiles the R^2 ranged from 0.988 to 0.140 and slopes with R^2 less than 0.600 had changes in concentration that were near the analytical limits of detection.

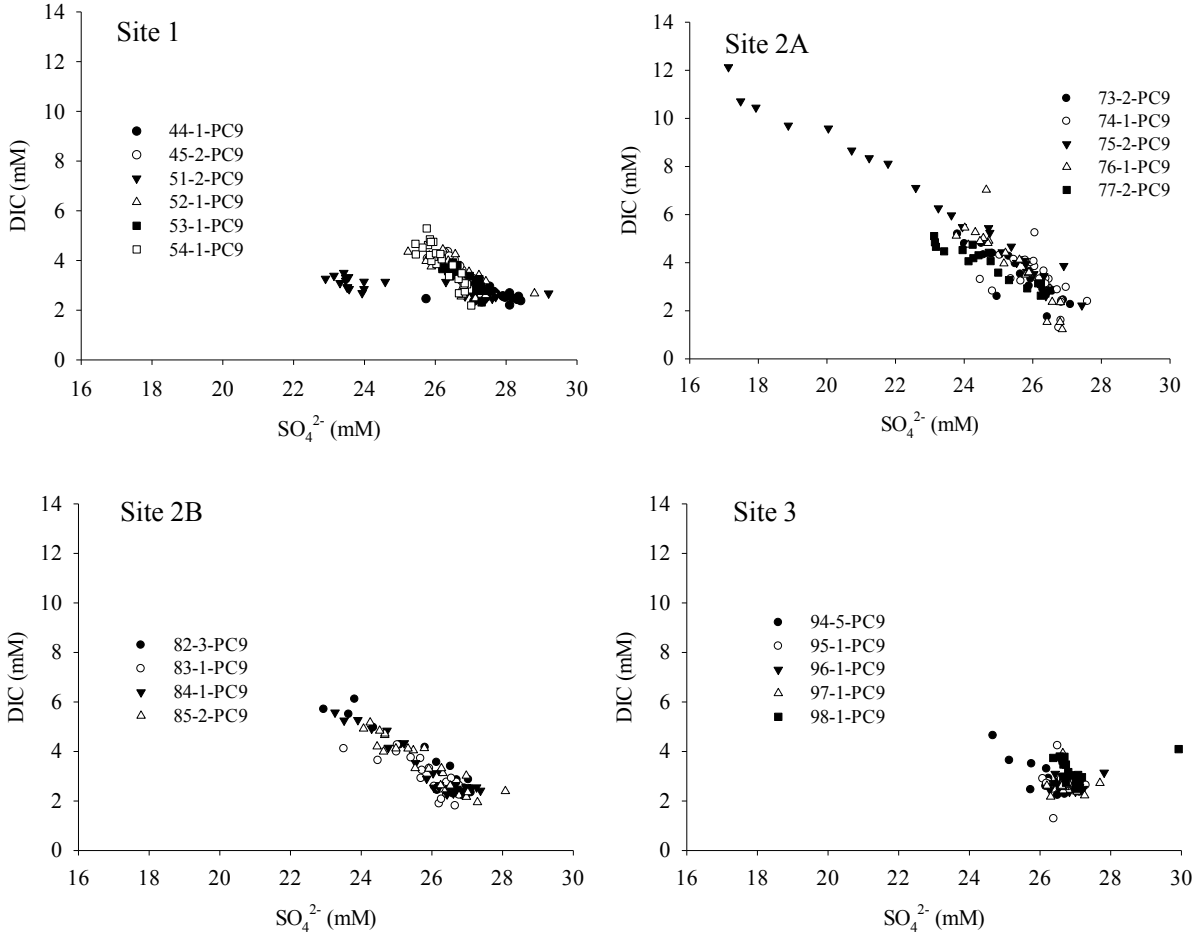

Figure 6.5.3.5. Reduction of porewater SO_4^{2-} relative to DIC production compared through cores and between the coring locations.

Table 6.5.3.6. Estimates for the depth of SO_4^{2-} minimum created by anaerobic oxidation of methane and/or organoclastic sulfate reduction. These estimates are based on observation of similar, inverse variations in the DIC and SO_4^{2-} concentrations in porewaters. These estimates will be assessed for AOM with laboratory analysis of porewater sulfide concentrations and stable carbon isotope analyses of dissolved inorganic carbon.

Site	Core ID	SO_4^{2-} Minimum (mbsf)	R2, N
1	44-1-PC9	34.4	0.140, 18
1	45-1-PC9	101.8	0.829, 25
1	51-1-PC9	22.1	0.549, 21
1	52-1-PC9	69.0	0.607, 22
1	53-1-PC9	103.3	0.774,25
1	54-1-PC9	100.2	0.763, 27
2A	73-2-PC9	51.5	0.955, 18
2A	74-1-PC9	77.2	0.936, 17
2A	75-2-PC9	16.2	0.988, 27

2A	76-1-PC9	50.5	0.962, 24
2A	77-2-PC9	37.5	0.920, 23
2B	82-3-PC9	23.5	0.958, 13
2B	83-1-PC9	38.0	0.760, 13
2B	84-1-PC9	33.6	0.957, 14
2B	85-2-PC9	51.6	0.859, 12
3	94-1-PC9	66.5	0.653, 24
3	95-1-PC9	55.4	0.201, 19
3	96-1-PC9	77.8	0.185, 21
3	97-1-PC9	no slope	n.d.
3	98-1-PC9	117.3	0.622, 18

6.5.5. Radiocarbon Isotope Analyses Background Survey

Background samples were taken of the lab van and ship to assess any background ^{14}C levels that would interfere with the analyses of natural abundance. These tests were taken in the lab van and at different regions around the ship (Table 6.5.3.7.). Data showed a clean radiocarbon background and indicated no interference with radiocarbon natural abundance analyses.

The preliminary data obtained during the SO226/2 expedition provides the following information for completing the analysis of samples to address paleo-geochemical methane cycling across Chatham Rise.

1. Low current day methane vertical fluxes suggest there will not be an overlap of the modern day and paleo-geochemical carbon cycling.
2. A large variation in shallow sediment depths relative scoured regions will require careful selection of cores sites and thorough age profiles in the mixed sediment.
3. Current day organic and inorganic carbon sources will be determined with analysis of $\delta^{13}C$ of organic and inorganic sediment and porewater carbon.
4. Stable nitrogen isotope analysis of organic matter will be included in the evaluation to understand the shallow sediment carbon cycling.
5. Radioisotopes ($_{230}Th$, $_{210}Pb$, and $_{231}Pa$) will be examined through the core regions to determine the modern day sedimentation rates and spatial variations of sediment mixing.
6. Radioisotopes ($_{230}Th$, $_{210}Pb$, and $_{231}Pa$) will be compared with $\delta^{14}C$ of sediment inorganic and organic carbon to determine if methane contributed to shallow sediment carbon cycle during the previous climate change.

Table 6.5.3.7. Radiocarbon blank testing for back ground data in the NRL portable lab and the RV SONNE laboratories.

Sample ID	Sample Weight (mg)	Carbon Weight (mgC)	Conventional Radiocarbon Age (years BP)	$\delta^{13}C$ (‰)	Fraction Modern (pmc)
841, Lab Van, Whatman QMA filter ashed, no swipe or isopropanol	45.7	0.8	33654 ± 690	-26.2 ± 0.2	0.0152 ± 0.0013
842, Lab Van, Whatman QMA filter ashed, no swipe with isopropanol	44.7	0.9	23731 ± 199	-26.2 ± 0.3	0.0521 ± 0.0013
843, Lab Van, Whatman QMA filter ashed, swipe port side lab bench with isopropanol	45.9	1.0	15745 ± 75	-26.4 ± 0.2	0.1409 ± 0.0013
844, Lab Van, Whatman QMA filter ashed, swipe starboard side lab bench with isopropanol	45.5	1.1	10731 ± 39	-26.3 ± 0.2	0.2629 ± 0.0013
845, Lab Van, Whatman QMA filter ashed, swipe floor with isopropanol	44.8	1.1	14339 ± 60	-26.2 ± 0.2	0.1678 ± 0.0012
SONNE-1, Location 1	46.1	0.7	13206 ± 52	-23.3 ± 0.2	0.1932 ± 0.0013
SONNE-2, Location 2	45.3	1.2	26598 ± 282	-26.3 ± 0.2	0.0365 ± 0.0013
SONNE-3, Location 3	46.1	1	13945 ± 57	-26.2 ± 0.2	0.1762 ± 0.0013
SONNE-4, Location 4	45.9	1	13516 ± 55	-26.2 ± 0.2	0.1859 ± 0.0013
SONNE-5, Location 5	44.1	1	9095 ± 38	-26.3 ± 0.2	0.3223 ± 0.0015
SONNE-6, Location 6	45.3	1.1	12171 ± 46	-26.4 ± 0.2	0.2198 ± 0.0013
SONNE-7, Location 7	44.8	1.2	18021 ± 110	-26.7 ± 0.2	0.1061 ± 0.0015
SONNE-8, Location 8	44.8	1.1	12135 ± 46	-27.1 ± 0.2	0.2208 ± 0.0013
SONNE-9, Location 9	44.2	1	26609 ± 282	-26.5 ± 0.2	0.0364 ± 0.0013
SONNE-10, Location 10	44.8	1.2	42387 ± 2015	-26.2 ± 0.2	0.0051 ± 0.0013

6.6. Cores for stratigraphic and paleoceanographic analysis.

Core descriptions of the eight cores collected for the purposes of constraining the timing and paleoceanographic conditions during formation of the seafloor depressions on Chatham Rise are compiled below and summarised in Fig 6.6.1. Coordinates and further information on the core locations are listed in Tab. 6.5.1.

SO226-2-33-1: Chatham 1, Water Depth 899 m, Core Length 4.36 m.

Light olive grey sandy silt overlying and grading to grey silt, few bioturbation burrows and blebs, ~5% black minerals (glauconite/pyrite) sharp boundary at 70 cm. These deposits are likely to be from the last glacial cycle i.e. Marine Isotope Stage (MIS 1 and 2). Below lithified white biogenic (coccolith and foraminifera) ooze occurs to end of core. The latter deposit is potentially of Miocene age indicating a significant hiatus occurs at about 70 cm below seafloor (bsf).

SO226-2-45-1: Chatham 1, Water Depth 747 m, Core Length 6.85 m.

Light olive grey sandy silt grades at 98 cm to an olive gray silt which extends to 185 cm bsf. Minor presence of bioturbation structures and evidence of heavy minerals (glauconite/pyrite). These deposits are likely to be from the last glacial cycle, MIS 1 and 2. Underlying is a succession of alter-

nating light olive grey and olive grey silts, exhibiting minor presence of bioturbation structures and evidence of heavy minerals (glauconite/pyrite). Evidence of a slope failure/turbiditic deposit is noted at 400 cm bsf. These latter deposits may represent sediments that extend up to MIS8.

SO226-2-57-1: Chatham 1, Water Depth 634 m, Core Length 1.86 m

Olive grey sandy silt grading, at 17 cm to a gray silt deposit that extends to 74 cm bsf. Underlying is a firm light olive grey silt with bioturbation and presence of glauconite both increasing down the unit from ~10% to 30%. After an irregular bioturbated boundary sediments are heavily bioturbated sandy silts with significant lenses of concentrated glauconite. Sediments within the upper 2 units of the core are likely to from the last glacial cycle.

SO226-2-75-1: Chatham 2, Water Depth 963 m, Core Length 6.50 m

Light olive grey, homogenous sandy silt grades into stiffer homogenous gray silt at 116 cm bsf, this lower unit occurs to the end of core at 650 cm. A thick tephra unit occurs between 343 and 350 cm, this light grey sand is most likely a deposit of the widely dispersed Kawakawa Tephra, with a reported last glacial age of 25.45 cal ka BP. Therefore, these deposits represent an overthickened deposit from MIS1 and 2.

SO226-2-77-3: Chatham 2, Water Depth 936 m, Core Length 6.54 m

Olive grey sandy silt grades, at 14 cm, into gray silt which extends to 60 cm bsf. A thin gray tephra unit occurs at 32-36 cm, likely a deposit of the widely dispersed Kawakawa Tephra, with a reported last glacial age of 25.45 cal ka BP. Hence, these upper 2 units represent sediment from MIS 1 and 2. Underlying is a succession of alternating light grey, grey and olive grey silts, exhibiting minor presence of bioturbation structures and evidence of heavy minerals (glauconite/pyrite). Light grey units between 260 to 330 cm exhibit sandier textures dominiated by foraminifera and therefore likely represent deposits of the relatively warmer MIS 5 or other interglacial times. Hence this core also potentially extends to or past MIS8.

SO226-2-85-1: Chatham 2, Water Depth 973 m, Core Length 6.37 m

Olive grey sandy silt grades, at 7 cm, into gray silt which extends to 50 cm bsf. A thin gray tephra unit occurs at 29-30 cm, likely a deposit of the widely dispersed Kawakawa Tephra, with a reported last glacial age of 25.45 cal ka BP. These upper 2 units represent sediment from MIS 1 and 2, with the uppermost deposit representing MIS 1 potentially incomplete. Similar to core SO226-2-77-3, underlying is a succession of alternating light grey, grey and olive grey silts, exhibiting minor presence of bioturbation structures and evidence of heavy minerals (glauconite/pyrite). A light grey unit between 230 to 270 cm exhibits a sandier texture dominated by foraminifera and therefore likely represent deposits of the relatively warmer MIS 5 (particularly MIS5e) or other interglacial times. Hence this core also potentially extends to or past MIS8.

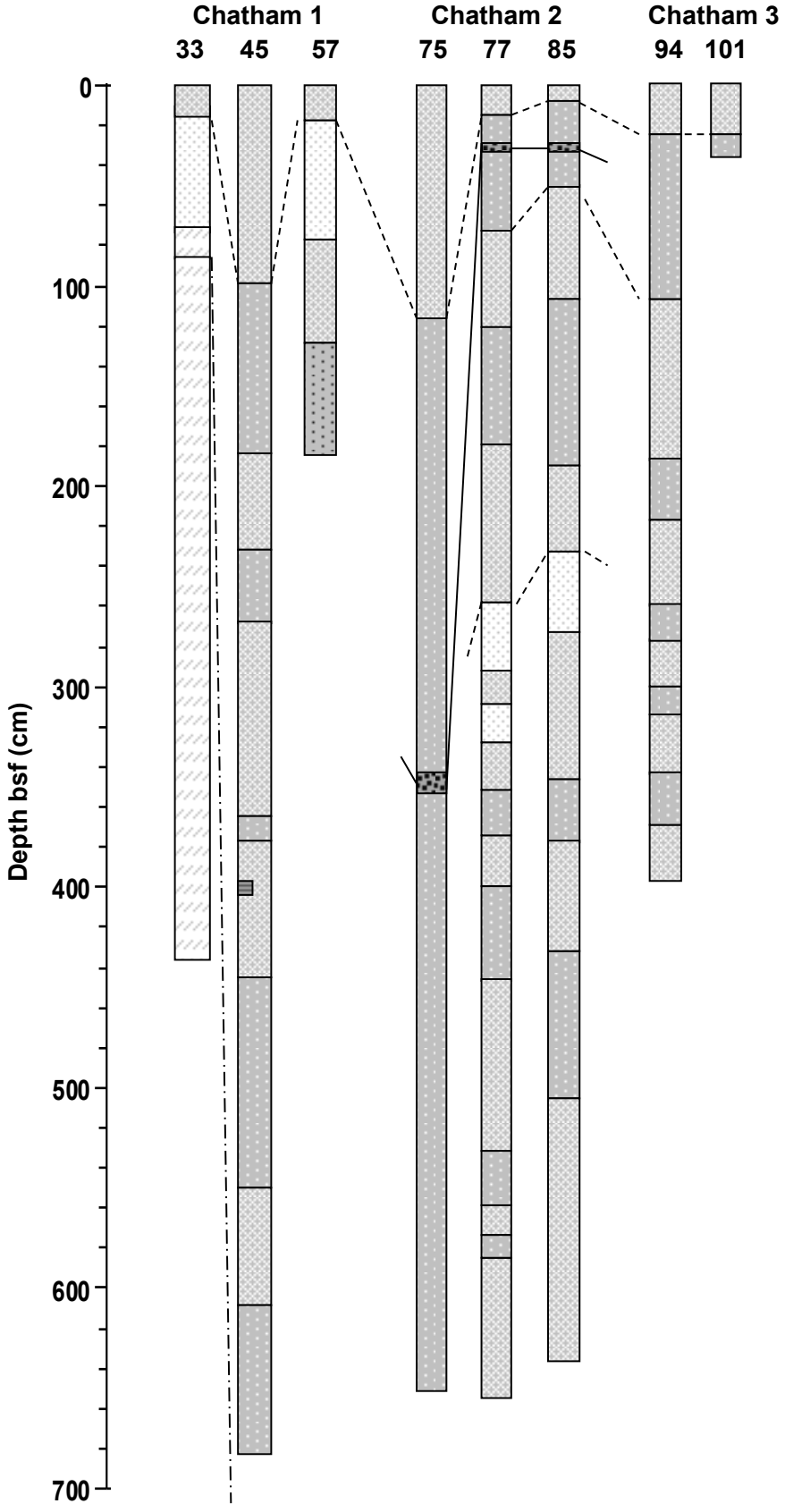

Figure 6.6.1. Summary of sedimentary units defined within the eight designated cores for paleoceanographic assessment.

SO226-2-94-3: Chatham 3, Water Depth 568 m, Core Length 4.43 m

Olive grey sandy silt grades, at 30 cm, into gray silt which extends to 121 cm bsf, these upper 2 units represent sediment from MIS 1 and 2. Similar to preceding cores SO226-2-77-3 and 85-1, underlying is a succession of alternating grey and olive grey silts, exhibiting minor presence of bio-turbation structures and evidence of heavy minerals (glauconite/pyrite). Several thin sandy units, distinguishable only by texture, are evident throughout the core and are potentially a consequence of current winnowing or preferential deposition of coarser material. Hence, this core potentially extends to or past MIS6.

SO226-2-101-1: Chatham 3, Water Depth 572 m, Core Length 0.49 m

Olive grey sandy silt grades, at 30 cm, into gray sandy silt which extends to 44 cm bsf. The base of the lower unit comprises stiff sandy silt, possibly the result of current winnowing of fines.

6.7. Multi-corer preliminary results

A total of 42 multi-corer deployments were undertaken: 18 in Area 1 (mega-pockmarks), 17 in Area 2 (medium pockmarks) and 7 in Area 3 (small pockmarks). In general, the multi-corer was deployed with 4 core tubes to maximize sediment returns, and there were repeat sampling only required at one site (Station 70).

At all multi-corer sampling sites, one core was sectioned at 1 cm intervals to 5 cm and then every 10 cm to the base of the core and samples stored frozen (-20° C) until analysis for physical (i.e., grain-size, water content, carbonate content – Nodder, NIWA) and biogeochemical sediment parameters (i.e., organic carbon, sediment pigment concentrations (chlorophyll *a*, phaeopigments) – Nodder, NIWA). A second core was also sectioned at 1 cm intervals, and will be analyzed for Pa and Th radio-isotopes to determine the degree of lateral transport across the study area (Rose, NRL).

At selected locations, typically inside and outside pockmark areas (see Table 1 below), a suite of multi-cores were collected for characterising the sediment infaunal communities and their functioning (Nodder). Typically, from these locations, one core was sectioned at 0-1 cm intervals to the base of the core and stored frozen (-20°C) in Whirlpak bags, three cores were used in sediment community oxygen consumption (SCOC) incubations and three cores were used for meiofauna and bacterial analyses, as outlined below.

In the SCOC incubations, sediment was extruded from the multi-corer tubes into incubation chambers and the consumption of oxygen by infauna was monitored over time (from 47-53 hours) in these chambers incubated at bottom water temperatures (~5° C) in self-regulating water baths. The %O2 reduction was monitored over time in the sediment chambers and in one chamber with water collected from each site (blank) using a PreSens Fibox3 LCD trace v7 oxygen meter and a PSt3 oxygen sensor from the University of Waikato, Hamilton, New Zealand (Dr Conrad Pilditch). Two point calibrations were completed immediately prior to each set of incubations using Na_2SO_4 (0% oxygen) and a 100% oxygen standard. At the completion of the incubations, these cores were processed for macrofauna (>300 μm over 0-5 and 5-10 cm and 10 cm to the base of the incubation core (typically 11-13 cm) depth intervals) and preserved with 10% formalin.

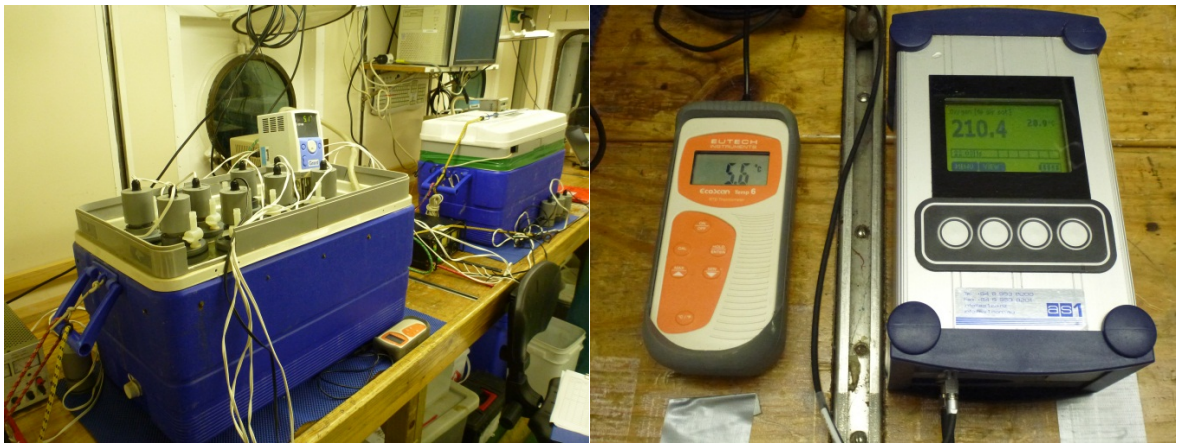

Figure 6.7.1. Sediment Community Oxygen Consumption (SCOC) incubation set-up (left) and PreSens oxygen sensor system (right).

Figure 6.7.2. Examples of SCOC incubation chambers

In addition, three cores from each site were sampled using 29 mm diameter sub-cores for meiofauna (>32 µm over 0-1, 1-3 and 3-5 cm intervals), stained with Rose Bengal and preserved with 10% formalin. These same cores were also processed for bacteria in the water immediately overlying the sediment-water interface (50 ml subsample) and in the surface sediments (~30 ml sediment). For the latter, a surface scrape of sediment was taken antiseptically, placed in a 50 ml centrifuge tube, made into a slurry using Phosphate Buffer Solution (volume made up to 40 ml) and sub-sampled for bacterial abundance (e.g., sediments with no PBS – 2 x 3 ml, with PBS – 2 x 3 ml and with 1 ml RNALater – 1 x 2 ml) and productivity using ^{3}H-thymidine incorporation methods (for each core – 2 x 5 ml sediment, plus one control).

All water and sediment samples were stored frozen (-20°C), except for the sediment bacterial productivity samples, which were incubated at ambient bottom water temperatures (~5°C) in the water baths used for the SCOC incubations for 3 hours, poisoned with 5 ml 5% formaldehyde and then frozen (-20°C). The bacterial productivity control samples were poisoned with 2 ml 5% formaldehyde and not incubated. All the bacterial productivity samples were refrigerated at 4°C until processing onland.

6.8. Methane sensor results

On Saturday 16th February the Hisem sensor was attached to the video sled OFOS on SONNE that was deployed during a several hours lasting tow-track. Due to its high sensitivity even nanomolar methane peaks in the water column should have appeared as an elevated signal in the data. However, no elevated methane concentration was found at a tow depth of 824 m in working area "A" corresponding to very low methane concentration within several piston cores and visual observations without any seepage related benthic organisms. The measured methane partial pressure was converted into methane concentration in water after Wiesenburg and Guinasso (1979), and Weiss (1970) to 1.9 nmol / L. This value represents typical oceanic methane background methane concentrations (0.5-3nmol/L) as also measured in the North off New Zealand at the Hikurangi margin by Faure et al. (2010).

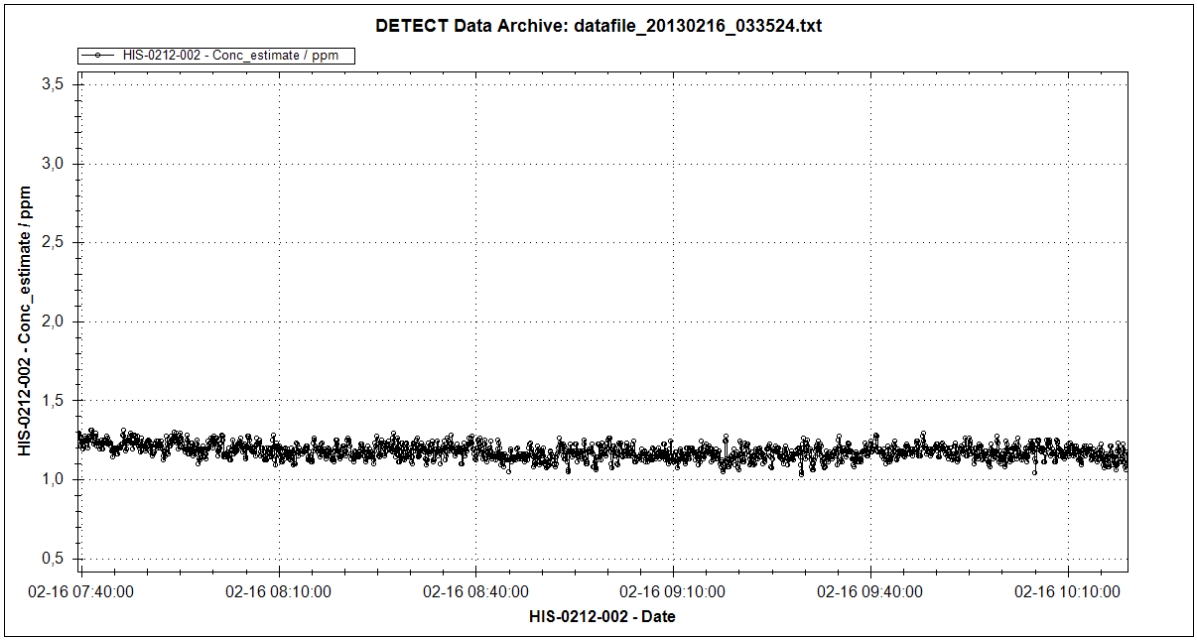

Figure 5.5.2. HISEM_Data CH4 on the OFOS

On Monday, the 18th February the methane sniffer was attached to a CTD (945 m) to potentially locate layers with elevated methane concentration in the water column. Such elevations can be caused by seepage or by the abundant zooplankton layers that were found by active acoustics throughout the cruise in the water column. However, no signal in the water column has been observed. To test the device the CTD trigger-weight was dumped into the sediment to cause some sediment suspension and the CTD rested close to the seabed for 2 min. A slight signal might be visible with a time delay of 10 min after approaching the seafloor. However, the signal is difficult to see as the impacts of the temperature changes have to be evaluated.

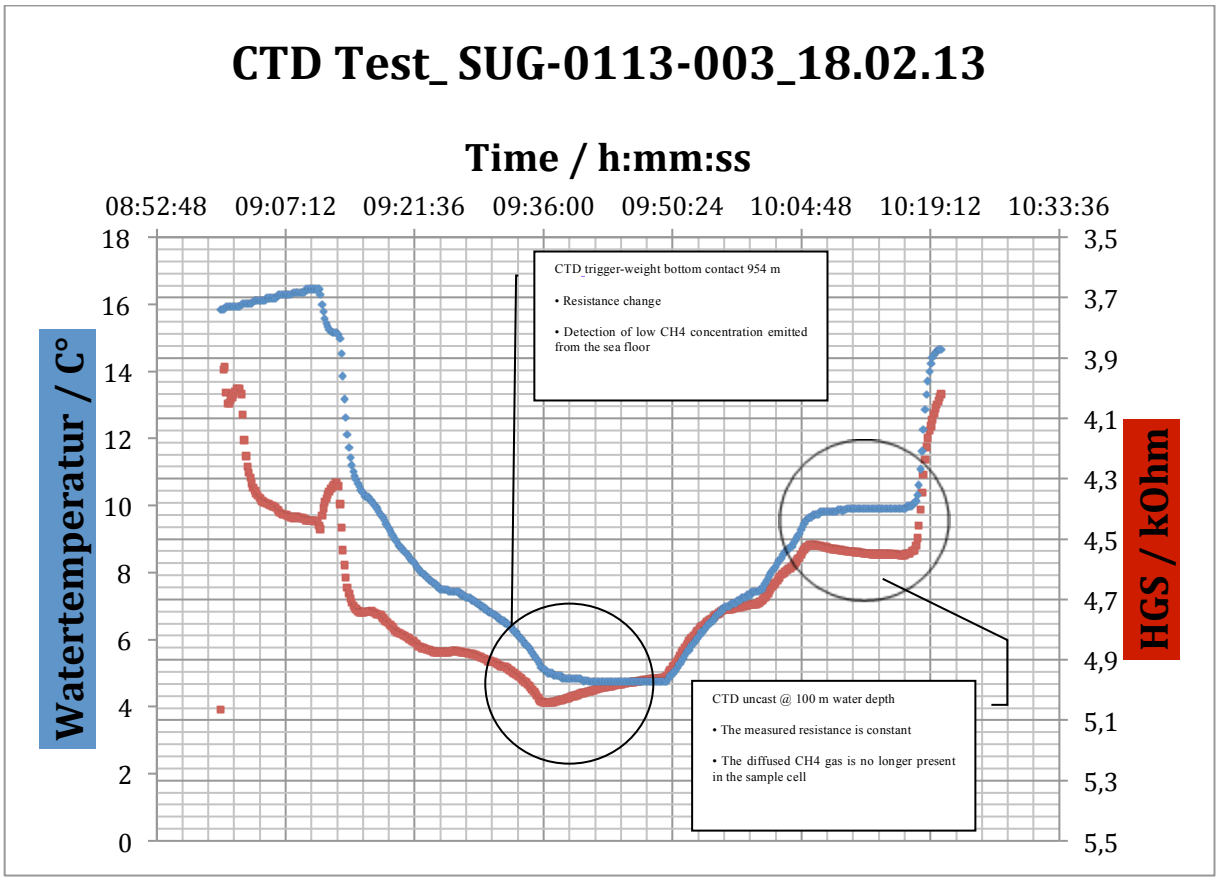

Figure 5.5.3. CTD Test_ SUG-0113-003_ Sniffer

Furthermore, this sensor has been integrated into the side-scan towfish during its deployment on Wednesday the 20th February 2013. The results show a similar temperature-dependent curve as the CTD profile. The measured resistance values do not show a clear signal that could be indicative for elevated methane concentration.

7. Acknowledgments

The cruise SO226 CHRIMP Leg 1 and 2 was financed by the German Federal Ministry for Education and Research (Bundesministerium für Bildung und Forschung, BMBF) under project No. 03G0226. We are grateful to the continuous support of marine sciences with an outstanding platform such as R/V SONNE.

We acknowledge the financial support of the 3D seismic acquisition by GNS

The authors wish to express their gratitude to all the colleagues who have supported the work before, during and after the cruise. Much of the work done during the cruise was only made possible by the scientists', technicians' and the crews' experience.

Particular thanks are directed to Captains Lutz Mallon and Oliver Meyer and to the entire crew of R/V SONNE for their excellent support throughout the cruise.

8. References

Adams C. J., H. J. Campbell & W. J. Griffin (2008): Age and provenance of basement rocks of the Chatham Islands: An outpost of Zealandia, New Zealand Journal of Geology and Geophysics, 51:3, 245-259

Bialas, J. & E. R. Flueh (1999) Ocean bottom seismometers: New instrument package demonstrates value of recording full wavefield; shows that interpretations of sediment shear wave velocities are reliable. Sea Technology, 40, 41-46.

Bialas, J., E. R. Flueh, J. Phipps Morgan, K. Schleisiek & G. Neuhaeuser. 2002. Ocean-bottom seismology in the third millennium. In SCIENCE TECHNOLOGY SYNERGY FOR RESEARCH IN THE MARINE ENVIRONMENT: CHALLENGES FOR THE XXI CENTURY, eds. L. Beranzoli, P. Favali & G. Smriglio, 37-44. UK: Elsevier Science Pub Co.

Bradshaw, J. D. (1989), Cretaceous dispersion of Gondwana: Continental and oceanic spreading in the southwest Pacific-Antarctic sector, in Geological Evolution of Antarctica, edited by M. R. A. Thomson et al., pp. 581–585, Cambridge Univ. Press, New York

Borowski, W. S., C. K. Paull, and W. Ussler III. 1999. Global and local variations of interstitial sulfate gradients in the deep-water, continental margin sediments: Sensitivity to underlying methane and gas hydrates. Mar. Geol. 159:131-154.

Carter, L., Carter, R.M., 1993. Sedimentary evolution of the Bounty Trough: a Cretaceous rift basin, southwestern Pacific Ocean. In: Ballance, P.F. (Ed.), South Pacific Sedimentary Basins. Sedimentary Basins of the World, 2. Elsevier, Amsterdam, pp. 51-67.

Carter, L., Garlick, R.D., Sutton, P., Chiswell, S., Oien, N.A., Stanton, B.R., 1998. Ocean Circulation New Zealand. National Institute of Water and Atmospheric Research Chart, Misc. Ser. 76.

Carter, R.M., McCave, I.N., Richter, C., Carter, L., et al., (1999), Proceedings of the Ocean Drilling Program, Initial Reports Volume 181.

Carter, L., Neil, H.L. and McCave, I.N. 2000), Glacial to interglacial changes in non-carbonate and carbonate accumulation in the SW Pacific Ocean, New Zealand, Palaeogeogr. Palaeoclimatol. Palaeoecol., 162(3–4), 333–356, doi:10.1016/S0031-0182(00)00137-1.

Carter, L.; R.M. Carter, I.N. McCave (2004), Evolution of the sedimentary system beneath the deep Pacific inflow off eastern New Zealand, Marine Geology, 205, 9-27

Cathles, L. M., Z. Su, and D. Chen (2010), The physics of gas chimney and pockmark formation, with implications for assessment of seafloor hazards and gas sequestration, Marine and Petroleum Geology, 27(1), 82-91.

Chiswell, S.M., 1994. Acoustic Doppler current profiler measurements over the Chatham Rise. N.Z. J. Mar. Freshwater Res. 28, 167-178.

Chiswell, S. M. (2002), Temperature and salinity mean and variability within the subtropical front over the Chatham rise, New Zealand, New Zealand Journal of Marine and Freshwater Research, 36(2), 281-298.

Coffin, R.. B., C. L. Osburn, R. Plummer, and K. S. Grabowski (Submitted-A) Deep sediment methane incorporation into shallow sediment carbon pools in Atwater Valley, Texas-Louisiana Shelf, Gulf of Mexico. Marine Petroleum and Geology.

Coffin, R.B., Hamdan, L.J., Plummer, R.E. Smith, J.P., Osburn, C.L., Yoza, B. Pecher, I., Rose, P.S., Montgomery, M.T. (Submitted-B). Plate convergence forcing influence on shallow sediment carbon cycling: Porangahau Ridge, Hikurangi Margin, New Zealand. Marine Petroleum and Geology.

Cullen, D.J., 1987. The submarine phosphate resource on central Chatham Rise. Div. Mar. Freshwater Sci. Rep. 2, DSIR,22 pp.

Davy, B., and R. A. Wood (1994), Gravity and magnetic modelling of the Hikurangi Plateau, Mar. Geol., 118, 139–151, doi:10.1016/0025-3227(94)90117-1.

Davy, B., K. Hoernle, and R. Werner (2008), Hikurangi Plateau: Crustal structure, rifted formation, and Gondwana subduction history, Geochem. Geophys. Geosyst., 9, Q07004, doi:10.1029/2007GC001855

Davy, B., I. Pecher, R. Wood, L. Carter, and K. Gohl (2010), Gas escape features off New Zealand: Evidence of massive release of methane from hydrates, Geophysical Research Letters, 37(21), n/a-n/a.

Dickens, G. R., M. M. Castillo, and J. C. G. Walker (1997), A blast of gas in the latest Paleocene: Simulating first-order effects of massive dissociation of oceanic methane hydrate, Geology, 25(3), 259-262.

Dickens, G. R. (2001), The potential volume of oceanic methane hydrates with variable external conditions, Org. Geochem., 32, 1179-1193.

Donahue DJ, Linick TW, Jull AJT. 1990. Isotope-ratio and background corrections for accelerator mass spectrometry radiocarbon measurements. Radiocarbon 32(2):135.

Faure, K., Greinert, J., Schneider von Deimling, J., McGinnis, D. F., Kipfer, R., & Linke, P. (2010). Methane seepage along the Hikurangi Margin of New Zealand: Geochemical and physical data from the water column, sea surface and atmosphere. Marine Geology, 272, 170-188. doi:10.1016/j.margeo.2010.01.001.

Flueh, E. R. & J. Bialas (1996) A digital, high capacity ocean bottom recorder for seismic investigations. Underwater Systems Design.

Goff, J.A., Kraft, B.J. Mayer, L.A. Schock, S.G. Sommerfield, C.K. Olson, H.C. Gulick, S.P.S. & Nordfjord, S.(2004). Seabed characterization on the New Jersey middle and outer shelf: correlatability and spatial variability of seafloor sediment properties. Marine Geology, 209, 147-172.

Heath, R.A., 1972. The Southland current. N.Z. J. Mar. Freshwater Res. 6, 497-533.

Heath, R. A. (1972) Choice of reference surface for geostrophic currents around New Zealand. New Zealand Journal of Marine and Freshwater Research, 6, 148-177.

Heath, R.A., 1985. A review of physical oceanography of the seas around New Zealand - 1982. N.Z. J. Mar. Freshwater Res. 19, 79-124.

Herzer, R.H., 1981. Ellesmere sediments. New Zealand Oceanographic Institute Coastal Chart Series 1:200 000 sediments.

Judd, A. G., and M. Hovland (2007), Seabed Fluid Flow, Cambridge University Press, New York.

Karoui, I., Fablet, R., Boucher, J. M. & Augustin, J. M. 2009. Seabed Segmentation Using Optimized Statistics of Sonar Textures. IEEE Transactions on Geoscience and Remote Sensing, 47, 1621-1631.

Kennett, J. P., K. G. Cannariato, I. L. Hendy, and R. J. Behl (2000), Carbon Isotopic Evidence for Methane Hydrate Instability During Quaternary Interstadials, Science, 288(5463), 128-133.

Lewis, K. B., D. J. Bennett, R. H. Herzer, C. C. von der Borch (1986), Seismic stratigraphy and structure adjacent to an evolving plate boundary, Western Chatham Rise, New Zeland, in Kennet, J.P et al. Initial Reports DSDP, 90, Washington, 1325-1337

McDougall, J. C. (1982), Bounty sediments, New Zealand Oceanographic Institute chart, oceanic series, 1:1000000.

McGinnis, D. F., J. Greinert, Y. Artemov, S. E. Beaubien, and A. Wüest (2006), Fate of rising methane bubbles in stratified waters: How much methane reaches the atmosphere?, Journal of Geophysical Research, 111(C9).

Nodder, S., D. Bowden, and J. Hewitt (2009), New Zealand's Ocean Survey 20/20 programme: Understanding the relationships between seabed habitats and biodiversity using broad-scale mapping, paper presented at GeoHab 2009 conference, Geol. Surv. of Norway, Trondheim, Norway.

Paull, C. K., W. Ussler, and W. P. Dillon (1991), Is the extent of glaciation limited by marine gas-hydrates?, Geophys. Res. Lett., 18, 432-434.

Reyners, M., et al., Tracking repeated subduction of the Hikurangi Plateau beneath New Zealand, Earth Planet. Sci. Lett. (2011), doi:10.1016/j.epsl.2011.09.011

Sandwell, D. T., and W. H. F. Smith (1997), Marine gravity anomaly from Geosat and ERS 1 satellite altimetry, J. Geophys. Res., 102(B5), 10,039 – 10,054, doi:10.1029/ 96JB03223.

Sikes, E. L., W. R. Howard, H. L. Neil, and J. K. Volkman (2002), Glacial-interglacial sea surface temperature changes across the subtropical front east of New Zealand based on alkenone unsaturation ratios and foraminiferal assemblages, Paleoceanography, 17(2), PA1012.

Schmale, O., J. Greinert, and G. Rehder (2005), Methane emission from high-intensity marine gas seeps in the Black Sea into the atmosphere, Geophysical Research Letters, 32(7).

Schneider von Deimling, J. & C. Papenberg (2012) Technical Note: Detection of gas bubble leakage via correlation of water column multibeam images. Ocean Sci. Discuss., 8, 1757-1775.

Schneider von Deimling, J., W. Weinrebe, Z. Toth, H. Fossing, G. Rehder & V. Spiess (2013) A low frequency multibeam assessment: Spatial mapping of shallow gas by enhanced penetration and angular response anomaly. Geophysical Research Letters.

Smirnov, A., B. N. Holben, I. Slutsker, D. M. Giles, C. R. McClain, T. F. Eck, S. M. Sakerin, A. Macke, P. Croot, G. Zibordi, P. K. Quinn, J. Sciare, S. Kinne, M. Harvey, T. J. Smyth, S. Piketh, T. Zielinski, A. Proshutinsky, J. I. Goes, N. B. Nelson, P. Larouche, V. F. Radionov, P. Goloub, K. Krishna Moorthy, R. Matarrese, E. J. Robertson, and F. Jourdin (2009), Maritime Aerosol

Network as a component of Aerosol Robotic Network, J. Geophys. Res., 114, D06204, doi:10.1029/2008JD011257.

Solomon, E. A., M. Kastner, I. R. MacDonald, and I. Leifer (2009), Considerable methane fluxes to the atmosphere from hydrocarbon seeps in the Gulf of Mexico, Nature Geosci, 2(8), 561-565.

Stanton, B. R. (1981) An oceanographic survey of the Tasman Front. New Zealand Journal of Marine and Freshwater Research, 15, 289-297.

Stanton, B. R. (2002) Antarctic Intermediate Water variability in the northern New Zealand region. New Zealand Journal of Marine and Freshwater Research, 36, 645-654.

Stuiver, M. & H. A. Polach (1977) DISCUSSION: REPORTING OF 14C DATA. Radiocarbons, 19, 355-363.

Sutton, P. (2001), Detailed structure of the Subtropical Front over Chatham Rise, east of New Zealand, J. Geophys. Res., 106(C12), 31,045-031,056.

Svensen, H., S. Planke, A. Malthe-Sorenssen, B. Jamtveit, R. Myklebust, T. Rasmussen Eidem, and S. S. Rey (2004), Release of methane from a volcanic basin as a mechanism for initial Eocene global warming, Nature, 429(6991), 542-545.

Tomczak, M. and J. S. Godfrey (1994) Regional Oceanography: an Introduction. Pergamon, Oxford. 422p.

Wiesenburg, D. A., & Guinasso, N. L. jr. (1979). Equilibrium solubilities of methane, carbon monoxide, and hydrogen in water and seawater. J. Chem. and Engin. Data, 24(4), 356-360.

Wood, R.A., Andrews, P.B., Herzer, R.H., 1989. Cretaceous and Cenozoic geology of the Chatham Rise Region, South Island, New Zealand. N.Z. Geol. Surv. Basin Stud. 3, 75 pp.

Wood, R. A., and R. H. Herzer (1993), The Chatham Rise, New Zealand, in South Pacific Sedimentary Basins, edited by P. F. E. Ballance, pp. 329–349, Elsevier, Amsterdam.

Wood, R., and B. Davy (1994), The Hikurangi Plateau, Mar. Geol., 118, 153–173, doi:10.1016/0025-3227(94)90118-X.

9. Appendices

Table 9.1. Multi-core station locations and site details from SO-226-2.

SO226/2 Station #	Date (UTC) (dd/mm/yyyy)	Time corer on bottom (UTC)	Latitude °S (DD MM,mm)	Longitude °E (DD MM,mm)	Water depth (m)	Site selection comments
37-1	14/02/13	6:26	43° 59,10' S	178° 45,35' E	700	Area 1 – NE mega pockmark; sed infill outside pockmark (W); Seismic Line 6110, shot #7780
38-1	14/02/13	7:29	43° 59,02' S	178° 46,05' E	700	Area 1 – NE mega pockmark; outside pockmark above possible subsurface faulting (W); ; Seismic Line 6110, shot #8408
39-1	14/02/13	8:40	43° 58,93' S	178° 46,73' E	828	Area 1 – NE mega pockmark; inside pockmark at deepest point; Seismic Line 6110, shot #8980
40-1	14/02/13	9:40	43° 58,90' S	178° 46,96' E	812	Area 1 – NE mega pockmark; inside pockmark; Seismic Line 6110, shot #9162
41-1	14/02/13	11:50	43° 58,80' S	178° 47,65' E	740	Area 1 – NE mega pockmark; sed infill inside pockmark, above area with no buried lenses; Seismic Line 6110, shot #9719
42-1	14/02/13	13:05	43° 58,90' S	178° 48,88' E	678	Area 1 – NE mega pockmark; outside pockmark (E); Seismic Line 6110, shot #10869
48-1	15/02/13	9:41	43° 58,90' S	178° 47,21' E	782	Area 1 - NE mega pockmark; inside pockmark on lowermost feather edge of sed infill; Seismic Line 6110
49-1	15/02/13	11:19	43° 58,82' S	178° 47,81' E	755	Area 1 - NE mega pockmark; inside pockmark on uppermost feather edge of sed infill; Seismic Line 6110
50-1	15/02/13	12:36	43° 57,95' S	178° 47,62' E	702	Area 1 - NE mega pockmark; inside pockmark on uppermost conformable sequence of sed infill; Seismic Line 6112, shot #1747
50-2	15/02/13	13:34	43° 57,95' S	178° 47,60' E	700	Area 1 - NE mega pockmark; inside pockmark on uppermost conformable sequence of sed infill; Seismic Line 6112, shot #1747 - REPEAT
51-1	15/02/13	15:05	43° 58,22' S	178° 46,80' E	770	Area 1 - NE mega pockmark; inside pockmark on drape deposit on inner margin of sed infill; Seismic Line 6112, shot #2467
61-1	17/02/13	6:39	44° 5,75' S	178° 31,20' E	903	Area 1 - old mega-pockmark; outside pockmark (W); SO226-2 Stn33 site
62-1	17/02/13	8:25	44° 6,60' S	178° 35,62' E	986	Area 1 - old mega-pockmark; deepest point inside pockmark (E); TAN0902 site
62-2	17/02/13	9:23	44° 6,60' S	178° 35,63' E	984	Area 1 - old mega-pockmark; deepest point inside pockmark (E); TAN0902 site
63-1	17/02/13	11:02	44° 6,05' S	178° 40,02' E	878	Area 1 - old mega-pockmarks; SO226-2 Stn 31 "CONTROL" site
63-2	17/02/13	11:56	44° 6,05' S	178° 40,00' E	878	Area 1 - old mega-pockmarks; SO226-2 Stn 31 "CONTROL" site

64-1	17/02/13	13:57	43° 58,92' S	178° 46,74' E	826	Area 1 – NE mega-pockmark; inside pockmark at deepest point; SO226-2 Stn 39
64-2	17/02/13	14:49	43° 58,99' S	178° 46,67' E	825	Area 1 – NE mega-pockmark; inside pockmark at deepest point; SO226-2 Stn 39
68-1	20/02/13	6:32	44° 14,34' S	177° 11,17' E	933	Area 2 - NE pockmark transect; outside pockmark, conformable sed infill; Seismic line 7114, shot #7783
69-1	20/02/13	7:50	44° 14,37' S	177° 10,38' E	967	Area 2 - NE pockmark transect; inside pockmark on feather edge of sed infill above highly upwardly disrupted reflectors; Seismic line 7114, shot #7112
70-1	20/02/13	8:39	44° 14,37' S	177° 10,29' E	971	Area 2 - NE pockmark transect; inside pockmark on innermost feather edge of sed infill above highly upwardly disrupted reflectors; Seismic line 7114, shot #7032
70-2	20/02/13	9:51	44° 14,39' S	177° 10,31' E	971	Area 2 - NE pockmark transect; inside pockmark on innermost feather edge of sed infill above highly upwardly disrupted reflectors; Seismic line 7114, shot #7033
71-1	20/02/13	11:17	44° 14,38' S	177° 9,01' E	967	Area 2 - NE pockmark transect; inside pockmark on central sed infill; Seismic line 7114, shot #5948
72-1	20/02/13	12:19	44° 14,38' S	177° 8,55' E	960	Area 2 - NE pockmark transect; inside pockmark on small "hill" in central sed infill above buried fault zone; Seismic line 7114, shot #5554
73-1	20/02/13	13:22	44° 14,38' S	177° 8,42' E	965	Area 2 - NE pockmark transect; inside pockmark on W side of small "hill" in central sed infill above buried fault zone; Seismic line 7114, shot #5451
77-4	21/02/13	9:24	44° 14,38' S	177° 11,15' E	935	Area 2 - NE pockmark transect; outside pockmark, conformable sed infill; Seismic line 7114, shot #7783
77-5	21/02/13	10:29	44° 14,37' S	177° 11,15' E	935	Area 2 - NE pockmark transect; outside pockmark, conformable sed infill; Seismic line 7114, shot #7783
78-1	21/02/13	11:50	44° 14,38' S	177° 8,41' E	962	Area 2 - NE pockmark transect; inside pockmark on W side of small "hill" in central sed infill above buried fault zone; Seismic line 7114, shot #5451
78-2	21/02/13	12:46	44° 14,39' S	177° 8,40' E	962	Area 2 - NE pockmark transect; inside pockmark on W side of small "hill" in central sed infill above buried fault zone; Seismic line 7114, shot #5451
79-1	21/02/13	14:26	44° 17,55' S	177° 3,41' E	972	Area 2 - NE pockmark transect; outside pockmark, conformable sed infill; Seismic line 7109, shot #6430
80-1	21/02/13	15:51	44° 18,29' S	177° 2,58' E	1017	Area 2 - SW pockmark transect; inside pockmark above buried uplifted strata; Seismic line 7109, shot #5313
80-2	21/02/13	16:50	44° 18,28' S	177° 2,59' E	1017	Area 2 - SW pockmark transect; inside pockmark above buried uplifted strata; Seismic line 7109, shot #5313
81-1	21/02/13	17:50	44° 18,37' S	177° 2,48' E	1019	Area 2 - SW pockmark transect; inside pockmark on side of small "hill" above buried uplifted strata; Seismic line 7109, shot #5128

82-1	21/02/13	18:51	44° 18,49' S	177° 2,38' E	1021	Area 2 - SW pockmark transect; inside pockmark above buried uplifted strata; Seismic line 7109, shot #5001
82-2	21/02/13	19:45	44° 18,48' S	177° 2,37' E	1022	Area 2 - SW pockmark transect; inside pockmark above buried uplifted strata; Seismic line 7109, shot #5001
90-1	25/02/13	10:08	43° 59,42' S	174° 28,08' E	573	Area 3 - NW-SE pockmark transect; outside pockmark on conformable near-surface strata; Seismic line 9103, shot #1916
91-1	25/02/13	10:56	43° 59,25' S	174° 27,96' E	572	Area 3 - NW-SE pockmark transect; inside pockmark; Seismic line 9103, shot #2155
92-1	25/02/13	12:00	43° 59,22' S	174° 27,92' E	574	Area 3 - NW-SE pockmark transect; inside pockmark; Seismic line 9103, shot #2197
93-1	25/02/13	12:52	43° 59,16' S	174° 27,87' E	573	Area 3 - NW-SE pockmark transect; inside pockmark, poss fluid efflux; Seismic line 9103, shot #2289
93-2	25/02/13	13:45	43° 59,15' S	174° 27,86' E	567	Area 3 - NW-SE pockmark transect; inside pockmark, poss fluid efflux; Seismic line 9103, shot #2289
94-1	25/02/13	14:47	43° 59,43' S	174° 28,08' E	568	Area 3 - NW-SE pockmark transect; outside pockmark on conformable near-surface strata; Seismic line 9103, shot #1916
94-2	25/02/13	15:37	43° 59,44' S	174° 28,05' E	569	Area 3 - NW-SE pockmark transect; outside pockmark on conformable near-surface strata; Seismic line 9103, shot #1916

Table 9.2. Multi-core sampling details from SO-226-2.

SO226/2 Station #		Core #1	Core #2	Core #3	Core #4	Core #5	Core #6	Core #7	Core #8
37-1	Parameter					PaulaR (NRL)		Seds	
	Sed depth (cm)	No sample		No sample		13		13	
38-1	Parameter			Seds				PaulaR (NRL)	
	Sed depth (cm)	No sample		9		No sample		6	
39-1	Parameter	Sample discarded	PaulaR (NRL)		Seds		Sample discarded		
	Sed depth (cm)	39	40		41		37		
40-1	Parameter					PaulaR (NRL)		Sample	Seds

								discarded	
	Sed depth (cm)			No sample		14		12	14.5
41-1	Parameter			Seds	Sample discarded			PaulaR (NRL)	
	Sed depth (cm)			24	21.5		No sample	24	
42-1	Parameter					Seds			PaulaR (NRL)
	Sed depth (cm)	No sample		No sample		15			14.5
48-1	Parameter	Seds	PaulaR (NRL)		Sample discarded	Sample discarded			
	Sed depth (cm)	25	22		22	26			
49-1	Parameter			Sample discarded			PaulaR (NRL)	Seds	Sanple discarded
	Sed depth (cm)			23			27	26.5	23
50-1	Parameter								
	Sed depth (cm)	No sample		No sample		No sample		No sample	
50-2	Parameter		Sample discarded		Sample discarded	Seds		PaulaR (NRL)	
	Sed depth (cm)		35		28	36		36	
51-1	Parameter						Seds	Sample discarded	PaulaR (NRL)
	Sed depth (cm)			No sample			10	11	11.5
61-1	Parameter	Seds				Sample discarded		PaulaR (NRL)	Sample discarded
	Sed depth (cm)	31.5				24		35	22
62-1	Parameter		Seds	SCOC/macro	Bact only		SCOC/macro		
	Sed depth (cm)		29	37.5	24		37		
62-2	Parameter	Meio/bact				SCOC/macro		SCOC/macro	Meio/bact seds only

	Sed depth (cm)	38				39.5		38.5	35
63-1	Parameter		Meio/bact	SCOC/macro	SCOC/macro		PaulaR (NRL)		
	Sed depth (cm)		24	32	27		35.5		
63-2	Parameter	Meio/bact				Seds		Meio/bact	SCOC/macro
	Sed depth (cm)	31				30		37	23
64-1	Parameter	Sample discarded - disturbed			SCOC/macro		Sample discarded - disturbed		
	Sed depth (cm)	15			18		12		No sample
64-2	Parameter								
	Sed depth (cm)	No sample		No sample		No sample		No sample	
68-1	Parameter		Sample discarded	Seds		PaulaR (NRL)			Sample discarded
	Sed depth (cm)			28		34			23.5
69-1	Parameter	Seds			Sample discarded		Sample discarded	PaulaR (NRL)	
	Sed depth (cm)	17			16.5		13.5	19	
70-1	Parameter								Seds
	Sed depth (cm)	No sample		No sample		No sample			
70-2	Parameter								
	Sed depth (cm)	No sample		No sample		No sample		No sample	
71-1	Parameter		Sample discarded	Seds	Sample discarded	PaulaR (NRL)			
	Sed depth (cm)		11.5	16	11.5	17.5			
72-1	Parameter	Sample discarded					PaulaR (NRL)	Sample discarded	Seds
	Sed depth (cm)	18					12.5	20.5	11

73-1	Parameter			PaulaR (NRL)	Sample discarded	Seds			
	Sed depth (cm)		No sample	17.5	17	17			
77-4	Parameter	Seds	Meio/bact				SCOC/macro		SCOC/macro
	Sed depth (cm)	35	22				35		24
77-5	Parameter			Meio/bact	Sample discarded	Meio/bact		SCOC/macro	
	Sed depth (cm)			36	38	41		44.5	
78-1	Parameter	SCOC/macro	Meio/bact				SCOC/macro		Meio/bact
	Sed depth (cm)	17	14				14.5		14.5
78-2	Parameter			SCOC/macro	Sample discarded	Meio/bact		Seds	
	Sed depth (cm)			16.5	12.5	17.5		17.5	
79-1	Parameter	Seds	Sample discarded				PaulaR (NRL)		Sample discarded
	Sed depth (cm)	39	26				43		40
80-1	Parameter								
	Sed depth (cm)	No sample		No sample		No sample		No sample	
80-2	Parameter			PaulaR (NRL)	Sample discarded	Sample discarded			Seds
	Sed depth (cm)			21	19	20			20.5
81-1	Parameter	PaulaR (NRL)	Sample discarded				Sample discarded		Seds
	Sed depth (cm)	27	14				25		23
82-1	Parameter								
	Sed depth (cm)	No sample		No sample		No sample		No sample	
82-2	Parameter			PaulaR (NRL)	Sample discarded	Seds		Sample discarded	

	Sed depth (cm)			28.5	19	21.5		9	
90-1	Parameter	PaulaR (NRL)		Meio/bact		Seds			Meio/bact
	Sed depth (cm)	22.5		23		22			20
91-1	Parameter		Sample discarded		Seds		PaulaR (NRL)	Sample discarded	
	Sed depth (cm)		29		35		38	31	
92-1	Parameter	PaulaR (NRL)		Sample discarded		Sample discarded			Seds
	Sed depth (cm)	23		27		25.5			24.5
93-1	Parameter		Meio/bact		Sample discarded		PaulaR (NRL) & Seds	SCOC/macro	
	Sed depth (cm)		31.5				42.5	41	
93-2	Parameter	SCOC/macro		SCOC/macro		Meio/bact			Meio/bact
	Sed depth (cm)	39		27		34			26
94-1	Parameter		SCOC/macro		Sample discarded		Meio/bact		Sample discarded
	Sed depth (cm)		32.5		-		32.5		-
94-2	Parameter	SCOC/macro		SCOC/macro	Sample discarded			SCOC/macro	
	Sed depth (cm)	24		24	-			25	

Table 9.3. OFOS station locations and station details from SO-226-2.

SO226-2 Station #	Date (UTC)	Time (UTC)	Latitude (DD MM,mm)	Longitude (DD MM,mm)	Water depth (m)	Gear type	Station notes	
SO226/055-1	16/02/13	2:23	43° 58,91' S	178° 48,90' E	680	OFOS	Beginn Station	
SO226/055-1	16/02/13	2:39	43° 59,05' S	178° 48,99' E	680	OFOS	zu Wasser	W 2
SO226/055-1	16/02/13	3:00	43° 58,94' S	178° 48,97' E	676	OFOS	Bodensicht	SLmax: 673 m; rwK: 275°, d: 1 nm

SO226/055-1	16/02/13	5:11	43° 58,82' S	178° 47,58' E	741	OFOS	Kursänderung	rwk: 260°, d: 2 nm
SO226/055-1	16/02/13	9:05	43° 59,10' S	178° 45,34' E	699	OFOS	Beginn hieven	
SO226/055-1	16/02/13	9:25	43° 59,13' S	178° 45,44' E	698	OFOS	an Deck	
SO226/055-1	16/02/13	9:33	43° 59,14' S	178° 45,42' E	699	OFOS	Ende Station	
SO226/087-1	23/02/13	0:12	44° 17,52' S	177° 3,45' E	971	OFOS	Beginn Station	
SO226/087-1	23/02/13	0:15	44° 17,53' S	177° 3,46' E	972	OFOS	zu Wasser	W 2
SO226/087-1	23/02/13	0:46	44° 17,54' S	177° 3,41' E	971	OFOS	Bodensicht	SL: 963 m; rwK: 219°
SO226/087-1	23/02/13	4:04	44° 18,48' S	177° 2,35' E	1022	OFOS	Beginn hieven	SLmax: 1024 m; d: 1 nm
SO226/087-1	23/02/13	4:36	44° 18,40' S	177° 2,18' E	1030	OFOS	an Deck	
SO226/087-1	23/02/13	4:36	44° 18,40' S	177° 2,18' E	1030	OFOS	Ende Station	
SO226/105-1	26/02/13	20:06	44° 0,13' S	174° 28,61' E	572	OFOS	Beginn Station	
SO226/105-1	26/02/13	20:10	44° 0,14' S	174° 28,60' E	573	OFOS	zu Wasser	W 2
SO226/105-1	26/02/13	20:30	44° 0,12' S	174° 28,65' E	583	OFOS	Bodensicht	SLmax: 577 m
SO226/105-1	27/02/13	0:05	43° 58,92' S	174° 27,69' E	574	OFOS	Beginn hieven	
SO226/105-1	27/02/13	0:33	43° 58,94' S	174° 27,71' E	574	OFOS	an Deck	
SO226/105-1	27/02/13	0:39	43° 58,95' S	174° 27,73' E	573	OFOS	Ende Station	

9.4 Station List

Table with deployment and recovery times of operation, provided as complimentary Excel file

9.5 Winch Operation

Table with times and information on winch operations, provided as complimentary Excel file

GEOMAR
Helmholtz-Zentrum für Ozeanforschung Kiel

GEOMAR Reports

No.	Title
1	FS POSEIDON Fahrtbericht / Cruise Report POS421, 08. – 18.11.2011, Kiel - Las Palmas, Ed.: T.J. Müller, 26 pp, DOI: 10.3289/GEOMAR_REP_NS_1_2012
2	Nitrous Oxide Time Series Measurements off Peru – A Collaboration between SFB 754 and IMARPE –, Annual Report 2011, Eds.: Baustian, T., M. Graco, H.W. Bange, G. Flores, J. Ledesma, M. Sarmiento, V. Leon, C. Robles, O. Moron, 20 pp, DOI: 10.3289/GEOMAR_REP_NS_2_2012
3	FS POSEIDON Fahrtbericht / Cruise Report POS427 – Fluid emissions from mud volcanoes, cold seeps and fluid circulation at the Don-_Kuban deep sea fan (Kerch peninsula, Crimea, Black Sea) – 23.02. – 19.03.2012, Burgas, Bulgaria - Heraklion, Greece, Ed.: J. Bialas, 32 pp, DOI: 10.3289/GEOMAR_REP_NS_3_2012
4	RV CELTIC EXPLORER EUROFLEETS Cruise Report, CE12010 – ECO2@NorthSea, 20.07. – 06.08.2012, Bremerhaven – Hamburg, Eds.: P. Linke et al., 65 pp, DOI: 10.3289/GEOMAR_REP_NS_4_2012
5	RV PELAGIA Fahrtbericht / Cruise Report 64PE350/64PE351 – JEDDAH-TRANSECT -, 08.03. – 05.04.2012, Jeddah – Jeddah, 06.04 - 22.04.2012, Jeddah – Duba, Eds.: M. Schmidt, R. Al-Farawati, A. Al-Aidaroos, B. Kurten and the shipboard scientific party, 154 pp, DOI: 10.3289/GEOMAR_REP_NS_5_2013
6	RV SONNE Fahrtbericht / Cruise Report SO225 - MANIHIKI II Leg 2 The Manihiki Plateau - Origin, Structure and Effects of Oceanic Plateaus and Pleistocene Dynamic of the West Pacific Warm Water Pool, 19.11.2012 - 06.01.2013 Suva / Fiji – Auckland / New Zealand, Eds.: R. Werner, D. Nürnberg, and F. Hauff and the shipboard scientific party, 176 pp, DOI: 10.3289/GEOMAR_REP_NS_6_2013

For GEOMAR Reports, please visit:
https://oceanrep.geomar.de/view/series/GEOMAR_Report.html

Reports of the former IFM-GEOMAR series can be found under:
https://oceanrep.geomar.de/view/series/IFM-GEOMAR_Report.html

GEOMAR
Helmholtz-Zentrum für Ozeanforschung Kiel

Das GEOMAR Helmholtz-Zentrum für Ozeanforschung Kiel
ist Mitglied der Helmholtz-Gemeinschaft
Deutscher Forschungszentren e.V.

The GEOMAR Helmholtz Centre for Ocean Research Kiel
is a member of the Helmholtz Association of
German Research Centres

Helmholtz-Zentrum für Ozeanforschung Kiel / Helmholtz Centre for Ocean Research Kiel
GEOMAR
Dienstgebäude Westufer / West Shore Building
Düsternbrooker Weg 20
D-24105 Kiel
Germany

Helmholtz-Zentrum für Ozeanforschung Kiel / Helmholtz Centre for Ocean Research Kiel
GEOMAR
Dienstgebäude Ostufer / East Shore Building
Wischhofstr. 1-3
D-24148 Kiel
Germany

Tel.: +49 431 600-0
Fax: +49 431 600-2805
www.geomar.de